QUALITY OF FLEXIBLE PAVEMENT LONGITUDINAL JOINTS USING NON-DESTRUCTIVE TESTING

By

Hamad Bin Muslim

A DISSERTATION

Submitted to
Michigan State University
in partial fulfillment of the requirements
for the degree of

Civil Engineering – Doctor of Philosophy

2024

ABSTRACT

Hot-mix asphalt (HMA) compaction at longitudinal joints is critical for pavement performance and longevity. Many highway agencies face challenges maintaining deteriorated joints, often resulting in issues like raveling along the centerline. Despite extensive research and training on proper HMA placement and compaction, joint deterioration remains a leading cause of premature flexible pavement failure. Improving joint compaction during construction is critical to better pavement performance. The longitudinal joint construction includes various methods—differing laying conditions, joint geometry, rolling patterns, and techniques. While each has advantages, these methods also carry risks in consistently achieving optimal compaction. Current quality assurance (QA) methods, such as coring and density gauges, are labor-intensive, time-consuming, costly, and offer limited coverage, increasing the likelihood of missing low-density areas. The variability in construction methods and limitations of traditional QA testing raises the risk of inadequate joint compaction, potentially compromising pavement's durability and performance.

The Dielectric Profiling System (DPS) offers a nondestructive alternative for assessing compaction quality, providing continuous real-time coverage by measuring dielectric values, which correlate with HMA density but need a calibrated relationship. Adopting DPS for QA testing requires alternative methods (other than air voids) to quickly assess joint density during construction. This study compared various longitudinal joint construction methods using dielectric measurements from Minnesota and Michigan road projects. The continuous dielectric data were discretized into subsections for analyses using relative dielectric differences that indicated over 2% more air voids at the joint than at the mat.

This study used a coreless calibration method with lab-prepared pucks to develop a new model for converting dielectric values to predicted air voids for similar analyses. Project- and group-wise calibrations were performed; project-specific models aligned well with cores collected during DPS and QA testing. Minor HMA production fluctuations across different days displayed minimal impact on air void predictions. Additionally, HMA mixtures were grouped for group-wise calibrations using recorded dielectric values and mix characteristics, which demonstrated reasonable accuracy. This approach highlights the potential for direct DPS data use in the field without needing project-specific models.

Statistical analyses revealed that unconfined joints had the highest air void content, with 50 to 100% of subsections showing significant differences, indicating over 2% more air voids than the adjacent mat. Additionally, 60 to 100% of unconfined joint subsections fell below the 60% Percent Within Limits (PWL), the rejectable quality level (RQL). In contrast, all other joint types showed similar compaction to the mat, with negligible subsections below 60% PWL. These findings were consistent when using predicted air voids. Similarly, the probabilistic analysis showed a 30 to 60% likelihood that unconfined joints had significantly lower dielectric values than the mat, while other joints exhibited minimal differences or better compaction.

This study introduces a Longitudinal Joint Quality Index (LJQI) that enables the direct use of dielectric values to enhance the field applicability of DPS. A threshold of 70% LJQI was established for joint quality acceptance. LJQI comparisons revealed that unconfined joints had higher void content than the adjacent mat in 11 to 89% of stations across multiple projects. According to all the analyses conducted, it was consistently found that constructing either butt or tapered joints while avoiding unconfined joint construction can lead to achieving better joint density. Moreover, it has been observed that smaller subsections are efficient in identifying local compaction problems, and for practical reasons, it is suggested to use 100 ft subsections during analyses.

Many State Highway Agencies (SHAs) rely on specifications that focus on as-constructed air voids to assess construction quality and determine pay factors (PF) for contractor payments, often neglecting the performance of longitudinal joints. This study proposes a Performance-Related Specification (PRS) framework that leverages the DPS's continuous data to link joint service life to void content, used as the Acceptance Quality Characteristic (AQC). By using air void content as AQC and PWL quality measure, SHAs can more accurately assess joint quality and make informed pay adjustments, ensuring durable, high-quality pavements while minimizing overpayments.

I dedicate this dissertation to my parents, Dr. Muslim Khan and Huma Muslim, whose unwavering encouragement and prayers have always fueled my success. I also dedicate it to my spouse, Fatima Hayat, and my children, Armughan Bin Hamad, and Adan Hamad, for their constant support throughout this journey. Additionally, I dedicate this work to my siblings, Dr. Fahad Bin Muslim, Saima Misbah, Dr. Faiqa Farah Muslim, Bushra Khan, and Alza Farah Muslim, whose love and encouragement have been invaluable.

ACKNOWLEDGMENTS

First and foremost, I would like to thank Almighty Allah for granting me the opportunity to be part of such a prestigious institution and giving me the strength to achieve this significant milestone in my life.

I would like to express my sincere gratitude to my advisor, Dr. Syed Waqar Haider, for his exceptional support and guidance throughout this study. Dr. Haider has been a remarkable mentor, imparting invaluable lessons about the research process and providing constant motivation through his approachability and willingness to help. This research would not have been possible without his insightful input and time. His extensive experience, thorough knowledge, patience, and active involvement at every stage were instrumental in helping me complete the work successfully.

I would also like to extend my heartfelt thanks to my committee members, Drs. Muhammed Emin Kutay, Kirk D. Dolan, and Karim Chatti, for serving on my Ph.D. committee. I am particularly grateful to Dr. Kutay for his guidance and the time he dedicated to my research. I also acknowledge Dr. Dolan for teaching me essential numerical modeling and parameter estimation lessons, which were instrumental in my dissertation work. Lastly, I sincerely appreciate Dr. Chatti for his constructive feedback and support.

I express my deepest gratitude to my spouse, Fatima Hayat, and my children, Armughan and Adan, for their unwavering support and patience throughout this challenging yet rewarding journey. I could not have achieved this milestone without them. I also want to thank my parents, Dr. Muslim Khan and Huma Muslim, whose daily prayers have been a constant source of strength and motivation for me during this time. Additionally, I am grateful to my siblings for their care and support in looking after our parents in my absence.

Finally, I would like to thank all my fellow graduate students who made this journey unforgettable and enjoyable. I feel fortunate to have had the opportunity to learn and work with Drs. Angela Farina, Mahdi Ghazavi, Mumtahin Hasnat, Ceren Aydin, Peng Chen, Wasif Naqvi, Celso Santos, Rahul Raj Singh, and Farhad Abdollahi. I am also thankful for the support, help, and companionship of Poornachandra Vaddy, Faizan Ahmed Lali, Muhamad Yaman Fares, and Ahmad Albdour throughout my academic journey. I also want to thank Dr. Fawaz Kaseer and Ethan Akerly from the Michigan Department of Transportation (MDOT) for their help with data collection.

TABLE OF CONTENTS

CHAPTER 1 - INTRODUCTION

1.1 PROBLEM STATEMENT

Asphalt pavements minimize disruptions in traffic flow as these can be paved and opened to traffic quickly. Typically, during asphalt pavement construction, one lane is paved at a time while traffic is maintained in an adjacent lane. Consequently, a longitudinal joint is constructed between the lanes. As in all engineering materials, joints are considered potential weak points, which also hold for asphalt pavements. An inadequately constructed longitudinal joint can result in the premature deterioration of an otherwise sound pavement (*1*). The issue has been thoroughly investigated to find methods to improve the quality of longitudinal joints since the 1960s (*2*).

Foster et al. pointed out that a low-density zone within the joint area of flexible pavements leads to long-term performance issues (*3*). This is a direct consequence of paving a single lane at a time. Once the first lane is paved, the mat is compacted with an unconfined edge. During compaction, the unsupported condition at the edge results in lateral sloughing of the fresh asphalt material, resulting in a lower density. Additionally, the asphalt material along the edge of the mat tends to cool more quickly than the material within the mat. Thus, the cooler material at the edge inhibits proper compaction and decreases density at the joint. Although the cold edge of the first paved mat presents a confined edge for compaction of hot asphalt material of the second lane, it may lead to an uneven surface along with a bonding problem between the edges, hindering the achievement of a monolithic mat (*4*).

According to Estakhri et al., the structural support and temperature differences while paving and compacting the two adjacent lanes result in lower density, higher permeability, higher segregation, and lower adhesion at the joint (*1*). Insufficient asphalt material at the joint while compacting is also anticipated for the lower longitudinal joint density (*5*). The low-density weak bonded centerline joint within the pavement eventually cracks, leading to water and moisture infiltration—such ingress of water results in debonding due to stripping. Also, the infiltrated water can undergo freeze-thaw cycles, especially in the colder regions, and increase the chances of joint failure and pavement raveling near the joint (*6*). Several studies estimated that a 1% decrease in air void content in the compacted asphalt mat could enhance a pavement's service life by approximately 10% (*7-11*). Thus, compaction is the most critical construction-

related factor directly related to the in-place density and air void content of asphalt pavements and improving it can provide long-term serviceability (*12*).

1.2 RESEARCH MOTIVATION

Several ways are employed to construct the asphalt pavements' centerline longitudinal joints. These ways differ in the laying conditions, joint geometry, rolling patterns, and construction techniques. Considering conditions, the longitudinal joint can be laid as a hot joint, a semi-hot, or a cold joint. Also, the longitudinal joint can be confined or unconfined based on the project (new construction or overlay). As far as the joint's geometry is concerned, it can either be a vertical (or butt joint) or a tapered joint (with or without a notch). In addition, different rolling patterns are used to compact the longitudinal joints. The joint can be rolled using the hot overlap, hot pinch, or cold roll methods. Another method-based technique, the Maryland Method, is used for constructing confined joints. Moreover, techniques such as echelon paving, sequential mill, and fill, wedge construction, edge restrain, joint maker, and cut back are used to construct the longitudinal joints at different projects. Each of these construction methods is known to have some merits and demerits in achieving the required compaction levels at the joints. Thus, risk is involved in using any techniques to construct the joint and achieve better joint quality and performance.

Conventional joint quality evaluation methods either involve destructive ways, such as coring, or non-destructive ways, such as nuclear and non-nuclear gauges. The cores extracted from the pavements are used to measure the air voids in the laboratory and evaluate the achieved level of compaction in the field. One of the most significant limitations of either way is their limited coverage of asphalt pavements. Quality acceptance programs rely on random coring measuring less than 1% of the total asphalt mixtures produced and laid (*13*). Thus, the chances of missing localized areas with compaction issues increase manifolds. While many measurements can be taken quickly and non-destructively using nuclear and non-nuclear gauges, these also have several demerits. Seating the gauge over the joint, especially at the crown, is a known problem (*14*). The density gauges are known to underestimate density since they measure joint density by placing them very close to the joint but not over it (*15*). The use of several longitudinal joint construction methods and the limited coverage provided by the conventional quality evaluation methods increase the chances of not achieving adequate compaction at the joints.

Since the longitudinal joint quality and performance appear to be influenced by the overall density achieved at the joint, it is essential to compare the density achieved using different longitudinal joint construction methods. In addition, using the recently developed Dielectric Profiling System (DPS) provides a better alternative than conventional joint quality evaluation methods. A DPS is a Ground Penetrating Radar (GPR) based equipment that evolved from research conducted under the National Academies of Science sponsored second Strategic Highway Research Program (SHRP2) (*16; 17*). The system utilizes specially designed GPR sensors, whose collected data helps determine the dielectric constant of the hot-mix asphalt (HMA) layer in real-time. The obtained HMA dielectric values can be correlated with the pavement's air void percentage and density. The DPS gives the equivalent of about 100,000 cores per mile, aiding better monitoring and evaluation of the joint's quality (*18*).

While the DPS dielectric data has been used to evaluate the compaction of the asphalt mat and the accompanying joint, a comprehensive comparison has not been performed between different longitudinal joint types and their construction techniques, especially when incorporating the continuous coverage capability of the DPS equipment. This study compares several different asphalt centerline longitudinal joint types and construction techniques using DPS in-field dielectric measurements at various road projects from Minnesota and Michigan. Additionally, best practices for longitudinal joint construction are identified using literature, conducting a survey, and DPS data analysis. Moreover, the use of DPS is demonstrated in evaluating the joint quality and identifying any special needs for its implementation in the field.

Furthermore, since the DPS provides dielectric values rather than air voids, incorporating it into the quality assurance (QA) and quality control (QC) processes for asphalt pavements during construction requires alternative methods to assess the relative compaction quality achieved at the joint quickly. Moreover, most SHAs rely on as-constructed density or air voids as the primary performance indicators for the asphalt mat and longitudinal joints. However, the difficulty in achieving the required minimum density at joints, combined with the limitations of core sampling, puts agencies at risk of fully paying for substandard joints. Exploring the possibility of developing performance-related specifications (PRS) utilizing the DPS's enhanced sampling capability may aid SHAs in enforcing quality requirements effectively, ensuring achieving the desired quality without overpayments.

1.3 RESEARCH OBJECTIVE AND METHODOLOGY

It is well-known that the quality of longitudinal joint construction is critical to the life of flexible pavements. The maintenance activities caused by longitudinal joint deterioration's direct or indirect effects have become challenging for many highway agencies. A 2009 Federal Highway Administration (FHWA) survey of their divisional offices found that about 50% of their engineers were unhappy with longitudinal joints' performance. Local agencies report problems with deterioration (raveling) along the centerline paving joint of asphalt roadways. Several questions are raised to understand this widespread problem, including whether the source of the issue is material, specification, constructional quality, method-related, or a combination of these issues.

Consequently, academia, highway agencies, and industry have made numerous research efforts in the last 30 years. Besides, training on the placement and compaction of HMA pavements is available within the industry. Despite all these efforts, longitudinal joint deterioration is still one of the prime causes of premature failure of flexible pavements. Improving longitudinal joint construction can improve density and decrease permeability. It is probably the single most crucial remedy to enhance pavement performance.

The overall goal of this study is to compare the different asphalt longitudinal joint construction types and practices, identify best practices used in the states of Minnesota and Michigan, and investigate the use of DPS in the quality evaluation of the different joint types. The following are the specific objectives to achieve these goals:

- Review existing longitudinal joint construction practices and literature, compare methods and issues, and identify the current longitudinal joint construction practices in Minnesota and Michigan.
- Collect HMA in-field dielectric data using DPS and statistically and stochastically analyze it to compare different longitudinal joint construction methods.
- Investigate and potentially demonstrate the direct use of the recorded dielectric data.
- Demonstrate using DPS data for longitudinal joint quality evaluation, quality control (QC), and quality assurance (QA).
- Recommend best practices for the construction and repair of longitudinal joints, their quality evaluation during construction, and construction specifications for the potential use of DPS in longitudinal joint QA testing.

- Establish a PRS framework for longitudinal joints by developing a performance relationship between a suitable acceptance quality characteristic (AQC) and the performance measure.

The methodology primarily involves conducting a detailed literature review of the existing practices and comparing various approaches for longitudinal joint construction and identification of issues. The study focused on three main areas: (a) construction practices, (b) evaluation of the longitudinal joint quality, and (c) repair and remedial measures. In addition, a survey was conducted to determine the state of practice for HMA longitudinal joint construction within Minnesota and Michigan. Comparing the current practices with the literature, best practices are identified for improving the longitudinal joints' quality, eventually resulting in longer-lasting pavements. In addition, DPS dielectric data were collected from different project sites in Minnesota and Michigan using varying longitudinal joint construction methods and techniques. Statistical and stochastic analysis were employed to compare the compaction ability of different joints. Based on the literature review, survey, and DPS data analyses, final recommendations are made to improve longitudinal joint quality and construction practices.

Moreover, this study investigated the potential direct use of the DPS's dielectric data in the field without needing the project-specific dielectric-air void relationship to compare the compaction ability of various joint types relative to the mat. Finally, this study developed a performance-related specifications (PRS) framework utilizing DPS's continuous data for joint quality evaluation and subsequent determination of pay factors based on the developed PRS.

1.4 DISSERTATION OUTLINE

This dissertation contains seven chapters. Chapter 1 contains the problem statement and highlights the motivation behind this study. It also includes the research objectives. Chapter 2 documents the literature review and the survey results conducted in Minnesota and Michigan. Chapter 3 discusses the DPS data collection and presents the project-wise and group-wise dielectric-air void calibration relationships and their validation using the collected pavement cores and QA cores. Chapter 4 describes the data analysis methods, provides example analyses, and summarizes the results. Chapter 5 presents the Longitudinal Joint Quality Index (LJQI), demonstrates its usage, and analyzes different thresholds. Chapter 6 shows examples of in-field compaction evaluation for selected projects, illustrates a framework to determine the longitudinal joint's air void-service life relationship, and discusses the developed joint PRS and related pay

factors. Chapter 7 summarizes this study's conclusions, recommendations, and future scope. Each chapter has a summary at the end, which outlines the overall content of that chapter.

REFERENCES

1. Estakhri, C. K., T. J. Freeman, and C. H. Spiegelman, "Density evaluation of the longitudinal construction joint of hot-mix asphalt pavements," Texas Transportation Institute, Texas A & M University System, 2001.
2. Buncher, M. S., and C. Rosenberger, "Best Practices for Constructing and Specifying HMA Longitudinal Joints," *Final Report, Asphalt Institute, Washington, DC*, 2012.
3. Foster, C., S. Hudson, and R. Nelson, "Constructing longitudinal joints in hot mix asphalt pavements," *Highway Research Record,* vol. 51, pp. 124-136, 1964.
4. McDaniel, R. S., A. Shah, and J. Olek, "Longitudinal Joint Specifications and Performance," 2012.
5. Zinke, S., J. Mahoney, E. Jackson, and G. Shaffer, "Comparison of the use of notched wedge joints vs. traditional butt joints in Connecticut," 2008.
6. Buchanan, M. S., "Evaluation of notched-wedge longitudinal joint construction," *Transportation Research Record,* vol. 1712, pp. 50-57, 2000.
7. Aschenbrener, T., E. R. Brown, N. Tran, and P. B. Blankenship, "The FHWA's demonstration project for enhanced durability of asphalt pavements through increased in-place pavement density," *Transportation Research Record,* vol. 2672, pp. 57-67, 2018.
8. Tran, N., P. Turner, and J. Shambley, "Enhanced compaction to improve durability and extend pavement service life: A literature review," 2016.
9. Linden, R. N., J. P. Mahoney, and N. C. Jackson, "Effect of compaction on asphalt concrete performance," *Transportation Research Record,* 1989.
10. Kim Willoughby, P., W. Olympia, J. P. Mahoney, and J. Walter, "An Assessment of WSDOT's Hot-Mix Asphalt Quality Control and Assurance Requirements," 2007.
11. Sebaaly, P. E., and J. C. Barrantes, "Development of a Joint Density Specification: Phase I-Literature Review and Test Plan," 2004.
12. Hughes, C. S., *Compaction of asphalt pavement*. Washington, D.C., 1989.
13. Steiner, T., K. Hoegh, E. Z. Teshale, and S. Dai, "Method for assessment of modeling quality for asphalt dielectric constant to density calibration," *Journal of Transportation Engineering, Part B: Pavements,* vol. 146, p. 04020054, 2020.
14. Williams, S. G., "HMA longitudinal joint evaluation and construction," University of Arkansas, Fayetteville. Dept. of Civil Engineering, 2011.
15. Kandhal, P. S., T. L. Ramirez, and P. M. Ingram, "Evaluation of eight longitudinal joint construction techniques for asphalt pavements in Pennsylvania," *Transportation Research Record,* vol. 1813, pp. 87-94, 2002.
16. Sebesta, S., T. Scullion, and T. Saarenketo, *Using infrared and high-speed ground-penetrating radar for uniformity measurements on new HMA layers*. Transportation Research Board, 2013.

17. Khazanovich, L., K. Hoegh, and R. Conway, "Non-destructive Evaluation of Bituminous Compaction Uniformity Using Rolling Density," 2017.

18. Hoegh, K., T. Steiner, E. Zegeye Teshale, and S. Dai, "Minnesota Department of Transportation case studies for coreless asphalt pavement compaction assessment," *Transportation Research Record*, vol. 2674, pp. 291-301, 2020.

CHAPTER 2 - LITERATURE REVIEW AND STATE OF PRACTICE

2.1 BACKGROUND

During asphalt pavement construction, typically, one lane is paved at a time while traffic flows in an adjacent lane, creating a longitudinal joint between lanes. These joints are potential weak points within the pavement structure. It has been established that poorly constructed longitudinal joints can lead to the premature deterioration of an otherwise structurally sound pavement (*1*). Therefore, extensive research has been conducted to find methods to improve the quality of these joints since the 1960s (*2*). Foster et al. identified that a low-density zone within the joint area of flexible pavements leads to long-term performance issues (*3*). This problem arises from paving one lane at a time. During paving the first lane, the absence of a confined edge causes lateral movement of the fresh asphalt material instead of volume reduction during compaction, resulting in lower density. Additionally, the material along the edge of the asphalt mat cools quicker than the material at its center, thus inhibiting proper compaction and reducing density.

While the cold edge of the first paved mat provides a confined edge for compacting the hot asphalt material of the second lane, it may cause an uneven surface and bonding problems between the edges, preventing the formation of a monolithic mat (*4*). The variations in structural support and temperature differences during paving and compaction of adjacent lanes lead to lower density, higher permeability, increased segregation, and reduced adhesion at the joint (*1*). Starving the joint due to insufficient asphalt material while compacting is also anticipated for the lower longitudinal joint density (*5*). This weakly bonded joint with low density at the pavement's centerline eventually develops a crack, allowing water and moisture infiltration. Such water ingress results in debonding due to stripping. Moreover, repeated freeze-thaw cycles of the infiltrated water increase the likelihood of joint failure and pavement raveling near the joint in colder regions (*6*). Several studies estimated that a 1% decrease in air void content in the compacted asphalt material over 7% could increase a pavement's service life by approximately 10% (*7-11*). Thus, compaction is the most critical construction-related factor directly related to the in-place density, and its improvement can result in longer-lasting asphalt pavements (*12*).

2.2 TYPE OF LONGITUDINAL JOINTS

Several methods are used in the literature to construct longitudinal joints in asphalt pavements. Based on the laying conditions of HMA layers, the resulting longitudinal joint can be of the following three broad types (*3; 4; 13*):

2.2.1 Hot Joints

A hot joint is formed when parallel lanes are paved simultaneously using the echelon technique, where two pavers are spaced so that the asphalt material in the first lane does not significantly cool before the second lane is laid beside it. This method results in a nearly seamless joint that is expected to achieve the highest density compared to other joint types.

2.2.2 Semi-Hot Joints

A semi-hot or warm joint is created when a paver lays asphalt material in the first lane for a certain distance and then returns to pave the adjacent lane shortly after. As a result, the HMA material in the first lane cools to about 120 to 140°F before the adjoining lane is paved, where the material is still hot.

2.2.3 Cold Joints

A cold joint is formed when two adjacent lanes are paved on different days. Consequently, the edge of the HMA material from the first day is completely cooled when the second lane is paved. Additionally, a cold joint can occur if the temperature of the first lane drops below 120°F before the second lane is placed.

2.3 LONGITUDINAL JOINT GEOMETRY

Two different geometries are used while constructing a longitudinal joint, as described below:

2.3.1 Butt Joint

The vertical or butt joint is the most commonly used type of joint in asphalt pavement construction. In this method, the hot material from the second lane being laid is "butted" against the cold material's edge from the lane laid earlier or the night before, creating a vertical interface between the two lanes (*5*). When constructed with careful attention to detail, a butt joint can perform well. However, improper construction can result in poor performance of the butt joints (*4*).

2.3.2 Wedge Joint

The tapered or wedge joint is a sloped edge joint that gradually tapers down to the surface. However, continuous tapering can be problematic, especially when using a large nominal maximum aggregate size (*4*). The notched wedge joint was introduced and used in Michigan in the mid-1980s (*6*). The wedge's slope and the notch's size and location can vary. The wedge joint is believed to significantly reduce the risk of transverse migration of the hot asphalt material during compaction. It features a sloped interface overlapped by the hot asphalt material. The thin asphalt layer on the sloped surface of the wedge joint heats up when covered by the hot lane's asphalt, allowing for better aggregate interlock at the joint during compaction and resulting in improved density (*14*).

2.4 LONGITUDINAL JOINT ROLLING METHODS

Constructing a longitudinal joint involves compacting the asphalt material using a steel drum roller followed by pneumatic tire rollers, employing various methods and patterns. These methods impact the joint's density differently, thereby affecting its performance. Figure 2-1 shows the schematics of different techniques, and their brief overview is discussed below.

2.4.1 Hot Overlap Rolling Method

In this method, the compaction at the joint takes place from the hot side. Most of the breakdown steel drum roller is on the hot lane while overlapping 6 inches onto the cold lane, as illustrated in Figure 2-1(a). The compaction is usually accomplished using the roller in vibratory mode.

2.4.2 Hot Pinch Rolling Method

The hot pinch method differs from the hot overlap method in that the breakdown roller's drum is entirely on the hot side, with the drum's edge kept at least 6 inches away from the joint, as shown in Figure 2-1(b). Rolling in vibratory mode is believed to push the hot asphalt material toward the joint, enhancing the density achieved with the hot pinch method. This method is recommended for compacting tender mixes or thick lifts, as these conditions can push the asphalt material toward the joint (*13*). The initial pass may create a slight hump over the joint, which helps achieve a uniform surface with improved density (*15*). Studies indicate that using a pneumatic tire roller during compaction is more beneficial than a steel roller. A pneumatic tire roller can knead low-density areas near the joint, improving joint density, which is impossible with a steel drum roller due to the bridging effect (*14*).

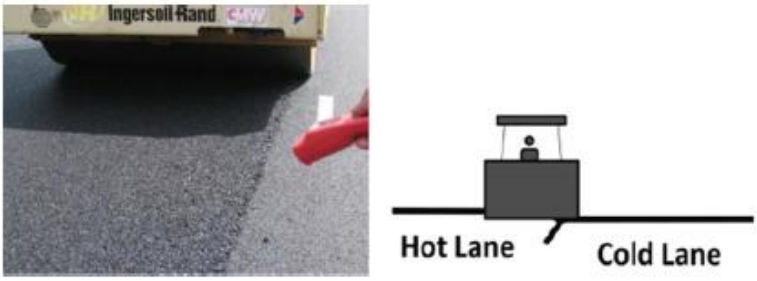

(a) The hot overlap method

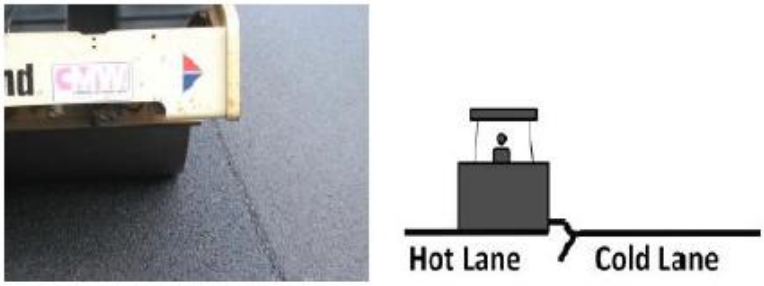

(b) The hot pinch method

(c) The cold roll method

Figure 2-1 Different longitudinal joint rolling methods (*14*)

2.4.3 The Cold Roll Method

This rolling method performs compaction with most of the roller's drum on the cold side, overlapping the hot side by 6 to 12 inches, Figure 2-1(c). The roller should be used in static mode to prevent cracking on the cold side. Timing is crucial with this method; as compaction begins on the cold side, the hot side loses heat when the roller covers the entire width of the hot side. This cooling effect impairs the compaction of the hot asphalt mat. A pneumatic tire roller is unsuitable for this method, as it tends to push the hot material away from the joint when compacting at the free edge of the cold side. Instead, a steel drum roller is recommended (*14*).

2.5 LONGITUDINAL JOINT CONSTRUCTION TECHNIQUES

Various techniques are employed to construct longitudinal joints in asphalt pavements, each affecting the quality and performance of the joint. This section briefly overviews these different longitudinal joint construction techniques while Figure 2-2 illustrates some of them.

2.5.1 Tandem or Echelon Paving

Echelon paving is a construction technique that allows for the simultaneous paving of multiple adjacent lanes using at least two pavers positioned close together, one following the other. Tandem paving is similar but involves pavers spaced further apart than in echelon paving. Both techniques ensure the creation of a hot joint, resulting in a seamless mat.

2.5.2 Sequential Mill and Fill Technique

This technique is typically used in a mill and fill project, where one lane is milled and filled at a time rather than milling all lanes at once and then laying asphalt lane by lane. In the sequential mill and fill method, it is essential to thoroughly clean the milled surface and the confined edge before laying down fresh asphalt material. This approach creates a confined edge for the hot lane, achieving better density during compaction.

2.5.3 Wedge Construction Technique

The free edge of the longitudinal joint is constructed with a wedge shape. This involves using a special plate attached to the paver's screed to shape the edge at the unconfined edge, as illustrated in Figure 2-2(a). The wedge joint can be built with or without a notch at the top. Compaction of the wedge is achieved using truck tires, a steel side roller wheel, a rubber side roller wheel, or a tag-along roller attached to the compactor (*16; 17*). Different wedge compaction techniques can create varying degrees of sloped surfaces, such as slopes of 3:1, 6:1, or 12:1.

(a) A notched wedge joint (15)

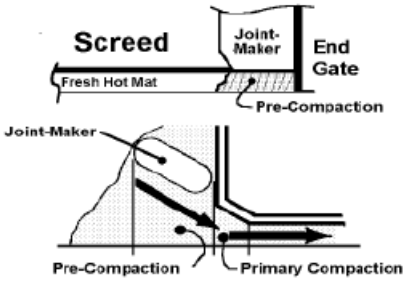

(b) A joint maker (*18*)

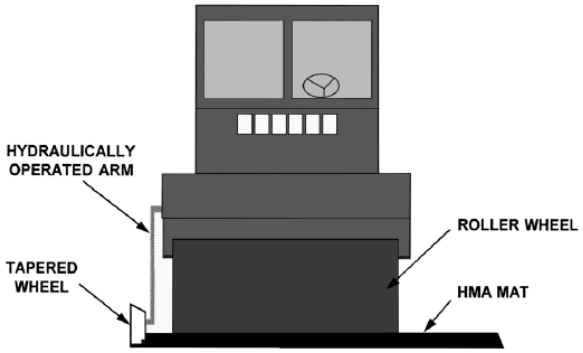

(c) A schematic of an edge restraining device (*19*)

(d) Cutting wheel attached to grader (*2*)

(e) Application of joint adhesive and sealants (*14*)

Figure 2-2 Different longitudinal joint construction techniques

2.5.4 Joint Maker Technique

This technique also supports the unsupported edge of the mat using an inclined, rounded-edge metal mass attached to the side of the paver screed, Figure 2-2(b). The device aids in pre-compacting the asphalt material before it is fed into the screed for subsequent laying. An excess

material kicker plate attached to the end of the paver's screed racks the extra material back into the joint, helping to create a more vertical edge and a smoother joint (*14*). This joint-making technique can also be combined with the notched wedge method to construct a longitudinal joint.

2.5.5 Edge Restraint Technique

Like the wedge construction, this technique involves an additional fixture attached to the compaction roller, as shown in Figure 2-2(c), which pinches the unconfined edge of the first-laid lane towards the roller. This method provides lateral resistance to prevent the hot material from moving away from the joint (*13; 19; 20*). The edge created with the edge restraint technique is steeper than the edge constructed using the wedge technique.

2.5.6 Cutting Wheel Technique

A 10-inch diameter cutting wheel is used to trim the unconfined edge (usually 2 to 6 inches) of the freshly laid asphalt while it is still in a plastic state (*13; 14*). This cutting wheel may be mounted on a roller or other plant equipment, as shown in Figure 2-2(d). Removing the low-density edge material from the cold lane provides a high-density, smooth, and cleaner confined edge for the adjacent lane that will be constructed next.

2.5.7 Joint Adhesives and Sealants

Various products are used to seal longitudinal joints and prevent water and air from penetrating the joint. Joint adhesives and sealers are believed to improve bonding between lanes and seal the pavement's surface. This helps minimize the risk of the lanes separating at the joint and maintains the joint's integrity. Sealants are typically applied on top of the joint after construction to reduce permeability, as illustrated in Figure 2-2(e). Adhesives can be applied to the edge of a cold lane before laying and compacting the hot asphalt material for the adjacent lane. They can also be applied over the joint after compacting both sides. Additionally, adhesives can be applied to the underlying layer before paving either of the asphalt layers. The heat from the hot material helps spread the adhesive into the joint, theoretically reducing interconnected voids (*14*).

Void-reducing asphalt membranes (VRAM) are also used to construct longitudinal joints. These membranes are applied to the surface at the joint location before laying the asphalt material for either lane. The concept is that when hot asphalt material is laid over the VRAM, it heats up, migrates upwards, and fills 50 to 70 percent of the joint's air voids, making the joint impermeable (*21*).

2.5.8 Infrared Joint Heaters

The density differential between the joint and adjacent areas is a major cause of issues when hot asphalt is laid against the already cold edge of the previous lane. The cold edge needs to be warmed before laying the hot lane to achieve a hot joint. Infrared joint heaters operate on this principle by pre-heating the cold edge before laying the adjacent hot lane. Like echelon paving, this process helps ensure better adhesion between the two lanes and improves compaction. Joint heaters have been used for over 30 years, with modern versions employing propane-powered, highly efficient infrared technology mounted on a trailer. These heaters can travel ahead of the paver, heating the joint area to a relatively soft state. They typically move at speeds comparable to the paver and can raise the pavement temperature to 200 to 250°F (*14*).

2.5.9 Warm Mix Asphalt (WMA)

The use of Warm Mix Asphalt (WMA) is effective in achieving higher-density longitudinal joints in Canada. WMA's ease of compaction improves its capacity to produce denser joints. Additionally, the reduced temperature difference between the hot asphalt material and the cold edge material, which absorbs heat and becomes slightly workable, contributes to tighter joints with better density and enhanced adhesion at the joint interfaces (*22; 23*).

2.5.10 The Maryland Method

It is a method-based specification used for the construction of longitudinal butt joints and clearly defines sequential HMA paving and rolling steps as follows (*2*):

1. Overlap the edge of the previously constructed adjoining mat by 1 to 1.5 inches with the hot asphalt material during paving. Remove any excess HMA material that extends beyond 1.5 inches. Do not bump back the overlapped material. Moreover, ensure sufficient HMA material accounting for a 0.25-inch per 1-inch of rolling down.
2. Begin compacting the hot asphalt material with the roller 6 to 12 inches from the longitudinal joint. This step consolidates and locks the hot asphalt material, pushing extra material into the joint. The roller's drum overlaps the joint on the second pass.
3. Finally, the maximum vibratory force of the roller is used to compact and push the hot HMA material into the confined space, achieving optimal joint density. A thin white line on the top of the longitudinal joint signifies the successful application and completion of the Maryland Method.

2.6 COMPARISON OF LONGITUDINAL JOINT CONSTRUCTION METHODS

Table 2-1 presents the benefits and drawbacks of all the longitudinal joint construction types, methods, and techniques explained earlier.

Table 2-1 Benefits and drawbacks of longitudinal joint construction methods

Construction method	Benefits	Drawbacks
Hot overlap rolling method	• An efficient method, as most of the roller sits over the HMA material (*15*) • Minimizes vertical differential between lanes, enhancing the bond (*13; 14; 24*)	• It may move the HMA material away from the joint laterally (*2; 15*)
Hot pinch rolling method	• Preferred for tender mixes and thick lifts as it pushes HMA material towards the joint (*13; 15*) • Enhances joint performance (*14; 25*)	• Forms a hump that may hinder neighboring material compaction (*14*) • Can cause secondary cracks along the pinch line (*2; 14*)
Cold roll method	• Provides good initial compaction and reduces vertical differential at the joint (*14*) • Proven to produce joints with minimal cracking and better performance (*14; 26*)	• Placing most of the roller over the compacted mat wastes compaction energy; static mode rolling provides less compaction (*14*) • Hot asphalt of the second lane loses heat during rolling, hindering its compaction (*13; 14; 19*)
Tandem or echelon paving technique	• Avoids constructing cold joints, providing good performance (*4*) • Delivers excellent joint quality, reducing maintenance needs (*23*) • Saves time (*15*) • Achieves similar joint and mat density (*27*)	• Used under no traffic (echelon paving) or traffic control at the site (tandem paving); needs two pavers with crew; increasing costs; needs a high-capacity plant (*4*)
Sequential mill and fill technique	• Enhances joint density by providing a confined edge for hot asphalt (*25*) • Eliminates uneven surface issues at the joint; no special equipment is needed (*15*)	• Delays projects, as milling must wait for paving, may increase costs (*4; 27*) • Milling may damage adjacent new mix, causing wastage (*4*) • Thorough cleaning of milled surface before paving is challenging, especially at night (*27*)

Table 2-1 (cont'd)

Construction method	Benefits	Drawbacks
Edge restraint technique	• Increases joint density (*4; 13; 18*) • Reduces permeability (*18*) • Creates a uniform edge (*17*)	• Quality relies on operator skill (*4; 13; 18; 19; 28*) • Challenging the operator to maintain position requires excess material removal from the adjacent lane (*17*)
Joint maker technique	• Claimed to improve joint density and aggregate interlock at the joint if used properly	• No significant joint density improvement with the joint maker (*13; 18; 29*)
Cutting wheel technique	• Removes low-density material from the joint (*4; 17*)	• Wastes new mix; needs equipment and manpower for cutting and cleaning; quality depends on operator skill (*4; 13; 17*)
Joint adhesives	• Reduces permeability (*18*) • Improves adhesion at the interface with no negative impacts on performance (*4*)	• Not always effective in reducing permeability (*4*) • Requires special equipment and manpower that increases costs (*4*) (*18*)
Joint sealants	• Can reduce joint permeability; no additional equipment needed; no negative performance impact (*4*)	• Not always effective in reducing permeability (*4*) • Increases costs (*4*)
Void-reducing asphalt membrane (VRAM)	• Dries within 15-30 minutes and can be driven over by construction traffic; reduces permeability and air voids; may improve cracking resistance (*21*)	• Higher initial material cost, but benefits may offset this (*21*)
Infrared joint heaters	• Avoids cold joints; increases adhesion at the interface (*4*) • Most effective for reducing joint cracking by enhancing compaction, increasing density, and decreasing permeability (*14; 30; 31*) • Improves IDT strength; reduces cracking and segregation (*18; 31; 32*)	• Requires extra equipment and fuel; lengthens paving train; interferes with paving operations; poses safety risks; can scorch the mix (*4; 18*) • Efficiency may drop, and the top layer may scorch on thicker lifts (*15*) • High wind conditions may reduce effectiveness in raising the joint temperature (*23*)
Warm mix asphalt (WMA)	• Reduces temperature differential between joints, lowers asphalt aging; versatile in various climates; fewer fumes, lower energy use, and more eco-friendly; reduces joint permeability (*22; 23*)	

2.7 JOINT QUALITY EVALUATION

Longitudinal joints have been identified as a primary cause of flexible pavement deterioration since the 1960s when they were first highlighted as "low-density zones" (*3*). Several studies concluded that a well-constructed longitudinal joint should have 1-2% lower density than the mat, and 5-10% lower if poorly constructed (*1; 3; 13; 18; 33*). Another study estimated the effect of air voids on the overall service life of HMA pavements—if the mat density reduces from 92% (8% air voids) to 88 and 90% (10-12% air voids), a reduction of 17-36% is expected in the service life (Figure 2-3) (*9*). Seed et al. concluded that a 1 percent decrease in air voids of a flexible pavement improves its fatigue performance by 8-43% and rutting resistance by 7-66% (*34*). Thus, the longitudinal joint quality is usually determined by estimating its density. The NCAT study presented the joint density and performance data generated by various joint construction techniques but did not identify their effectiveness. The study reports the following general findings (*11; 19; 33; 35; 36*):

- The performance of the longitudinal joint is influenced by the density achieved at the joint.
- Joint density should be within 2% of the mat density.
- Use cores to measure joint density, as the nuclear gauge is impractical.

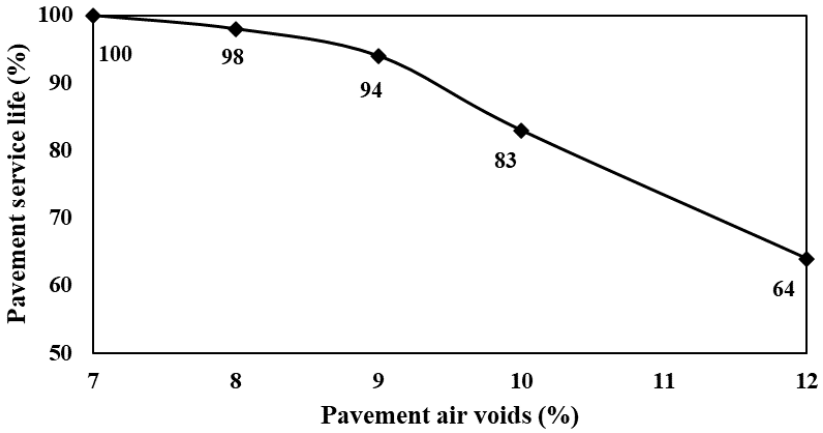

Figure 2-3 Effect of in-place density on service life (*9*)

Several measurement methods are used to determine the as-constructed HMA mat and longitudinal joint density. Using pavement cores for determining density in the laboratory is most common, while some highway agencies also use nuclear and non-nuclear density gauges.

2.7.1 Using Pavement Cores

Laboratory-measured density using pavement cores is widely considered the most accurate method (*36*). However, there is no specific recommendation for the best method to determine density from pavement cores in the laboratory (*14*). Various procedures such as Saturated Surface Dry (SSD), vacuum sealing, parafilm, CoreReader, dimensional analysis, and X-ray tomography are used. The AASHTO T166 method (bulk specific gravity (Gmb) of compacted asphalt mixtures using saturated surface dried SSD specimens) is particularly common. Cores used for density determination are prevalent among State Highway Agencies (SHAs). An NCAT report indicates that 38 SHAs use pavement cores to assess in-field compaction (*7*). Nonetheless, using cores for compaction assessment has both advantages and disadvantages (*37; 38*):

Advantages

- Easy to obtain and test.
- Useful for post-construction analysis.
- Often used as primary components of quality assurance (QA).

Disadvantages

- Destructive in nature.
- Expensive and time-consuming.
- Provides limited coverage, i.e., increases chances of missing localized problem areas.
- Unable to provide real-time feedback about the compaction during construction.
- Results have a longer turnaround time (1-2 days).
- If the longitudinal joint is cored with the core barrel centered over the joint line, the retrieved core will have a larger portion of the cold lane, i.e., the lane laid first, especially in the case of a wedge joint (39).

2.7.2 Using Nuclear and Non-Nuclear Density Gauges

Nuclear and non-nuclear gauges were developed as non-destructive alternatives to pavement coring for density determination. The nuclear density gauge measures HMA density by emitting gamma rays into the pavement and detecting the scattered rays. The scattering or absorption of gamma rays depends on the quantity of HMA material rather than the number of air voids (*40*). Non-nuclear gauges operate by sending an electric field into the pavement; the

response is influenced by the dielectric constant of the pavement components multiplied by their volumes (*41; 42*). The advantages and disadvantages of nuclear and non-nuclear gauges include:

Advantages

- Many measurements can be taken quickly
- Non-destructive

Disadvantages

- Seating over the joint, particularly at the crown, is problematic (*14*). Density gauges tend to underestimate density, so these devices are used to measure joint density by placing them very close to, but not directly over, the joint (*36*).
- The nuclear gauge requires special handling, training, and certification due to the presence of radioactive material.
- Provides limited coverage, i.e., increases chances of missing localized problem areas
- Require calibration.

2.7.3 Using Ground Penetrating Radar (GPR) Technology

Ground penetrating radar (GPR) employs electromagnetic waves to investigate the subsurface and has been widely used to detect free water (*43*). By estimating the dielectric properties of pavement materials, GPR can assess layer thicknesses and the density of HMA layers (*44-49*). It can also estimate in-field HMA density variability through variations in dielectric properties (*50*). Traditional methods for determining HMA layer dielectric properties using GPR involve measuring reflections' round trip travel time at the HMA layer depth or surface. However, this approach requires prior knowledge of the HMA thickness, which is often unknown or highly variable. Additionally, the construction of HMA layers in multiple lifts or the presence of overlays complicates the analysis of travel time from various lifts and layers.

To compute the bulk dielectric constant (εr) of the HMA, the asphalt concrete (AC) surface reflection method relates the amplitude (A_0) of the GPR signal reflection from air to the HMA surface with the incident amplitude (A_i), characterized by the reflection from a metal plate (Figure 2-4) (*51*). The dielectric constant of the surface is calculated using Equation 1 (*52*). For layers thicker than 1.2 inches, the measurement of HMA surface reflection pertains solely to the properties of the upper layer, which is advantageous for accurately characterizing the layer of interest.

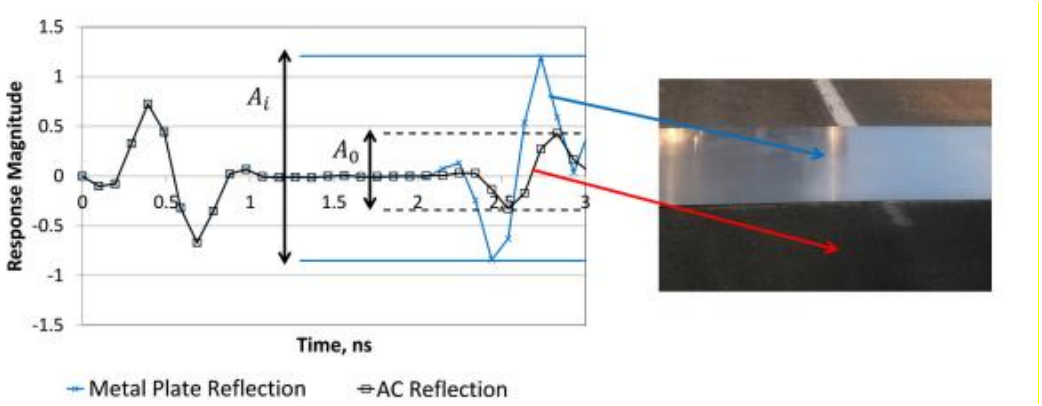

Figure 2-4 GPR reflection signals (*51*)

$$\varepsilon_r = \left(\frac{1 + \left(\frac{A_0}{A_i}\right)}{1 - \left(\frac{A_0}{A_i}\right)} \right)^2 \qquad \text{Equation 1}$$

The bulk dielectric response of an HMA mixture (i.e., the effective dielectric constant) depends on the dielectric response of its components, influenced by their dielectric constant and volume fractions (*53*). Although aggregates' types and volumetric proportions significantly impact HMA's bulk dielectric properties, air volume primarily varies the dielectric constant if the mix contains similar aggregates with uniform proportions (*46; 53; 54*). This finding allows the GPR technology to estimate HMA compaction uniformity in the mat and longitudinal joint. A rolling density meter (RDM - Figure 2-5), a GPR-based dielectric profiling system (DPS), evolved from recent research under the National Academies of Science's second Strategic Highway Research Program (SHRP2) (*37; 55*). The system utilizes three specially designed GPR sensors, whose collected data helps determine the dielectric constant of the HMA layer in flexible pavements. The collected data by the GPR sensors is analyzed and processed within the system's concentrator box. At the same time, an onboard computer reports the real-time dielectric constant values of the HMA surface. The obtained HMA dielectric values can be correlated with the newly constructed pavement's air void percentage and density.

Figure 2-5 Three-sensor dielectric profiling system (DPS)

Several field studies have demonstrated the device's high accuracy (*37; 56-60*). When assessing a fully formed longitudinal joint, it is recommended to position the DPS sensor at a 0.5 ft offset from the joint on its unconfined side. This is because (a) the DPS's sensor has a footprint of 6 inches, and (b) the variations of the joint geometry cause inaccurate and inconsistent dielectric measurements. Comparing the measured joint dielectric properties with those of the mat away from the joint (i.e., 3.5-4 ft offset from the joint) can indicate compaction quality: a lower dielectric constant at the joint suggests higher air void content. In contrast, a similar dielectric constant indicates comparable compaction levels as the mat. The dielectric constants measured by DPS can be correlated with the percent air voids and density using lab-measured air void content from cores or Superpave gyratory compactor (SGC) specimens (*58; 59; 61; 62*).

A field trial in Minnesota identified low joint compaction as a critical issue during compaction (*37*). Figure 2-6(a) shows the variation in DPS-measured dielectric constants for the inner and outer lanes, as well as the confined and unconfined sides of the joint, across different stations of a 1,000-ft section of HWY-52 near Zumbrota, Minnesota. The inner and outer lanes exhibit similar and uniform compaction levels across various stations. However, the unconfined side of the joint shows lower dielectric values (higher air void content) than the confined side. In some areas, the confined side of the joint also showed lower dielectric values than the unconfined side. These results indicated inconsistency in joint compaction, providing real-time feedback to the construction crew. Low dielectric values highlighted poor compaction at

locations where the roller pattern was reset. Consequently, the joint rolling pattern was adjusted to resolve the issue (*37*).

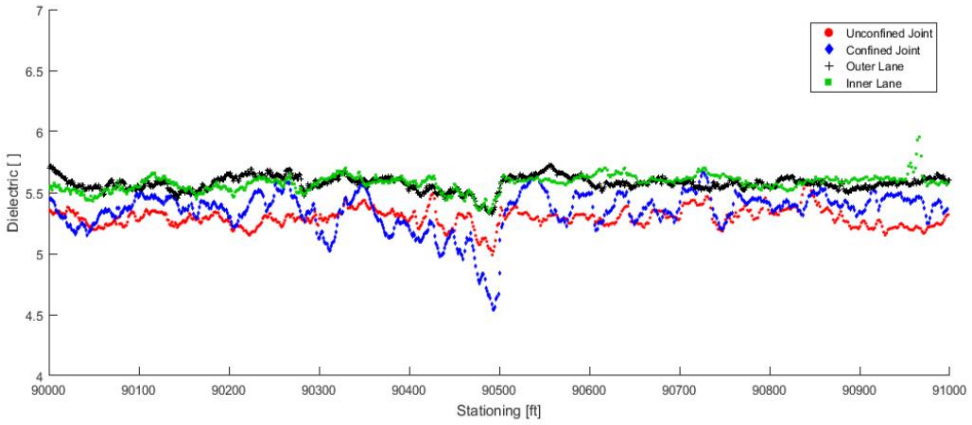

	Unconfined Joint
Median	5.31
Mean	5.29
Lift	Wear
Station Range 1 [ft]	90000 to 91000
Offset Range 1 [ft]	-1.5 to 0

	Confined Joint
Median	5.41
Mean	5.34
Lift	Wear
Station Range 1 [ft]	90000 to 91000
Offset Range 1 [ft]	0 to 1.5

	Inner Lane
Median	5.58
Mean	5.57
Lift	Wear
Station Range 1 [ft]	90000 to 91000
Offset Range 1 [ft]	-8 to -4

	Outer Lane
Median	5.59
Mean	5.57
Lift	Wear
Station Range 1 [ft]	90000 to 91000
Offset Range 1 [ft]	4 to 8

(a) Variation in measured HMA dielectric values using DPS

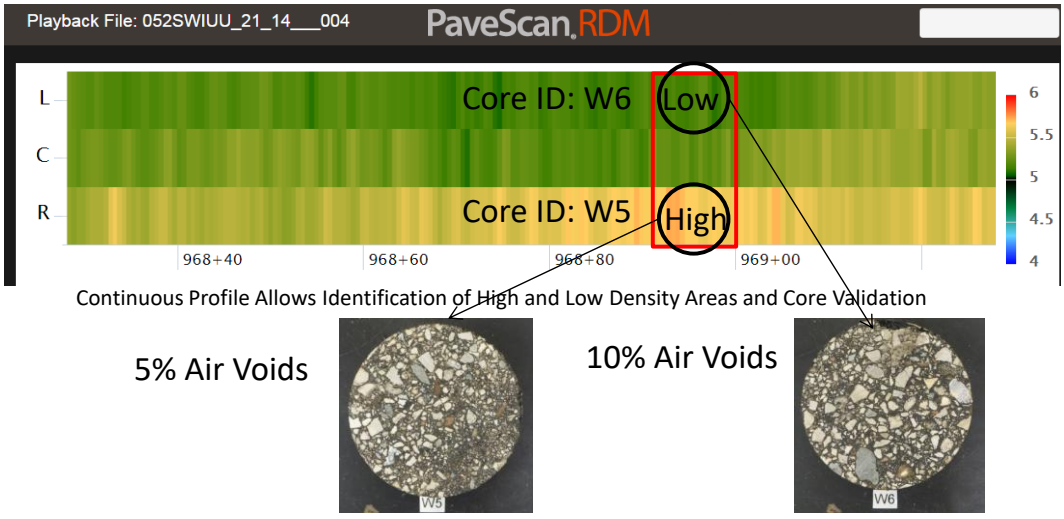

(b) Real-time dielectric data visualization and comparison with cores

Figure 2-6 Using the field-measured HMA dielectric values by DPS (*37*)

The long-term, flexible pavement performance is significantly influenced by the overall compaction quality of the mat, notably the longitudinal joint. Traditional methods like coring or nuclear gauges fail to provide rapid and continuous data collection, essential for minimizing traffic delays on major highways. This makes DPS an appealing alternative. DPS allows for fast, continuous data collection, ensuring greater coverage and real-time results during compaction. The DPS gives the equivalent of about 100,000 cores per mile compared to the spot tests

provided by the conventional methods, aiding better monitoring and evaluation of the in-place pavement density (*63*). As shown in Figure 2-6(b), a DPS survey can identify areas with higher dielectric constants, indicating good compaction, and areas with lower dielectric values, indicating poor compaction. This real-time dielectric (or compaction) profile aids contractors and inspectors, making DPS an efficient and reliable quality control tool that helps achieve optimal compaction and improve the as-built density and subsequent performance of flexible pavements.

2.8 REPAIR AND MAINTENANCE

Once deterioration appears on longitudinal joints, immediate repair is necessary. The timing of these repairs is crucial, as it determines whether to use preventive treatments (less expensive) or reactive methods (most costly). A brief description of the different longitudinal joint distress repair techniques is presented.

2.8.1 Slot Paving

Slot paving involves milling a narrow section around a distressed longitudinal joint, cleaning the slotted area, applying tack to the sides and bottom, and repaving with HMA. The Ohio Department of Transportation (ODOT) has effectively used this technique to repair medium to high-severity joint distresses, Figure 2-7(a). Slot widths range from 4 to 12 feet, requiring a standard paver for larger slots, while a "berm" box attachment on a paver fills smaller slots. According to an ODOT supervisor, successful slot construction requires at least one foot of width for each inch of depth. The estimated treatment life for slot paving is 4.3 years (*64*). However, this method creates two joints to maintain instead of one and places the joints closer to the wheel path.

2.8.2 Spray Injection

The spray injection technique replaces traditional pothole patching by using air to clean the pothole, applying emulsified asphalt, mixing aggregate chips with the asphalt, and filling the area with the blend using compressed air. The pavement is then opened to traffic, with or without compaction, after applying an aggregate layer over the repaired joint. ODOT uses a semi-automated spray injection process to repair longitudinal joints, Figure 2-7(b). While primarily a corrective repair, spray injection can serve as preventive maintenance if applied on time. ODOT estimates a service life of 2.2 years for this treatment, which is suitable for medium to high-severity joint distress levels (*64*).

(a) Slot paving

(b) Spray injection

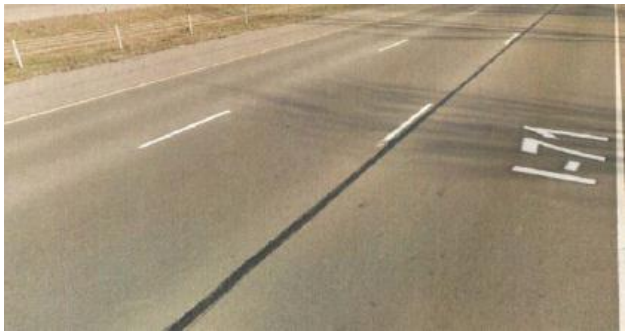

(c) Crack sealing

(d) Overbanding

Figure 2-7 Distressed longitudinal joint repair techniques (*64; 65*)

2.8.3 Crack Sealing

Crack sealing is a common treatment that fills distressed longitudinal joints to prevent moisture, debris, and air infiltration. This involves injecting bituminous materials into the crack, Figure 2-7(c). According to ODOT practices, crack sealing is the most cost-effective treatment for low to medium-level distressed joints, with an expected service life of 4.5 years (*64*). The Minnesota Department of Transportation (MnDOT) also uses it as a preventive maintenance treatment, with satisfactory performance for up to three years when applied timely (*66; 67*).

2.8.4 Overbanding

Joint sealing is a treatment applied after construction, typically when joint density does not meet specifications and is implemented early in the pavement's life, Figure 2-7(d). It is quick, causes minimal traffic disruptions, and is cost-effective. However, caution is necessary when considering overbanding for cracks, particularly on curves, as it can cause slipping issues for motorcycle traffic (*66*).

2.8.5 Additional Repair/Maintenance Options

MnDOT has used chip seals, fog seals, and sealants for preventive maintenance over longitudinal joints to prevent severe deterioration. Fog seal applications, including diluted

emulsions and rejuvenators, are applied up to two feet in width over the joints (*67*). These effectively reduce permeability without aesthetic issues (*68*). Moreover, sealants help reduce water ingress but do not limit deterioration in low-density areas near the joint. For medium to high-severity distresses, MnDOT has employed cold mix patching, micro surface, and mastic treatments to address safety concerns (*67*). The literature recommends using crack sealing and micro surfacing for longitudinal joint maintenance and repair until the cracks become too severe. These methods are more cost-effective than other options, as shown in Table 2-2. For medium to severe joint deterioration, spray injection treatment is suggested. Slot paving should be the last resort due to its higher cost and the creation of two joints closer to the wheel path.

Table 2-2 Cost comparison between different longitudinal joint repair techniques (*64*)

Treatment	Life (years)	Cost (per mile)	Cost (per mile per year)
Crack sealing	4.5	$3,362	$747
Spray injection	2.2	$12,763	$5,801
Slot paving	4.3	$104,644	$24,336

2.9 PRACTICES FOR LONGITUDINAL JOINT CONSTRUCTION

Table 2-3 summarizes the longitudinal joint construction, specification, and/or repair practices used by different states in the US and provinces of Canada.

Table 2-3 Longitudinal joint-related practices (*2; 4; 21; 64; 69; 70*)

State/province	Longitudinal joint practices
California	• **Construction**: All top surface joints are constructed at the lane lines of the pavement; joints need to be staggered 6 inches in lower asphaltic layers; lifts thicker than 1.8 inches require a notched wedge joint with 0.75-inch vertical notches at the top and bottom with a 1-foot wedge in the middle of the two notches; laying hot HMA against an existing pavement require saw cutting and removal of the edge material; tack coat is needed for all surfaces. • **Density measurements**: Uses calibrated density gauges for density testing at random locations 6 inches from the upper vertical notch after laying off the adjacent lane before opening to traffic. Also, 4- or 6-inch diameter cores are taken 6 inches from the upper vertical notch after placement of the adjacent lane and before opening to traffic for every 3,000 feet at engineer-selected locations. • **Specifications**: Both confined and unconfined edge (wedge as well) and the mat require a minimum 91% relative density measured through density gauge and testing of cores in the laboratory; disincentivize contractors for densities below 91% and above 97% of the TMD.
Colorado	• **Construction**: For lifts greater than 1 inch, the contractor can choose between butt or wedge joints, while any wedge configuration can be used as long as it prevents edge drop-offs greater than 1 inch for traffic safety. Most wedges have a 3:1 slope and a notch only at the top. Butt joints are used for lifts thinner than 1 inch. • **Density measurements**: Cores of 6 inches are centered within ±1 inch of the visible joint, with density calculations based on the average G_{mm} of both sides of the joint. • **Specifications**: A Percent-within-limits (PWL) method with an 88% lower limit is used. If PWL is ≥80.0%, full payment is granted. This specification applies to joints in all lifts, requiring one core per joint per sublot for Quality Assurance (QA) and two cores per 2,500 linear feet for Quality Control (QC).
Connecticut	• **Construction**: A notched wedge joint is used for lifts with a thickness between 1.5 and 3 inches, featuring a notch of 0.5 to 1.5 inches at the top and bottom, with a wedge slope between 8:1 and 12:1, as chosen by the contractor. A tack coat is applied to the cold face, and specifications require wedge compaction. For lifts less than 1.5 inches or greater than 3 inches, a butt joint is used. If site conditions prevent using a notched wedge, a butt joint with hot-poured rubberized asphalt treatment is constructed. • **Density measurements**: For notched wedge joints, cores should be taken with the core's center 5 inches from the visible joint on the hot side of the mat. For butt joints, cores should be taken within 1 inch of the joint, also from the hot side, using 4 to 6-inch cores. • **Specifications**: An incentive/disincentive system is applied, requiring a minimum of 91% of Theoretical Maximum Density (TMD) for full payment. If the density is ≤86.9%, removal and replacement is required.

Table 2-3 (cont'd)

Illinois	• **Construction**: Joints should be placed at the centerline or lane lines of the pavement. For stage construction, there must be a 3-inch offset from the joint of the previous layer. A notched wedge joint is required for lifts greater than 2 inches, featuring a vertical notch of 1 inch or up to 1.5 inches (for thicker lifts) at both the top and bottom of the lift, with a 9–12-inch width between notches. Notched wedge joints require a tack coat. An 18-inch-wide longitudinal joint sealant (LJS), with a thickness of 3/16 inch for the top course, should be applied centered under all joints, with or without a tack coat, to reduce air voids. Rolling should start at the lower elevation edge and move towards the other end, overlapping the previous pass. Unconfined edges should not be overlapped, but if allowed, a pneumatic tire roller should be used. For confined edges, the first pass should use the hot pinch method (staying no more than 6 inches from the joint), and the second pass should use the hot overlap rolling method (overlapping the cold side by no more than 12 inches). Subsequent rolling should continue from the lower elevation edge, ensuring some overlap on each pass. • **Density measurements**: Density measurements are not taken within 12 inches of the LJS applied joint between adjacent lanes. For SP mixes, a density of 92.5% is required at the confined edge and 90.5% at the unconfined edge. For SMA mixes, the required densities are 93.5% at the confined edge and 91.5% at the unconfined edge. Joint density testing should be conducted at a distance equal to the lift thickness or at least 4 inches from each pavement edge. • **Repair**: Micro surfacing is used for joint repairs, with a two-layer application if the joint is severely distressed. The repair should cover an 18-inch area centered over the joint.
Indiana	• **Construction**: Recommends using a notched wedge joint with a 0.5-inch notch and a 12-inch taper, though the specifics of butt joint construction are at the contractor's discretion. Joints must be placed on lane lines with a 6-inch offset from joints in underlying layers. A joint adhesive should be used on the unconfined edges of the surface course and the top of the intermediate layer. Apply a 12-inch-wide fog seal of emulsified asphalt on either side of the joint, but only on the top layer. • **Density measurements**: Density for joint evaluation is measured using cores taken from random locations, with cores collected no less than 6 inches from the unconfined edge and 3 inches from the confined edge. • **Specifications**: The minimum acceptable joint density is set at 91% of the percent Gmm.
Maine	• **Construction**: All cold edges must be coated with emulsified asphalt, including a 3-inch coating on the overlaid pavement. Butt joints are not required for echelon paving. • **Density measurements**: Joint density is not monitored, and cores for mat density testing cannot be taken within 9 inches of the joint.
Maryland	• **Construction**: Only butt joints are used, following a method specification that clearly outlines the placement and rolling procedures for longitudinal joints.

Table 2-3 (cont'd)

Massachusetts	• **Construction**: All joints must be treated with hot pour rubberized asphalt before laying hot asphalt material. This treatment is not required if echelon paving is used, and the material temperature is at least 95°C on the first laid edge before continuing with the hot material. Joint reheating is prohibited. • **Density measurements**: There is no specific density requirement for joints. Cores for density measurements cannot be taken within 12 inches of an unconfined edge or joint.
Michigan	• **Construction**: There are two types of longitudinal joints. Type 1 joints are used where new HMA pavement abuts; if a butt joint is used, the adjacent lane must be laid on the same day. A notched wedge joint can also be used, with a notch of 0.5 to 1 inch on the top and a taper not steeper than 1:12, extending beyond the lane width. Type 2 joints are used when a mat abuts existing pavement (HMA, PCC) or curb and gutter, and they must meet mat density specifications. All joints must align with painted lane lines. Tack coats are required, with a double coat on the vertical face of Type 2 joints. For butt joints, the unconfined edge should be rolled with the roller 3 to 6 inches away from the joint on the first pass and overlapping 3 to 6 inches over the joint on the second pass. For confined edges, use the hot pinch method on the first pass (keeping the roller 6 to 8 inches from the joint) and the hot overlap method on the second pass (overlapping the cold side by 6 to 8 inches). When using wedge joints, adjacent lanes must be laid within 24 hours. • **Density measurements**: Joint density is assessed with 6-inch diameter cores taken at the center of the joint. If different mixes are used on either side of the joint, the core should be taken 4 inches off-center on the cold side. • **Specifications**: The contractor must halt laying asphalt and adjust to improve density if the average joint density from five consecutive cores is below 89%. A joint density below 88% requires sawing or routing and sealing. If the density is below 86%, the entire lane 6 inches past the joint must be removed and replaced. An incentive and disincentive payment system is used for longitudinal joints.
Missouri	• **Construction**: All top surface joints should be placed at the lane lines of the pavement, avoiding pavement markings over the joint. Overlying layers must have a 6-inch stagger in the joint location. The engineer may require a light coating of bituminous material on the exposed edges before laying the hot material. • **Specifications**: Density specifications for confined edges are based on the mat density (92% for SP mixes and 94% for SMA mixes). The minimum density within 6 inches of the joint must be at least 2% below the required mat density for the unconfined edge (90% for SP mixes and 92% for SMA mixes).
New Hampshire	• **Construction**: Hot asphalt material must overlap the cold side by 1-2 inches. Compaction begins with the hot pinch method, where the roller is kept 6 inches away from the joint, followed by the hot overlap method, which involves a 6-inch overlap on the cold side. There is no specific joint density requirement, and cores are not allowed within 1 foot of the edge or joint.

Table 2-3 (cont'd)

Minnesota	• **Construction**: Joints should be placed at the centerline or lane lines of the pavement, avoiding the wheel path. They must be offset by 6 inches in the overlying layer. For HMA over concrete pavements, align the HMA longitudinal joints with the concrete's longitudinal joints. A tack coat is required unless a joint adhesive is used. The Maryland joint method involves a 1 to 1.5-inch overlap with a thickness of 0.25 inches over the adjacent lane. • **Density measurements**: Cores are taken from both sides of the joints, with the edge of each core 6 inches from the joint. A companion core is taken 12 inches longitudinally from the first core. Additionally, two cores are collected from the pavement mat, 2 feet to the right and left of the joint, to measure density. • **Specifications**: For wear course joints, a minimum density of 89.5% is required along confined edges and 88.1% at unconfined edges. For lower layers, 90.5% for confined edges and 89.1% for unconfined edges. An incentive and disincentive payment system is used to manage the quality of longitudinal joints. • **Repair**: Preventive maintenance treatments include chip seals, fog seals, and sealants. Treatments such as micro-surfacing, cold mix patching, and mastic are recommended for medium to high-severity distressed joints.
New York	• **Construction**: Either a butt or wedge joint can be used. A tapered wedge joint should be used for joints longer than 100 feet that will cool overnight before the next lane is laid. A butt joint requires an overlap of 2 to 3 inches of HMA material over the cold edge. Notched wedge joints have a 0.5-inch notch on top, a wedge slope no steeper than 1:8 and require a 1 to 1.5-inch overlap of hot asphalt over the cold edge. Hot asphalt material can be raked onto the joint but should not be broadcast back over the hot mat. • **Specifications**: No specific joint density requirement exists, but cores used for acceptance testing must be taken more than 23 inches from any edge.
North Dakota	• **Repair**: There is no ideal solution for joint distress; small equipment should be used to apply a microsurface seal over the distressed joint.
Ohio	• **Construction**: Either butt or notched wedge joints are used, with notched wedge joints being more common. Edges must be tack-coated before paving, with a maximum joint offset of 3 inches or less. A minimum 0.5-inch overlap of the joint edges is required. • **Density measurements**: Use 6-inch diameter cores for density measurements taken within 48 hours of joint construction. Core placement depends on the joint type: for butt joints, cores should be centered on the visible seam, while for notched wedge joints, cores should be taken 1 inch towards the wedge from the visible seam. • **Specifications**: As determined by the department, an incentive and disincentive payment system is used for longitudinal joints, based on Percent Within Tolerance (PWT). • **Repair**: For joint preventive maintenance and repair, use crack sealing followed by spray injection; slot paving is considered a last resort.
Tennessee	• **Repair**: Slot paving is used for joint repairs.

Table 2-3 (cont'd)

Pennsylvania	• **Construction**: A method specification (Maryland method) is used, but the choice of joint type is left to the contractor's discretion. • **Density measurements**: The minimum density specification now applies, with 6-inch cores taken centered over the joint for butt-type joints and centered over the wedge for wedge joints. • **Specifications**: If the joint density is below 88%, corrective action is required. An incentive/disincentive system is in place based on the joint's density. • **Repair**: Corrective action involves applying a 4-inch-wide band of PG-graded asphalt over the visible joint for surface courses and newly constructed joints, but only where the mats on either side of the joint were placed as part of the contract.
Rhode Island	• **Construction**: Sealants are applied over joints and edges of newly placed pavements. Joints in successive layers must be staggered by 6 inches. Hot asphalt material can be raked onto the joint but should not be broadcast back over the hot mat.
Texas	• **Construction**: The choice between butt or wedge joints is at the discretion of the Districts or the contractor. Butt joints are used for thinner lifts, while wedge joints are used for thicker HMA layers. Rolling patterns require overlapping unconfined edges by 6 inches during the first roller pass. Tack is applied over the entire wedge, and a rubber tire roller is used for intermediate rolling on most dense-graded jobs. • **Density measurements**: The minimum joint density is compared to the mat's density as measured by a density gauge. One measurement is taken near the core locations from the mat, and a second reading is taken 8 inches from the joint. Cores are used if the specified joint density is not met. • **Specifications**: Joint density is acceptable if it is within 3 pounds per cubic foot of the mat density measured at the same station. If the joint density is unacceptable, it is calculated using cores and compared with mat cores. A joint density is considered failing if the correlated density is less than 90% of the TMD. There is no bonus or penalty system in place.
Vermont	• **Construction**: Pavers must be equipped with a wedge or notched wedge forming devices and joint heaters. Wedge joints with a slope of 1:3 are used, and cold wedge joints must be heated to 95°C before placing the hot asphalt material for the adjacent lane. Compaction should start at the joint and proceed from the outer edge toward the center. • **Density measurements**: No specific joint density requirement exists, and coring for mat density testing is not allowed within 6 inches of the joint.
Washington	• **Construction**: Notched wedge joints are used. Sealing material must be applied to the vertical butt joint before paving the second lane. The layer is 1.8 inches thick and uses a half-inch nominal maximum aggregate size (NMAS).
West Virginia	• **Repair**: Uses micro surfacing centered 18- to 24-inch on the joint.

Table 2-3 (cont'd)

Wisconsin	• **Construction**: Joints are placed at the centerline or lane lines of the pavement. A wedge joint is used on all unconfined edges, featuring a 0.5- to 1-inch notch on top and tapering at a 12:1 ratio, extending beyond the lane width. All wedge layers must overlap directly and slope in the same direction. Wedge construction requires a strike-off device, and a roller with the same width as the wedge is needed to compact the initial portion of the wedge to near final density. Tack application to the wedge is mandatory. Confined edges must be cut back to achieve a full-depth butt joint, and the joint should be cleaned and painted with hot asphaltic, cutback, or emulsified asphalt. • **Specification**: There is a special provision for reheating HMA joints when abutting cold edges. An 8-inch-wide strip of the cold edge must be reheated to within 60°F of the temperature of the hot material used during paving.
Alberta, Canada	• **Repair**: Spray injection is used as a deteriorated joint repair treatment.
British Columbia, Canada	• **Repair**: Spray injection treatment is used to repair small potholes, cracks wider than 1 inch, and longitudinal joints.

2.10 CURRENT STATE OF PRACTICE – MINNESOTA AND MICHIGAN

This section presents the results of a survey conducted to document the current state of practice in Minnesota and Michigan in constructing longitudinal asphalt joints. The online survey was conducted to identify the best longitudinal joint construction practices, material usage, testing, and repair techniques. Figure 2-8 shows the distribution of the responses received from various road agencies. The majority (i.e., 39) of the responses received pertain to either city or county transportation agencies of the State of Minnesota. In contrast, six responses were received from the MDOT, representing the State's practices. Summarized survey results for the responses received from different Michigan and Minnesota transportation agencies are as follows:

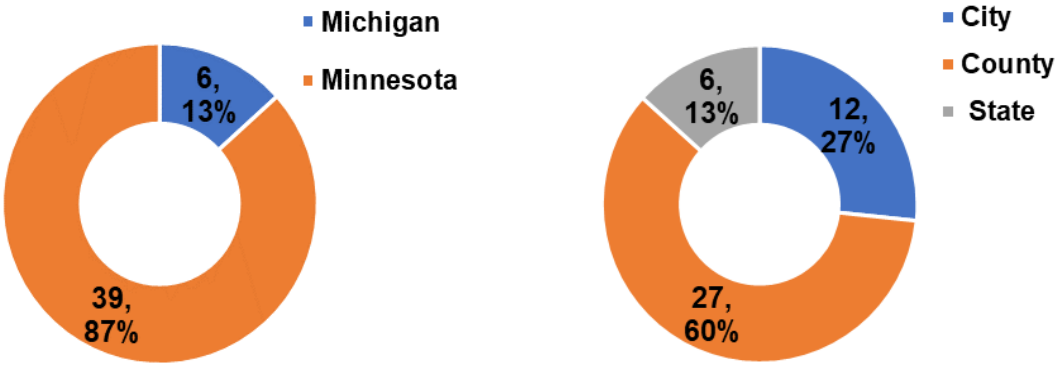

Figure 2-8 Representation of different agencies in the survey data

- The survey results show that 80% of the agencies (mostly local from Minnesota) do not specify the type of longitudinal joint to be constructed. Most longitudinal joints constructed are butt joints. However, tapered joints with a vertical notch are also used in Michigan.
- Only 22% of the responding agencies (i.e., 9 out of 41) specify the method to roll the joint with an unsupported edge; many of these agencies require compacting the unsupported edge with the roller's drum overhanging the edge by 6 inches.
- None of the agencies have any experience with using infrared joint heaters. Many of these agencies have cost, time, and benefit concerns against its use.
- About 27% of the agencies specify using either the hot pinch or the hot overlap method to compact joints against supported edges (i.e., confined joints).
- When asked about staggering the longitudinal joints in multiple AC lifts, 59% of agencies responded that these need to be staggered; most require staggering the joints by at least 6 inches.
- When asked about joint sealing, the responses showed that joint sealing is not usually required on the surface unless core results necessitate a corrective action. Most agencies only require a bond coat on the face of the cold longitudinal joint before laying the adjacent lane.
- The survey responses revealed that longitudinal joint quality is monitored via a special provision in Michigan that specifies density requirements for different joint types. However, many of the local agencies from Minnesota do not specify/measure the joint quality except one that requires joint density measurements using cores.
- 59% of the agencies believe that specifying minimum density requirements results in better joint compaction rather than method-based specifications. While using method-based specifications, the inspector's responsibility and experience are critical and are a major concern if specified.
- Only 33% of the agencies communicated that they monitor the longitudinal joint density for QA purposes. Out of these agencies, the majority use pavement cores for joint density evaluation. Not monitoring the joint density is a weak link even on well-constructed and good-performing pavements. The reason may be the additional required resources (equipment and workforce) and time. Another reason for not

monitoring the joint density can be the destructive nature of pavement coring, which is the most widely used option.

- Most agencies that use pavement cores for joint density evaluation utilize 6-inch diameter cores centered over the joint. Some use 4-inch diameter cores.
- About 45% of the responding agencies use the simple average as the quality measure for longitudinal joint, and 30% use PWL. A major concern about using a simple average is that half of the cores would have a density less than the specified values. On the contrary, the PWL is beneficial since a lower PWL specification limit typically represents 90% acceptable values with only 10% defective results for a 100% payment to the contractor.
- 47% of the responding agencies penalize contractors for poor joint density. Moreover, joint sealing was the popular option used for maintaining poor-performing joints of in-service pavements.
- Most survey respondents pointed out that asphalt mixture type plays a role in better construction and performance of the longitudinal joint; 9.5mm NMAS asphalt mixtures are better than the 12.5mm mixes. Some respondents believe that lift thickness is more critical instead. Regarding binder content, the responses do not clearly distinguish between mixes with greater and less than 6% binders in achieving better compaction quality at the joint.
- An MDOT respondent mentioned that MDOT allows a credit of up to 4 inches of removal at a joint before paving the second half of the joint. This allows the contractor to mill back 4 inches of the mix without deducting this quantity. Often, contractors will mill back more to remove additional material at their expense.

2.11 SUMMARY - BEST PRACTICES FOR LONGITUDINAL JOINT CONSTRUCTION

Most agencies in Michigan and Minnesota don't specify the type of longitudinal joint to be constructed, though literature indicates butt joints are common. Some states use tapered joints, with Michigan utilizing a vertical notch. Staggering longitudinal joints in multiple HMA layers is widely practiced, typically with a 6-inch offset. This practice prevents weak areas (joints) from aligning through the asphalt layers, reducing water ingress if the top layer's joint opens. A

successful joint requires a straight or smooth edge, especially on curves, to ensure better compaction when adjacent lanes are constructed.

Rolling significantly impacts joint density. Many agencies don't specify how to roll an unsupported/unconfined joint, but overhanging the joint by at least 6 inches from the hot side is common. Vibratory rolling with a 6-inch overhang helps prevent stress cracks, but excessive overhang can damage the joint edge. For confined joints, either the hot pinch or hot overlap methods involve vibratory rolling. The hot pinch method used first pushes hot material into the joint, creating a hump that is compacted back, ensuring the joint isn't starved of material. The hot overlap method is less effective if there's insufficient hot asphalt near the cold joint.

Overlapping the cold joint edge with hot asphalt by 1 ± 0.5 inches during adjacent lane paving is crucial for durability, with the overlapped material being at least 0.25 inches higher than the adjacent mat for compaction. Applying tack to the full lane width and the existing joint face is important. Some agencies use joint adhesive or a longitudinal joint seal like VRAM to improve bonding and reduce permeability. These materials melt and migrate into the lift, filling air voids in the unconfined edge.

Echelon paving is considered best for avoiding joint construction. Using a safety edge and matching lanes daily can also eliminate cold joints. Allowing for the removal of newly paved HMA from an unconfined edge before laying the adjacent lane enhances joint compaction. MDOT permits up to 4 inches of removal without penalty, which is believed to improve joint quality by eliminating high air void material from the edge.

Most agencies don't monitor joint density due to resource and time constraints and the destructive nature of coring, the most common method. While some agencies use Percent Within Limits (PWL) to measure quality, most use a simple average. Using a simple average means half the joint cores might fall below the specified density, unlike PWL, which represents 90% acceptable values for 100% payment. Therefore, using a simple average is ineffective for joint quality.

REFERENCES

1. Estakhri, C. K., T. J. Freeman, and C. H. Spiegelman, "Density evaluation of the longitudinal construction joint of hot-mix asphalt pavements," Texas Transportation Institute, Texas A & M University System, 2001.
2. Buncher, M. S., and C. Rosenberger, "Best Practices for Constructing and Specifying HMA Longitudinal Joints," *Final Report, Asphalt Institute, Washington, DC*, 2012.
3. Foster, C., S. Hudson, and R. Nelson, "Constructing longitudinal joints in hot mix asphalt pavements," *Highway Research Record*, vol. 51, pp. 124-136, 1964.
4. McDaniel, R., A. Shah, and J. Olek, "Longitudinal joint specifications and performance (Joint Transportation Research Program Publication No. FHWA/IN/JTRP-2012/29). West Lafayette, IN: Purdue University," 2012.
5. Zinke, S., J. Mahoney, E. Jackson, and G. Shaffer, "Comparison of the use of notched wedge joints vs. traditional butt joints in Connecticut (No. CT-2249-F-08-4)," Connecticut Transportation Institute, 2008.
6. Buchanan, M. S., "Evaluation of notched-wedge longitudinal joint construction," *Transportation Research Record*, vol. 1712, pp. 50-57, 2000.
7. Aschenbrener, T., E. R. Brown, N. Tran, and P. B. Blankenship, "The FHWA's demonstration project for enhanced durability of asphalt pavements through increased in-place pavement density," *Transportation Research Record*, vol. 2672, pp. 57-67, 2018.
8. Tran, N., P. Turner, and J. Shambley, "Enhanced compaction to improve durability and extend pavement service life: A literature review," 2016.
9. Linden, R. N., J. P. Mahoney, and N. C. Jackson, "Effect of compaction on asphalt concrete performance," *Transportation Research Record*, 1989.
10. Kim Willoughby, P., W. Olympia, J. P. Mahoney, and J. Walter, "An Assessment of WSDOT's Hot-Mix Asphalt Quality Control and Assurance Requirements," 2007.
11. Sebaaly, P. E., and J. C. Barrantes, "Development of a Joint Density Specification: Phase I-Literature Review and Test Plan," 2004.
12. Hughes, C. S., *NCHRP Synthesis of Highway Practice 152: Compaction of asphalt pavement*. TRB, National Research Council, Washington, D.C., 1989.
13. Kandhal, P. S., and R. B. Mallick, "Longitudinal Joint Construction Techniques for Asphalt Pavements. NCAT Report 97-4," *National Center for Asphalt Technology, Auburn University, Alabama*, 1997.
14. Williams, S. G., "HMA longitudinal joint evaluation and construction," University of Arkansas, Fayetteville. Dept. of Civil Engineering, 2011.
15. Putman, B. J., and E. M.-Y. Kim, "Best Practices for Longitudinal Joint Construction and Compaction," 2018.
16. Burati Jr, J. L., and G. B. Elzoghbi, "Study of joint densities in bituminous airport pavements," *Transportation Research Record*, 1987.

17. Toepel, A., *Evaluation of techniques for asphaltic pavement longitudinal joint construction*. Wisconsin Department of Transportation, Division of Transportation …, 2003.

18. Fleckenstein, L. J., D. L. Allen, and D. B. Schultz Jr, "Compaction at the longitudinal construction joint in asphalt pavements (KYSPR-00-208) (No. KTC-02-10/SPR208-00-1F)," 2002.

19. Kandhal, P. S., and S. S. Rao, "Evaluation of longitudinal joint construction techniques for asphalt pavements (Michigan and Wisconsin projects-interim report)," *NCAT Report*, pp. 94-91, 1994.

20. Crawford, C., and J. A. Scherocman, "Hot Mix Asphalt Joint Construction," 1990.

21. Williams, R. C., J. Podolsky, and J. Kamau, "Use of J-Band to Improve the Performance of the HMA Longitudinal Joint," Minnesota Department of Transportation, 2020.

22. OHMPA, "The ABCs of Longitudinal Joints ", Ontario Hot Mix Producers Association Ontario, Canada, 2013.

23. Uzarowski, L., G. Moore, M. Halloran, and V. Henderson, *Construction of Durable Longitudinal Joints - The Courage to Use Innovations Pays Off*.

24. Kronick, D., D. Brown, and D. Brown, "Factors affecting compaction of Asphalt Pavements," 2006.

25. Williams, R. C., C. Chen, T. Ahmed, and H. Lee, "Quality control/quality assurance testing for joint density and segregation of asphalt mixtures," Iowa. Dept. of Transportation, 2013.

26. Marquis, B., "Longitudinal joint study," Maine. Dept. of Transportation, 2001.

27. Hand, A. J., T. Aschenbrener, and M. Buncher, "Tech Brief: Improving Longitudinal Joint Performance," 2020.

28. Kassem, E., E. Masad, A. Chowdhury, and G. Claros, "Influence of Field Compaction Pattern on Asphalt Pavement Uniformity (With Discussion)," *Journal of the Association of Asphalt Paving Technologists,* vol. 77, 2008.

29. Marks, P., "Longitudinal Joint Compaction–Improving Paved Lanes," *RoadTalk, Ontario's Transportation Technology Transfer Digest,* vol. 10, 2004.

30. Baker, R. F., J. R. Croteau, J. J. Quinn, and E. J. Hellriegel, "Longitudinal Wedge Joint Study," *Transportation Research Record*, 1990.

31. Huang, B., X. Shu, J. Chen, and M. Woods, "Evaluation of longitudinal joint construction techniques for asphalt pavements in Tennessee," *Journal of Materials in Civil Engineering*, vol. 22, pp. 1112-1121, 2010.

32. Daniel, J. S., "Use of an infrared joint heater to improve longitudinal joint performance in hot mix asphalt pavements," *Journal of Performance of Constructed Facilities,* vol. 20, pp. 167-175, 2006.

33. Kandhal, P. S., and R. B. Mallick, "Study of longitudinal-joint construction techniques in hot-mix asphalt pavements," *Transportation Research Record,* vol. 1543, pp. 106-112, 1996.

34. Seeds, S. B., G. R. Hicks, G. E. Elkins, H. Zhou, and T. V. Scholz, "LTTP Data Analysis: Significance of 'As-Constructed'AC Air Voids to Pavement Performance," *Applied Pavement Technology, Inc., NCHRP Project,* pp. 20-50, 2002.

35. Kandhal, P. S., and R. B. Mallick, "Longitudinal joint construction techniques for asphalt pavements," National Center for Asphalt Technology, 1997.

36. Kandhal, P. S., T. L. Ramirez, and P. M. Ingram, "Evaluation of eight longitudinal joint construction techniques for asphalt pavements in Pennsylvania," *Transportation Research Record,* vol. 1813, pp. 87-94, 2002.

37. Khazanovich, L., K. Hoegh, and R. Conway, "Non-destructive Evaluation of Bituminous Compaction Uniformity Using Rolling Density," 2017.

38. Wilson, B., S. Sebesta, and T. Scullion, "Evaluation of the Rolling Density Meter for Rapid Continuous Measurement of Asphalt Mixture Density," 2019.

39. Prowell, B. D., *Practices and Specifications for Longitudinal Joints–A National Perspective*.

40. Smith, B., and B. Diefenderfer, "Comparison of Nuclear and Nonnuclear Pavement Density Testing Devices," *Transportation Research Record,* vol. 2081, pp. 121-129, 2008.

41. TransTech, "PQI 301 Operator's Handbook Manual," TransTech Systems, Inc., Schenectady, NY, 2002.

42. Henault, J. W., "Field Evaluation of a Non-Nuclear Density Pavement Quality Indicator," 2001.

43. Al-Qadi, I. L., D. K. Ghodgaonkar, V. K. Varada, and V. V. Varadan, "Effect of moisture on asphaltic concrete at microwave frequencies," *IEEE Transactions on Geoscience and Remote Sensing,* vol. 29, pp. 710-717, 1991.

44. Al-Qadi, I. L., S. Lahouar, and A. Loulizi, "In situ measurements of hot-mix asphalt dielectric properties," *NDT & e International,* vol. 34, pp. 427-434, 2001.

45. Al-Qadi, I. L., and S. Lahouar, "Measuring layer thicknesses with GPR–Theory to practice," *Construction and Building Materials,* vol. 19, pp. 763-772, 2005.

46. Leng, Z., I. L. Al-Qadi, and S. Lahouar, "Development and validation for in situ asphalt mixture density prediction models," *NDT & e International,* vol. 44, pp. 369-375, 2011.

47. Leng, Z., "Prediction of in-situ asphalt mixture density using ground penetrating radar: theoretical development and field verification," University of Illinois at Urbana-Champaign, 2012.

48. Shangguan, P., and I. L. Al-Qadi, "Calibration of FDTD simulation of GPR signal for asphalt pavement compaction monitoring," *IEEE Transactions on Geoscience and Remote Sensing,* vol. 53, pp. 1538-1548, 2014.

49. Shangguan, P., and I. L. Al-Qadi, "Content-based image retrieval approaches to interpret ground penetrating radar data," *Construction and Building Materials,* vol. 69, pp. 10-17, 2014.

50. Scullion, T., and Y. Chen, "Using ground-penetrating radar for real-time quality control measurements on new HMA surfaces," 1999.

51. Hoegh, K., L. Khazanovich, S. Dai, and T. Yu, "Evaluating asphalt concrete air void variation via GPR antenna array data," *Case Studies in Nondestructive Testing and Evaluation,* vol. 3, pp. 27-33, 2015.

52. Saarenketo, T., and T. Scullion, "Road evaluation with ground penetrating radar," *Journal of applied geophysics,* vol. 43, pp. 119-138, 2000.

53. Al-Qadi, I. L., Z. Leng, S. Lahouar, and J. Baek, "In-place hot-mix asphalt density estimation using ground-penetrating radar," *Transportation Research Record,* vol. 2152, pp. 19-27, 2010.

54. Leng, Z., *Prediction of in-situ asphalt mixture density using ground penetrating radar: theoretical development and field verification*. University of Illinois at Urbana-Champaign, 2011.

55. Sebesta, S., T. Scullion, and T. Saarenketo, *Using infrared and high-speed ground-penetrating radar for uniformity measurements on new HMA layers*. Transportation Research Board, 2013.

56. Hoegh, K., S. Dai, T. Steiner, and L. Khazanovich, "Enhanced Model for Continuous Dielectric-Based Asphalt Compaction Evaluation," *Transportation Research Record,* vol. 2672, pp. 144-154, 2018.

57. Teshale, E. Z., K. Hoegh, S. Dai, R. Giessel, and C. Turgeon, "Ground Penetrating Radar Sensitivity to Marginal Changes in Asphalt Mixture Composition," *Journal of Testing and Evaluation,* vol. 48, 2020.

58. Haider, S. W., H. B. Muslim, L. Khazanovich, M. E. Kutay, and B. Cetin, "BMP For Issues with Asphalt Centerline Joint and Intelligent Compaction for Local Agencies," Minnesota. Department of Transportation. Office of Research & Innovation, 2023.

59. Muslim, H. B., S. W. Haider, and L. Khazanovich, "Flexible pavement longitudinal joint quality evaluation using non-destructive testing," *Journal of Road Engineering,* vol. 4, pp. 189-202, 2024.

60. Muslim, H. B., S. W. Haider, and L. Khazanovich, "Non-destructive compaction evaluation and comparison of different asphalt centerline longitudinal joints," *Construction and Building Materials,* vol. 449, p. 138473, 2024.

61. Hoegh, K., R. Roberts, S. Dai, and E. Zegeye Teshale, "Toward core-free pavement compaction evaluation: An innovative method relating asphalt permittivity to density," *Geosciences,* vol. 9, p. 280, 2019.

62. Steiner, T., K. Hoegh, E. Z. Teshale, and S. Dai, "Method for assessment of modeling quality for asphalt dielectric constant to density calibration," *Journal of Transportation Engineering, Part B: Pavements,* vol. 146, p. 04020054, 2020.

63. Hoegh, K., T. Steiner, E. Zegeye Teshale, and S. Dai, "Minnesota Department of Transportation case studies for coreless asphalt pavement compaction assessment," *Transportation Research Record,* vol. 2674, pp. 291-301, 2020.

64. Duncan, G. M., L. V. Sibaja, S. B. Seeds, D. G. Peshkin, M. Sminchak, and S. Sophocleous, "Longitudinal Joint Repair Best Practices for the Ohio Department of Transportation," Ohio. Dept. of Transportation, 2017.

65. MDOT, "Capital Preventive Maintenance Manual," Michigan. Dept. of Transportation, Construction Field Services Division, 2020.

66. Johnson, A. M., "Best practices handbook on asphalt pavement maintenance," University of Minnesota. Center for Transportation Studies, Minnesota, 2000.

67. Watson, M., "Improving HMA Longitudinal Joints through Construction, Preventive Maintenance and Repairs," *Minnesota Department of Transportation*, 2011.

68. Watson, M., "Longitudinal Joint Fog Seal Test Sections, MnDOT Memo," *Minnesota Department of Transportation* 2009.

69. Zinke, S., and J. Mahoney, "Evaluation of longitudinal joint density specification on 2012 polymer modified warm-mix asphalt projects in Connecticut," Connecticut. Dept. of Transportation, 2015.

70. NRRA, "Longitudinal Joint Construction," *National Road Research Alliance*, vol. 19, 2018.

CHAPTER 3 - DIELECTRIC PROFILING SYSTEM (DPS) DATA COLLECTION AND CALIBRATION

3.1 THE DPS EQUIPMENT

The effective dielectric response of an HMA mixture is influenced by its components' dielectric properties (*1*). Given that an HMA mixture usually contains uniform aggregates with consistent proportions, the air volume primarily affects the mix's dielectric constant. The key assumption for using dielectric-based compaction assessment in HMA pavements is that dielectric changes due to mix variability are less significant than those caused by air content variability (*1-3*). This finding supports using ground penetrating radar (GPR) technology for non-destructive estimation of in-place HMA compaction uniformity. The density profiling system (DPS), a rolling density meter (RDM) developed under the Second Strategic Highway Research Program (SHRP2), employs three specially designed GPR sensors to measure the HMA dielectric constant in flexible pavements (*4; 5*). Studies have shown a strong correlation between DPS-measured dielectric values and the air voids in a newly constructed HMA layer, allowing for accurately determining in-place density (*4; 6; 7*).

This study used the PaveScan RDM v2.0, developed by Geophysical Survey Systems Inc. (GSSI). This device meets the strict short- and mid-term dielectric stability requirements and the inter-antenna dielectric variation limits that ensure consistent dielectric measurements without bias set forth by the American Association of State Highway and Transportation Officials (AASHTO) (*4; 8*). It is a portable device that uses three high-frequency (2.2 GHz) GPR sensors mounted on a wheeled cart (Figure 2-5) (*4*). The spacing between the three sensors can be altered based on the number of DPS passes desired for the complete coverage of a pavement lane. For optimal testing, the operator must stroll the cart at a walking speed of no more than 3 mph for optimum testing (*9*), collecting 10 readings per foot of travel (*4*). It also provides a statistical summary, including the mean (of every 5 measurements) and standard deviation of the collected dielectric data for every 6 inches, and suggests core locations based on the recoded low, medium, and high dielectric values (*4*).

The standard operating procedures of the DPS involve several calibrations (*9; 10*). The calibrations include the DPS's survey wheel calibration so that it records survey lengths accurately. It also includes the DPS sensors' air and metal plate calibrations. Finally, the sensors also require calibration using the High-Density Polyethylene (HDPE) block. While the survey

wheel and the sensor's air and metal plate calibrations are needed daily before commencing the testing, the sensor HDPE calibration is occasionally required before using the DPS in the field. These calibrations ensure accurate dielectric measurements of the DPS sensors. In addition to the calibrations, a Swerve test/pass is recommended before data collection to ensure sensor values are within 0.08 of each other, indicating unbiased dielectric measurements (*11*). Swerving the DPS includes keeping the outer two sensors between 2 and 10 ft from the centerline longitudinal joint while the middle sensor remains between 4 and 8 ft. It is performed so that the test starts and ends at the same location with the DPS swerved over the pavement so that each outer sensor touches the 2 ft and 10 ft offset locations twice from the start till the end point. A complete swerve test includes testing a short lot (say 100 ft) starting at point A, reaching point B, and turning around following the same path (and offsets) to reach point A at the end (Figure 3-1).

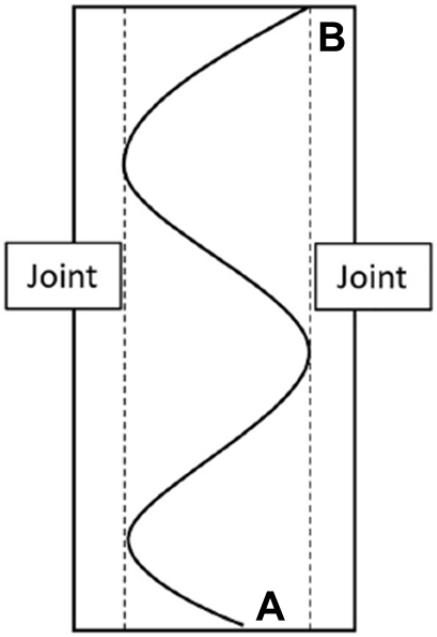

Figure 3-1 Schematic of a Swerve test (*11*)

The DPS equipment has also been successfully used to measure the continuous dielectric values of the longitudinal joint (*4; 11; 12*). While testing the compaction quality at the longitudinal joint, the DPS sensor is placed at a 6-inch offset of the joint's visible seam per the recommendation and usage in previous studies (*11; 12*). This is because the approximate footprint of a DPS sensor is 6 inches. Moving the sensor closer than that to the joint results in erroneous dielectric readings caused by the variable geometry at the interface.

3.2 DPS TESTING AND DATA COLLECTION

The DPS data collection involved testing (mainly) 1,000-foot pavement sections at different project sites in Minnesota and Michigan constructed during 2022 and 2023. The surface HMA lift (i.e., the wearing course) was tested at each project site. Each site underwent multiple DPS runs, with three sensor passes per run, each pass offset differently from the centerline longitudinal joint to ensure full pavement coverage, as illustrated schematically in Figure 3-2. After completing its final pass, the DPS testing followed the Finish roller, and the water sprayed by the compacting pneumatic tire rollers dried out. Different longitudinal joint configurations were tested in this study, including confined and unconfined cold joints, tapered joints, and hot joints constructed using echelon paving. The following sections will briefly explain the joint testing sequence at different project sites using the varying longitudinal joint configurations.

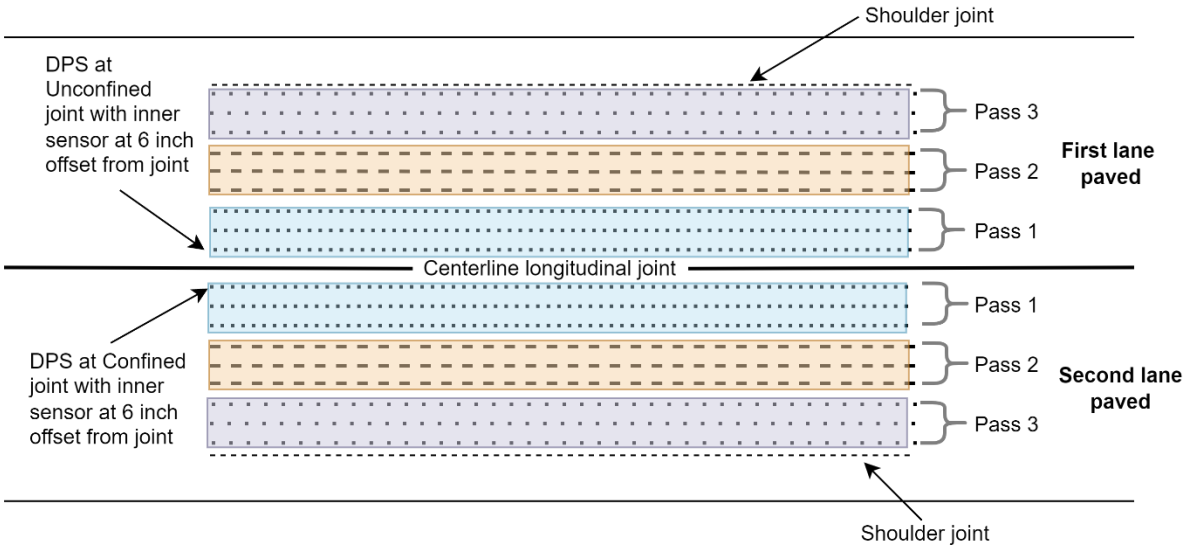

Figure 3-2 Schematic of DPS testing and data collection sequence

3.2.1 Minnesota Project Sites

In 2022, DPS testing in Minnesota was conducted at Xerxes Avenue in the City of Bloomington and Manning Trail in Washington County. On Xerxes Avenue, the paving involved laying an asphalt concrete overlay on 20-foot lanes (one in each direction). The 40-foot wearing course was completely milled and reconstructed lane-wise. DPS data were collected from two sections of this project. The first section's data were gathered for the unconfined (side of the) joint between 84th and 90th Streets when the first lane was paved, followed by dielectric measurements of the confined joint constructed when the adjacent lane was paved later that day

as illustrated in Figure 3-3(a) and 3-3(b). The joint sensor was offset 6 inches from the visible joint line, with the other two sensors measuring data at 2 feet and 3.5 feet offsets.

The second section's data involved dielectric measurements on the unconfined joint only between 98th and 102nd Streets using the same sensor offsets. In addition to DPS data, pavement cores, and loose HMA mixture samples were also collected to calibrate/validate the dielectric-air void relationship. As mentioned, the DPS suggests core locations with low, medium, or high dielectric values. The suggested locations were used to cut and retrieve cores from the pavement. Note that surveying the core locations before cutting is recommended after these are identified, as it is necessary for accurate spot measurements of dielectric values. However, the identified locations were not re-surveyed after they were identified; instead, dielectric values recorded during the field testing were used.

At the Manning Trail site, a wearing lift was constructed on a 12-foot lane with an extended 8-foot shoulder paved using the echelon method. The southbound lane had been paved a day earlier, resulting in a confined butt joint at the centerline that was constructed using the Maryland method. The DPS data were collected from two sections, with sensor offsets similar to those previously mentioned, on both the confined joints and the hot echelon-paved shown in Figure 3-3(c), 3-3(d), and 3-3(e). No pavement cores were collected from this project site, and only loose HMA mix samples were obtained.

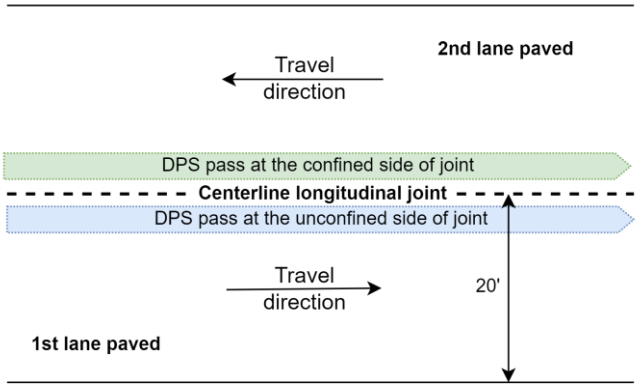

(a) Testing at Xerxes Avenue

(b) Unconfined joint, Xerxes Avenue

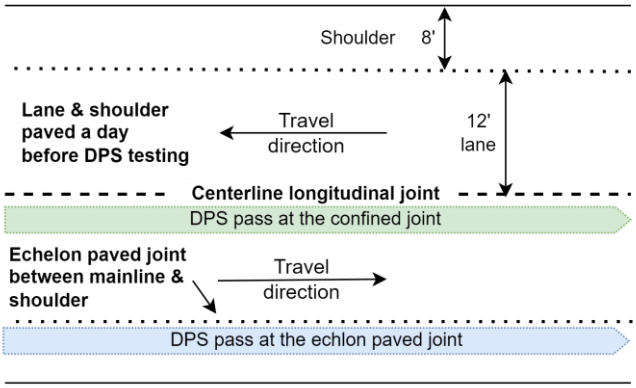

(c) Testing at Manning Trail, MN

(d) Confined joint, Manning Trail

(e) Hot joint, Manning Trail

Figure 3-3 Joint testing at projects in Minnesota

3.2.2 Michigan Project Sites

DPS testing in Michigan included data collection at 25 pavement projects, six during 2022 and 19 during the 2023 construction seasons. These projects are part of the Michigan Trunkline Highway System, encompassing Interstate routes, US Highways, and Michigan State Trunkline highways (M routes). MDOT operates seven regional offices: North and Superior Regions located in the state's Upper Peninsula, which primarily handles low-traffic and rural routes, while the remaining five regions are located in the state's Lower Peninsula, including the University and Metro Regions in the South, which deal with high traffic volumes. Figure 3-4 shows the region-wise locations of each of the project sites. Given that these projects are spread across the state, they utilized various HMA mix types and different rolling patterns for HMA layer compaction and constructed the centerline longitudinal joints with varying configurations between pavement lanes.

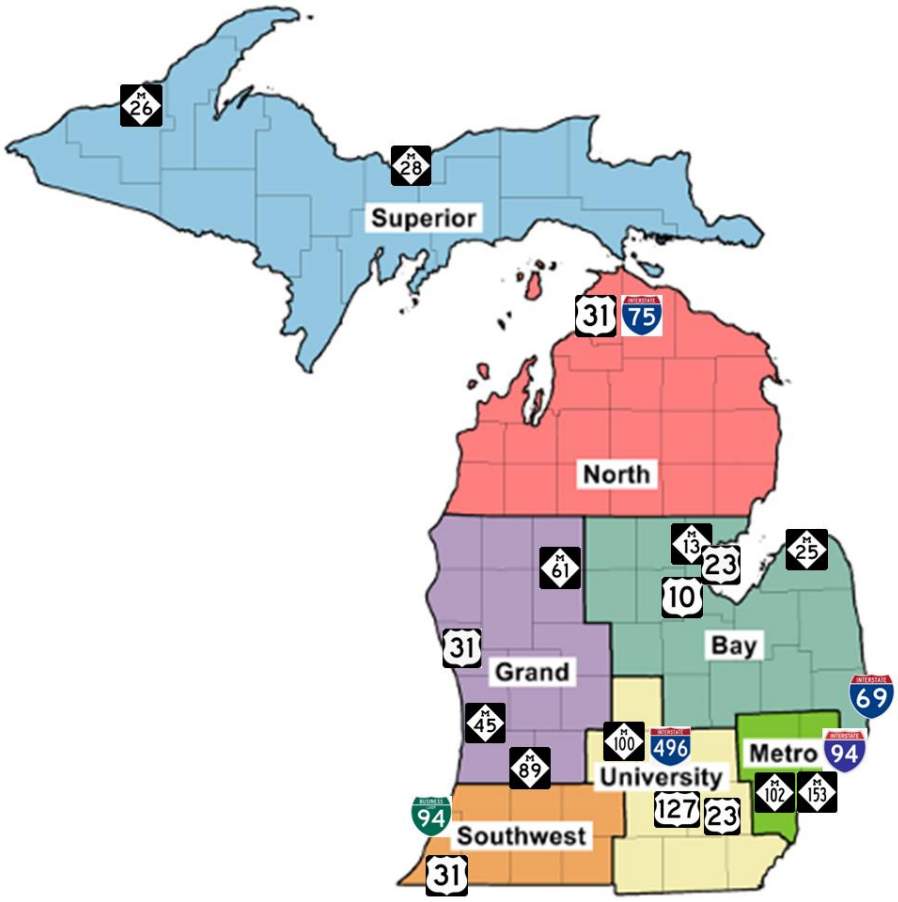

Figure 3-4 Region-wise pavement project sites in Michigan

Construction at the M-89 and M-25 projects (for both years), and the M-100, M-45, and I-94BL projects, involved cold milling and HMA resurfacing using the sequential mill and fill technique, constructing confined butt joints every time [Figure 3-5(a)]. DPS data were collected either on a single lane of these projects (i.e., on M-100, M-45, I-94BL, and both M-89 projects) or both lanes, as was the case with the M-25 projects from both years. The M-28, M-61, and M-26 projects involved constructing the surface layer in both directions using tapered joints. At the M-28 and M-61 projects, the DPS data were collected on the first day when the unconfined taper joint was constructed [Figure 3-5(b)], followed by measurements on the second day when the adjacent lane was built with a confined taper joint [Figure 3-5(c)]. At the M-28 project, testing occurred at two 1,000 ft pavement sections, testing two unconfined and confined joints per day of paving at the exact station locations. At the M-26 project, both unconfined and confined joints were constructed on the same day but at different times, thus resulting in a warm tapered joint between the lanes. Either side of the tapered joint (i.e., unconfined and confined) was tested using DPS. Note that, unlike Minnesota, a 2-foot offset was used between the DPS sensors while testing in Michigan.

At the US-10 project site and the US-31 sites in Holland, Allendale, and Niles, the HMA pavements were constructed using the echelon paving method. Construction at the US-10 project used three pavers [Figure 3-5(d)]. One paver laid the inside shoulder, and the next laid the inner pavement lane, creating an echelon joint between the lane and shoulder. The outer lane and shoulder were paved simultaneously with a third paver. DPS measurements were taken on both joints at the US-10 site. At I-75, the HMA surface layer was laid in echelon with the shoulder using a different mix, resulting in an echelon-paved joint with the shoulder and a cold confined joint at the centerline. The US-31 in the Allendale (2023) project followed a similar pattern; thus, dielectric values were measured for the resulting echelon joint. The centerline echelon-paved joints were tested at the US-31 projects in Holland (2022) and Niles (2023). Moreover, the construction of the I-69 project also involved echelon paving over three lanes and shoulders, forming hot joints between the lanes. However, the location of the echelon joints during the DPS testing could not be located accurately at the site due to inconsistent paving operations followed by the paving crews during construction. Thus, this project data was not included in the joint-related analysis.

(a) Confined butt joints at M-45, MI

(b) Tapered (unconfined) joint at M-61, MI

(c) Tapered (confined) joint at M-61, MI

(d) Echelon paving at US-10, MI

Figure 3-5 Joint testing at projects in Michigan

The surface layers on the US-23 and I-94 projects used a stone matrix asphalt (SMA) mix. For the I-94BL project, dielectric data were measured on an unconfined joint. The US-23 project involved paving each lane on consecutive days, with DPS data collected over the unconfined joint on the first day and over the confined joint on the second day at the same locations but with a shorter section length—the construction of M-153 and M-13 projects involved milling and resurfacing. At the M-153 project, where milling and resurfacing of the surface HMA layer was conducted, data were collected from an unconfined joint first, followed by DPS measurements at the warm confined joint on one side and another unconfined joint after paving the adjacent lane. Testing at the M-13 project site involved dielectric measurements on a confined joint on one end while an unconfined joint at the other end of the same lane. The M-102 project involved nighttime construction, testing both unconfined joints of a single lane as part of a milling and two-course overlay project, as shown in Figure 3-6(a).

The I-496 project in Lansing was tested in both 2022 and 2023. In 2022, the contractor used the cutback method, paving more than 12 ft lane and trimming back about 6 inches of the freshly laid HMA material before paving the adjacent lane [Figure 3-6(b)]. DPS data were collected with a 6 in offset from the unconfined joint. In 2023, the same practice was followed. The center lane of a three-lane section was tested on the first day, with measurements taken from both the confined and unconfined joints. On the second day, after the first two lanes were opened to traffic, the third lane was constructed, forming a confined joint after trimming 6 inches of HMA material. DPS measurements were made on this joint. Additional data were collected at the cutback joint on the center lane using a single DPS sensor at a 6-inch offset from the new centerline due to traffic constraints.

(a) Unconfined joints at M-102, MI

(b) Cutback unconfined joint at I-496, MI

Figure 3-6 Joint testing at M-102 and I-496 (2023) projects in Michigan

In addition to DPS data, pavement cores were also collected from all project sites except the M-89 (Richland) and M-100 (Grand Ledge) projects. Moreover, loose HMA mixture samples were collected from all pavement sites. The cores and loose mix samples were used to calibrate/validate the dielectric-air void relationship. While it is recommended that the identified core locations be re-surveyed for spot dielectric measurements before cutting the cores, the identified core locations were not re-surveyed at the US-31 (Holland), I-496 (2022), M-25 (Port Austin), US-31 (Holland), M-28 (Munising), and the M-89 (Fennville) project sites. The dielectric values measured during the field survey were retrieved from the DPS and used for the cores at these sites. Moreover, Quality Assurance (QA) field cores, which are required for mix acceptance according to MDOT's standard specifications, were also collected on the same HMA production days for all projects except M-100 and M-89 (2023). Discussion about the utilization

of the QA cores will be presented in the subsequent chapters. Table 3-1 details the joint types, section lengths, lift thicknesses, and HMA mix specifics for the projects tested with DPS in this study.

Table 3-1 Project details with joint type and section lengths for DPS data collection

Project & section number	Year, Location, State	Joint type & construction details	Section length (ft)	Mix type & surface lift thickness (in)	NMAS (mm)	Binder grade & content (%)
Xerxes Rd-1	2022, City of Bloomington, MN	Unconfined	1000	SPWEB340(R), 2.0	12.5	58S-28, 5.00
Xerxes Rd-1		Confined butt (Cold)	1000			
Xerxes Rd-2		Unconfined	500			
Manning Tr-1	2022, Washington County, MN	Confined (Maryland method)	1000	SPWEB340(R), 2.0	12.5	58H-34, 5.50
Manning Tr-1		Echelon (Hot)	1000			
Manning Tr-2		Confined (Maryland method)	1000			
Manning Tr-2		Echelon (Hot)	1000			
US-23	2022, Standish, MI	Unconfined	1000	SMA, 1.5	9.5	70-28P, 6.77
US-23		Confined butt (Cold)	465			
I-94	2023, New Haven, MI	Unconfined	1000	SMA, 1.5	9.5	70-22P, 6.21
M-102-1	2023, Detroit, MI	Unconfined	1000	5EMH-HS, 1.5	9.5	70-28P, 5.96
M-102- 2		Unconfined	1000			
M-153-1	2023, Canton, MI	Unconfined	800	5EML, 1.5	9.5	64-28, 6.13
M-153-2		Unconfined	800			
M-153		Confined (Warm)	800			
I-496	2022, Lansing, MI	Unconfined (Cutback)	1000	5EMH, 2.0	9.5	64-28, 6.60
I-496	2023, Lansing, MI	Unconfined	1000			
I-496		Unconfined (Cutback)	1000			
I-496-1		Confined butt (Cold)	1000			
I-496-2		Confined butt (Cold)	1000			
M-28-1	2022, Munising, MI	Unconfined tapered	1000	5EML, 1.5	9.5	58-34, 6.22
M-28-2		Unconfined tapered	860			
M-28-1		Confined tapered (Cold)	1000			
M-28-2		Confined tapered (Cold)	1000			
M-61	2023, South Marion, MI	Unconfined tapered	1000	4EL, 2.0	9.5	64-28, 5.94
M-61		Confined tapered (Cold)	1000			
M-89	2022, Fennville, MI	Confined butt (Cold)	1000	5EL, 1.5	9.5	58-28, 6.03
M-89	2023, Richland, MI	Confined butt (Cold)	1000	5EML, 1.5	9.5	64-28, 6.46
M-25-1	2022, Port Austin, MI	Confined butt (Cold)	1000	5EL, 1.5	9.5	58-28, 6.42
M-25-2		Confined butt (Cold)	1000			
M-25-1	2023, Caseville, MI	Confined butt (Cold)	1000	5EML, 1.5	9.5	64-28, 6.50
M-25-1		Confined butt (Cold	1000			
I-75	2023, Mackinac, MI	Confined butt (Cold)	1000	5EMH, 1.5	9.5	64-34P, 6.25
I-75		Echelon (Hot)	1000			
I-94BL	2023, Benton Harbor, MI	Confined butt (Cold)	975	5EML,1.5	9.5	64-28, 6.46
M-100	2023, Grand Ledge, MI	Confined butt (Cold)	1000	5EML, 1.5	9.5	64-28, 6.59
US-10-1	2023, Bay City, MI	Echelon (Hot)	1000	5EMH, 1.5	9.5	64-28, 6.28
US-10-2		Echelon (Hot)	1000			
US-31	2022, Holland, MI	Echelon (Hot)	1000	4EMH, 2.25	9.5	64-28, 5.55
US-31	2023, Allanson, MI	Echelon (Hot)	1000	5EML, 1.5	9.5	64-34P, 6.47
US-31	2023, Niles, MI	Echelon (Hot)	1000	4EMH, 2.0	9.5	64-28, 5.32
I-69	Port Huron, MI	Echelon (Hot)	1000	5EMH, 1.5	9.5	64-28, 5.99
US-127	Jackson, MI	Confined & Unconfined	1000	5EMH, 1.5	9.5	64-28, 5.80
M-26	Mass City, MI	Tapered joint	1000	5EL, 1.5	9.5	58-34, 6.13
M-13	Standish, MI	Confined & Unconfined	1000	5EML, 1.5	9.5	64-28, 6.16
M-45	Allendale, MI	Confined	1000	5EMH, 1.5	9.5	64-28, 5.89
US-23	2023, Ann Arbor, MI	Confined	1000	5EMH, 1.5	9.5	64-28, 5.97

3.3 DIELECTRIC TO AIR VOID CALIBRATION PROCESS

The DPS provides compaction coverage as HMA dielectric values that do not directly indicate the mix's air void content. Thus, two calibration methods can be used to convert the recorded dielectric values into air void content. A dielectric vs. air void relationship can be calibrated either using cores drilled and retrieved from the newly laid and finished HMA pavement or it can be accomplished using a core-free method that requires laboratory-prepared samples using loose mix samples (*13*). The core-free method was utilized in this study, which uses six laboratory-prepared samples (referred to as pucks from now on). The method has shown promise in accurately converting dielectric data into air voids (*11; 12*). Each puck is 4 inches high and 6 inches in diameter and prepared using a Superpave Gyratory Compactor (SGC) from the loose mix samples obtained from each project site. The pucks are compacted such that each pair has 4-5%, 7-9%, and 11-14% air voids. The dielectric measurements of the pucks are recommended before bulking them for air void determination.

Hoegh et al. developed the procedure to measure the puck dielectric constant values (*13*). It involves measurements of EM responses in four steps: (1) two Delrin spacers are placed on the DPS sensor for 15 seconds, (2) a metal plate replaces the top Delrin spacer, and the response is recorded for 15 seconds, (3) the HMA puck replaces the metal plate for another 15-second scanning, and finally, (4) the metal plate is replaced over the HMA specimen recording EM response for 15 seconds. Processing the saved data from these four steps provides the dielectric constant of the puck. This procedure is repeated at least twice by rotating the sample 90 degrees for successive measurements. Any two measurements within 0.02 dielectric of each other are considered acceptable and averaged to get the puck's dielectric constant.

The dielectric values of the pucks were determined at the MDOT Construction Field Services (CFS) building using the DPS equipment, as shown in Figure 3-7. Once the dielectric values of the pucks were determined, their air voids were measured. The puck air voids were determined using the vacuum sealing method AASHTO T331 (Figure 3-7) since the saturated surface dry method (AASHTO T166) is known to underestimate the air void content of samples that absorb over 2% of water, indicating the presence of open or interconnected voids (*14*). In addition to the pucks, the air voids of the field cores were also determined. These cores were primarily collected for verification of the dielectric-air void model calibrated using pucks.

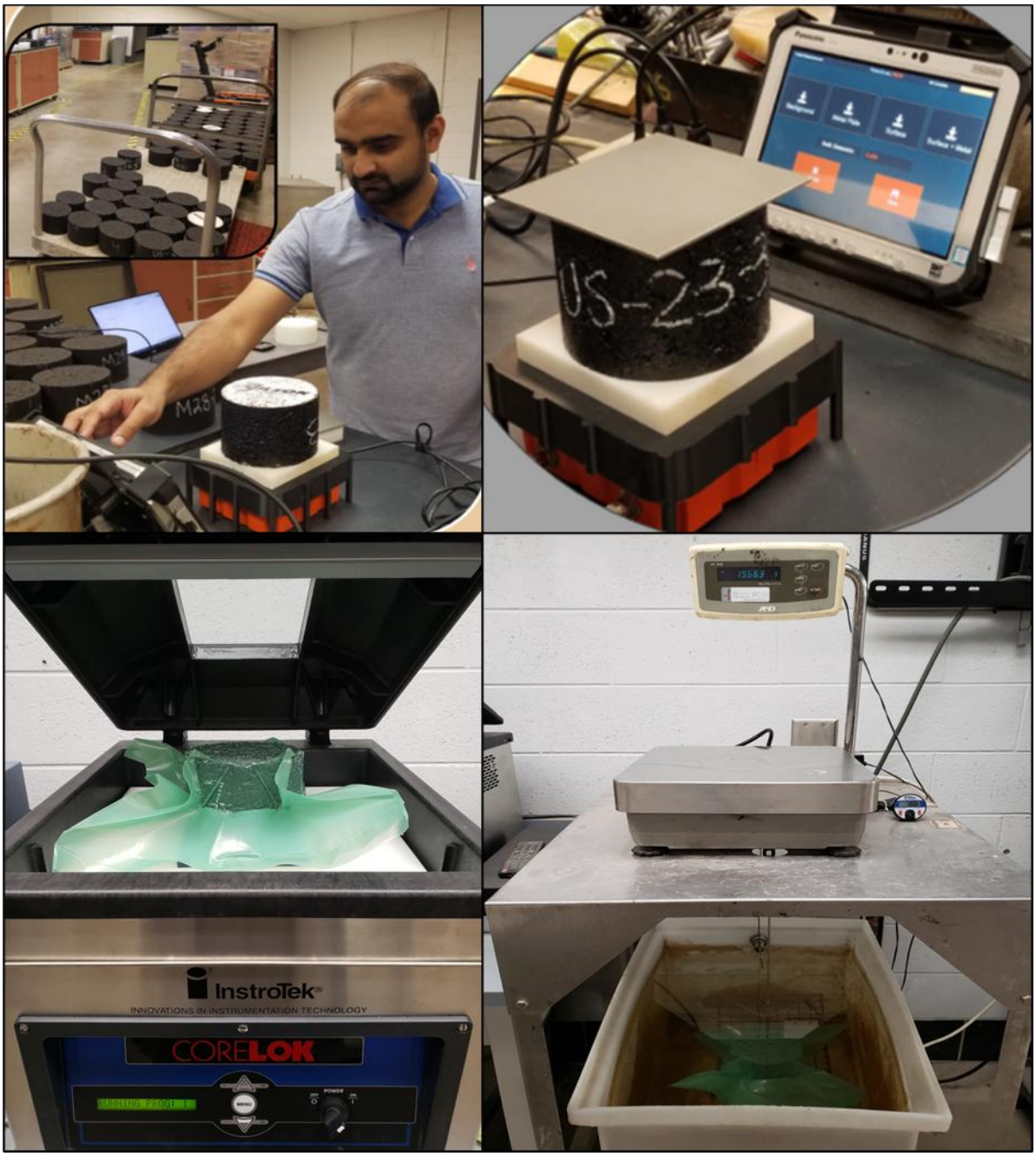

Figure 3-7 Puck dielectric constant and air void measurement

3.3.1 Model Selection

Dielectric values do not indicate air void content directly; thus, a conversion relationship is needed to translate dielectric data into as-constructed air voids for the newly constructed HMA layers. Al-Qadi et al. demonstrated that the HMA dielectric constant can be related to the dielectrics of its components (e.g., aggregate, binder, and air) through electromagnetic (EM) mixing models (*1*). These models simulate wave interactions with composite materials. Various

dielectric mixing models for AC mixes are documented, with different assumptions about EM wave and HMA component interactions (*1; 3; 15-17*). The most widely accepted models for estimating AC density from dielectric data include the Rayleigh, Bottcher, and Complex Refractive Index Model (CRIM) (*1*). While these models are theoretically sound, they require the dielectric values of individual HMA components, such as aggregate and binder, which are not easily measured (*1*). Moreover, Al-Qadi et al. noted that the aggregate dielectric can be back-calculated from density and dielectric data, but this process necessitates cutting cores from the pavement (*3*).

In addition to mechanistic mix-modeling, purely empirical models have effectively linked measured in-field dielectric values to pavement air voids. The most common and successful empirical models are linear (Equation 3-1) or exponential decay (Equation 3-2) functions (*5; 18-20*). While these models are restricted within the measured dielectric ranges, they have a significant limitation: these models underestimate void content when the dielectric value is 1.0 (i.e., air's dielectric constant value), failing to predict 100% (*6; 21*). This issue is crucial primarily when highway agencies use incentive-based systems and penalize contractors when high air voids are present in the field, such as at longitudinal joints. To address this, Hoegh et al. developed the Hoegh-Dai (HD) model (Equation 3-3), which correctly predicts 100% void content at a dielectric value of one (*6*). Nevertheless, the HD model did not align well with field core data trends due to overestimating the slope at higher air voids (≥ 14%), which may result in a higher penalty to the contractors relative to the actual achieved density in the field (*22*).

Moreover, the HD model is a three-parameter model compared to the conventional exponential (and linear) models with two parameters. An increased number of parameters increases the model's complexity and may result in unreasonable predictions and overfitting. Steiner et al. recently developed a five-parameter logistic-regression-based MnDOT model (Equation 3-4) to correlate in-place dielectric measurements with the air void content in asphalt concrete (*22*). Note that two parameters in the model, i.e., a and δ have been fixed to 0.2 and 0.0008. Fixing a at 0.2 is because field HMA air void content should not approach 20%, termed as an approximate physical limit of the possible air void content within an HMA core. The value 0.0008 for the δ parameter was determined based on more than 50 fits using $a = 0.2$ since using that value forces the fit to predict 100% air voids at a dielectric value of 1.0006 (*22*). This model provides a better fit for the experimental data compared to the HD model, mainly in the higher

air voids range (>12%) (*22*). Moreover, the MnDOT model demonstrated the highest accuracy and proved stable in predicting consistent air voids for the same HMA mix design produced on different days (*22*). Thus, the MnDOT model was selected for calibrating a dielectric vs. air void relationship in this study.

$$AV = a\varepsilon + b \quad \text{Equation 3-1}$$

$$AV = ae^{-b\varepsilon} \quad \text{Equation 3-2}$$

$$AV = e^{\left(-B\left(D^{\left|\frac{1}{\varepsilon-C}-\frac{1}{1-C}\right|-1}\right)\right)} \quad \text{Equation 3-3}$$

$$AV = \frac{a\ (=0.2)}{\left(1+\left(\frac{\varepsilon}{c}\right)^{b}\right)^{g}} + \frac{\delta\ (=0.0008)}{(\varepsilon-1)} \quad \text{Equation 3-4}$$

where;

AV = air voids (%),

ε = HMA dielectric values,

a,b,c,g,B,C,D = regression parameters.

3.3.2 New Model Development

Parameter estimation is essential when fitting a model to data to explain a phenomenon, and it is often equated with curve-fitting or optimization. However, there are distinct differences between these two processes. While optimization focuses solely on minimizing the sum of squares or another error criterion without considering the significance of the parameters, parameter estimation considers the errors in the parameters themselves (*23*). According to Beck and Arnold, parameter estimation is "a discipline that provides tools for the efficient use of data in the estimation of constants that appear in mathematical models and for aiding in modeling phenomena" (*24*).

Microsoft Excel-based routines (such as Solver®) are commonly used to estimate nonlinear model parameters, but they typically do not compute parameter errors, limiting their application to curve-fitting (*23*). However, Geeraerd et al. suggest that Solver® can be adapted for parameter estimation by constructing a sensitivity matrix and using matrix multiplication to calculate parameter errors (*25*). According to Dolan, the sensitivity matrix, or Jacobian, is composed of the first derivatives of the model with respect to each parameter and has dimensions of *n*-by-*p*, where *n* represents the number of data points, and *p* denotes the number of parameters

(*26*). It is crucial to determine whether the parameters in a model are accurate and estimable, meaning that they are statistically significant, i.e., do not include zero within their confidence interval (CI). Therefore, reporting the CI of any estimated parameter is as crucial as accounting for parameter errors.

The identifiability of parameters hinges on the scaled sensitivity coefficients (SSC) and the minimization of the objective function (*23*). SSCs are instrumental in assessing whether a parameter is estimable and provide insights into its accuracy in terms of relative error. Several studies have used SSCs in various applications (other than pavements) to estimate the sensitivity of a parameter on a continuous scale of the independent variable (*23; 26; 27*). Recently, these have also been used in pavement-related research (*28; 29*). The i_{th} sensitivity coefficient of a model, $\eta(x,\beta)$, where x is an independent variable, and β represents the parameter vector, defined as $X_i = \partial\eta/\partial\beta_i$ and quantifies the extent of change in the response due to slight variations in the parameter (*24*). When dealing with a nonlinear model, where $\partial\eta/\partial\beta_i = f(\beta_i)$, an initial parameter value is necessary, and an iterative approach using a nonlinear regression algorithm is required for the solution (*24*). The parameter's SSC (X'_i) is the product of its sensitivity coefficient and the parameter itself, as shown in Equation 3-5.

$$X'_i = \beta_i \frac{\partial \eta}{\partial \beta_i} \qquad \text{Equation 3-5}$$

where;

X'_i = SSC of the i_{th} parameter,

β_i = Estimate of the i_{th} parameter,

$\frac{\partial \eta}{\partial \beta_i}$ = i_{th} sensitivity coefficient of the model w.r.t β_i.

Assume that a model $\eta(x,\beta)$ has three parameters (like the MnDOT model), β_1, β_2, and β_3. The sensitivity coefficients (X_i) and SSC (X'_i) w.r.t. each parameter is estimated using Equations 3-6 through 3-11. Suppose the parameters (β) are estimated using a nonlinear regression algorithm and the sensitivity coefficient matrix (i.e., Jacobian) J is obtained. In that case, the SSC for each parameter can then be approximated using Equations 3-12 through 3-14.

$$X_1 = \frac{\partial \eta}{\partial \beta_1} \approx \frac{\eta\big((1.001 * \beta_1), \beta_2, \beta_3\big) - \eta(\beta_1, \beta_2, \beta_3)}{0.001 * \beta_1} \qquad \text{Equation 3-6}$$

$$X_1' = \beta_1 \frac{\partial \eta}{\partial \beta_1} \approx \frac{\eta\big((1.001 * \beta_1), \beta_2, \beta_3\big) - \eta(\beta_1, \beta_2, \beta_3)}{0.001} \quad \text{Equation 3-7}$$

$$X_2 = \frac{\partial \eta}{\partial \beta_2} \approx \frac{\eta(\beta_1, (1.001 * \beta_2), \beta_3) - \eta(\beta_1, \beta_2, \beta_3)}{0.001 * \beta_2} \quad \text{Equation 3-8}$$

$$X_2' = \beta_2 \frac{\partial \eta}{\partial \beta_2} \approx \frac{\eta(\beta_1, (1.001 * \beta_2), \beta_3) - \eta(\beta_1, \beta_2, \beta_3)}{0.001} \quad \text{Equation 3-9}$$

$$X_3 = \frac{\partial \eta}{\partial \beta_3} \approx \frac{\eta\big(\beta_1, \beta_2, (1.001 * \beta_3)\big) - \eta(\beta_1, \beta_2, \beta_3)}{0.001 * \beta_3} \quad \text{Equation 3-10}$$

$$X_3' = \beta_3 \frac{\partial \eta}{\partial \beta_3} \approx \frac{\eta\big(\beta_1, \beta_2, (1.001 * \beta_3)\big) - \eta(\beta_1, \beta_2, \beta_3)}{0.001} \quad \text{Equation 3-11}$$

$$X_1' \approx \beta_1 * J(:,1) \quad \text{Equation 3-12}$$

$$X_2' \approx \beta_2 * J(:,2) \quad \text{Equation 3-13}$$

$$X_3' \approx \beta_3 * J(:,3) \quad \text{Equation 3-14}$$

The SSC of a parameter shares the same units as the model η, allowing for direct comparison between the two. Ideally, SSCs for the parameters should be large (the maximum value of an SSC should be at least 10% of the largest value of the dependent variable) relative to the model η and uncorrelated with each other (*23*). A larger SSC for a parameter implies a more significant impact on the model, making it easier to estimate. Moreover, the parameter with the largest SSC will also be the most accurate. However, if any SSCs are correlated—meaning one is a linear function of the other—those parameters cannot be estimated separately, as the model would respond to them identically. Thus, the SSCs serve multiple critical functions. They assess a parameter's sensitivity across a continuous scale of the independent variable, highlight any collinearity between coefficients, and provide insights into the accuracy of the parameter estimates, thereby increasing confidence in the results.

Figure 3-8(a) illustrates the SSCs for the three parameters of the MnDOT model shown in Equation 3-4, comparing them to the response variable, the air voids in percentage. It is important to note that estimating and plotting SSCs is a forward problem, requiring only initial guesses for the parameters rather than actual data. The model's response, or dependent variable (air voids), ranges from 0% to 20%. The SSC for parameter *c* is noticeably large relative to the

model (i.e., greater than 10% of the maximum value of the predicted air voids, Av-P), indicating that *c* should have the least error. However, parameters *c* and *g* peak at the same dielectric value (the independent variable), suggesting a correlation between them. As a result, parameters *c* and *g* are likely insignificant (i.e., may contain zero within the parameter CI) when estimated together, with parameter *g* expected to have a larger error than *c*. On the other hand, parameter *b* is estimable and is anticipated to have the least error, as it is significant relative to the independent variable and shows no correlation with the other parameters. In summary, parameter *b* is estimable and should have the most accuracy. In contrast, if estimated simultaneously, the other two parameters would result in erroneous values with the highest error in parameter *g*.

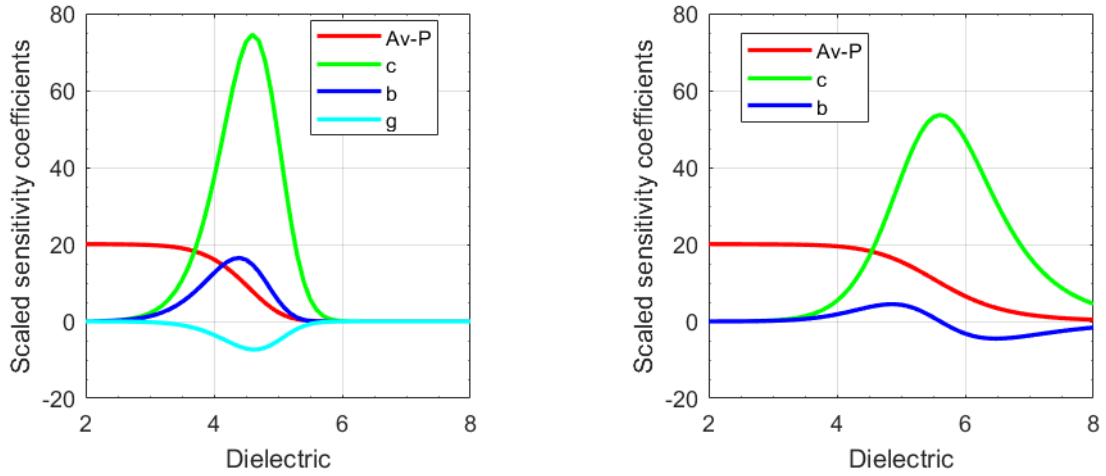

(a) MnDOT model with 3 parameters (b) Modified model with 2 parameters

Figure 3-8 Scaled sensitivity coefficients for the MnDOT and modified MnDOT model

While a separate dielectric vs. air void relationship is recommended for every HMA mix, a single relationship using the 3-parameter MnDOT model was calibrated using the puck dielectric and air void data from Michigan projects constructed in 2022 to verify the information provided by the SSCs in Figure 3-8(a). Table 3-2 presents the calibration results, including the three parameters' ordinary least squares (OLS) estimates, confidence intervals (CI), and relative errors. As the scaled sensitivity coefficients (SSCs) indicate, parameters *c* and *g* are statistically insignificant, as their CI includes zero. Also, the relative error for parameter *g* is the highest, followed by parameter *c*. Only the CI of parameter *b* does not include a zero, indicating a significant/estimable parameter with the lowest relative error.

The principle of parsimonious data modeling suggests that when two models fit a dataset equally well, the model with fewer parameters will likely have better predictive accuracy with new data (*30; 31*). A highly efficient parsimonious model achieves the same accuracy and results

as more complex models with fewer parameters and requiring significantly less data (*31*). Thus, based on the information provided by the SSCs, the 3-parameter MnDOT model is modified by just removing parameter *g*. The modified MnDOT model (the New model from now on) contains only two parameters, as shown in Equation 3-15. The New model's SSC plot in Figure 3-8(b) suggests that parameters *c* and *b* are not correlated. The SSC for parameter *c* is larger, indicating that it is estimable with the least error compared to parameter *b*. Table 3-3 shows the calibration results using the New model with only two parameters and the same data used for the results in Table 3-2 earlier. As indicated by the SSCs in Figure 3-8(b), the two parameters were uncorrelated, resulting in CI for each parameter that does not contain zero. i.e., showing that these parameters have a significant bearing on the response variable. Moreover, Parameter *c* was estimated to have the least relative error (of only 0.37%) compared to Parameter b, which had a 6% error.

Table 3-2 OLS estimates, CI, and relative errors – MnDOT model

Value of	Parameter *c*	Parameter *b*	Parameter *g*
Initial guess	5.61	10.74	8.35
Final OLS estimates	6.95	7.05	9.67
Parameter CI	-10.43 to 24.33	2.15 to 11.95	-137.74 to 157.08
Relative parameter error, %	125.08	34.78	762.64

$$AV = \frac{0.2}{1 + \left(\frac{\varepsilon}{c}\right)^{b}} + \frac{0.0008}{(\varepsilon - 1)} \qquad \text{Equation 3-15}$$

where;

AV = air voids (%),

ε = HMA dielectric values,

b,c = regression parameters.

Table 3-3 OLS estimates, CI, and relative errors – New model

Value of	Parameter *c*	Parameter *b*
Initial guess	5.61	10.74
Final OLS estimates	4.79	10.04
Parameter CI	4.76 to 4.83	8.83 to 11.26
Relative parameter error, %	0.37	6.04

Figure 3-9 compares the individual calibrated dielectric vs. air void relationships for some Michigan projects using the MnDOT and 2-parameter New models. The predictions from

the MnDOT model are very similar to those from the New model, confirming that the New model with fewer parameters is parsimonious compared to the MnDOT model. Thus, it is logical to use the modified, less complicated new model that would convert the dielectric data into air voids efficiently and with similar accuracy as the MnDOT model.

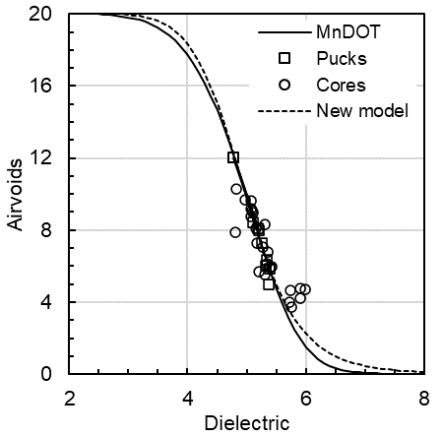

(a) M-25 Port Austin, MI

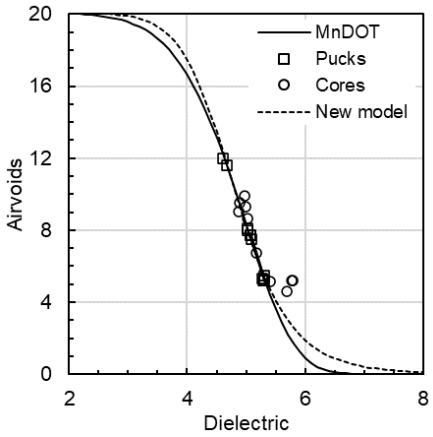

(b) M-28 Munising, MI

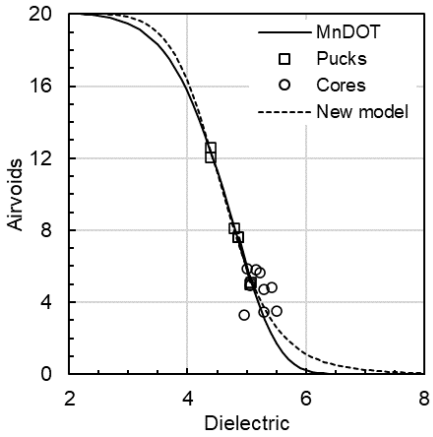

(c) I-496 (2022) Lansing, MI

Figure 3-9 Comparing the models – 3-parameter MnDOT vs. 2-parameter New model

3.3.3 Project-Wise Calibration

Using the New model, a dielectric vs. air void relationship was calibrated for every project using the puck dielectric and air void measurements. The OLS parameter estimation approach, which is a fundamental and widely used optimization technique, was used for calibration. This approach determines optimal parameter estimates that help minimize the sum of the squared differences between the measured/observed and the predicted data. The OLS estimation approach's basic assumption is that the errors (i.e., residuals) are normally and

independently identically distributed (NIID). Validation of these assumptions ensures that the statistical properties of the estimators (such as unbiasedness and efficiency) hold.

Additionally, to the OLS estimation method, a resampling technique called Bootstrapping was employed to increase confidence in the estimated parameters of the modified model. This method involves resampling the data with replacement, using random numbers from a uniform distribution, without making assumptions about the data distribution or the true parameter values. Unlike the Monte Carlo method, which generates synthetic data based on the model function and estimated parameters, while assuming specific distributions and true parameter values, bootstrapping makes no such assumptions. The key advantage of this resampling method is its ability to quantify variability by providing confidence intervals CI for both the estimated parameters and the corresponding model predictions.

Bootstrapping can be implemented in two ways: (a) by resampling the data or (b) by resampling the residuals. When bootstrapping data, *n* pairs of data points are randomly selected from the original dataset, with replacement, where *n* is the number of data points in the original set. This process involves generating *n* random numbers from a uniform distribution, allowing for the possibility of repeating data pairs. On the other hand, residual bootstrapping involves randomly selecting *n* residual pairs, with replacement, from the original residuals using *n* random numbers from a uniform distribution. These selected residuals are then added to the predicted data to create a new dataset of *n* pairs. Residual bootstrapping is generally preferred when dealing with smaller datasets, especially when the SSCs are large only within a narrow range of the independent variable. This study used residual bootstrapping since most of the projects in this study used data from six pucks only for calibration. Moreover, the SSCs for the New model are only large in a limited range of the dielectric values, as shown in Figure 3-8(b).

Table 3-4 displays the estimated parameters (*c* and *b*) for Michigan's M-153 project (as an example) along with their CI, relative errors, and model's root means squared error (RMSE) using the OLS method and bootstrap methods utilizing 1,000 bootstrap samples. It is observed that the CI of either parameter is significant, with parameter *c* having the lowest relative error (0.36%) compared to 7.33% of parameter *b*. This observation aligns with the information previously discussed about SSCs, which suggested that parameter *c* will be more accurately estimated than parameter *b*. Moreover, the model's RMSE is only about 0.45%, with a 98% coefficient of determination (R^2).

Table 3-4 OLS and bootstrap estimates, CI, relative errors – M-153 project, MI

Value of	For parameter *c*	For parameter *b*
Initial guess	5	12
Final OLS estimates	4.9289	12.2714
Parameter CI (OLS)	4.8791 to 4.9788	9.7737 to 14.7690
Standard error	0.018	0.899
Relative error, %	0.36	7.33
Model R^2, %	98.18	
Model RMSE, %	0.4531	
Bootstrap CI (using residuals)	4.9016 to 4.9613	10.8406 to 13.6761
Bootstrap RMSE, %	0.4551 *(using mean bootstrap estimated c and b values)*	

Figure 3-10 displays the calibrated model and its residual analysis plots. Figure 3-10(a) shows the calibrated model using the puck data. The green dashed lines show the confidence bands (CB) around the predicted air voids curve (Av-P), shown in black. The CB provides an interval within which the true model's response *η(x)* is expected to lie for a given predictor value *x* calculated using Equation 3-16 and Equation 3-17. The dotted blue lines show the prediction band (PB) for the model and provide an interval within which a new observation y_{new} is expected to fall based on a given predictor value *x*. The PB is calculated using Equations 3-18 and 3-19.

$$\hat{y}(x) \pm t_{\alpha/2,n-p} \,.SE\big(\hat{y}(x)\big) \qquad \text{Equation 3-16}$$

$$SE(\hat{y}(x)) = \sqrt{MSE \,.J(x) \,.C \,.J(x)^T} \qquad \text{Equation 3-17}$$

$$\hat{y}(x) \pm t_{\alpha/2,n-p} \,.SE_{pred}(x) \qquad \text{Equation 3-18}$$

$$SE_{pred}(x) = \sqrt{MSE \,.(1 + J(x) \,.C \,.J(x)^T)} \qquad \text{Equation 3-19}$$

where;

$\hat{y}(x)$ = predicted response using the model at a value *x*,

$t_{\alpha/2,n-p}$ = critical value from *t*-distribution with *n*−*p* degrees of freedom (i.e., *n* shows the total number of data points while *p* is the number of parameters) for a desired confidence level,

$SE\big(\hat{y}(x)\big)$ = standard error of the mean response at *x*,

$SE_{pred}(x)$ = standard error of the prediction at *x*,

$MSE = \frac{1}{n-p} \sum_{i=1}^{n} (y_i - \hat{y}_i)^2$ is the mean squared error,

$J(x)$ = Jacobian row vector of model's partial derivatives w.r.t. the parameters, evaluated at *x*, $C = (J^T J)^{-1}$ is the covariance matrix of the parameter estimates calculated using the Jacobian matrix, J of the model evaluated at all data points.

The standard statistical assumptions must be met for any regression model to yield meaningful conclusions. These assumptions require the errors to be (a) additive, (b) have a zero mean with a (c) constant variance, (d) they should be uncorrelated, and (e) normally distributed (*24*). Figure 3-10(a) shows that the residuals meet assumptions *a* through *d* as the residuals do not display any trend (e.g., do not fan out), their mean is almost zero, and their values have a constant variance (i.e., all values are within ±1 around zero). Figure 3-10(c) shows the confidence and prediction bands estimated using the OLS and bootstrap methods. Bootstrap bands are observed to be tighter than those estimated using the OLS estimation method. This is due to the resampling of 1,000 bootstrap samples, which results in more accurate estimates closer to the true population estimate values. Figure 3-10(d) shows the distribution of the bootstrap residuals; these are normally distributed with a zero mean. Moreover, Figures 3-10(e) and 3-10(f) display the distribution of the bootstrap estimated parameters. The bootstrap estimated parameters are normally distributed; their mean values are close to the ones estimated using the OLS method.

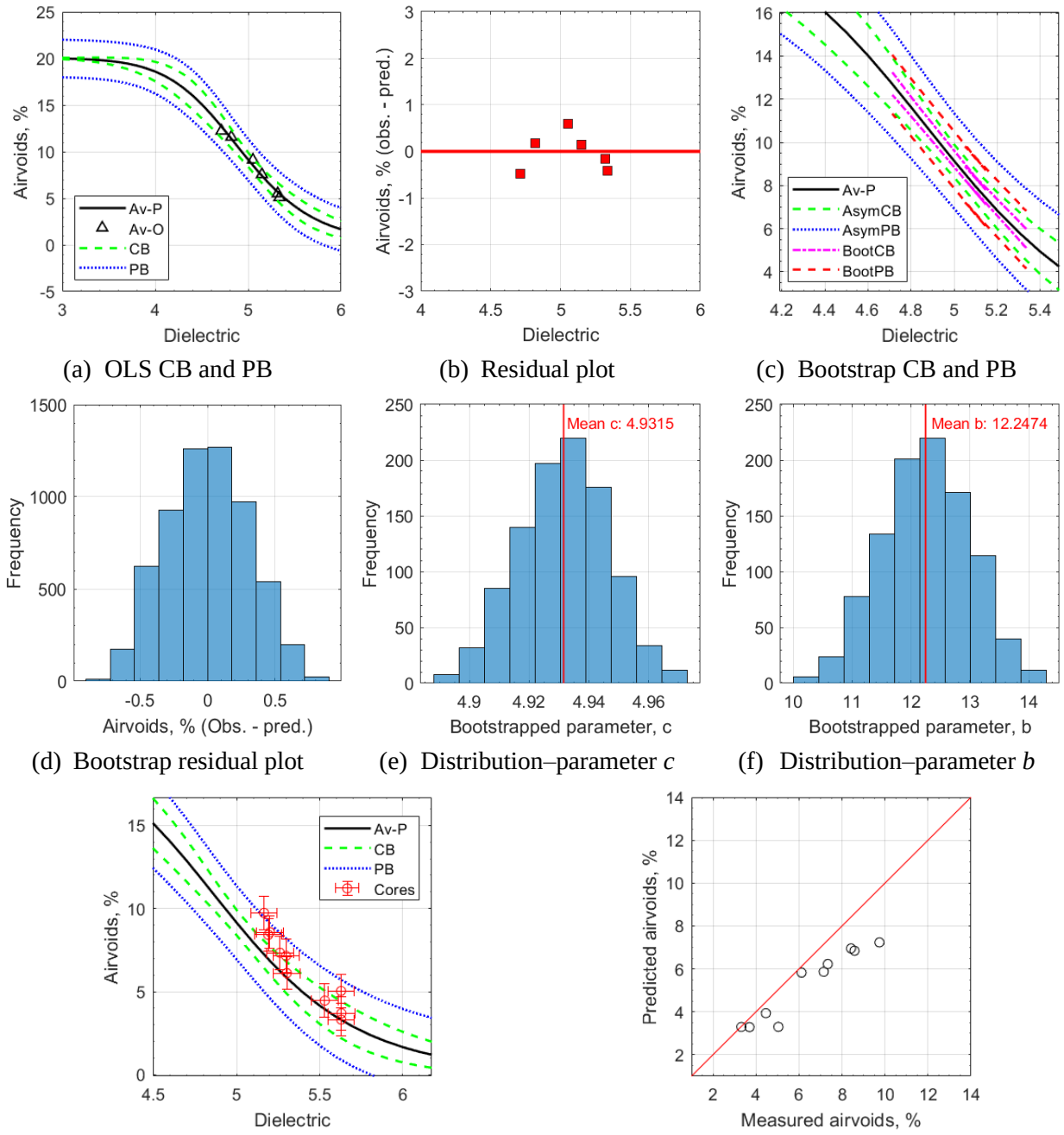

(a) OLS CB and PB (b) Residual plot (c) Bootstrap CB and PB

(d) Bootstrap residual plot (e) Distribution–parameter *c* (f) Distribution–parameter *b*

(g) Model validation using cores (h) One-to-one core validation

Figure 3-10 Calibrated model, residual analysis, confidence bands (CB), and prediction bands (PB) using OLS and bootstrap methods – M-153 project, MI

A typical pavement construction project often spans multiple days, producing the same (i.e., design) HMA material over several days. This makes it difficult to maintain consistent asphalt mix proportions across the entire project. Thus, highway agencies specify and use certain mix-property-related tolerances for accepting HMA mixes with a target job-mix formula (JMF) produced on multiple days, allowing for production variability. Table 3-5 presents the HMA

acceptance tolerances per the MDOT HMA production manual. To assess whether asphalt mix production variations resulting from multiple-day production impact the calibration curves between surface dielectric and air void content, HMA loose samples were collected on multiple construction days of some of the projects in Michigan along with their production JMFs. The idea was that if these curves differed between production days, the DPS might require daily calibration.

Table 3-5 HMA acceptance tolerances per MDOT HMA production manual (*32*)

HMA mixture volumetrics property	Tolerance value
Binder content	± 0.40
Bulk specific gravity of the mix, G_{mb}	± 0.020
Maximum specific gravity of the mix, G_{mm}	± 0.019
Air voids	± 1.00%
Voids in mineral aggregates (VMA)	± 1.20%

Seven projects (I-94, M-28, I-496, M-61, M-25, M-89, and M-26) using various mix types (SMA PG70-22P, 5EMH PG64-28, 5EML PG58-34, 5EL PG58-28, 5EL PG58-34, and 4EL PG64-28) were analyzed. Two separate puck dielectric-density calibration curves were established using loose mix samples collected on two production days. While the HMA production was only a day apart for most of the projects, the 5EMH PG64-28 mix on the I-496 project was sampled a year apart (i.e., in 2022 and 2023) to create separate calibration curves for the same design mix. Table 3-6 details the aggregate gradation, asphalt mix volumetrics for the target JMF, and the actual values from QA test reports on the different production days. The table highlights slight variations in the mix properties produced to either day compared to the design JMF for certain projects. For instance, the M-28 project exhibited a 0.36% difference in binder content (6.22% vs. 5.86%) and a 0.32% variation in VMA. Similarly, the VMA differences between the two production days of the M-61 project exhibited a 0.80% difference. However, most of these differences are within the HMA mix tolerances presented in Table 3-5. Moreover, the M-61 project showed differences in aggregate gradations of approximately 3-5% across different sieve sizes.

Despite these variations, the calibration curves remained unaffected, as observed in Figure 3-11. The calibration curves from either production day of all the projects are comparable. A slight shift can be observed in the two curves for the HMA mix in the I-94SMA and I-496 projects. However, the slight shift resulted in less than a 0.2% difference in the predicted air

voids. Such results suggest that the shift between the curves due to slight mix-proportion differences has an insignificant impact on the calculated density. Thus, it can be inferred that the mix's calibration is reproducible and independent of the HMA production day. Moreover, minor mix production fluctuations on different days do not impact the calibration curves between surface dielectric and air void content and hence predict similar density. Table 3-7 tabulates the final calibration coefficients for the New Model that were used to convert the dielectric into air voids for the analysis presented in the subsequent chapters. Note that the table also contains the dielectric values for 8% and 10% air voids resulting from the calibrated relationship for every project. These values will be referred to and used later in the analysis.

Table 3-6 HMA mix variability between design JMF and production mix QA testing

Sieve, in. (mm)	I-94: SMA (PG70-22P)			M-28: 5EML (PG58-34)			M-61: 4EL (PG64-28)		
	JMF	9/17/23	9/23/23	JMF	8/10/22	8/11/22	JMF	8/9/23	8/10/23
¾ (19.0)	100	100	100	100	100	100	100	100	100
½ (12.5)	99.9	94.87	97.04	100	99.68	100	93.2	92.06	92.84
⅜ (9.5)	90.5	82.67	81.69	97.7	96.67	96.73	84.6	82.2	84.44
No.4 (4.75)	45.3	44.18	42.43	79.8	76.72	76.5	68.3	63.73	68.57
No.8 (2.36)	27.3	26.01	24.63	58.7	58.52	58.12	54.2	50.83	54.68
No.16 (1.18)	19.3	18.04	17.02	46.4	46.73	46.35	42.4	39.88	42.99
No.30 (0.6)	15.4	13.99	13	36.3	38.07	37.81	30	28.32	31.39
No. 50 (0.3)	12.7	11.12	10.4	20.3	21.61	21.47	14.1	13.59	13.62
No.100 (0.15)	10.7	8.57	8.34	9.4	8.42	8.61	7	7.01	6.81
No.200 (0.075)	8	6.93	6.79	6.4	5.11	5.29	4.9	4.88	4.72
Asphalt, %	6.21	5.81	6.09	6.22	6.22	5.86	5.94	5.88	6.02
G_{mm}	2.672	2.684	2.695	2.467	2.462	2.478	2.477	2.499	2.492
VMA	17.95	17.41	17.6	16.36	15.9	15.58	15.24	14.27	15.07

Sieve, in. (mm)	M-25: 5EL (PG58-28)			M-89: 5EL (PG58-28)			M-26: 5EL (PG58-34)		
	JMF	9/14/22	9/15/22	JMF	7/18/22	7/19/22	JMF	7/31/23	8/1/23
¾ (19.0)	100	100	100	100	100	100	100	100	100
½ (12.5)	99.5	99.76	98.88	100	99.73	99.39	100	100	100
⅜ (9.5)	97.2	97.52	96.96	95.8	96.69	97.18	92.7	94.74	94.47
No.4 (4.75)	82.1	80.5	80.92	71.8	70.37	67.87	70.9	73.28	73.7
No.8 (2.36)	61	59.96	60.57	56	55.84	54.06	54.3	57.31	58.34
No.16 (1.18)	45.8	45.09	46	42.1	43.62	42.84	42.6	46.53	46.69
No.30 (0.6)	33.5	3308	34.09	30.8	33.03	33.73	33.6	36.85	36.37
No. 50 (0.3)	18.8	18.41	19.28	15.6	17.49	17.17	20.6	25.59	24.75
No.100 (0.15)	9.9	9.1	9.54	7.3	7.02	7.31	9.4	11.01	10.18
No.200 (0.075)	5.9	5.99	6.24	4.6	4.33	4.64	5.6	5.75	5.38
Asphalt, %	6.42	6.53	6.43	6.03	6.2	6.02	6.13	6.27	6.38
G_{mm}	2.452	2.455	2.46	2.495	2.508	2.5	2.479	2.479	2.476
VMA	15.8	15.8	15.6	16.05	16.41	16.01	15.56	15.77	15.94

Sieve, in. (mm)	I-496: 5EMH (PG64-28)			
	JMF	11/4/22	8/29/23	
¾ (19.0)	100	100	100	
½ (12.5)	99.9	99.71	99.68	
⅜ (9.5)	95.6	96.44	94.76	
No.4 (4.75)	69.4	70.7	69.19	
No.8 (2.36)	50.4	53.17	51.97	
No.16 (1.18)	36.1	39.66	38.5	No data.
No.30 (0.6)	26.4	30.43	28.97	
No. 50 (0.3)	17.4	20.06	19.12	
No.100 (0.15)	7.4	8.89	8.57	
No.200 (0.075)	4.2	4.8	5.07	
Asphalt, %	5.59	5.59	5.42	
G_{mm}	2.534	2.526	2.532	
VMA	15.83	16.21	15.47	

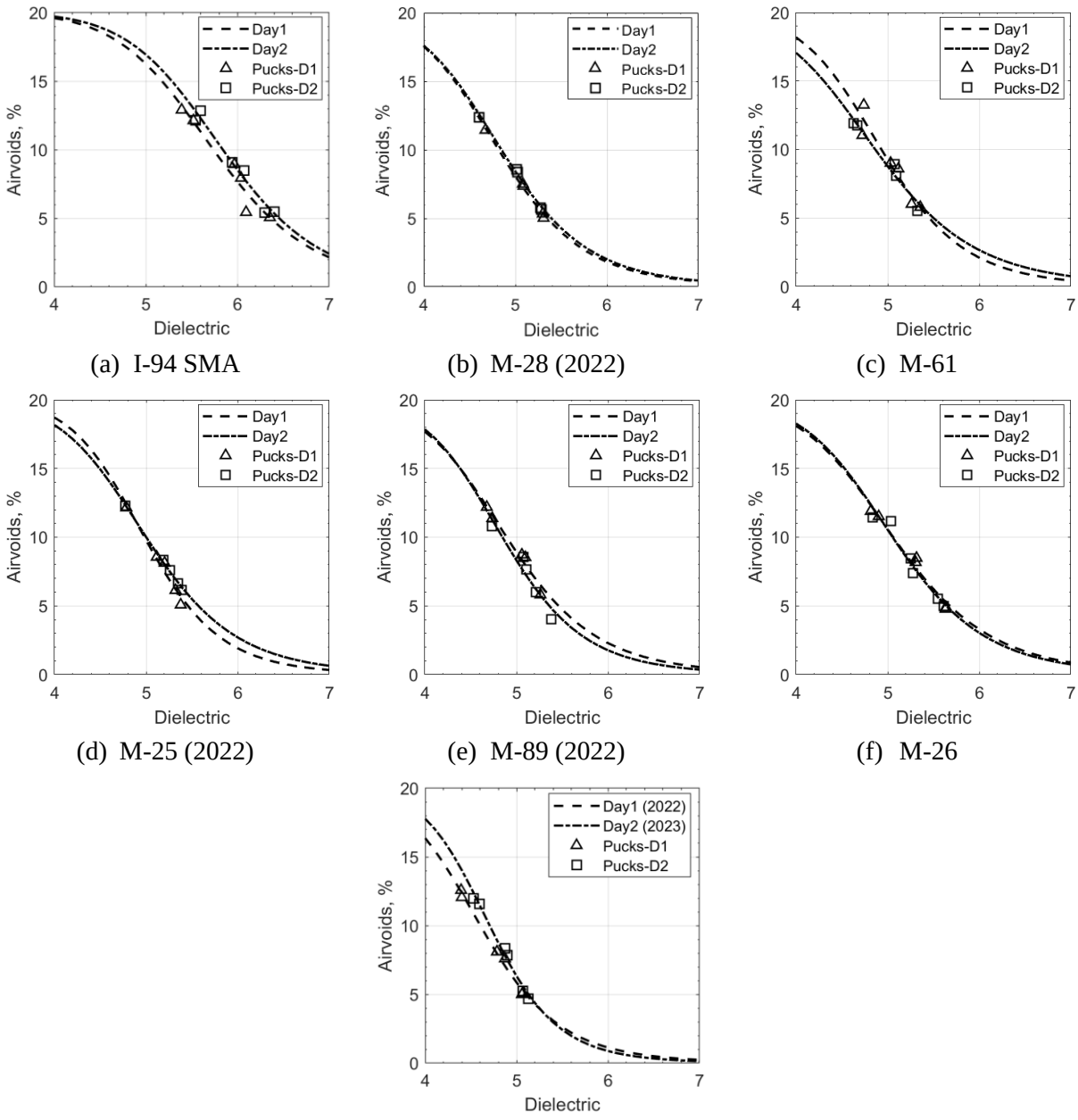

(a) I-94 SMA (b) M-28 (2022) (c) M-61

(d) M-25 (2022) (e) M-89 (2022) (f) M-26

(g) I-496

Figure 3-11 Puck calibrated models using loose HMA samples produced on multiple days

Table 3-7 New Model calibration coefficients for individual project's HMA

Project	Parameter *c*	Parameter *b*	Dielectric (8% Av)	Dielectric (10% Av)	Dielectric difference for ≥ 2% Av difference
I-75	4.98	12.45	5.143	4.978	0.165
I-94BL	5.01	11.89	5.183	5.009	0.174
I-94 SMA	5.72	10.94	5.937	5.721	0.216
I-496	4.65	11.18	4.822	4.650	0.172
M-28 (2022)	4.82	10.38	5.014	4.822	0.192
M-25 (2022)	4.97	11.07	5.157	4.972	0.185
M-25 (2023)	4.94	11.56	5.123	4.946	0.177
M-61	4.83	10.04	5.027	4.828	0.199
M-89 (2022)	4.83	10.71	5.018	4.832	0.186
M-89 (2023)	4.95	11.08	5.141	4.956	0.185
M-100	4.61	12.53	4.766	4.614	0.152
M-102	5.11	11.86	5.288	5.110	0.178
M-153	4.93	12.27	5.096	4.930	0.166
US-10	5.264	12.557	5.438	5.266	0.172
US-31 (2022)	4.77	11.28	4.946	4.772	0.174
US-31N (2023)	5.24	12.14	5.421	5.242	0.179
US-31A (2023)	4.55	9.43	4.752	4.552	0.200
I-69 (2023)	4.94	12.22	5.110	4.943	0.167
M-45	5.21	12.59	5.382	5.212	0.170
M-26	5.06	9.74	5.277	5.062	0.215
US-127	5.12	12.49	5.291	5.122	0.169
M-13	4.58	11.34	4.750	4.583	0.167
US-23 SMA (2022)	4.92	14.89	5.057	4.921	0.136
US-23 (2023)	4.93	13.08	5.084	4.928	0.156
XX Project, MN	4.78	13.54	4.927	4.782	0.145
Manning Trail, MN	4.84	12.12	5.006	4.842	0.164

Note: Av = Air voids; US-31N = US-31 (Niles); US-31A = US-31 (Allanson); XX = Xerxes.

Validation Using Field Cores

For validating the calibrated models, pavement cores were extracted from all the projects except for one in Minnesota (the Manning Trail project) and two in Michigan (M-100 and M-89 projects in Grand Ledge and Richland, respectively). Figure 3-12 shows the calibrated model for every project and its core validation (where cores were available). The red circles in the figure represent air void measurements from field cores. Per AASHTO PP98-19, a dielectric measurement variation threshold of 0.08 is acceptable between any two air-coupled GPR sensors (i.e., dielectric values within 0.08 of each other are considered similar) (*8*). Thus, the figure shows horizontal error bars indicating dielectric constant measurement variability of ± 0.08. On the other hand, the vertical error bars show the measured core air voids ± 1% since the MDOT QA/QC procedures tolerate air void measurement differences of 1% (Table 3-5) (*32*).

Considering the variability shown by error bars, it can be inferred that the coreless calibration method reasonably predicts the as-constructed HMA density represented by the core data, albeit with slightly elevated error in some cases. For instance, Xerxes Rd (MN), M-89, US-23 SMA, and US-31 (Holland) from the 2022 projects show discernable differences between the predicted air voids and the core data. These differences can be partly attributed to data collected during field testing and not re-surveying the indicated core locations for spot dielectric measurement (recommended) before cutting and retrieving the cores. In the case of the US-23 (2022) project, these differences might also be because of the SMA mix used in the construction. Nevertheless, the calibrated models still perform reasonably. While most 2023 projects show agreement between the predicted and measured (core) air voids, six projects exhibited noticeable differences. Of these six, three projects, including the M-26, US-127, and US-23, showed the highest differences between the calibrated model predictions and the measured core air voids. The remaining three projects (i.e., M-45, M-13, and US-31 in Niles) show comparatively more minor differences between the model predictions and measured core data.

Note that the HMA dielectric value ranges between 3 and 7, depending upon its constituent components and their dielectric values (i.e., 2.6 – 2.8 for the asphalt binder, 4.5 – 6.5 for the aggregates, and about 1.006 for air) (*33; 34*). In contrast, water has a dielectric constant value of ~81 (*35-37*). Thus, moisture on the HMA surface from water spraying on the roller tires during compaction may change (i.e., increase) the recorded dielectric values and potentially incorporate bias in the calibration process (*38*). Evans et al. found that a 1% increase in the gravimetric moisture content of asphalt mix, on average, bumps up its dielectric value by 0.91 (*39*). The presence of moisture during the DPS field measurements on the six previously mentioned projects was suspected to result in increased core dielectric values compared to the pucks (and the resulting model prediction). Although DPS testing was typically conducted shortly after the finish roller, in many cases, testing was delayed until the surface layer appeared dry. However, on some sites, the excessive water used by compacting rollers may have caused DPS testing to be conducted on surfaces that seemed dry but still retained moisture within the mix. Furthermore, certain aggregates may absorb and retain water longer, increasing dielectric values if not heated for sufficient time during the HMA production process, leaving moisture entrapped between the aggregate and the binder coating.

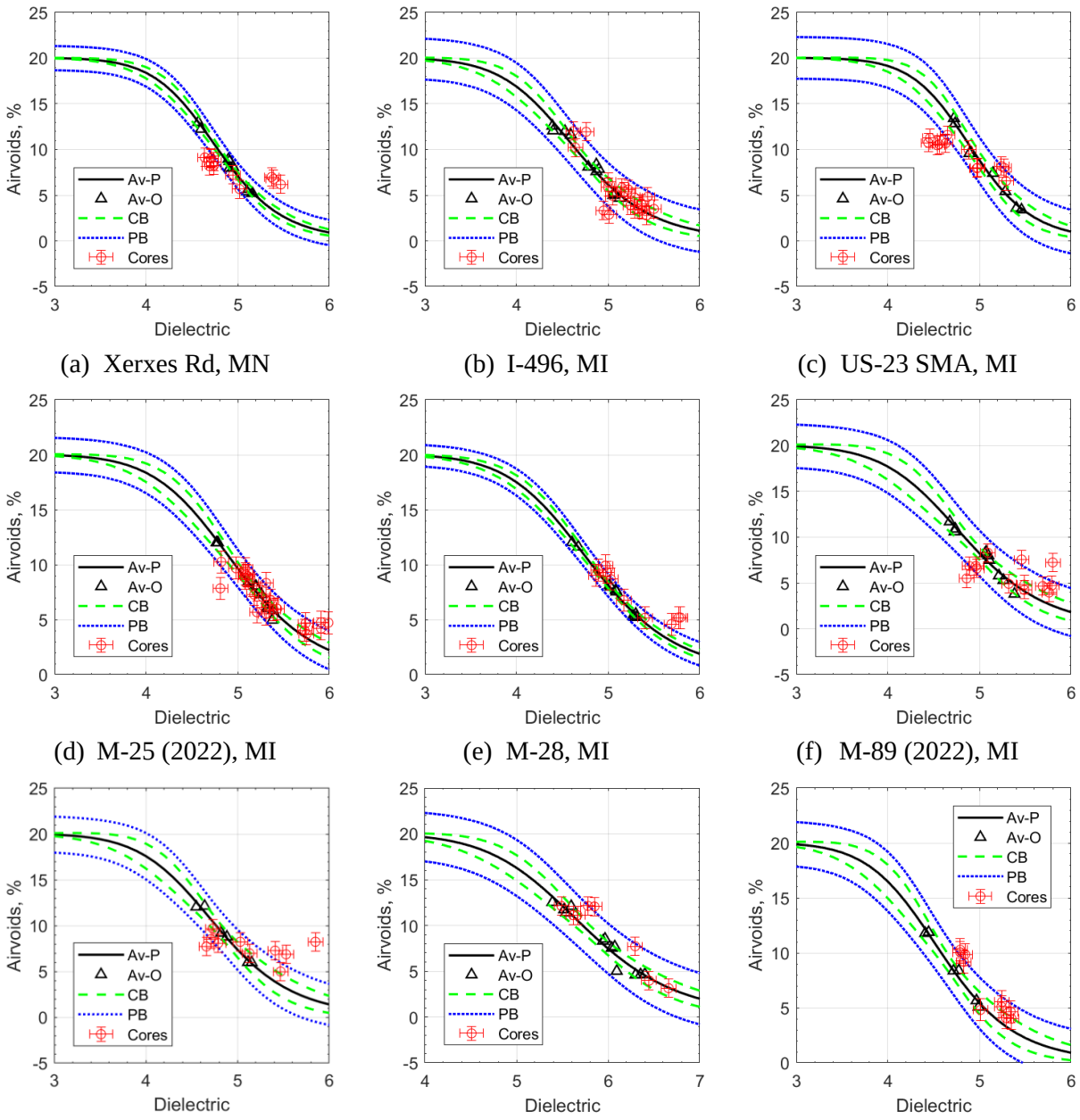

(a) Xerxes Rd, MN (b) I-496, MI (c) US-23 SMA, MI

(d) M-25 (2022), MI (e) M-28, MI (f) M-89 (2022), MI

(g) US-31 (2022), MI (h) I-94 SMA, MI (i) M-13, MI

Note: Av-P = Predicted air voids; Av-O = Observed air voids; CB = 95% confidence bands; PB = 95% prediction bands

Figure 3-12 Puck-calibrated models and validation using field cores (if available)

Figure 3-12 (cont'd)

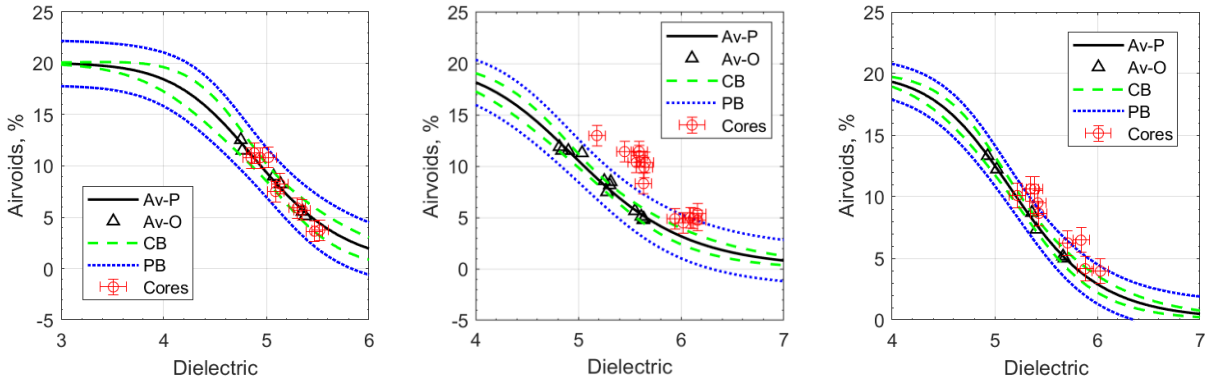

(j) M-25 (2023), MI (k) M-26, MI (l) M-45, MI

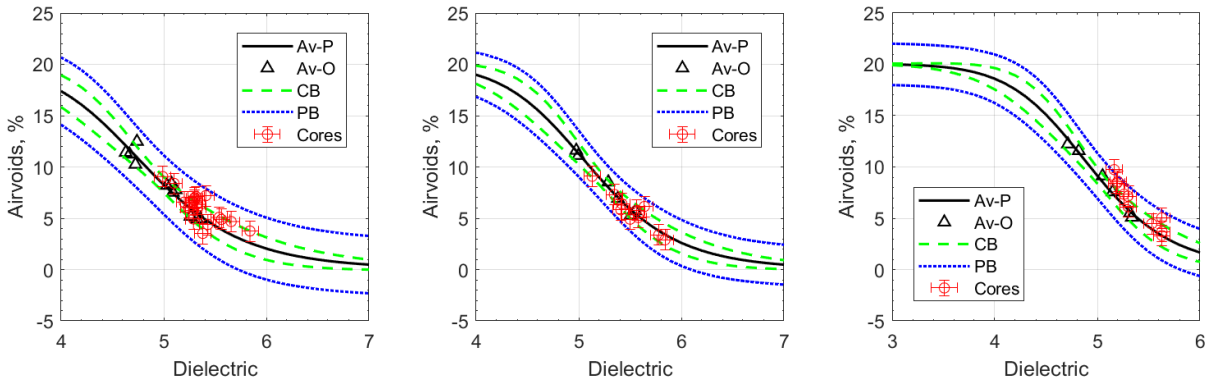

(m) M-61, MI (n) M-102, MI (o) M-153, MI

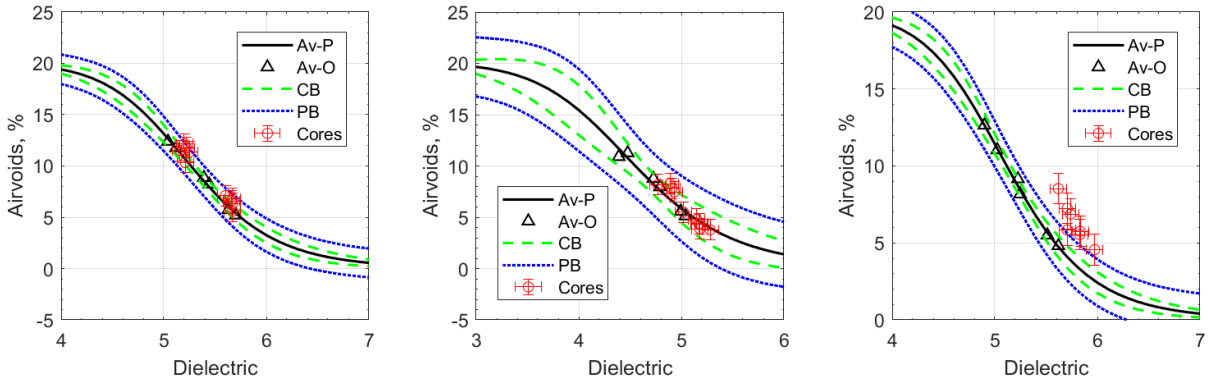

(p) US-10, MI (q) US-31 Allansen, MI (r) US-127, MI

Note: Av-P = Predicted air voids; Av-O = Observed air voids; CB = 95% confidence bands; PB = 95% prediction bands

Figure 3-12 (cont'd)

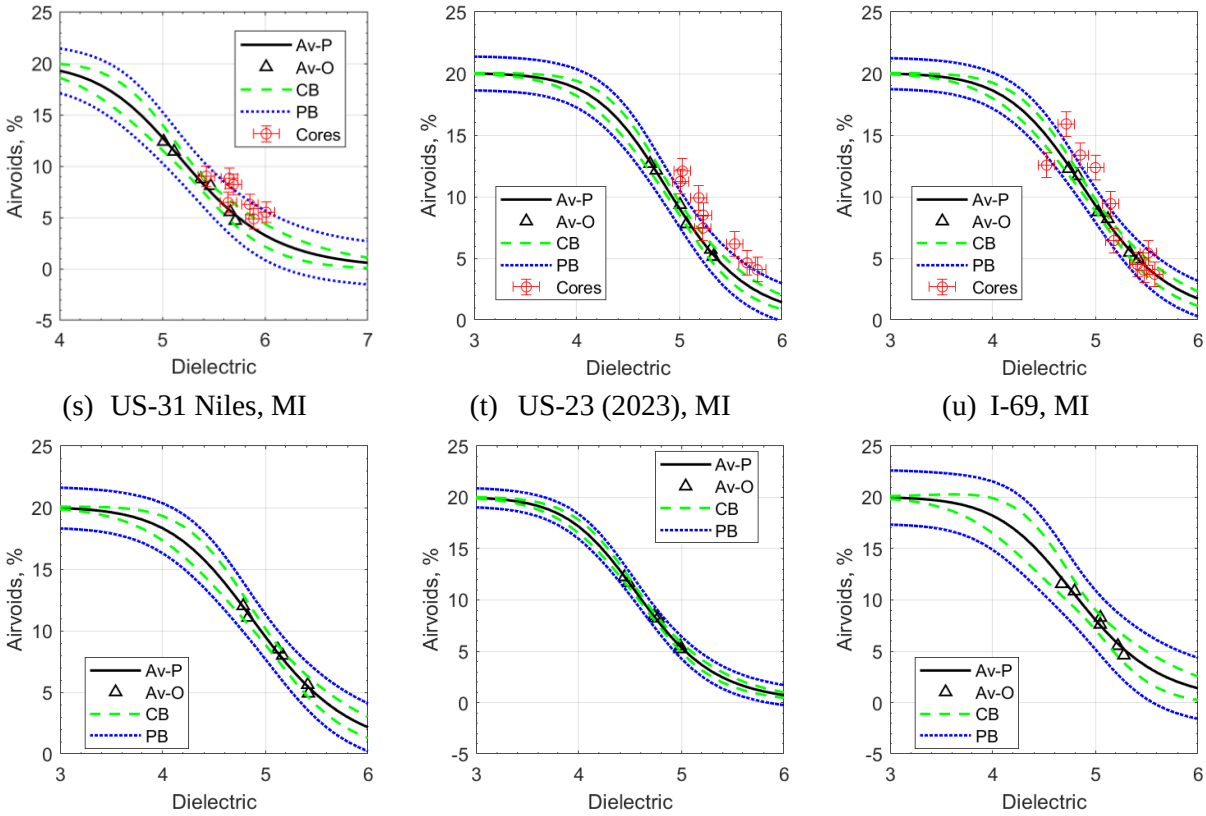

(s) US-31 Niles, MI (t) US-23 (2023), MI (u) I-69, MI

(v) M-89 (2023), MI (w) M-100, MI (x) Manning Trail, MN

Note: Av-P = Predicted air voids; Av-O = Observed air voids; CB = 95% confidence bands; PB = 95% prediction bands

Dielectric measurements were re-evaluated for selected samples (pucks and cores) from three of the six projects to investigate potential moisture presence during DPS field testing. These re-measurements occurred a couple of months after the initial testing during which the samples were stored at room temperature in the lab. The re-testing was conducted at the GSSI facility in New Hampshire using a different DPS unit than the one used in the original study. The re-testing process included dielectric measurements at three different temperatures. First, the dielectric values for every sample were repeated at room temperature. Next, the samples were frozen overnight at -40°C before dielectric measurements. Ice exhibits lower dielectric values (between 3 and 4) compared to ~81 for liquid water (*36; 40; 41*). This dielectric value reduction is due to the differences in the molecular arrangement and mobility of liquid and frozen water. Measuring the dielectric values of frozen samples aimed to minimize the influence of water on dielectric values that might be present within the HMA matrix. Finally, the samples were heated at 50°C for 8 hours to observe their dielectric response at elevated temperatures.

Figure 3-13 shows the dielectric responses of the HMA puck and core samples for the US-127 project and core sample responses for the US-31 (Niles) project. For the US-127 project, Figure 3-13(a) shows that the dielectric values of the pucks, measured initially at room temperature (21°C) in the laboratory and later remeasured at GSSI, were consistent and within a 0.08 difference for Pucks 2 and 4. However, Puck 5 exhibited a slightly more significant discrepancy between the two sets of measurements. Nonetheless, it can be inferred that DPS measurements are repeatable.

When comparing the dielectric values measured at frozen conditions (-40°C) to those at room temperature (Rep.) of 21°C, there was a slight reduction in dielectric values. However, these differences were minor, i.e., within 0.08. Conversely, the dielectric values slightly increased when measured at 50°C compared to the room temperature values, but again, the difference remained within 0.08. On average, the dielectric values showed a linear increase of 0.007 to 0.009 for every 10°C rise in temperature from -40°C to 50°C. Given that these changes are lower than 0.08, it can be concluded that the puck dielectric values remained nearly constant across the three different temperatures.

In Figure 3-13(b), the dielectric values for the US-127 project cores show a significant increase (ranging from 0.34 to 0.47) when these were remeasured at GSSI at 21°C compared to the initial field (spot) testing. This substantial change likely resulted from the HMA surface not being completely dry during the field measurements. While one might reason that the temperature increase during field testing could be responsible, this is unlikely. The dielectric differences between measurements at 21°C and 50°C are minimal, ranging from -0.012 to 0.012, well within the ±0.08 range. Since field measurements were also conducted at approximately 50°C (122-124°F), data does not support the hypothesis that higher temperatures caused the increase in dielectric values. The differences between dielectric values recorded at -40°C and 50°C are between 0.039 and 0.078, also below the 0.08 threshold. On average, the dielectric values of the cores changed by 0.002 to 0.009 for every 10°C increase in temperature from -40°C to 50°C.

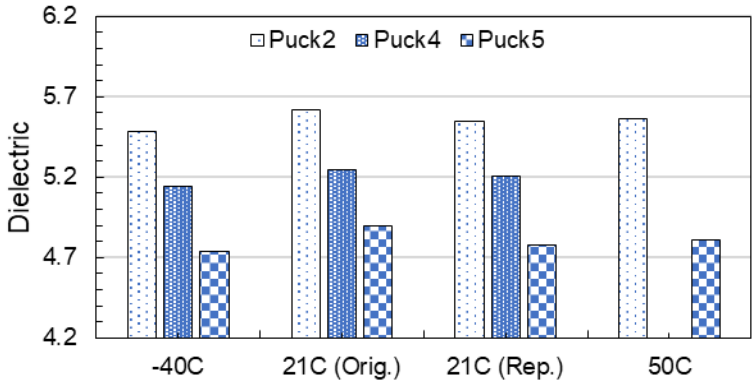

(a) Puck dielectric measurements – US-127, MI

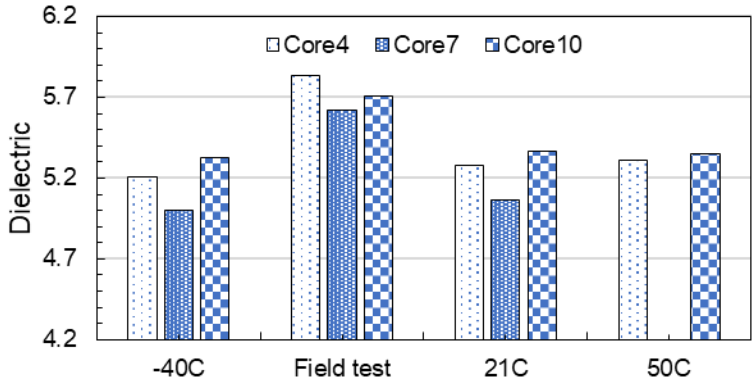

(b) Core dielectric measurements – US-127, MI

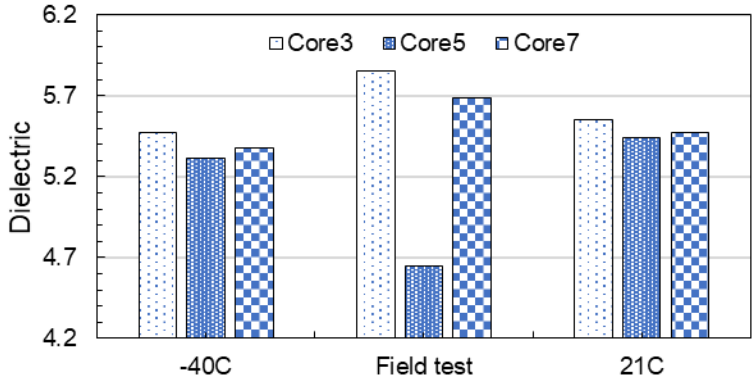

(c) Core dielectric measurements – US-31 project (Niles), MI

Figure 3-13 Dielectric measurements at different temperatures

In Figure 3-13(c), the core dielectric values for the US-31 (Niles) project show a significant reduction (ranging from 0.20 to 0.30) when remeasured, which could indicate that the initial field measurements were likely taken on an HMA surface that wasn't completely dry. Additionally, the dielectric differences exceeded the 0.08 threshold when measured at -40°C compared to room temperature (21°C), with the change estimated at 0.016 for every 10°C increase from -40°C to 21°C. This change in dielectric values for the US-31 (Niles) project is higher than that observed in the US-127 project, suggesting the presence of residual moisture

trapped within the HMA matrix—specifically between the aggregate and binder coating (i.e., moisture absorbed by the aggregates)—that persisted even months after the initial field testing and core extraction.

Figure 3-14 shows the dielectric values measured at various temperatures for the pucks and cores of the M-26 project. In Figure 3-14(a), the puck data reveals minimal differences between the original dielectric values (Orig.) measured at 21°C and those remeasured at GSSI. The differences at 21°C are within 0.08 for pucks 1 and 6, although slightly higher for puck 10. Despite using different DPS equipment for these measurements, this consistency indicates that dielectric values are generally repeatable even when a different DPS device is utilized.

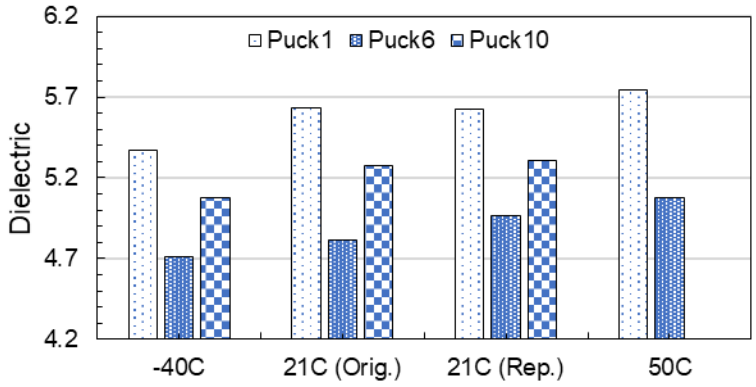

(a) Puck dielectric measurements

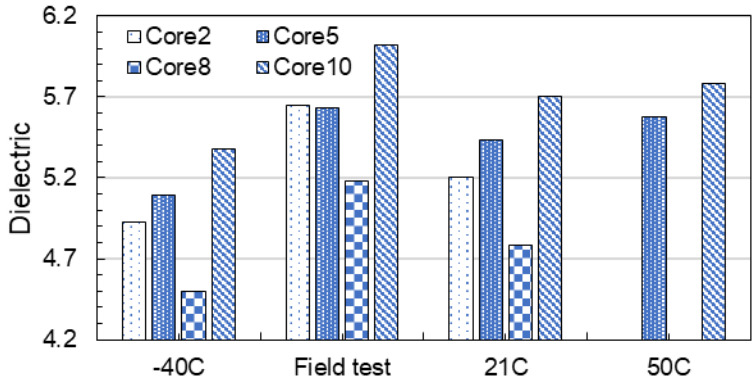

(b) Core dielectric measurements

Figure 3-14 Dielectric measurements at different temperatures – M-26 project, MI

For the pucks, Figure 3-14(a) indicates that dielectric values at -40°C are significantly lower, by 0.23 to 0.26, compared to those at 21°C. When the temperature increased from 21°C to 50°C, the dielectric values rose by 0.10 to 0.12. On average, there was a 0.04 increase in dielectric values for every 10°C rise from -40°C to 21°C. This rate of change is about 2.5 times higher than that observed in the US-31 (Niles) cores. Note that the pucks were fabricated by

reheating the loose mix in the laboratory, and the dielectric values were measured before determining the puck air void contents. Therefore, the changes in dielectric values are likely due to aggregate-absorbed moisture trapped within the binder-coated matrix.

For the cores, Figure 3-14(b) shows a significant reduction in dielectric values between the field measurements and those remeasured at GSSI at 21℃, with reductions ranging from 0.20 to 0.45. This suggests the presence of moisture during field testing. Comparing dielectric values at room temperature (21℃) and -40℃, a reduction of 0.27 to 0.38 is observed. When comparing dielectric values recorded at 21℃ and 50℃, an increase of 0.08 to 0.15 is seen. On average, core dielectric values changed by 0.045 for every 10℃ change from -40℃ to 50℃, about 2.8 times higher than the change observed in the US-31 (Niles) cores. In part, the initial reduction in core dielectric values between field-recorded and remeasured values at 21℃ at GSSI indicates moisture presence during field testing due to the rolling operation. However, the significant core and puck differences (on the order of about 0.04 change for every 10℃ rise from -40℃ to 50℃), observed at various temperatures suggest the presence of residual aggregate-absorbed moisture within the HMA matrix, persisting even months after initial field testing and core extraction, reheating in case of pucks.

As is known, highly absorptive aggregates can retain water longer and thus require adequate heating time before being mixed with asphalt binder to produce an HMA. However, suppose they are not heated for sufficient time during the HMA production process. In that case, aggregate-absorbed moisture is entrapped between the aggregate and the binder coating, which may lead to stripping even with adequate road drainage. The results from the dielectric measurements conducted at different temperatures show the DPS (and GPR technology) ability to detect aggregate-absorbed moisture within the HMA matrix entrapped by the binder coating using field cores or laboratory-prepared pucks. This could be important in forensic investigation to determine stripping causes in cases where the pavement is adequately drained.

Figure 3-15 presents the calibrated dielectric-air void relationships for the US-27, US-31 (Niles), and M-26 projects. The figure compares the core dielectric values measured in the field with their corrected values, measured at GSSI at 21℃. Notably, the corrected core dielectric values are lower than the field-recorded values and align well with the model's predictions based on puck dielectric values. This alignment validates the model and supports the presence of moisture in the asphalt mix during field DPS testing for these projects. Moreover, these findings

highlight the need for caution when using DPS for compaction evaluation of asphalt pavements during construction. It is crucial to allow sufficient time for the evaporation of water sprayed during the rolling operation before commencing DPS testing to ensure the recording of accurate dielectric values.

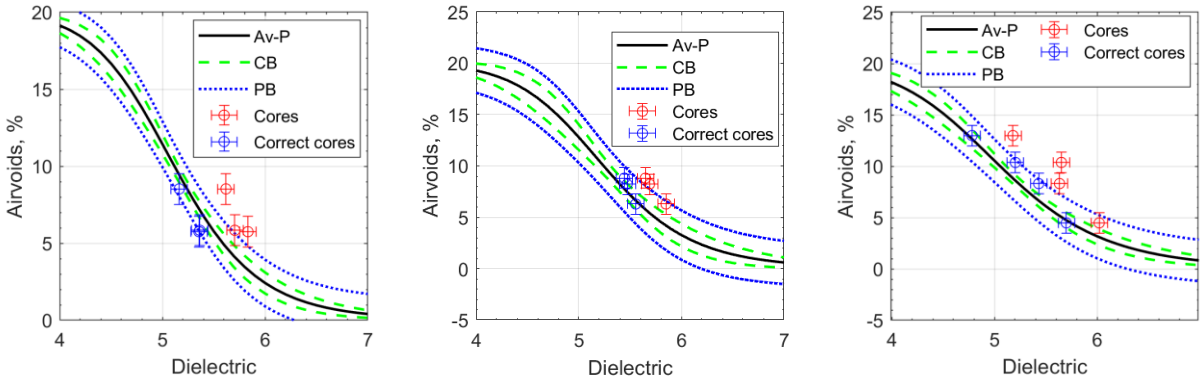

(a) US-127, MI (b) US-31 (Niles), MI (c) M-26, MI

Note: Av-P = Predicted air voids; Av-O = Observed air voids; CB = 95% confidence bands; PB = 95% prediction bands

Figure 3-15 Validation of calibrated models after corrected core dielectric values

3.3.4 Group-Wise Calibration

For optimal use of the DPS, it will be beneficial that the recorded dielectric values are directly integrated into the QA process during construction without the need for calibration. This can be achieved by establishing a comprehensive database of all the agency's HMA mixes and determining the minimum acceptable mat and joint dielectric values that can be referred to during field compaction evaluation during construction. These values could be determined based on a single model calibrated group-wise for mixes with similar aggregates and binders (i.e., sources and proportions) that exhibit similar dielectric-air void relationships. Hoegh et al. have previously demonstrated cases where data can be consolidated for a single calibration relationship (*6*).

For classifying the different HMA mixes into groups based on the recorded dielectric values and HMA mix characteristics, a machine-learning algorithm known as Classification and Regression Trees (CART®) was used. CART analysis is an advantageous tool for identifying critical patterns and relationships between continuous responses and predictors utilizing non-parametric methods, particularly when the data does not follow a certain distribution. Moreover, CART analysis facilitates the interpretation of complex relationships by displaying them in

visually comprehendible formats, making the process simpler and more straightforward and interpretation (*42*).

Before conducting the CART analysis, it was essential to determine the mix characteristics for grouping the various available HMA mixtures. Thus, a correlation analysis was performed. This analysis considered the mix's maximum specific gravity (G_{mm}), the aggregate's effective specific gravity (G_{se}), the aggregate's bulk specific gravity (G_{sb}), the lab-measured bulk specific gravity of the mix (G_{mb_M}), binder percentage (P_b), and the percentage passing the No. 4 and No. 200 sieves. The results in Table 3-8 indicate that G_{mm}, P_b, and the percentage passing the No. 4 and No. 200 sieves are appropriate HMA mix characteristics for the CART analysis. Other mix characteristics were excluded as they exhibited a strong correlation (>0.80) with one of these four parameters or with each other.

Table 3-8 Results of the correlation analysis

Mix characteristic	Dielectric	G_{mm}	G_{se}	G_{sb}	G_{mb_M}	Pb (%)	P No.4 (%)
G_{mm}	0.603	-	-	-	-	-	-
G_{se}	0.622	0.954	-	-	-	-	-
G_{sb}	0.618	0.965	0.978	-	-	-	-
G_{mb_M}	0.896	0.571	0.547	0.557	-	-	-
Pb (%)	-0.041	-0.323	-0.025	-0.135	-0.180	-	-
P No.4 (%)	-0.312	-0.519	-0.524	-0.601	-0.325	0.108	-
P No. 200 (%)	0.428	0.341	0.517	0.520	0.216	0.497	-0.409

Note: (-) No data.

Figure 3-16 displays the optimal tree from the CART analysis, showing that G_{mm} and the percentage passing the No. 200 sieve alone can categorize the tested HMA mixtures into four groups. Figure 3-17 presents the group-wise dielectric-air void relationships and their correspondence to the individual project calibration curves. Note that the I-94 SMA project is not part of any groups. That is because the CART analysis categorized the project's SMA mix as entirely different from the other mixtures. And since it was the only project within its CART-based classification, it was excluded from the group-wise calibration process. Observing the group-wise calibration curves, one can infer that the combined model (for a group) should reasonably predict the air voids as long as the HMA mix's characteristics remain within the limits identified by the CART analysis. Moreover, developing and using the group-wise calibration curves can reduce the need for individual calibrations, enhancing the usage and applicability of the DPS in the field.

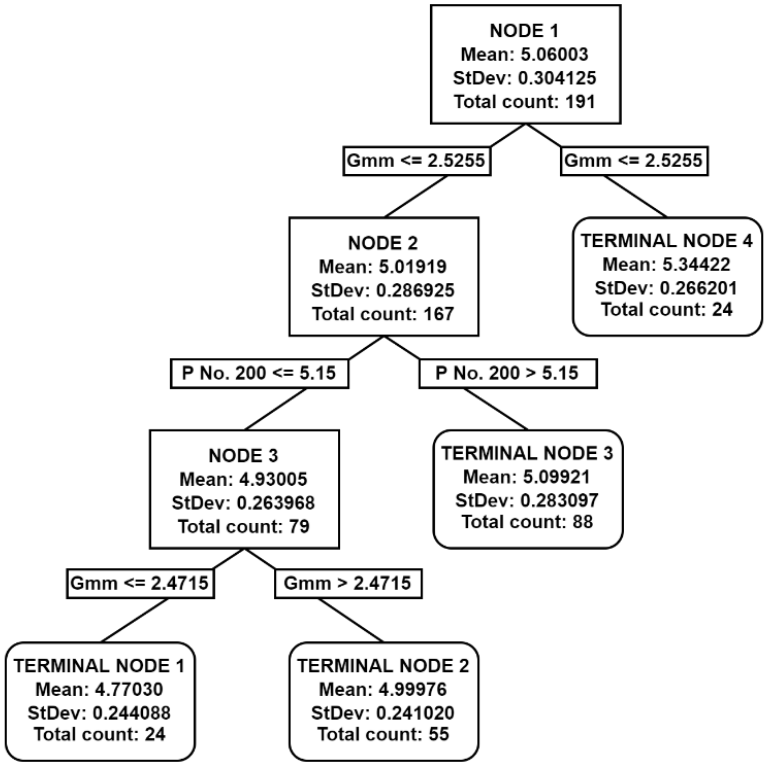

Figure 3-16 Optimal tree diagram for recorded dielectric values and selected HMA mix characteristics

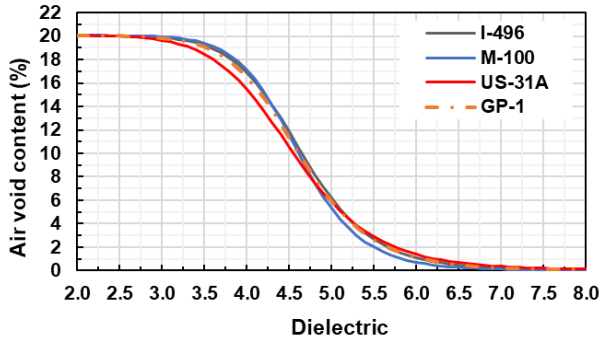

Projects	Mix type	Binder grade
I-496	5EMH	PG64-28
M-100	5EML	PG64-28
US-31A	5EML	PG64-34P[1]

(a) Group 1

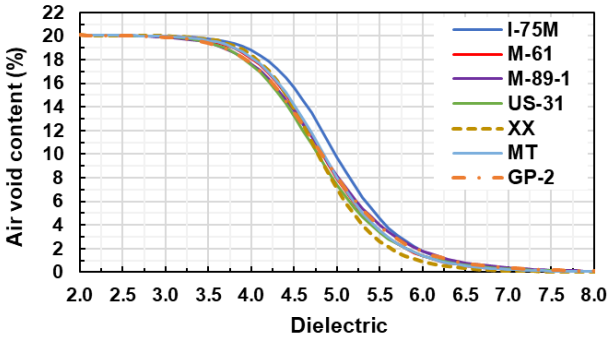

Projects	Mix type	Binder grade
I-75M	5EMH	PG64-34P
M-61	4EL	PG64-28
M-89	5EL	PG58-28
US-31	4EMH	PG64-28
XX Rd	SPWEB340(R)	PG58S-282
M.Tr.	SPWEB340(R)	PG58H-343

(b) Group 2

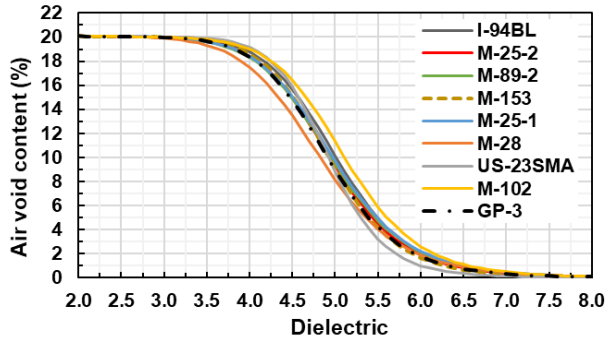

Projects	Mix type	Binder grade
I-94BL	5EML	PG64-28
M-25	5EL	PG58-28
M-89	5EML	PG64-28
M-153	5EML	PG64-28
M-25	5EML	PG64-28
M-28	5EML	PG58-34
US-23	SMA	PG70-28P
M-102	5EMH	PG70-28P

(c) Group 3

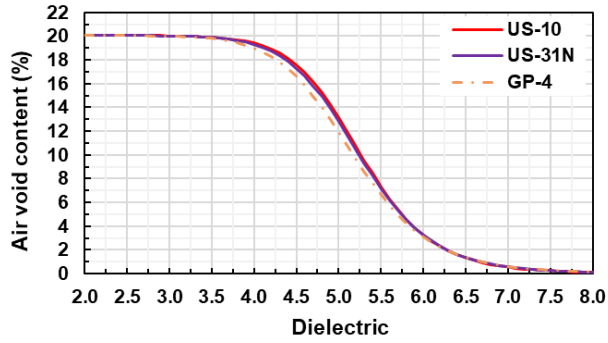

Projects	Mix type	Binder grade
US-10	5EMH	PG64-28
US-31N	4EMH	PG64-28

(d) Group 4

[1] Polymer-modified asphalt binder; [2,3] Multiple stress creep recovery (MSCR) based designation for standard (S) and heavy (H) traffic loading.

Figure 3-17 Groupwise calibration of the dielectric-air void relationships

3.4 CHAPTER SUMMARY

This study utilizes PaveScan RDM v2.0, a DPS device developed by Geophysical Survey Systems Inc. (GSSI), which uses three GPR sensors and provides three dielectric profiles per DPS pass. The DPS data were collected at two pavement projects in Minnesota and 25 projects in Michigan. Each data collection involved testing the asphalt centerline longitudinal joint and the adjacent asphalt mat. Each of these projects used different HMA mix types and varying rolling patterns for asphalt layer compaction. They also built longitudinal joints between pavement lanes using varying joint configurations. In addition to the DPS field data collection, pavement cores, and loose HMA mix samples were also collected.

A new model was developed by modifying the regression-based MnDOT model using the information provided by the SSCs to convert dielectric into air voids. The new model has two parameters in contrast to the MnDOT model, which needed to estimate three parameters instead. With the advantage of estimating one less parameter, the parsimonious New Model predicts the air voids similar to the ones predicted by the MnDOT model. The collected loose mix samples were used to individually develop dielectric-air void relationships for each project and calibrate group-wise models. This was accomplished using the coreless calibration method, which utilizes laboratory-prepared pucks compacted using SGC. Additionally, pavement cores were collected to validate the calibrated models.

The project-wise puck calibration showed reasonable agreement with the extracted core data for most projects. Moreover, minor mix production fluctuations on different days do not impact the calibration curves between surface dielectric and air void content and hence predict similar density. Thus, inferring that the mix's calibration is reproducible and independent of the HMA production day. However, higher dielectric differences were observed for six projects even after spot dielectric measurements at the core locations before core extraction. This was hypothesized to result from HMA surfaces that were not completely dry during the DPS testing after being sprayed on with water by the compacting rollers.

Testing pucks and core samples from three (out of six) projects to remeasure their dielectric values after recording them in the field confirmed that hypothesis. Thus, care must be exercised to ensure the HMA surface is moisture-free before commencing DPS testing in the field. Furthermore, measuring the dielectric values of samples at room temperature (21°C), after freezing them overnight at -40°C, and after heating them to 50°C for eight hours was found to

detect aggregate-absorbed moisture entrapped by binder coating within the HMA mix. This capability of the GPR-based DPS can be beneficial in investigating HMA stripping in pavements with otherwise adequate drainage.

Finally, group-wise model calibration was explored for HMA mixtures classified based on their recorded dielectric values and mix characteristics using the machine-learning technique known as CART analysis. Comparing the individual project calibration curves with their respective group's calibrated model showed reasonable agreement. Group-wise calibration is particularly advantageous for determining the acceptable minimum joint and mat dielectric values, enabling the direct use of dielectric values in the field during testing without a model calibration. Moreover, developing and using group-wise calibration curves can simplify and enhance the field applicability and usage of DPS for QA and QC processes.

REFERENCES

1. Al-Qadi, I. L., Z. Leng, S. Lahouar, and J. Baek, "In-place hot-mix asphalt density estimation using ground-penetrating radar," *Transportation Research Record,* vol. 2152, pp. 19-27, 2010.
2. Leng, Z., *Prediction of in-situ asphalt mixture density using ground penetrating radar: theoretical development and field verification*. University of Illinois at Urbana-Champaign, 2011.
3. Leng, Z., I. L. Al-Qadi, and S. Lahouar, "Development and validation for in situ asphalt mixture density prediction models," *NDT & e International,* vol. 44, pp. 369-375, 2011.
4. Khazanovich, L., K. Hoegh, and R. Conway, "Non-destructive Evaluation of Bituminous Compaction Uniformity Using Rolling Density," 2017.
5. Sebesta, S., T. Scullion, and T. Saarenketo, *Using infrared and high-speed ground-penetrating radar for uniformity measurements on new HMA layers*. Transportation Research Board, 2013.
6. Hoegh, K., S. Dai, T. Steiner, and L. Khazanovich, "Enhanced Model for Continuous Dielectric-Based Asphalt Compaction Evaluation," *Transportation Research Record,* vol. 2672, pp. 144-154, 2018.
7. Teshale, E. Z., K. Hoegh, S. Dai, R. Giessel, and C. Turgeon, "Ground Penetrating Radar Sensitivity to Marginal Changes in Asphalt Mixture Composition," *Journal of Testing and Evaluation,* vol. 48, 2020.
8. AASHTO, "Asphalt Surface Dielectric Profiling System Using Ground Penetrating Radar, PP98-19," AASHTO, Washington, D.C., 2019.
9. MnDOT, *Density Profiling System Protocol.* Minnesota Department of Transportation. https://www.dot.state.mn.us/materials/dps/training.html. Accessed July 30, 2024.
10. GSSI, *PaveScan® RDM 2.0 Manual.* Geophysical Survey Systems, Inc. . https://www.geophysical.com/wp-content/uploads/2022/03/MN36-716E-PaveScan-RDM-2.0-System-User-Manual.pdf. Accessed July 30, 2024.
11. Hoegh, K., T. Steiner, E. Zegeye Teshale, and S. Dai, "Minnesota Department of Transportation case studies for coreless asphalt pavement compaction assessment," *Transportation Research Record,* vol. 2674, pp. 291-301, 2020.
12. Haider, S. W., H. B. Muslim, L. Khazanovich, M. E. Kutay, and B. Cetin, "BMP For Issues with Asphalt Centerline Joint and Intelligent Compaction for Local Agencies," Minnesota. Department of Transportation. Office of Research & Innovation, 2023.
13. Hoegh, K., R. Roberts, S. Dai, and E. Zegeye Teshale, "Toward core-free pavement compaction evaluation: An innovative method relating asphalt permittivity to density," *Geosciences,* vol. 9, p. 280, 2019.
14. Cooley, L. A., B. D. Prowell, M. R. Hainin, M. S. Buchanan, and J. Harrington, "Bulk specific gravity round-robin using the Corelok vacuum sealing device," National Center for Asphalt Technology (US), Washington, DC., 2002.

15. Leng, Z., "Prediction of in-situ asphalt mixture density using ground penetrating radar: theoretical development and field verification," University of Illinois at Urbana-Champaign, 2012.

16. Araujo, S., L. Delbreilh, L. Laguerre, H. Dumont, É. Dargent, and C. Fauchard, "Rock permittivity characterization and application of electromagnetic mixing models for density/compactness assessment of HMA by means of step-frequency radar," *Near Surface Geophysics,* vol. 14, pp. 551-562, 2016.

17. Fernandes, F. M., A. Fernandes, and J. Pais, "Assessment of the density and moisture content of asphalt mixtures of road pavements," *Construction and Building Materials,* vol. 154, pp. 1216-1225, 2017.

18. Saarenketo, T., and T. Scullion, "Road evaluation with ground penetrating radar," *Journal of applied geophysics,* vol. 43, pp. 119-138, 2000.

19. Hoegh, K., L. Khazanovich, S. Dai, and T. Yu, "Evaluating asphalt concrete air void variation via GPR antenna array data," *Case Studies in Nondestructive Testing and Evaluation,* vol. 3, pp. 27-33, 2015.

20. Maser, K., and A. Carmichael, "Ground penetrating radar evaluation of new pavement density," Washington (State). Dept. of Transportation. Office of Research and Library, 2015.

21. Rashidi, M., and H. Azari, "On the Empirical Relationships Between the Air Content and Dielectric Constant of Hot-Mix Asphalt."

22. Steiner, T., K. Hoegh, E. Z. Teshale, and S. Dai, "Method for assessment of modeling quality for asphalt dielectric constant to density calibration," *Journal of Transportation Engineering, Part B: Pavements,* vol. 146, p. 04020054, 2020.

23. Dolan, K. D., and D. K. Mishra, "Parameter Estimation in Food Science," *Annual Review of Food Science and Technology,* vol. 4, pp. 401-422, 2013.

24. Beck, J. V., and K. J. Arnold, *Parameter estimation in engineering and science*. James Beck, 1977.

25. Geeraerd, A., V. Valdramidis, and J. Van Impe, "GInaFiT, a freeware tool to assess non-log-linear microbial survivor curves," *International Journal of Food Microbiology,* vol. 102, pp. 95-105, 2005.

26. Dolan, K., "Estimation of kinetic parameters for nonisothermal food processes," *Journal of Food Science,* vol. 68, pp. 728-741, 2003.

27. Mishra, D. K., K. D. Dolan, J. V. Beck, and F. Ozadali, "Use of scaled sensitivity coefficient relations for intrinsic verification of numerical codes and parameter estimation for heat conduction," *Journal of Verification, Validation and Uncertainty Quantification,* vol. 2, p. 031005, 2017.

28. Singh, R. R., "Local Calibration of Pavement-ME Performance Models Using Maximum Likelihood Estimation," In *Civil and Environmental Engineering Department,* Ph.D. Dissertation - Michigan State University, East Lansing, MI, 2024.

29. Lali, F. A., "Comparison Between Pavement Mechanistic-Empirical Design Approaches for Rubblized Pavements in Michigan," In *Civil and Environmental Engineering Department*, MS Thesis - Michigan State University, East Lansing, 2023.

30. Seasholtz, M. B., and B. Kowalski, "The parsimony principle applied to multivariate calibration," *Analytica Chimica Acta,* vol. 277, pp. 165-177, 1993.

31. Gauch, J. H. G., Parsimony and efficiency. In *Scientific Method in Brief,* Cambridge University Press, Cambridge, 2012, pp. 174-198.

32. MDOT, "HMA Production Manual," Construction Field Services, Michigan Department of Transportation, Lansing, MI, 2020.

33. Wilson, B., S. Sebesta, and T. Scullion, "Evaluation of the Rolling Density Meter for Rapid Continuous Measurement of Asphalt Mixture Density," 2019.

34. Hector, L., and H. Schultz, "The dielectric constant of air at radiofrequencies," *Physics,* vol. 7, pp. 133-136, 1936.

35. Zeng, Z.-f., S.-X. Liu, and X. Feng, "Ground Penetrating Radar Theory and Applications," *Publishing House of Electronics Industry,* 2010.

36. Davis, J. L., and A. P. ANNAN, "Ground-penetrating radar for high-resolution mapping of soil and rock stratigraphy 1," *Geophysical Prospecting,* vol. 37, pp. 531-551, 1989.

37. Lunt, I. A., S. S. Hubbard, and Y. Rubin, "Soil moisture content estimation using ground-penetrating radar reflection data," *Journal of Hydrology,* vol. 307, pp. 254-269, 2005.

38. Cao, Q., and I. L. Al-Qadi, "Effect of moisture content on calculated dielectric properties of asphalt concrete pavements from ground-penetrating radar measurements," *Remote Sensing,* vol. 14, p. 34, 2022.

39. Evans, R., M. Frost, and R. Morrow, *Assessing the influence of moisture on the dielectric properties of asphalt.* IEEE.

40. Evans, S., "Dielectric properties of ice and snow–a review," *Journal of Glaciology,* vol. 5, pp. 773-792, 1965.

41. Camp, P. R., and D. J. Halchin, *Electrical Properties of Ice-Solid Interfaces.* National Research Council, Transportation Research Board, Special Report, Hanover, New Hampshire185.

42. Gong, H., Y. Sun, X. Shu, and B. Huang, "Use of random forests regression for predicting IRI of asphalt pavements," *Construction and Building Materials,* vol. 189, pp. 890-897, 2018.

CHAPTER 4 - METHODS AND DPS DATA ANALYSIS

4.1 METHODS FOR DATA ANALYSIS

Various methods are used in practice for constructing longitudinal joints between adjacent lanes, each with advantages and disadvantages in achieving the desired compaction levels. However, each technique carries some risk regarding the joint's overall quality and long-term performance. Thus, to investigate the compaction ability of the different joint types and construction techniques, the dielectric measurements provided by the DPS were utilized to evaluate as-constructed compaction quality. DPS records a dielectric value every six inches per sensor, equating to about 6,000 data points recorded on every DPS pass (with three sensors) within a 1,000 ft section. The continuous dielectric data were visualized using line plots, histograms, and box plots to assess relative compaction differences between the joint and the adjacent asphalt mat. Additionally, statistical and probabilistic approaches were applied after segmenting the data into subsections of varying lengths (i.e., 25, 50, 100, and 200 ft) to conduct a more detailed analysis. This approach further aided in identifying potential compaction differences between the joint and mat, allowing for a comparison of different joint construction techniques.

4.1.1 Statistical Approaches

The discretized data were analyzed statistically using two approaches: (1) paired *t*-tests and (2) percent within limits. A description of each of these approaches is as follows:

Paired t-tests

A paired *t*-test is an inferential statistics procedure that compares samples of two related groups to determine whether their means significantly differ and, thus, conclude about populations. Paired *t*-tests are particularly useful when the datasets are paired meaningfully, such as before and after measurements conducted on the same subjects or two measurements taken simultaneously on the same material but at different locations. Accounting for the natural pairing within the data sets, a paired *t*-test provides a more precise comparison by eliminating some of the variability within unpaired data sets.

The paired *t*-test works by calculating the difference between each pair of observations and determining if their average difference is significantly different from a hypothesized value (zero or another specific value). Equation 4-1 and Equation 4-2 are used to calculate the individual pairs' differences and their mean difference, while Equation 4-3 and Equation 4-4 are

used to calculate the test statistic (*t*-value). Using the *t*-value, the degrees of freedom (computed using Equation 4-5), and a desired significance level (α), the *p*-value is determined. The *p*-value shows the probability of obtaining test results as extreme as the observed ones, assuming that the null hypothesis (H_0) is true. If the obtained *p*-value is less than the desired significance level ($p < \alpha$), the H_0 is rejected, indicating a statistically significant difference between the two paired groups and that the alternate hypothesis (H_a) is true.

$$d_i = X_i - Y_i \quad \text{Equation 4-1}$$

$$\bar{d} = \frac{1}{n}\sum_{i=1}^{n} d_i \quad \text{Equation 4-2}$$

$$s_d = \sqrt{\frac{1}{n}\sum_{i=1}^{n}\left(d_i - \bar{d}\right)^2} \quad \text{Equation 4-3}$$

$$t = \frac{\bar{d} - \mu_0}{\frac{s_d}{\sqrt{n}}} \quad \text{Equation 4-4}$$

$$df = n - 1 \quad \text{Equation 4-5}$$

where;

d_i = difference between the any two paired observations,

X_i = value of the first variable,

Y_i = value of the second variable,

$\bar{d}$ = mean difference,

n = number of pairs,

s_d = standard deviation of the differences,

μ_0 = hypothesized difference (either zero or another specific value),

$\frac{s_d}{\sqrt{n}}$ = standard error of the mean difference,

df = degrees of freedom.

This study used an air void content of 8% as the upper threshold for the asphalt mat, with the corresponding upper limit for the longitudinal joint set at 10%. This joint limit aligns with the commonly accepted joint density criterion, which specifies that the joint density should not exceed a 2% reduction compared to the mat density. Table 3-7 presents the project-specific dielectric values corresponding to 8% and 10% air voids. The table also contains the relative

dielectric differences that would result in a 2% or greater air void difference between the joint and the mat for each project.

Paired *t*-tests were conducted to analyze the mean dielectric values for each subsection statistically, testing the null hypothesis that the mean dielectric difference between the mat and the joint results in an air void difference exceeding 2%. Suppose that, for any specific project, a dielectric difference *x* (as in Table 3-7) leads to an air void difference greater than 2%; the H_0 and H_a for the paired *t*-test would be formulated as shown in Equation 4-6 and Equation 4-7, respectively.

$$H_0 : \bar{d} = x \qquad \text{Equation 4-6}$$

$$H_a : \bar{d} > x \qquad \text{Equation 4-7}$$

Percent Within Limits

Percent within limits (PWL) and percent defective (PD) are widely recognized quality assurance measures, gaining popularity due to their effectiveness in simultaneously assessing both the mean and variability of data (*1; 2*). In this study, PWL is also employed to compare the compaction quality achieved at the joint, for various longitudinal joint construction methods. The PWL is defined as "*the percentage of the lot falling above the lower specification limit (LSL), beneath the upper specification limit (USL), or between the LSL and the USL*" (*3*). The calculation of PWL relies on the quality index, also known as the Q-value, which measures the distance of the sample mean from the specification limit in units of the sample's standard deviation.

The Q-values for the upper and lower specification limits (USL and LSL) are determined using Equation 4-8Equation 4-9, respectively. Once the Q-values are calculated, the PWL is determined using tables or a beta distribution (*4*). One-sided PWL for the *LSL* uses Q_L value, while one-sided PWL for the *USL* is determined using Q_U. The two-sided PWL for specification limits where PWL_U represents the percentage below the *USL* (based on Q_U), PWL_L represents the percentage above the LSL (based on Q_L), and PWL_T is the percentage within the two determined using Equation 4-10. These are schematically illustrated in Figure 4-1.

$$Q_L = \frac{\bar{x} - LSL}{s} \qquad \text{Equation 4-8}$$

$$Q_U = \frac{USL - \bar{x}}{s} \quad \text{Equation 4-9}$$

$$PWL_T = PWL_U + PWL_L - 100 \quad \text{Equation 4-10}$$

where;

Q_L = quality index for *LSL*,

Q_U = quality index for *USL*,

$\bar{x}$ = sample mean,

s = sample standard deviation.

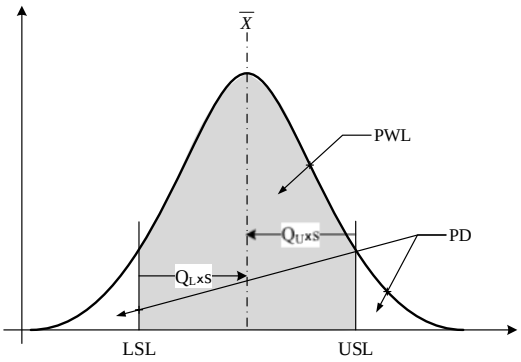

(a) PWL based on double-sided specification limits

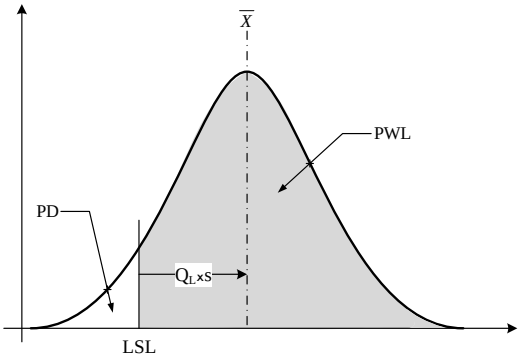

(b) PWL based on lower specification limits

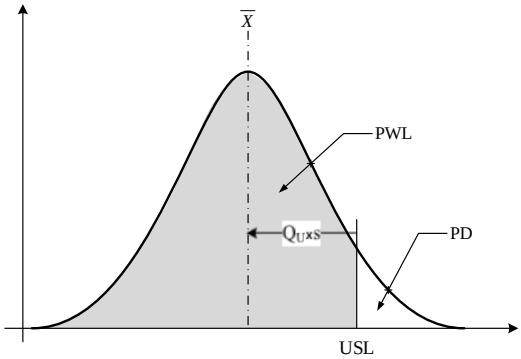

(c) PWL based on upper specification limits

Figure 4-1 Schematic illustrating the PWL and PD concept for different specification limits (*5*)

While the accuracy of PWL analysis improves with increased sampling, it requires balancing the cost of additional sampling and testing (*6*). Conventional compaction assessment methods often limit the sample size, but the higher sampling rate of the DPS makes PWL analysis more efficient and valuable. Even when sections are divided into smaller subsections, there are still enough data points to reliably determine PWL for each subsection, unlike traditional methods that rely on limited cores per lot of asphalt. Using continuous dielectric data,

one-sided PWL was calculated for both the mat and the joint, and the difference between them was calculated for each subsection.

The PWL for the mat and joint were calculated using project-specific *LSL* values, while the PWL for the mat–joint difference used a *USL* based on the difference between the mat's and joint's specified *LSL* values. The dielectric values corresponding to 8% air voids for the mat and 10% for the joint, as shown in Table 3-7, were used as *LSL* for each. Additionally, the dielectric difference values from the table, which are expected to result in more than a 2% air void difference between the joint and mat, were used as *USL* when calculating the difference-based PWL.

In any PWL-based acceptance plan that determines pay adjustments, specific quality acceptance thresholds, known as the acceptable quality level (AQL) and rejectable quality level (RQL), are essential. The AQL represents the minimum quality level at which the product is accepted, while the RQL defines the point at which it is rejected. In this study, an AQL of 90% is used per the AASHTO *Quality Assurance/Quality Control Guide Specification Status Report (7)*, and an RQL of 60% is used in the PWL analysis as a reference. Moreover, an acceptance limit of 60% was used.

4.1.2 Probabilistic Approach

In addition to statistical methods, a probabilistic approach using conditional probability was applied to compare various longitudinal joint construction methods. Conditional probability is the probability of an event occurring, given that another event has already occurred. More specifically, it measures how the likelihood of one event changes when information about another related event is available. This concept is vital in probability theory and helps refine predictions by incorporating additional information about related events. It is widely used in statistics, machine learning, and decision-making processes to improve accuracy by considering known outcomes or evidence-based analysis. Mathematically, the conditional probability of event A, given that event B has already happened, is denoted by $P(A|B)$. It is determined using Equation 4-11 where $P(A \cap B)$ represents the joint probability of the two events A and B happening together and $P(B)$ is the probability of event B occurring.

$$P(A|B) = \frac{P(A \cap B)}{P(B)} \qquad \text{Equation 4-11}$$

The dielectric values for each type of joint and its corresponding mat from each project section (not the subdivided data) were classified into ten groups, as shown in Table 4-1. Similarly, the predicted air void for each project using the project-specific calibrations were also divided into ten groups per Table 4-1. The conditional probability for each dielectric and air void category was calculated for both the mat and the joint using Equation 4-12. Equation 4-12 represents the condition probability equation (Equation 4-11) in the content of dielectric/air void values of the mat and the longitudinal joint. The conditional probabilities for a particular compaction level at the longitudinal joint (Event B) were determined, given that a specific compaction level had already been achieved at the asphalt mat (Event A). Consequently, a probabilistic comparison was then conducted to evaluate the compaction level achieved at the joint, given that the mat's density fell within a specific range.

$$P(Joint|Mat) = \frac{P(Joint \cap Mat)}{P(Mat)} \qquad \text{Equation 4-12}$$

Table 4-1 Categories used for probabilistic analysis

Category	Dielectric ranges	Air void ranges
1	< 4.6	≥ 18
2	≥ 4.6 < 4.8	≥ 16 < 18
3	≥ 4.8 < 5.0	≥ 14 < 16
4	≥ 5.0 < 5.2	≥ 12 < 14
5	≥ 5.2 < 5.4	≥ 10 < 12
6	≥ 5.4 < 5.6	≥ 8 < 10
7	≥ 5.6 < 5.8	≥ 6 < 8
8	≥ 5.8 < 6.0	≥ 4 < 6
9	≥ 6.0 < 6.2	≥ 2 < 4
10	≥ 6.2	< 2

4.2 PROJECTWISE DATA ANALYSIS

This section presents an example of project wise data analyses conducted to achieve this study's objectives. The subsequent sections will include the summarized results. As mentioned earlier, each DPS pass contains three dielectric profiles recorded at various offsets from each other. Figure 4-2 presents the recorded dielectric profiles collected at the Xerxes Road project in MN. In Figure 4-2(a) and (c), the dielectric profiles recorded by the sensor at 0.5 ft offset from both the unconfined joints (Xerxes Rd #1 and #2) show lower dielectric values throughout the section's length than the mat dielectric profiles recorded at 2 and 3.5 ft offsets from the joint. On

the contrary, Figure 4-2(b) shows that the three dielectric profiles measured at the confined joint and the corresponding asphalt mat are very similar.

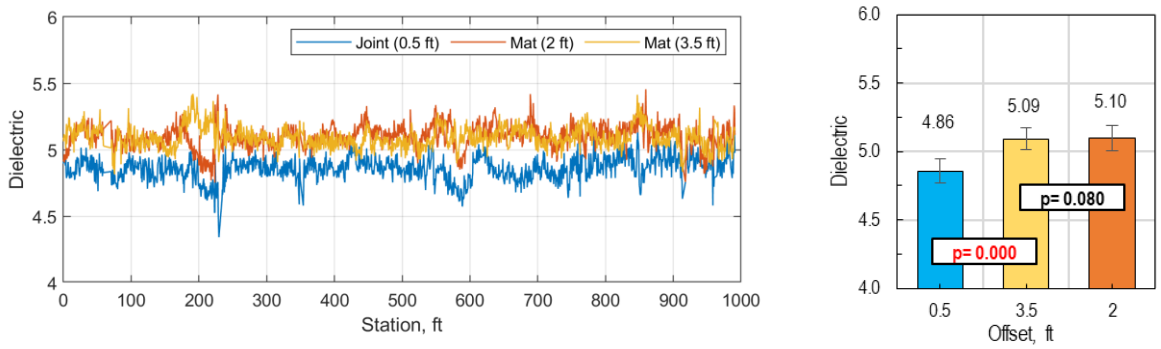

(a) Unconfined joint, Xerxes Road #1

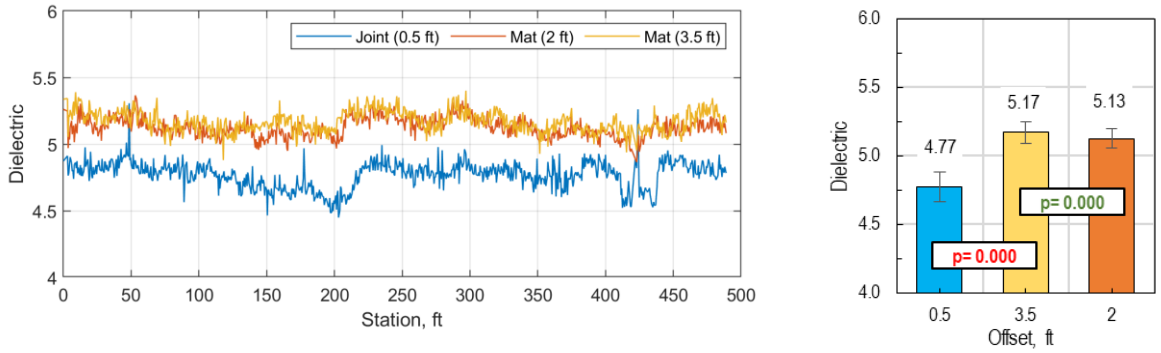

(b) Unconfined joint, Xerxes Road #2

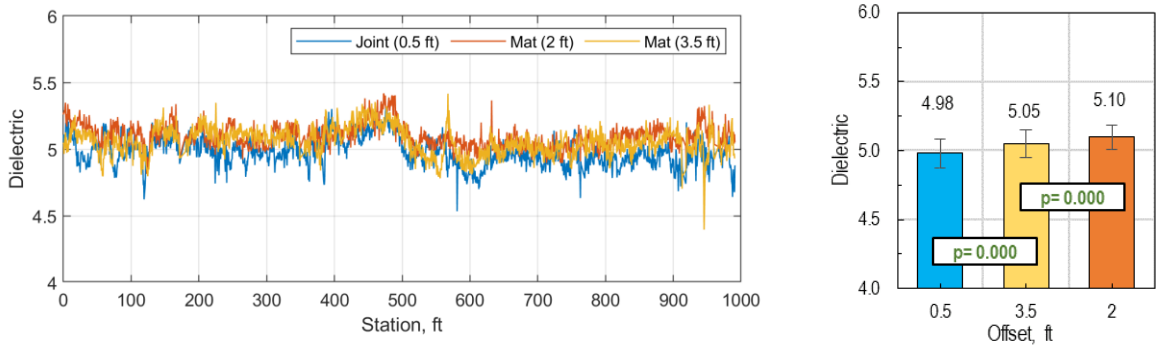

(c) Confined joint, Xerxes Road #1

Figure 4-2 Comparing dielectric values of confined and unconfined joints – Xerxes Road project

To further explore the dielectric differences, the figure also displays the mean values for each profile, along with their variation, represented by error bars (showing one standard deviation above and below the mean). This study compared joint dielectric values to mat dielectric values recorded at a 3.5 ft offset from the joint for the MN projects and at a 4.5 ft offset for MI projects. However, to ensure that any observed differences between the joint and the mat are attributed to variations in joint construction methods, rather than differences in overall

compaction effort, the mat dielectric profiles (measured at 2 ft and 3.5 ft offsets) were also compared for consistency.

The *p*-values shown on each pair of column bars indicate whether the two dielectric profiles are similar ($p > \alpha$) or dissimilar ($p < \alpha$), using a 5% significance level ($\alpha = 0.05$). These are color-coded as follows: (1) black font indicates no significant difference, (2) green font signifies a statistically significant difference but one that is practically insignificant (< 0.08), and (3) red font denotes both a statistically and practically significant difference. For instance, the mat dielectric values measured at 2 ft and 3.5 ft offsets while testing the unconfined joint at the Xerxes Road #1 project are statistically similar ($p = 0.080$). However, the profiles are statistically different when comparing the mat dielectric values at the same offsets for the unconfined and confined joints at Xerxes Road #1 and #2 projects, respectively ($p = 0.000$). Despite this, the mean dielectric difference between the two offsets (2 ft and 3.5 ft) is less than 0.08, which is within the acceptable range for dielectric variations as measured by air-coupled GPR sensors according to AASHTO guidelines (*8*). Therefore, while the profiles may be statistically different, they are practically similar based on dielectric variation thresholds.

Moreover, Figure 4-3 compares the dielectric values recorded over the asphalt mat using different offsets from the longitudinal joint. The figure shows each profile's mean dielectric values and variability, denoted by one standard deviation above and below it. The figure shows that the mean asphalt mat dielectric values are very similar and are within the range between 5.0 and 5.15, except for the profiles measured at the 19.5 ft offset. That is expected since the 19.5 ft values are recording dielectric values only 0.5 ft away from the outside joint of the road with a cement curb, which prohibits compaction at the edge. Thus, one can infer that there were no differences in the compaction effort on either day of construction.

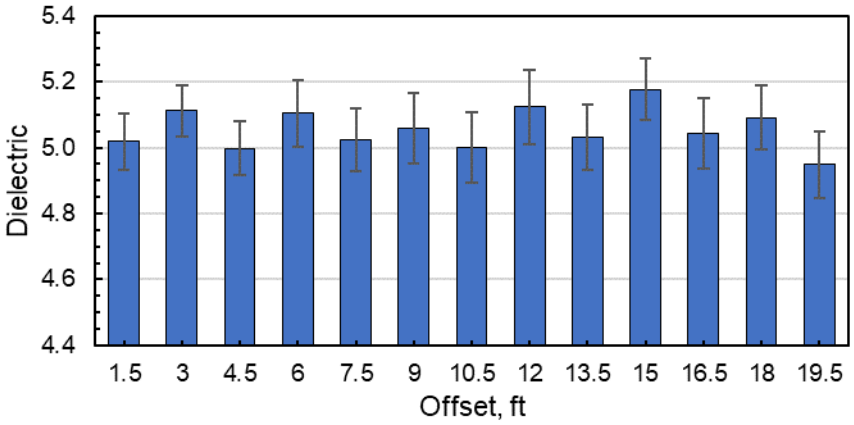

(a) Asphalt mat of 1st constructed lane, Xerxes Road #1

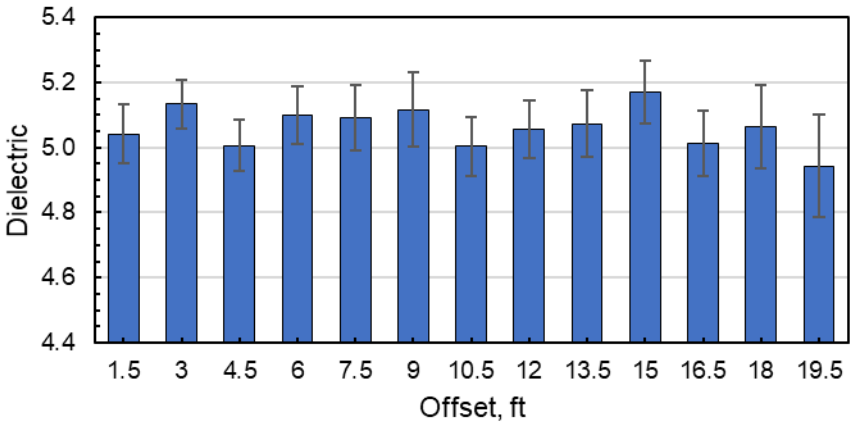

(b) Asphalt mat of 1st constructed lane, Xerxes Road #2

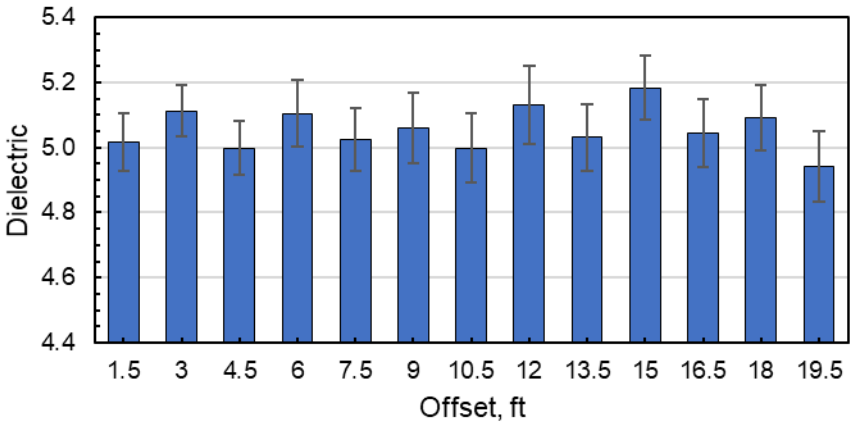

(c) Asphalt mat of 2nd constructed lane, Xerxes Road #1

Figure 4-3 Comparison of the asphalt mat dielectric values – Xerxes Road project

The unconfined joint dielectric values (i.e., values from 0.5 ft offset) are significantly different from those recorded at 3.5 ft offset (p = 0.000), with a practically large difference ranging between 0.23 and 0.4. However, the confined joint displays a statistical difference that is not practically significant (< 0.08). One can observe their distributions to understand further the

dielectric differences the three sensors recorded. Figure 4-4 shows the distribution of the dielectric values recorded at different offsets from the longitudinal unconfined joints of the Xerxes Road project. The figure also shows the distribution of differences between the recorded dielectric values at 3.5 ft and 0.5 ft offset (i.e., mat–joint). The figure shows that the mat dielectric values are similar and higher than 4.93, corresponding to less than 8% air voids. However, about a quarter to half of the dielectric values of the unconfined joints are lower than 4.78, corresponding to 10% air void.

Comparing the mat (3.5 ft offset) and the joint (0.5 ft offset) dielectric values, the mat dielectric values are higher than both of the unconfined butt joints values, with only a fraction of them overlapping throughout the section's length. This resulted in over half of the dielectric differences greater than 0.14, corresponding to greater than 2% air void differences between the mat and the joint. On the contrary, the mat and confined butt joint dielectric values are very similar, as seen in Figure 4-5. The figure shows that the dielectric values recorded at the three offsets are similar, with only a fraction of the dielectric differences greater than 0.14.

The dielectric trends illustrated by Figure 4-2 suggest that constructing a confined longitudinal joint by compacting against the edge of a previously built lane helps achieve better density at the seam rather than constructing an unconfined joint. The same can be observed from Figure 4-4 and Figure 4-5, which also reinforces (as Figure 4-2) that an unconfined joint construction may result in dielectric differences that would result in over 2% relative air void differences between the joint and the mat. While these figures illustrate that the unconfined joint results in relatively lower dielectric values (and higher air voids) than the accompanying mat compared to a confined joint, the data exhibits significant variability. Moreover, the analysis presented data from the whole section. However, the true utilization of the DPS's continuous data would be to discretize the data into subsections and undertake a more detailed analysis to fully understand the compaction ability differences between the various longitudinal joint types and construction methods.

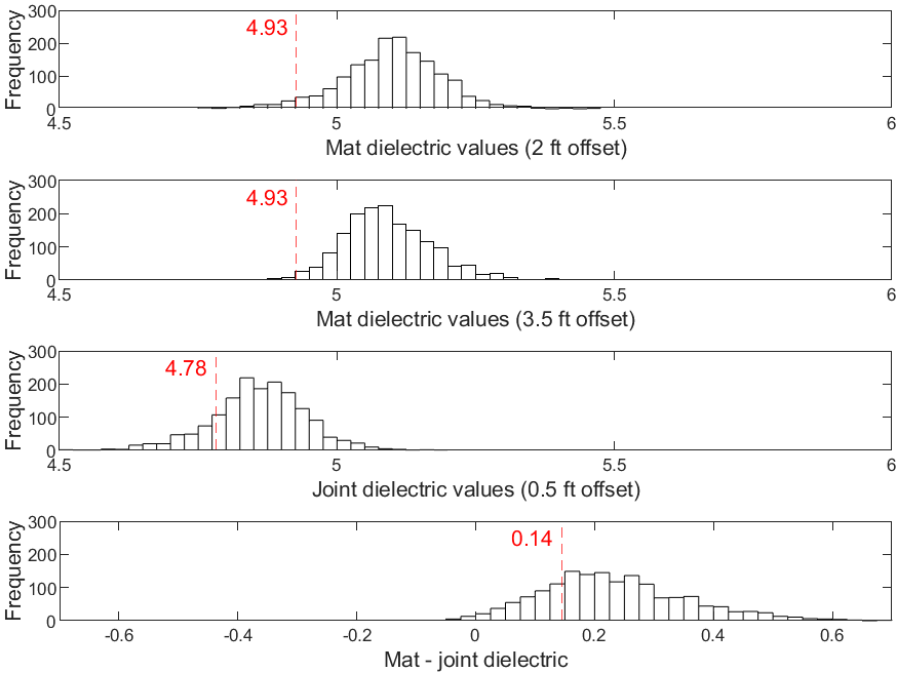

(a) Unconfined joint DPS pass, Xerxes Road #1

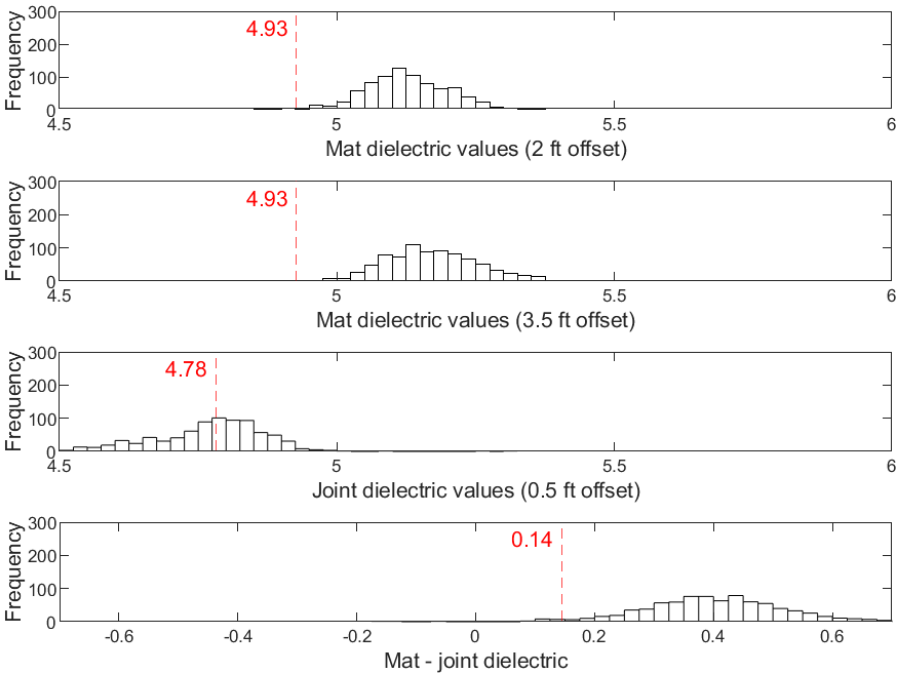

(b) Unconfined joint DPS pass, Xerxes Road #1

Figure 4-4 Dielectric value and their difference (3.5 ft – 0.5 ft offset) distributions of the two unconfined joints – Xerxes Road project

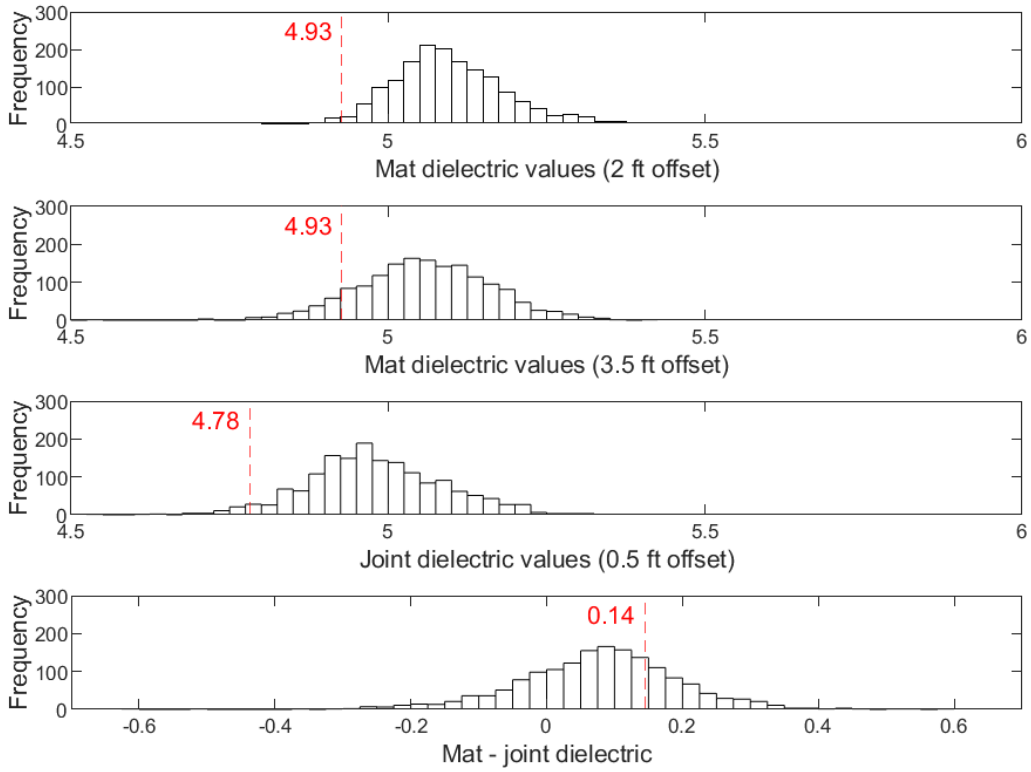

Figure 4-5 Dielectric value and their difference (3.5 ft – 0.5 ft offset) distributions of the confined joints – Xerxes Road project

4.2.1 Paired *t*-test Analysis

For in-depth data analysis of the recorded continuous dielectric profiles, the data from the two sections of the Xerxes Road project were discretized into smaller subsections 25, 50, 100, and 200 ft long. The discretization into different lengths was aimed at determining a suitable subsection length that could better explain the variability of the dielectric data and help differentiate areas with similar and dissimilar compaction. The mean dielectric values from each subsection were compared statistically using paired *t*-tests using the hypothesis discussed earlier to quantify the dielectric differences between a joint and its accompanying asphalt mat. Note that this study used the dielectric profiles measured at a 3.5 ft offset from the joint for the MN projects and a 4.5 ft offset for MI projects to compare with the joint dielectric values recorded 0.5 ft away from it. Table 4-2 presents the summarized *t*-test results for the unconfined butt joints of the Xerxes Road project. The data was divided into 25 ft subsections each. Out of the 40 *t*-tests (one per 25 ft subsection) of the Xerxes Road #1 project, about 78% revealed a significant difference ($p < \alpha$) between the joint and the accompanying mat, using a 5% Type 1 error rate ($\alpha = 0.05$). In comparison, all 20 (100%) subsections of the Xerxes Road #2 project displayed significant differences between the unconfined butt joint and mat dielectric values.

Table 4-2 Summary of *t*-tests for both unconfined joints of the Xerxes Road project

Subsection number	Unconfined joint – Xerxes Road #1				Unconfined joint – Xerxes Raod #2			
	No. of data points	Mean difference	Std.	*p*-value	No. of data points	Mean difference	Std.	*p*-value
1	43	0.26	0.09	0.000	32	0.49	0.09	0.000
2	42	0.25	0.08	0.000	41	0.38	0.08	0.000
3	30	0.28	0.07	0.000	42	0.36	0.10	0.000
4	35	0.24	0.11	0.000	42	0.32	0.10	0.000
5	42	0.19	0.09	0.001	41	0.34	0.08	0.000
6	41	0.24	0.08	0.000	42	0.38	0.09	0.000
7	42	0.16	0.07	0.178	42	0.49	0.07	0.000
8	42	0.35	0.13	0.000	41	0.46	0.10	0.000
9	41	0.47	0.08	0.000	42	0.58	0.08	0.000
10	36	0.44	0.12	0.000	42	0.44	0.08	0.000
11	42	0.22	0.08	0.000	41	0.43	0.07	0.000
12	41	0.19	0.06	0.000	42	0.39	0.10	0.000
13	42	0.20	0.08	0.000	42	0.40	0.07	0.000
14	42	0.24	0.07	0.000	41	0.38	0.09	0.000
15	35	0.25	0.12	0.000	42	0.35	0.09	0.000
16	42	0.19	0.07	0.000	42	0.37	0.12	0.000
17	42	0.21	0.07	0.000	41	0.32	0.10	0.000
18	41	0.10	0.06	1.000	37	0.42	0.30	0.000
19	42	0.20	0.07	0.000	42	0.27	0.11	0.000
20	42	0.17	0.07	0.026	41	0.42	0.08	0.000
21	41	0.21	0.07	0.000	No data.			
22	42	0.18	0.08	0.005				
23	42	0.30	0.13	0.000				
24	41	0.37	0.09	0.000				
25	42	0.26	0.14	0.000				
26	42	0.19	0.09	0.001				
27	41	0.31	0.10	0.000				
28	42	0.36	0.07	0.000				
29	42	0.20	0.09	0.000				
30	41	0.26	0.08	0.000				
31	41	0.26	0.09	0.000				
32	37	0.26	0.11	0.000				
33	41	0.16	0.07	0.065				
34	42	0.14	0.09	0.677				
35	42	0.37	0.11	0.000				
36	41	0.14	0.08	0.725				
37	38	0.16	0.08	0.193				
38	40	0.17	0.10	0.056				
39	35	0.15	0.13	0.337				
40	42	0.11	0.07	0.995				
Summary	31/40 *100 = 77.5%				20/20 * 100 = 100%			

Note: A *p*-value less than 0.05 ($\alpha = 0.05$) suggests that the mean dielectric difference between the mat and the joint is greater than 0.2 which corresponds to over 2% joint air voids as compared to the mat.

In contrast, the dielectric values for the confined joint from the Xerxes Road #1 project shown in Table 4-3 show no significant differences compared to the mat values ($p > \alpha$) for 95%

of the subsections. The results presented in both tables suggest that constructing an unconfined joint may result in higher than 2% relative air void differences between the joint and the mat. Moreover, building a confined joint produces joint densities that are comparable to those of the asphalt mat. This implies that constructing confined joints should be preferred whenever feasible.

4.2.2 PWL Analysis

Another statistical approach used to evaluate the compaction differences between the different joint types was to estimate the percent within limits for each subsection. Figure 4-6 shows the dielectric-based PWL for each 25 ft long subsection of the two unconfined joints with their accompanying asphalt mats of the Xerxes Road project. Reference AQL of 90% and RQL of 60% are also displayed. Figure 4-6(a) shows that for most subsections, the individual mat (recorded at 3.5 ft offset) and joint PWL values fall within acceptable limits at the Xerxes Raod #1 project. However, 38 out of the 40 subsections (95%) show unacceptable PWL based on the project's dielectric difference USL value of 0.14 (Table 3-7).

The PWL for the unconfined joint of the Xerxes Road #2 in Figure 4-6(b) shows that the individual mat has over 90% PWL for all subsections, and almost 50% (9 out of 20) of the subsections display below 60% PWL for the joint. However, PWL, based on the relative dielectric differences, exhibits that all subsections have near-zero PWL (all subsection PWLs are lower than the acceptance limit of 60%). These PWL results agree with those from the paired *t*-tests for this unconfined joint. Comparing the PWL results of the unconfined joints to those of the confined joint (shown in Figure 4-7), one can observe that only 18% (7 out of 40) subsections have PWL below 60% based on the dielectric differences. This percentage is considerably lower compared to those observed for the unconfined joint.

Thus, the PWL analysis also infers that constructing a confined joint will produce better joint densities, resulting in higher PWL than unconfined joints. Note that some of the PWL-based results contrast with the paired *t*-test findings. For instance, paired *t*-tests indicated that 78% (Table 4-2) and 5% (Table 4-3) of the subsections had a dielectric difference exceeding 0.14 between the mat and the joints (unconfined and confined) of the Xerxes Road #1 projects, respectively. However, the PWL results show 95% and 18% subsection with lower than 60% dielectric-difference-based PWLs for the same joints of the same project. This disagreement arises because the paired *t*-test focuses on statistically significant differences between mean values, while PWL reflects the probability of dielectric differences being less than 0.14.

Table 4-3 Summary of *t*-tests for confined butt joint of the Xerxes Road #1 project

Subsection no.	No. of data points, N	Mean difference	Standard deviation	*p*-value
1	43	-0.01	0.10	1.000
2	42	0.18	0.07	0.001
3	41	-0.06	0.12	1.000
4	42	0.06	0.14	1.000
5	42	0.01	0.08	1.000
6	41	0.04	0.14	1.000
7	42	0.05	0.10	1.000
8	29	0.01	0.08	1.000
9	41	0.12	0.08	0.983
10	42	0.14	0.11	0.713
11	42	0.15	0.07	0.345
12	41	0.15	0.08	0.379
13	42	0.12	0.07	0.984
14	42	0.11	0.08	0.993
15	32	0.12	0.09	0.949
16	42	0.07	0.17	0.998
17	42	0.03	0.10	1.000
18	41	0.09	0.08	1.000
19	42	0.09	0.08	1.000
20	42	0.02	0.06	1.000
21	41	0.10	0.07	1.000
22	42	-0.02	0.10	1.000
23	42	-0.06	0.15	1.000
24	41	0.13	0.14	0.766
25	42	0.10	0.08	0.999
26	42	0.09	0.07	1.000
27	41	0.04	0.07	1.000
28	42	0.08	0.07	1.000
29	42	0.07	0.07	1.000
30	41	0.07	0.11	1.000
31	39	0.05	0.17	1.000
32	37	0.13	0.07	0.889
33	41	0.11	0.09	0.979
34	42	0.12	0.07	0.995
35	42	0.10	0.08	0.999
36	41	0.10	0.06	1.000
37	38	0.20	0.13	0.003
38	39	0.04	0.12	1.000
39	33	0.04	0.23	0.991
40	42	0.10	0.14	0.974
Summary	2/40 * 100 = 5%			

Note: A *p*-value less than 0.05 ($\alpha = 0.05$) suggests that the mean dielectric difference between the mat and the joint is greater than 0.2 which corresponds to over 2% joint air voids as compared to the mat.

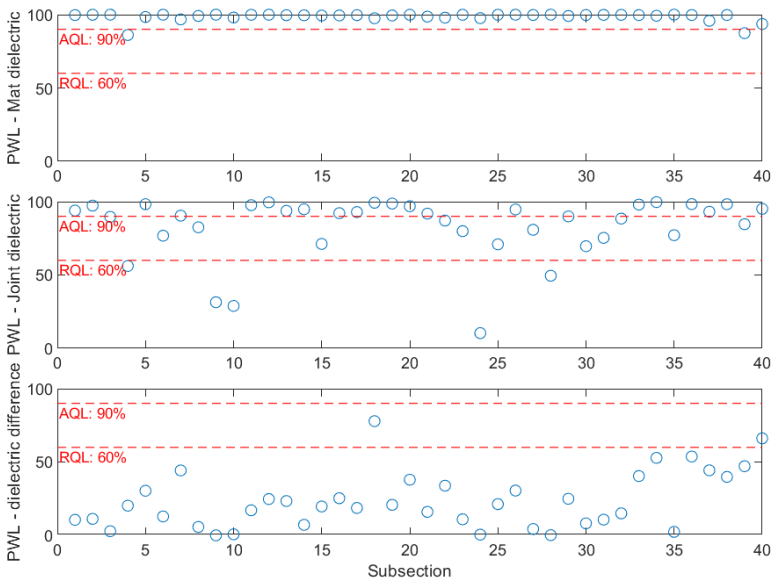

(a) Unconfined joint, Xerxes Road #1

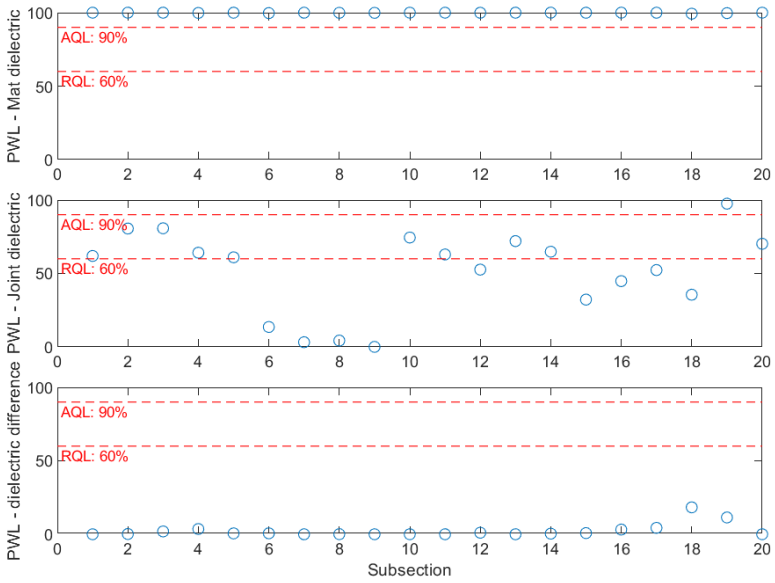

(b) Unconfined joint, Xerxes Road #2

Figure 4-6 Dielectric-based PWL for the unconfined joints, accompanying mats (3.5 ft offset), and their dielectric differences (3.5 ft – 0.5 ft offset) – Xerxes Road project

To understand the variability of PWL values, one can examine the recorded dielectric data. The box plots in Figure 4-8(a) show that most mat dielectrics are above LSL value (i.e., 4.93, corresponding to 8% air voids). Both the unconfined joint dielectrics are lower than the accompanying mat's dielectrics but with some data below the joint's LSL value (i.e., 4.78, equating to 10% air voids). The unconfined joint PWL for subsections 4, 9, 10, 24, and 28 of the Xerxes Road #1 project are lower than the acceptance limit of 60%. The dielectrics for these sections show that most of the data lie below the LSL of 4.78 for the joint.

In contrast, the dielectric values for the mat and confined joint in Figure 4-8(b) show greater variation, with most joint dielectrics exceeding 4.78, leading to higher PWL values (Figure 4-7). Meanwhile, several mat subsections have dielectric values below the threshold of 4.93, resulting in lower PWL values for the mat. While the dielectric-difference-based PWL remains within the acceptable quality limits (AQL and RQL) for nearly the entire 1,000 ft section, their variations are explained by the higher variability of the dielectric values for each subsection. The box plots also imply that constructing an unconfined joint will result in significant relative compaction differences from the accompanying mat compared to a confined joint. Such an in-depth pavement compaction analysis is impossible when using traditional density evaluation methods that rely on spot tests using cores and/or density gauges.

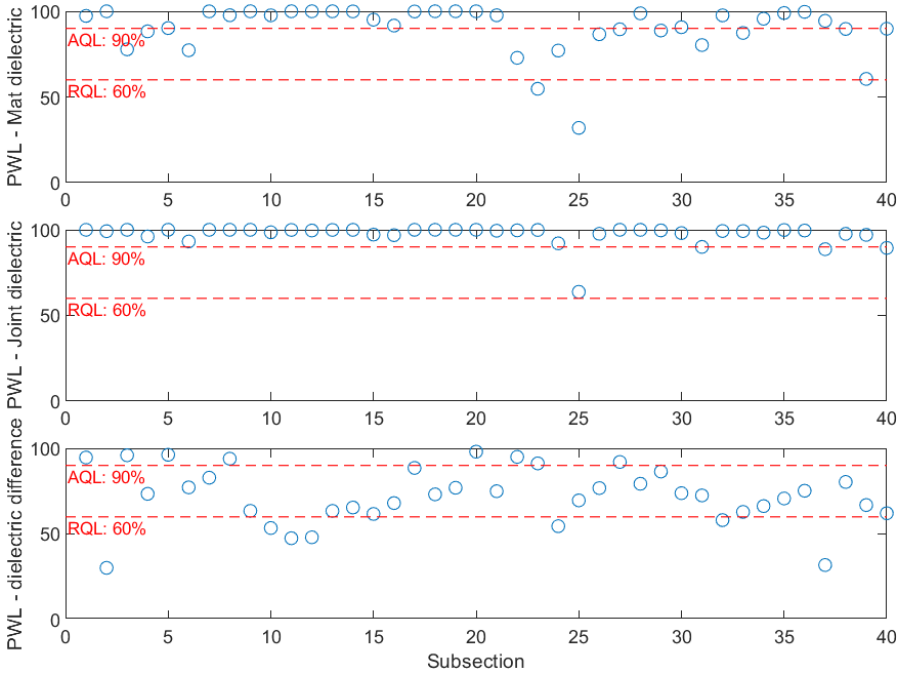

Figure 4-7 Dielectric-based PWL for the confined joint, accompanying mat (3.5 ft offset), and their dielectric differences (3.5 ft – 0.5 ft offset) – Xerxes Road project

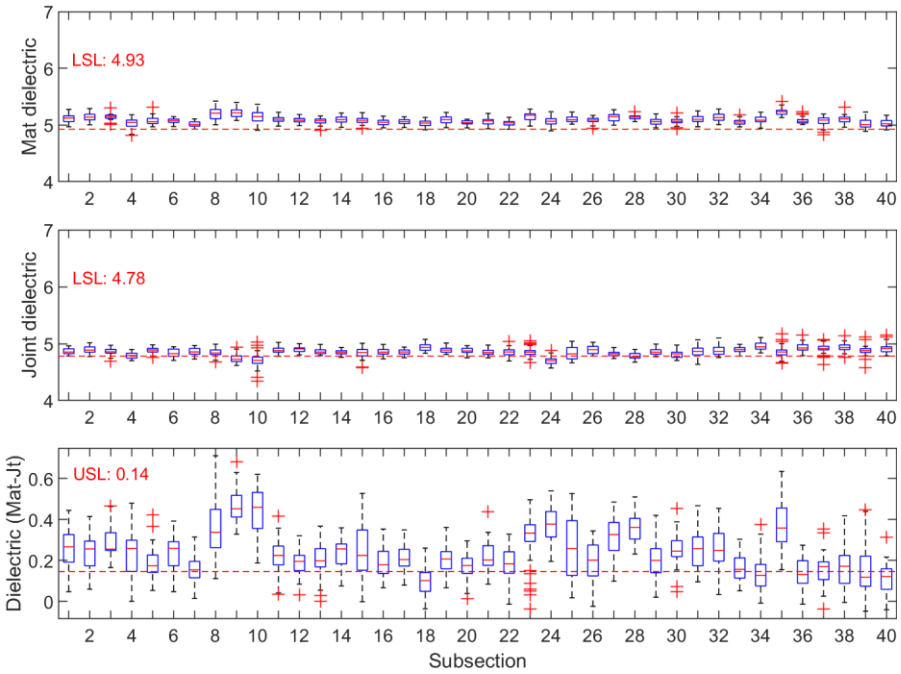

(a) Unconfined joint

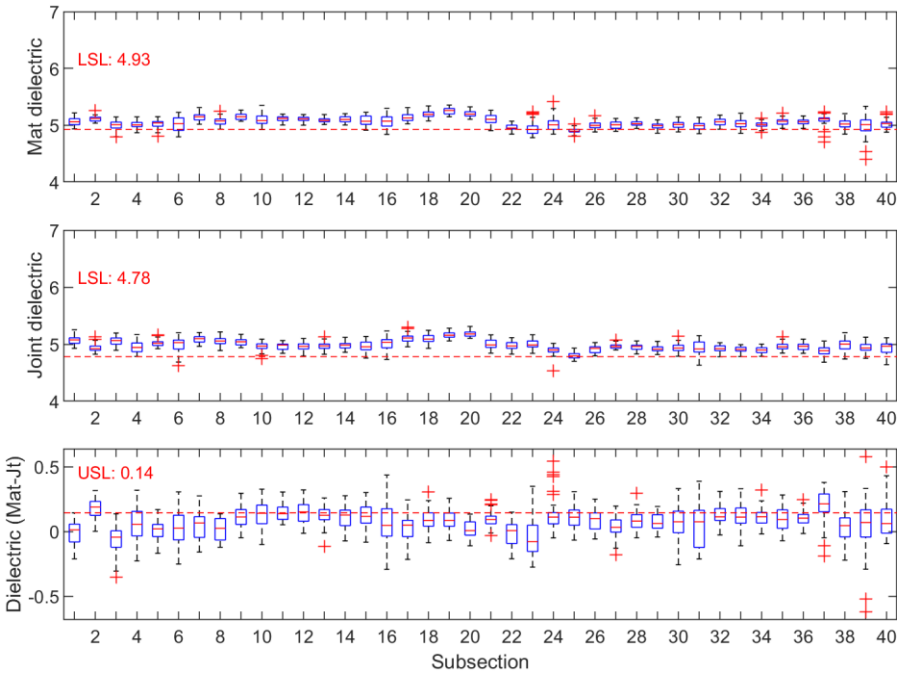

(b) Confined joint

Figure 4-8 Box plots of the recorded mat (3.5 ft) and joint dielectric data along with their dielectric differences (3.5 ft – 0.5 ft offset) – Xerxes Road #1 project

4.2.3 Probabilistic Analysis

The asphalt mat and joint dielectric values were also analyzed using a probabilistic approach. Tables 4-4 through 4-6 present the conditional probabilities for various dielectric value

categories of the mat and joint at the Xerxes Road project (as outlined in Table 4-1). For example, when the mat dielectric values are between 4.8 and 5.0, the probability that the unconfined joint dielectric values will fall below 4.6, within 4.6-4.8, or between 4.8-5.0 is 2%, 17%, and 80%, respectively, based on data from Xerxes Road #1. In contrast, the corresponding probabilities for Xerxes Road #2 are 18%, 46%, and 36%, respectively, for the same dielectric ranges. Furthermore, the likelihood that the unconfined joint dielectric values will fall between 4.8 and 5.0 shifts from 80% to 33% (and from 36% to 100% for Xerxes Road #2) when the mat dielectric values increase from 4.8-5.0 to 5.0-5.2, 5.2-5.4, or 5.4-5.6, respectively.

Table 4-4 Conditional probabilities for the unconfined butt joint – Xerxes Road #1 project

Mat / Joint	< 4.6	≥ 4.6 < 4.8	≥ 4.8 < 5.0	≥ 5.0 < 5.2	≥ 5.2 < 5.4	≥ 5.4 < 5.6
< 4.6	-	-	2%	-	-	-
≥ 4.6 < 4.8	-	-	17%	19%	36%	34%
≥ 4.8 < 5.0	-	-	80%	76%	56%	33%
≥ 5.0 < 5.2	-	-	1%	5%	8%	33%
≥ 5.2 < 5.4	-	-	-	-	-	-

Note: (-) means no data in that probability group.

Table 4-5 Conditional probabilities for the unconfined butt joint – Xerxes Road #2 project

Mat / Joint	< 4.6	≥ 4.6 < 4.8	≥ 4.8 < 5.0	≥ 5.0 < 5.2	≥ 5.2 < 5.4	≥ 5.4 < 5.6
< 4.6	-	-	18%	8%	4%	0.0%
≥ 4.6 < 4.8	-	-	46%	58%	40%	0.0%
≥ 4.8 < 5.0	-	-	36%	34%	56%	100.0%
≥ 5.0 < 5.2	-	-	-	-	-	-
≥ 5.2 < 5.4	-	-	-	-	-	-

Note: (-) means no data in that probability group.

Table 4-6 Conditional probabilities for the Confined butt joint – Xerxes Road #1 project

Mat / Joint	< 4.6	≥ 4.6 < 4.8	≥ 4.8 < 5.0	≥ 5.0 < 5.2	≥ 5.2 < 5.4	≥ 5.4 < 5.6
< 4.6	-	-	-	-	-	-
≥ 4.6 < 4.8	-	-	9%	3%	2%	-
≥ 4.8 < 5.0	-	60%	66%	56%	12%	100%
≥ 5.0 < 5.2	100%	40%	25%	39%	70%	-
≥ 5.2 < 5.4	-	-	-	2%	16%	-

Note: (-) means no data in that probability group.

Observing the probabilities in Table 4-6, there is a 60%, 66%, 56%, 12%, and 100% chance that the confined joint dielectric values would fall between 4.8 and 5.0 if the mat values

are within 4.6-4.8, 4.8-5.0, 5.0-5.2, 5.2-5.4, or 5.4-5.6, respectively. Interestingly, despite the mat dielectric values shifting toward lower groups compared to those shown in Tables 4-4, and 4-5, the confined joint values tend to shift higher, indicating improved joint compaction. For instance, when the mat dielectric values are between 4.8 and 5.0, there is a 0% probability that the confined joint dielectric values will fall below 4.6 and only a 9% chance they will be in the 4.6-4.8 range. In contrast, there is a 66% probability that the confined joint dielectric values will match those of the mat and a 25% chance that the joint will be even better compacted, with dielectric values falling between 5.0 and 5.2. These findings suggest that confined joints achieve higher compaction than unconfined ones, as reflected by their higher dielectric values.

4.3 COMPACTION COMPARISON BETWEEN DIFFERENT JOINT TYPE

Similar analyses, as presented in the previous section, were undertaken for all the projects and their longitudinal joint types. This section presents the summarized results from the statistical and probabilistic analysis comparing the compaction ability of the different longitudinal joint types evaluated in this study.

4.3.1 Summarized Results - Paired *t*-test Analysis

Table 4-7 summarizes the paired *t*-test results for the varying longitudinal joint types using different subsection lengths. The fractions shown in the table indicate the number of subsections out of the total available based on the subsection length, where the relative dielectric difference between the mat and joint is large enough (per Table 3-7) to result in an air void difference of 2% or more. The numbers in parentheses show the percentage of such subsections. Observing the percentages, the table indicates that constructing an unconfined joint, in most cases, may result in inadequate relative compaction between the mat and a joint based on dielectrics. For instance, the data for the unconfined joint of the Xerxes Road #1 project shows that about 78% of the 25 ft subsections have greater than 0.145 (Table 3-7) dielectric differences, large enough to cause over 2% air void difference between the unconfined joint and the accompanying asphalt mat. Similar higher percentages of subsections are seen for almost all the unconfined joints except one section of the M-102 project.

Table 4-7 Summarized paired *t*-test results using dielectric data

Project & section no.	Year	Joint geometry, type, and/or construction method	Subsection length			
			25 ft	50 ft	100 ft	200 ft
Xerxes Rd-1	2022	Unconfined	31/40 (78)	17/20 (85)	9/10 (90)	5/5 (100)
Xerxes Rd-2	2022	Unconfined	20/20 (100)	10/10 (100)	5/5 (100)	3/3 (100)
US-23 SMA	2022	Unconfined	33/40 (83)	18/20 (90)	10/10 (100)	5/5 (100)
I-94 SMA	2023	Unconfined	40/40 (100)	20/20 (100)	10/10 (100)	5/5 (100)
M-102-1	2023	Unconfined	0/40 (0)	0/20 (0)	0/10 (10)	0/5 (0)
M-102-2	2023	Unconfined	26/40 (65)	13/20 (65)	8/10 (80)	4/5 (80)
M-153-1	2023	Unconfined	15/32 (47)	8/16 (50)	6/8 (75)	3/4 (75)
M-153-2	2023	Unconfined	16/32 (50)	8/16 (50)	5/8 (63)	3/4 (75)
I-496	2023	Unconfined	40/40 (100)	20/20 (100)	10/10 (100)	5/5 (100)
I-496	2023	Unconfined (Cutback)	21/40 (53)	11/20 (55)	6/10 (60)	4/5 (80)
I-496	2022	Unconfined (Cutback)	1/40 (3)	1/20 (5)	0/10 (0)	0/5 (0)
M-28-1	2022	Unconfined tapered	0/40 (0)	0/20 (0)	0/10 (0)	0/5 (0)
M-28-2	2022	Unconfined tapered	0/36 (0)	0/18 (0)	0/9 (0)	0/5 (0)
M-61	2023	Unconfined tapered	3/40 (8)	2/20 (10)	0/10 (0)	0/5 (0)
I-496-1	2023	Confined butt (Cold)	0/40 (0)	0/20 (0)	0/10 (0)	0/5 (0)
I-496-2	2023	Confined butt (Cold)	15/40 (38)	6/20 (30)	3/10 (30)	1/5 (20)
Xerxes Rd-1	2022	Confined butt (Cold)	2/40 (5)	0/20 (0)	0/10 (0)	0/5 (0)
M-89	2022	Confined butt (Cold)	2/40 (5)	0/20 (0)	0/10 (0)	0/5 (0)
M-89	2023	Confined butt (Cold)	0/40 (0)	0/20 (0)	0/10 (0)	0/5 (0)
M-25-1	2022	Confined butt (Cold)	10/40 (25)	3/20 (15)	1/10 (10)	1/5 (20)
M-25-2	2022	Confined butt (Cold)	0/40 (0)	0/20 (0)	0/10 (0)	0/5 (0)
M-25-1	2023	Confined butt (Cold)	34/40 (85)	18/20 (90)	9/10 (90)	5/5 (100)
M-25-2	2023	Confined butt (Cold	25/40 (63)	14/20 (70)	7/10 (70)	4/5 (80)
US-23 SMA	2022	Confined butt (Cold)	1/19 (5)	0/10 (0)	0/5 (0)	No data
I-75	2022	Confined butt (Cold)	2/40 (5)	0/20 (0)	0/10 (0)	0/5 (0)
I-94BL	2023	Confined butt (Cold)	1/39 (3)	1/20 (5)	0/10 (0)	0/5 (0)
M-100	2023	Confined butt (Cold)	1/40 (3)	0/20 (00)	0/10 (0)	0/5 (0)
M-153	2023	Confined (Warm)	1/32 (3)	0/16 (0)	0/8 (0)	0/4 (0)
Manning Tr-1	2022	Confined (Maryland method)	0/40 (0)	0/20 (0)	0/10 (0)	0/5 (0)
Manning Tr-2	2022	Confined (Maryland method)	0/40 (0)	0/20 (0)	0/10 (0)	0/5 (0)
M-28-1	2022	Confined tapered (Cold)	7/40 (18)	3/20 (15)	2/10 (20)	0/5 (0)
M-28-2	2022	Confined tapered (Cold)	0/40 (0)	0/20 (0)	0/10 (0)	0/5 (0)
M-61	2023	Confined tapered (Cold)	0/40 (0)	0/20 (0)	0/10 (0)	0/5 (0)
Manning Tr-1	2022	Echelon (Hot)	10/40 (25)	5/20 (25)	2/10 (20)	2/5 (40)
Manning Tr-2	2022	Echelon (Hot)	20/40 (50)	9/20 (45)	5/10 (50)	3/5 (60)
US-31H	2022	Echelon (Hot)	15/40 (37.5)	7/20 (35)	4/10 (40)	2/5 (40)
US-10-1	2023	Echelon (Hot)	26/40 (65)	14/20 (70)	8/10 (80)	5/5 (100)
US-10-2	2023	Echelon (Hot)	0/40 (0)	0/20 (0)	0/10 (0)	0/5 (0)
I-75	2023	Echelon (Hot)	27/40 (68)	15/20 (75)	8/10 (80)	4/5 (80)
US-31A	2023	Echelon (Hot)	4/40 (10)	1/20 (5)	0/10 (0)	0/5 (0)

Note: The fraction indicates the number of subsections out of the total, where the relative dielectric difference between the mat and joint is large enough to result in an air void difference of 2% or more. The percentage of such subsections is shown in parentheses.

The table also indicates that the compaction of unconfined joints improves when a portion of the compacted HMA mat is cut back before paving the adjacent lane, as demonstrated in the I-496 project. For confined joints, including those constructed using the Maryland method

(Manning Trail projects), the majority of subsections do not display higher dielectric difference that results in over 2% relative air void differences, as reflected in the lower percentages (shown in parentheses) for most projects, except for the M-25 (2023) project. Likewise, both tapered joints—confined or unconfined—show lower percentages. Counterintuitively, most of the echelon joints show higher percentages of subsection with greater dielectric differences, indicating over 2% relative air void differences. The higher percentage for the I-75 project can be due to different HMA mixes, which were paved in the echelon while the mainline pavement and the adjacent shoulder were constructed simultaneously. Moreover, irregular rolling patterns were observed during the construction of the echelon paved joint of the US-10 project.

The table also compares different subsection lengths to assess their efficacy in analyzing relative dielectric differences between the mat and the joint. Data from the unconfined joint of the Xerxes Road #1 project reveals that using a longer subsection length of 200 ft results in 100% of the subsections within the 1,000 ft section having a dielectric difference greater than 0.145 corresponding to over 2% air void difference. For subsection lengths of 100, 50, and 25 ft, the percentages of subsections with significant differences greater than 0.145 are 78%, 85%, and 90%, respectively. These findings suggest that longer subsections may lead to rejecting a pavement section due to compaction differences between the mat and longitudinal joint, even though certain smaller subsections may have acceptable compaction. This implies that longer subsections might overlook localized compaction issues. Analyzing data with smaller subsection lengths highlights the value of continuous dielectric data, especially for flexible pavement QA.

To accomplish a similar comparison (i.e., using paired *t*-tests), the predicted air voids estimated by individual project-calibrated models were used. While the accuracy of these models was verified using pavement cores from the project sites, these were further validated using QA field cores. Note that the QA cores were collected only for Michigan projects. Mix acceptance procedures require collecting and testing pavement field cores per MDOT's standard specifications. The QA cores used in this study were not necessarily collected within the 1,000 ft pavement section that was tested. However, all cores were collected on the DPS testing days, sampling the HMA being laid that day. The collected cores ranged from 4 to 14 for various projects and were retrieved on the same production day(s).

Figure 4-9 presents the validation results using QA cores from both the asphalt mat and, where available, longitudinal joints. To achieve full lane coverage (typically 12 ft wide), three

DPS passes were conducted along the 1,000 ft pavement sections, resulting in nine sensor passes and generating two dielectric readings per foot. Excluding the two sensor passes that measured dielectric at a 6-inch offset from the joint on either edge of the pavement lane, the DPS-determined asphalt mat air voids shown represent an average of approximately 14,000 (7×1000×2) readings recorded daily. For the joint, the average air voids were calculated based on about 4,000 (2×1000×2) readings recorded by the two sensors positioned at a 6-inch offset from the joint at either edge of the lane. The error bars in the figure indicate ± one standard deviation from the average void content values. It's important to note that DPS testing and field core sampling were carried out over two separate HMA production and pavement construction days for some projects.

Since there were significant differences in sample sizes and variances between the two datasets—ranging from 4 to 14 field cores compared to the DPS's higher sampling rates (14,000 for the mat and 4,000 for the joint), traditional *t*-tests could not be used for comparison. This is because a traditional *t*-test equal variance among the two competing datasets. Hence, a Welch's *t*-test was used to statistically compare the air voids. A Welch's *t*-test does not require assuming equal variances, making it a more suitable and reliable method for such analyses. Equation 4-13 and Equation 4-14 were used to calculate Welch's *t*-statistic and degrees of freedom for the test, respectively. Equation 4-14, known as the Welch-Satterthwaite equation, weights the contribution of each group based on their variances and sample sizes. This approach ensures accurate results when assessing whether there is a statistically significant difference between the air voids measured using QA field cores and the DPS-predicted air voids.

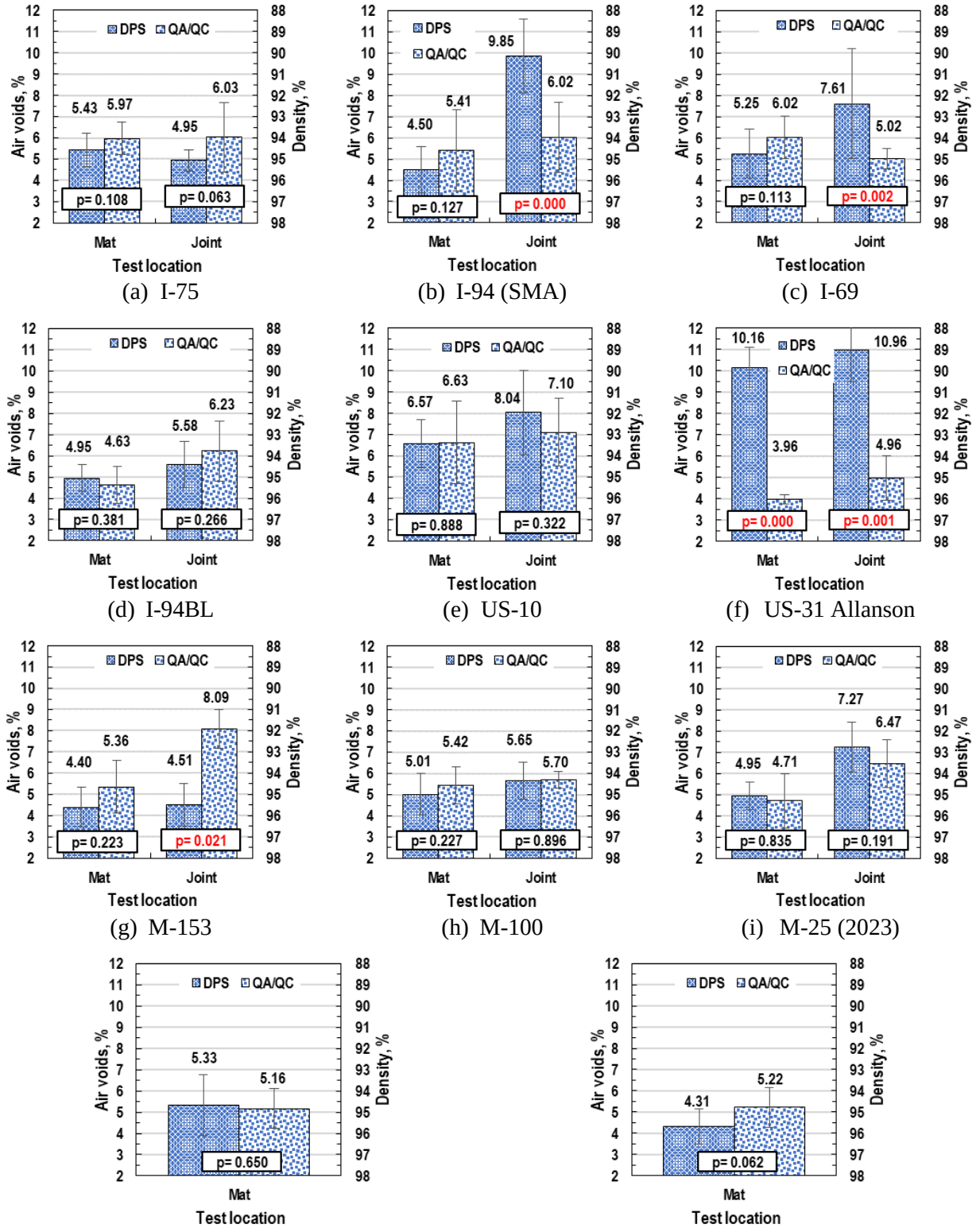

(a) I-75 (b) I-94 (SMA) (c) I-69

(d) I-94BL (e) US-10 (f) US-31 Allanson

(g) M-153 (h) M-100 (i) M-25 (2023)

(j) US-31 (2022) Holland (k) M-102

Figure 4-9 Comparison between QA cores air voids and DPS-estimated air voids

Figure 4-9 (cont'd)

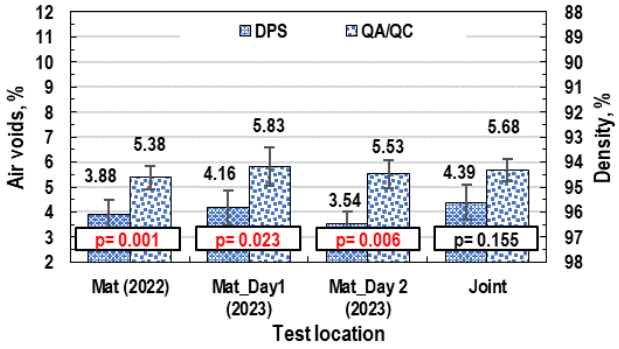

(l) I-496

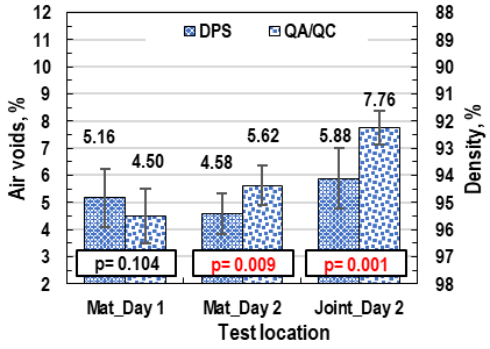

(m) M-28 (2022)

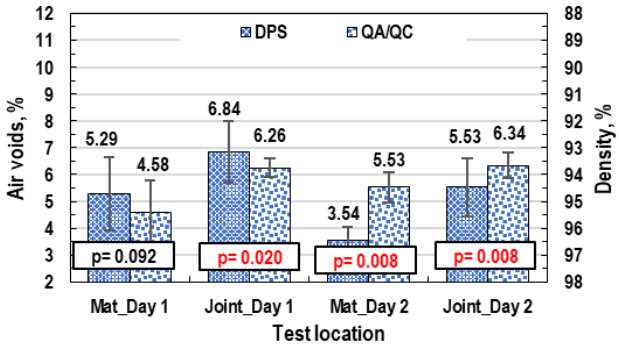

(n) M-25 (2022)

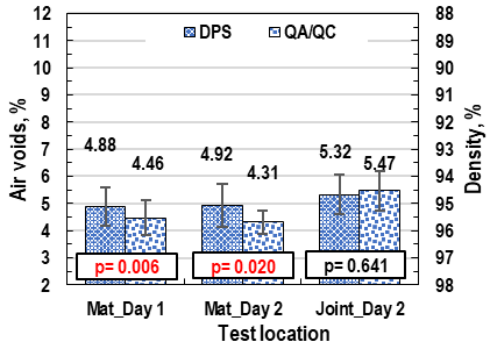

(o) M-61

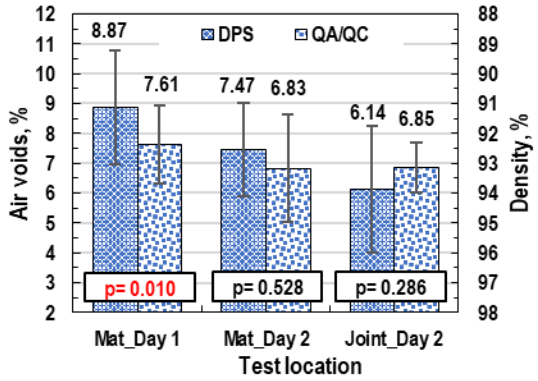

(p) US-23 (2022)

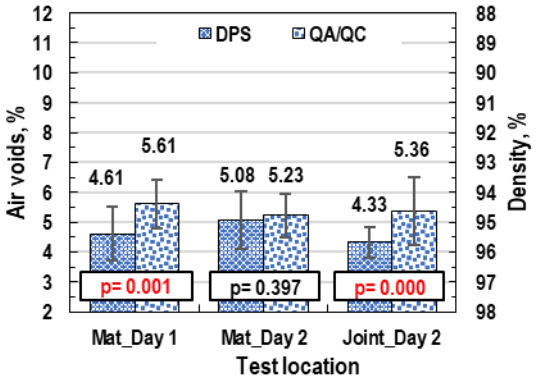

(q) M-89 (2022)

$$t = \frac{\bar{X}_1 - \bar{X}_2}{\sqrt{\frac{s_1^2}{n_1} + \frac{s_2^2}{n_2}}}$$

Equation 4-13

$$df = \frac{\left(\frac{s_1^2}{n_1} + \frac{s_2^2}{n_2}\right)^2}{\frac{\left(\frac{s_1^2}{n_1}\right)^2}{n_1 - 1} + \frac{\left(\frac{s_2^2}{n_2}\right)^2}{n_2 - 1}}$$

Equation 4-14

where;

t = Welch's *t*-statistic,

$\bar{X}_1, \bar{X}_2$ = sample means of the two groups,

s_1^2, s_2^2 = sample variances of the two groups,

n_1, n_1 = sample sizes of the two groups,

df = Welch's *t*-test degrees of freedom.

At a 5% significance level (α = 0.05), indicating a 95% confidence that the two means are similar, Figure 4-9 displays whether the two air content measurements for each project are statistically similar (*p*-value > 0.05) or significantly different (*p*-value ≤ 0.05). Considering the asphalt mat comparisons, most projects display agreement between the QA field cores and DPS-based air voids (*p-value* > 0.05), indicating that their air void contents are not statistically different. While some projects show a statistically significant difference (*p-value* < 0.05), the air void difference is close to ±1%, showing a trivial difference. For instance, the mean difference between the QA cores and DPS air void data shows a statistically significant difference for the mat of the M-61 project on both paving days. However, the mat air voids from the two daily datasets are within 1% of each other, showing practically similar void contents. Similarly, the QA core air voids of the asphalt mat measured on the 2nd paving day of the M-28 (2022) project are only 1.04% higher than the DPS-predicted ones, declared as statistically significant by Welch's *t*-test.

Projects such as I-496, US-31 in Alanson, the second day's mat data for M-25 (2022), and the first day's mat data for US-23 (2022) show notable differences between the mat QA cores and the predicted air voids from DPS data. Figure 3-12 indicated that the calibrated models for these projects aligned reasonably well with field core data collected during DPS testing within the pavement section. These differences may be attributed to the fact that the QA cores were not taken from the same sections tested with DPS. A more plausible explanation is that the QA cores were not collected from representative stations. This underscores the importance of using continuous dielectric data for compaction evaluation, as relying solely on limited core samples can be problematic—especially when payments are based on core densities. DPS data can help prevent overpayments by an agency for subpar work and underpayment to a contractor due to testing of non-representative cores from well-compacted pavement sections.

Figure 4-9 shows that most joint QA core air void measurements align with DPS-estimated air voids. In cases with statistically significant differences, these often reflect minor practical differences. For instance, the M-25 (2022) and M-89 (2022) projects show air void discrepancies within ±1% between DPS estimates and QA core measurements, with the DPS indicating slightly lower densities than the cores. For projects with larger air void discrepancies, non-representative core sampling is likely the main reason for the mismatch. The US-31 (Alanson) project, in particular, exhibits the most notable difference between the two datasets, emphasizing the importance of continuous compaction evaluation over only relying on a limited number of core samples. Overall, Figure 4-9 demonstrates reasonable agreement between DPS-predicted air voids and QA core data, validating the calibrated models and confirming the effectiveness of DPS for field compaction evaluation.

Table 4-8 shows similar summarized paired *t*-test results using the predicted air voids estimated by the calibrated models for the different longitudinal joint types using different subsection lengths of all the projects. The results are very similar to those shown in Table 4-7. The table shows similar findings that an unconfined joint produces the highest air void differences relative to its accompanied mat. However, slight variations can be observed between the summarized results in the two tables, especially in the case of the echelon joints. While these differences can partly be due to the model's variability affecting the predicted air voids, the use of different HMA mixes, as in the case of the I-75 project, for paving the mainline and shoulder in the echelon. Moreover, the results for the US-10 project majorly remained unchanged. As noted earlier, a likely explanation can be the irregular rolling pattern observed during data collection on this project site.

Table 4-8 Summarized paired *t*-test results using predicted air voids

Project & section no.	Year	Joint geometry, type, and/or construction method	Subsection length			
			25 ft	50 ft	100 ft	200 ft
Xerxes Rd-1	2022	Unconfined	30/40 (75)	16/20 (80)	8/10 (80)	5/5 (100)
Xerxes Rd-2	2022	Unconfined	20/20 (100)	10/10 (100)	5/5 (100)	3/3 (100)
US-23 SMA	2022	Unconfined	32/40 (80)	17/20 (85)	10/10 (100)	5/5 (100)
I-94 SMA	2023	Unconfined	40/40 (100)	20/20 (100)	10/10 (100)	5/5 (100)
M-102-1	2023	Unconfined	0/40 (0)	0/20 (0)	0/10 (10)	0/5 (0)
M-102-2	2023	Unconfined	5/40 (13)	2/20 (10)	1/10 (10)	0/5 (0)
M-153-1	2023	Unconfined	1/32 (3)	0/16 (0)	0/8 (0)	0/4 (0)
M-153-2	2023	Unconfined	10/32 (31)	5/16 (31)	3/8 (38)	2/4 (50)
I-496	2023	Unconfined	40/40 (100)	20/20 (100)	10/10 (100)	5/5 (100)
I-496	2023	Unconfined (Cutback)	6/40 (15)	3/20 (15)	2/10 (20)	0/5 (0)
I-496	2022	Unconfined (Cutback)	0/40 (0)	0/20 (0)	0/10 (0)	0/5 (0)
M-28-1	2022	Unconfined tapered	0/40 (0)	0/20 (0)	0/10 (0)	0/5 (0)
M-28-2	2022	Unconfined tapered	0/36 (0)	0/18 (0)	0/9 (0)	0/5 (0)
M-61	2023	Unconfined tapered	1/40 (3)	0/20 (0)	0/10 (0)	0/5 (0)
I-496-1	2023	Confined butt (Cold)	0/40 (0)	0/20 (0)	0/10 (0)	0/5 (0)
I-496-2	2023	Confined butt (Cold)	0/40 (0)	0/20 (0)	0/10 (0)	0/5 (0)
Xerxes Rd-1	2022	Confined butt (Cold)	1/40 (3)	0/20 (0)	0/10 (0)	0/5 (0)
M-89	2022	Confined butt (Cold)	0/40 (0)	0/20 (0)	0/10 (0)	0/5 (0)
M-89	2023	Confined butt (Cold)	0/40 (0)	0/20 (0)	0/10 (0)	0/5 (0)
M-25-1	2022	Confined butt (Cold)	3/40 (8)	2/20 (10)	0/10 (0)	0/5 (0)
M-25-2	2022	Confined butt (Cold)	0/40 (0)	0/20 (0)	0/10 (0)	0/5 (0)
M-25-1	2023	Confined butt (Cold)	31/40 (78)	16/20 (80)	8/10 (80)	5/5 (100)
M-25-2	2023	Confined butt (Cold	16/40 (40)	7/20 (35)	3/10 (30)	2/5 (40)
US-23 SMA	2022	Confined butt (Cold)	1/19 (5)	0/10 (0)	0/5 (0)	No data
I-75	2022	Confined butt (Cold)	1/40 (3)	0/20 (0)	0/10 (0)	0/5 (0)
I-94BL	2023	Confined butt (Cold)	1/39 (3)	0/20 (0)	0/10 (0)	0/5 (0)
M-100	2023	Confined butt (Cold)	0/40 (0)	0/20 (0)	0/10 (0)	0/5 (0)
M-153	2023	Confined (Warm)	0/32 (0)	0/16 (0)	0/8 (0)	0/4 (0)
Manning Tr-1	2022	Confined (Maryland method)	0/40 (0)	0/20 (0)	0/10 (0)	0/5 (0)
Manning Tr-2	2022	Confined (Maryland method)	0/40 (0)	0/20 (0)	0/10 (0)	0/5 (0)
M-28-1	2022	Confined tapered (Cold)	3/40 (8)	2/20 (10)	0/10 (0)	0/5 (0)
M-28-2	2022	Confined tapered (Cold)	0/40 (0)	0/20 (0)	0/10 (0)	0/5 (0)
M-61	2023	Confined tapered (Cold)	0/40 (0)	0/20 (0)	0/10 (0)	0/5 (0)
Manning Tr-1	2022	Echelon (Hot)	3/40 (8)	2/20 (10)	1/10 (10)	0/5 (0)
Manning Tr-2	2022	Echelon (Hot)	4/40 (10)	2/20 (10)	1/10 (10)	1/5 (20)
US-31H	2022	Echelon (Hot)	10/40 (25)	6/20 (30)	1/10 (10)	1/5 (20)
US-10-1	2023	Echelon (Hot)	25/40 (63)	13/20 (65)	6/10 (60)	4/5 (80)
US-10-2	2023	Echelon (Hot)	0/40 (0)	0/20 (0)	0/10 (0)	0/5 (0)
I-75	2023	Echelon (Hot)	18/40 (45)	8/20 (40)	5/10 (50)	3/5 (60)
US-31A	2023	Echelon (Hot)	1/40 (3)	1/20 (5)	0/10 (0)	0/5 (0)

Note: The fraction indicates the number of subsections out of the total, where the relative air voids difference between the mat and joint is over 2%. The percentage of such subsections is shown in parentheses.

The overall results from the paired t-tests suggest that constructing unconfined joints without additional techniques, such as tapering or cutting back, tends to result in inadequate compaction, leading to significantly higher air voids in the joint compared to the adjacent mat. Therefore, it is recommended to avoid unconfined joints whenever possible. In contrast,

confined, tapered (both confined and unconfined), and echelon joints generally achieve compaction levels closer to that of the mat. Furthermore, when examining the effect of subsection length on compaction assessment, the data shows that the percentage of sections displaying significant compaction differences increases as the subsection length increases from 25 ft to 200 ft. This indicates that using longer subsections may result in pavement rejection due to compaction differences between the mat and the longitudinal joint, even if compaction is acceptable over shorter sections. However, identifying localized compaction issues is more effective with smaller subsection lengths. Despite this, using 25- or 50-foot lengths may not be practical. As a result, when employing DPS for compaction evaluation, a subsection length of 100 feet is recommended as a balanced approach.

4.3.2 Summarized Results - PWL Analysis

Table 4-9 summarizes the PWL values for subsections of varying lengths across different longitudinal joint types. The table presents the number of subsections with PWL values below the 60% RQL as a fraction (numerator) of the total subsections for that length (denominator), with the percentage shown in parentheses. The data suggests that unconfined joints generally exhibit inadequate relative compaction between the mat and the joint, as indicated by dielectric measurements. For instance, in the first section of the Xerxes Road project, approximately 95% of the 25 ft subsections have PWL values below the RQL, showing a dielectric difference (mat–joint) of 0.145 or greater. Similar trends of low PWL values (below 60%) are observed in most unconfined joints, except for one section of the M-102 project.

The table also illustrates that cutting a portion of the compacted HMA mat before paving the adjacent lane improves the quality of unconfined joints, as demonstrated in the I-496 project. Moreover, for confined joints, including those constructed using the Maryland method, PWL values rarely fall below the 60% RQL, as reflected by the lower percentages (in parentheses) for most projects, except for the M-25 (2023) project. Likewise, both tapered joints, whether confined or unconfined, generally show PWL values above the RQL. However, similar to the paired *t*-test results, the echelon-paved joints show higher percentages of sections with lower than 60% PWL.

Table 4-9 Summarized PWL results using dielectric data

Project & section no.	Year	Joint geometry, type, and/or construction method	Subsection length			
			25 ft	50 ft	100 ft	200 ft
Xerxes Rd-1	2022	Unconfined	38/40 (95)	20/20 (100)	10/10 (100)	5/5 (100)
Xerxes Rd-2	2022	Unconfined	20/20 (100)	10/10 (100)	5/5 (100)	No data
US-23 SMA	2022	Unconfined	40/40 (100)	20/20 (100)	10/10 (100)	5/5 (100)
I-94 SMA	2023	Unconfined	40/40 (100)	20/20 (100)	10/10 (100)	5/5 (100)
M-102-1	2023	Unconfined	3/40 (8)	0/20 (0)	0/10 (10)	0/5 (0)
M-102-2	2023	Unconfined	35/40 (88)	20/20 (100)	10/10 (100)	5/5 (100)
M-153-1	2023	Unconfined	24/32 (75)	13/16 (81)	7/8 (88)	3/4 (75)
M-153-2	2023	Unconfined	20/32 (63)	12/16 (75)	5/8 (63)	3/4 (75)
I-496	2023	Unconfined	40/40 (100)	20/20 (100)	10/10 (100)	5/5 (100)
I-496	2023	Unconfined (Cutback)	26/40 (65)	14/20 (70)	8/10 (80)	4/5 (80)
I-496	2022	Unconfined (Cutback)	6/40 (15)	3/20 (15)	1/10 (10)	0/5 (0)
M-28-1	2022	Unconfined tapered	0/40 (0)	0/20 (0)	0/10 (0)	0/5 (0)
M-28-2	2022	Unconfined tapered	0/36 (0)	0/18 (0)	0/9 (0)	0/5 (0)
M-61	2023	Unconfined tapered	11/40 (28)	5/20 (25)	3/10 (30)	1/5 (20)
I-496-1	2023	Confined butt (Cold)	0/40 (0)	0/20 (0)	0/10 (0)	0/5 (0)
I-496-2	2023	Confined butt (Cold)	21/40 (53)	8/20 (40)	5/10 (50)	2/5 (40)
Xerxes Rd-1	2022	Confined butt (Cold)	7/40 (18)	3/20 (15)	1/10 (10)	1/5 (20)
M-89	2022	Confined butt (Cold)	2/40 (5)	0/20 (0)	0/10 (0)	0/5 (0)
M-89	2023	Confined butt (Cold)	2/40 (5)	0/20 (0)	0/10 (0)	0/5 (0)
M-25-1	2022	Confined butt (Cold)	14/40 (35)	7/20 (35)	4/10 (40)	1/5 (20)
M-25-2	2022	Confined butt (Cold)	1/40 (2.5)	0/20 (0)	0/10 (0)	0/5 (0)
M-25-1	2023	Confined butt (Cold)	37/40 (93)	19/20 (95)	10/10 (100)	5/5 (100)
M-25-2	2023	Confined butt (Cold	32/40 (80)	17/20 (85)	9/10 (90)	5/5 (100)
US-23 SMA	2022	Confined butt (Cold)	1/19 (5)	0/10 (0)	0/5 (0)	No data
I-75	2022	Confined butt (Cold)	2/40 (5)	1/20 (5)	1/10 (10)	0/5 (0)
I-94BL	2023	Confined butt (Cold)	2/39 (5)	1/20 (5)	1/10 (10)	0/5 (0)
M-100	2023	Confined butt (Cold)	7/40 (18)	2/20 (10)	1/10 (10)	0/5 (0)
M-153	2023	Confined (Warm)	2/32 (6)	1/16 (6)	0/8 (0)	0/4 (0)
Manning Tr-1	2022	Confined (Maryland method)	0/40 (0)	0/20 (0)	0/10 (0)	0/5 (0)
Manning Tr-2	2022	Confined (Maryland method)	0/40 (0)	0/20 (0)	0/10 (0)	0/5 (0)
M-28-1	2022	Confined tapered (Cold)	10/40 (25)	5/20 (25)	2/10 (20)	1/5 (20)
M-28-2	2022	Confined tapered (Cold)	0/40 (0)	0/20 (0)	0/10 (0)	0/5 (0)
M-61	2023	Confined tapered (Cold)	0/40 (0)	0/20 (0)	0/10 (0)	0/5 (0)
Manning Tr-1	2022	Echelon (Hot)	22/40 (55)	10/20 (50)	5/10 (50)	2/5 (40)
Manning Tr-2	2022	Echelon (Hot)	32/40 (80)	17/20 (85)	9/10 (90)	5/5 (100)
US-31	2022	Echelon (Hot)	22/40 (55)	11/20 (55)	6/10 (60)	3/5 (60)
US-10-1	2023	Echelon (Hot)	33/40 (83)	17/20 (85)	10/10 (100)	5/5 (100)
US-10-2	2023	Echelon (Hot)	0/40 (0)	0/20 (0)	0/10 (0)	0/5 (0)
I-75	2023	Echelon (Hot)	31/40 (78)	16/20 (80)	8/10 (80)	5/5 (100)
US-31	2023	Echelon (Hot)	5/40 (13)	1/20 (5)	1/10 (10)	0/5 (0)

Note: The fraction shows sections that have PWL lower than 60% RQL out of the total subsections while the number in parenthesis shows their percentage.

Observing the effect of different subsection lengths, the percentage of sections having PWL less than 60% either remains the same or increases as the length increases from 25 ft to 200 ft. This suggests that using a smaller subsection can effectively identify local compaction issues. As mentioned before, the ability to analyze data using smaller subsection lengths demonstrates

the real value of the continuous dielectric data provided by DPS in flexible pavements QA procedures. However, 25- or 50-foot subsection length might not be practically feasible; using 100 ft is preferable for PWL analysis when utilizing DPS for pavement compaction evaluation. Table 4-10 summarizes similar PWL results based on the predicted air voids determined using the individual project's calibrated models. Like Table 4-9**,** the numbers in Table 4-10 display the percentage of subsections with greater than 2% relative air void difference between the mat and the joint. Table 4-10 presents results like those in Table 4-9, based on dielectric data.

However, for most echelon-paved joints, the percentage of subsections with more than 2% air void differences decreased significantly compared to Table 4-9, where dielectric difference values were used as the LSL. As mentioned earlier, the higher percentage of subsections with lower than 60% PWL in the I-75 project may have resulted from using two different HMA mixes for the mainline and shoulder, which were paved in the echelon. Meanwhile, the results for the US-10 project remained unchanged, likely due to the irregular rolling pattern observed during data collection. Additionally, the variations between the two tables can be attributed to the variability in the calibrated model used for these projects.

Comparing the overall PWL results, it can be inferred that constructing an unconfined joint without additional measures (such as tapering or cutting back) may lead to poor joint compaction and should be avoided if possible. On the other hand, the confined, tapered (both confined and unconfined), and echelon joints generally achieve compaction levels closer to that of the mat.

4.3.3 Summarized Results – Probabilistic Analysis

Figure 4-10 summarizes the conditional probabilities for different mat dielectric ranges by combining data from various projects for each type of longitudinal joint. The figure reveals that unconfined joints have a 61%, 38%, and 32% likelihood of having dielectric values between 4.6 and 4.8 when the mat dielectric falls within 4.8–5.0, 5.0–5.2, or 5.2–5.4, respectively. Regardless of the mat's dielectric range, unconfined joints are expected to have dielectric values lower by 0.2 or more than the mat. However, unconfined joints constructed with a cutback of the HMA before paving the adjacent lane (unconfined cutback joints) show the potential for higher dielectric values compared to the mat. For example, Figure 4-10(a) indicates that for a mat dielectric range of 4.8–5.0, the unconfined cutback joint's dielectric values may entirely fall within 5.0–5.2. Similarly, Figure 4-10(b) shows a 14% chance that the joint's dielectric values

may fall in the higher 5.2–5.4 category when the mat is within 5.0–5.2. This joint has the highest probability of its dielectric values falling within the 5.0–5.2 range, regardless of the mat's dielectric range.

Table 4-10 Summarized PWL results using predicted air voids

Project & section no.	Year	Joint geometry, type, and/or construction method	Subsection length			
			25 ft	50 ft	100 ft	200 ft
Xerxes Rd-1	2022	Unconfined	36/40 (90)	20/20 (100)	10/10 (100)	5/5 (100)
Xerxes Rd-2	2022	Unconfined	20/20 (100)	10/10 (100)	5/5 (100)	No data
US-23 SMA	2022	Unconfined	40/40 (100)	20/20 (100)	10/10 (100)	5/5 (100)
I-94 SMA	2023	Unconfined	40/40 (100)	20/20 (100)	10/10 (100)	5/5 (100)
M-102-1	2023	Unconfined	0/40 (0)	0/20 (0)	0/10 (0)	0/5 (0)
M-102-2	2023	Unconfined	14/40 (35)	8/20 (40)	3/10 (30)	2/5 (40)
M-153-1	2023	Unconfined	8/32 (25)	2/16 (12.5)	0/8 (0)	0/4 (0)
M-153-2	2023	Unconfined	14/32 (43.8)	8/16 (50)	3/8 (37.5)	2/4 (50)
I-496	2023	Unconfined	40/40 (100)	20/20 (100)	10/10 (100)	5/5 (100)
I-496	2023	Unconfined (Cutback)	14/40 (35)	6/20 (30)	2/10 (20)	1/5 (20)
I-496	2022	Unconfined (Cutback)	0/40 (0)	0/20 (0)	0/10 (0)	0/5 (0)
M-28-1	2022	Unconfined tapered	0/40 (0)	0/20 (0)	0/10 (0)	0/5 (0)
M-28-2	2022	Unconfined tapered	0/36 (0)	0/18 (0)	0/9 (0)	0/5 (0)
M-61	2023	Unconfined tapered	3/40 (7.5)	2/20 (10)	0/10 (0)	0/5 (0)
I-496-1	2023	Confined butt (Cold)	0/40 (0)	0/20 (0)	0/10 (0)	0/5 (0)
I-496-2	2023	Confined butt (Cold)	4/40 (10)	2/20 (10)	1/10 (10)	1/5 (20)
Xerxes Rd-1	2022	Confined butt (Cold)	3/40 (7.5)	1/20 (2.5)	0/10 (0)	0/5 (0)
M-89	2022	Confined butt (Cold)	0/40 (0)	0/20 (0)	0/10 (0)	0/5 (0)
M-89	2023	Confined butt (Cold)	0/40 (0)	0/20 (0)	0/10 (0)	0/5 (0)
M-25-1	2022	Confined butt (Cold)	9/40 (22.5)	3/20 (15)	1/10 (10)	0/5 (0)
M-25-2	2022	Confined butt (Cold)	0/40 (0)	0/20 (0)	0/10 (0)	0/5 (0)
M-25-1	2023	Confined butt (Cold)	34/40 (85)	17/20 (85)	9/10 (90)	5/5 (100)
M-25-2	2023	Confined butt (Cold	22/40 (55)	12/40 (30)	4/10 (40)	3/5 (60)
US-23 SMA	2022	Confined butt (Cold)	0/19 (0)	0/10 (0)	0/5 (0)	No data
I-75	2022	Confined butt (Cold)	2/40 (5)	1/20 (5)	1/10 (10)	0/5 (0)
I-94BL	2023	Confined butt (Cold)	1/39 (2.6)	1/20 (5)	0/10 (0)	0/5 (0)
M-100	2023	Confined butt (Cold)	1/40 (2.5)	0/20 (0)	0/10 (0)	0/5 (0)
M-153	2023	Confined (Warm)	1/32 (3.1)	0/16 (0)	0/8 (0)	0/4 (0)
Manning Tr-1	2022	Confined (Maryland method)	0/40 (0)	0/20 (0)	0/10 (0)	0/5 (0)
Manning Tr-2	2022	Confined (Maryland method)	0/40 (0)	0/20 (0)	0/10 (0)	0/5 (0)
M-28-1	2022	Confined tapered (Cold)	4/40 (10)	3/20 (15)	2/10 (20)	0/5 (0)
M-28-2	2022	Confined tapered (Cold)	0/40 (0)	0/20 (0)	0/10 (0)	0/5 (0)
M-61	2023	Confined tapered (Cold)	0/40 (0)	0/20 (0)	0/10 (0)	0/5 (0)
Manning Tr-1	2022	Echelon (Hot)	5/40 (12.5)	2/20 (10)	2/10 (20)	1/5 (20)
Manning Tr-2	2022	Echelon (Hot)	8/40 (20)	3/20 (15)	2/10 (20)	1/5 (20)
US-31	2022	Echelon (Hot)	18/40 (45)	8/20 (40)	5/10 (50)	2/5 (40)
US-10-1	2023	Echelon (Hot)	33/40 (82.5)	16/20 (80)	10/10 (100)	5/5 (100)
US-10-2	2023	Echelon (Hot)	0/40 (0)	0/20 (0)	0/10 (0)	0/5 (0)
I-75	2023	Echelon (Hot)	22/40 (55)	13/20 (65)	6/10 (60)	4/5 (80)
US-31	2023	Echelon (Hot)	4/40 (10)	1/20 (5)	0/10 (0)	0/5 (0)

Note: The fraction shows sections that have PWL lower than 60% RQL out of the total subsections while the number in parenthesis shows their percentage.

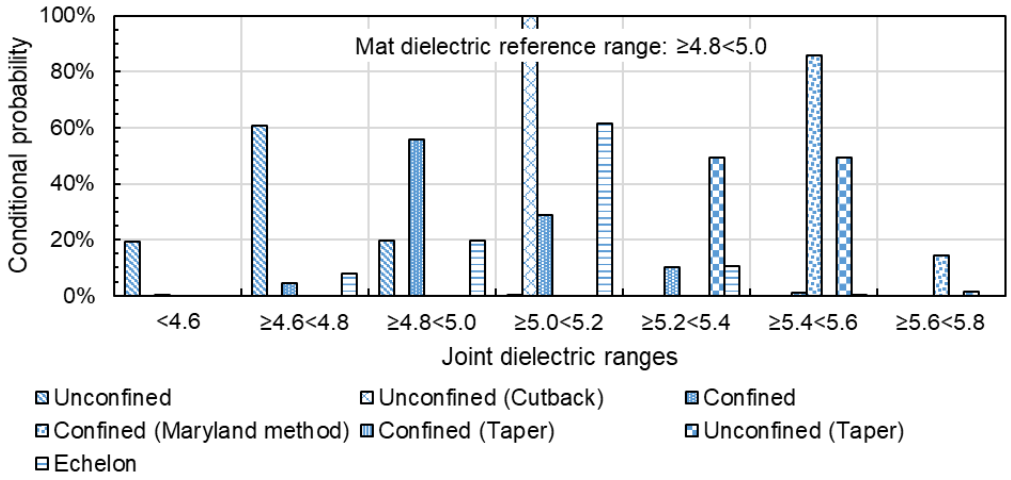

(a) Asphalt mat reference dielectric range of 4.8–5.0

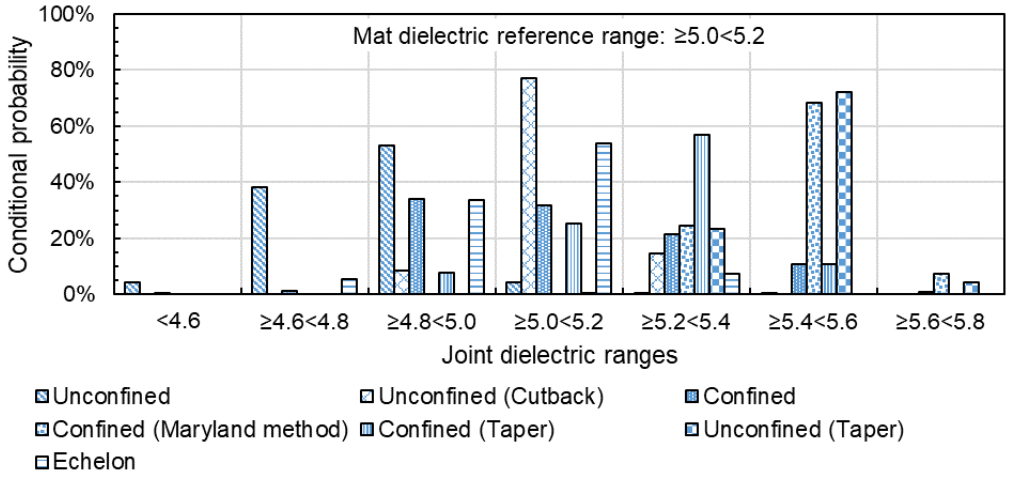

(b) Asphalt mat reference dielectric range of 5.0–5.2

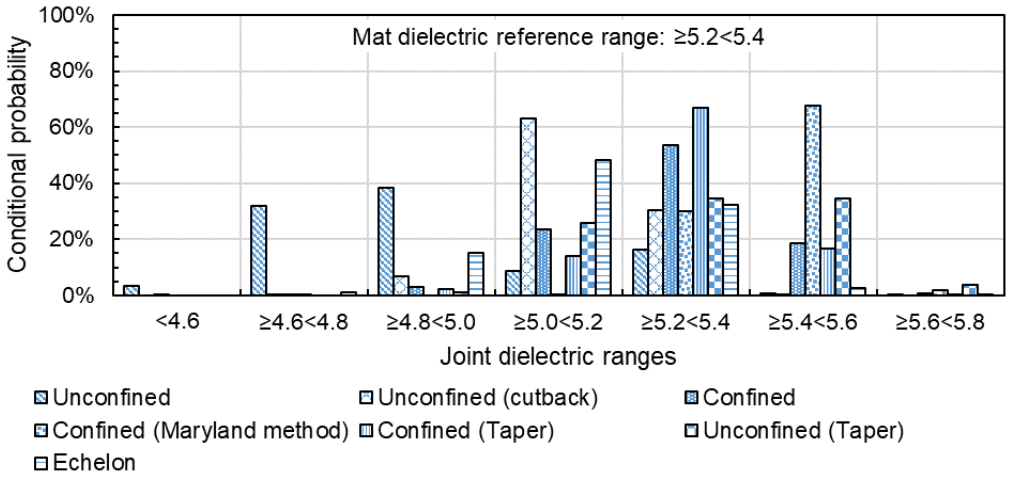

(c) Asphalt mat reference dielectric range of 5.2–5.4

Figure 4-10 Conditional probabilities of dielectric categories for varying mat dielectric reference ranges by joint type

For confined joints, the figure indicates a higher likelihood that the joint's dielectric values will align with the reference mat ranges. There is also a lower probability of the confined joint's dielectric values falling outside the mat's reference range, either higher or lower. Confined joints constructed using the Maryland method consistently show a greater chance of having dielectric values exceeding those of the reference mat. For instance, Figure 4-10(a) demonstrates that the dielectric values of a confined joint built with the Maryland method could all fall within the 5.4–5.6 range when the mat dielectric is between 4.8–5.0. Similarly, Figure 4-10(b) and Figure 4-10(c) show a 68% probability that the joint will have dielectric values within the same 5.4–5.6 range, even when the mat dielectric values are between 5.0–5.2 or 5.2–5.4.

A confined tapered joint has a 25% probability of matching the mat's dielectric values within the reference range of 5.0–5.2. Figure 4-10(b) shows a 57% chance that the joint will fall into a higher dielectric category. Furthermore, Figure 4-10(c) indicates a 67% probability that the joint will have dielectric values similar to the mat when the reference range is 5.2–5.4. Notably, Figure 4-10(a) shows no probability for the confined tapered joint because none of the associated mats from those projects had dielectric values in the 4.8–5.0 range. The unconfined tapered and echelon joints also exhibit chances of having dielectric values equal to or higher than the mat's reference ranges. However, the echelon joint shows a slight possibility of having dielectric values that are marginally lower than the corresponding mat values.

Figure 4-11 provides a probabilistic analysis using varying mat air void reference ranges, showing the conditional probabilities for different joint types based on air void categories (Table 4-1). Like the dielectric-based findings, Figure 4-11(a) indicates that unconfined joints have a considerable probability of higher air voids compared to the reference mat void content. For example, the unconfined joint has a 36% chance of falling within the 4–6% air void range when the mat is in the same range, along with a 31% and 20% probability of being in the higher 6–8% and 8–10% air void ranges, respectively. As the mat's reference void content increases, the probability of the unconfined joint having higher air voids also rises, reaching 48% for the 8–10% range per Figure 4-11(b) and 42% for the 12–14% range from Figure 4-11(c) when the reference mat void contents are 6–8% and 8–10%, respectively.

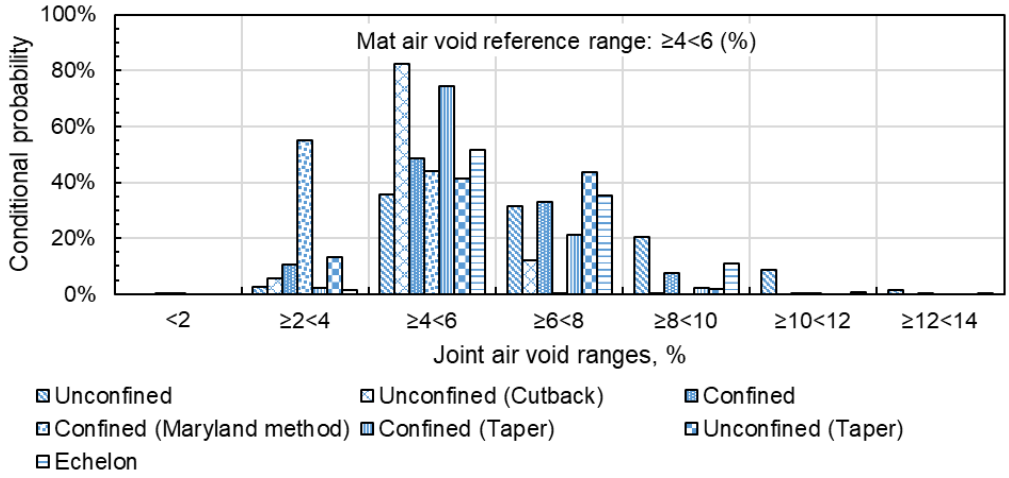

(a) Asphalt mat reference air void range of 4–6%

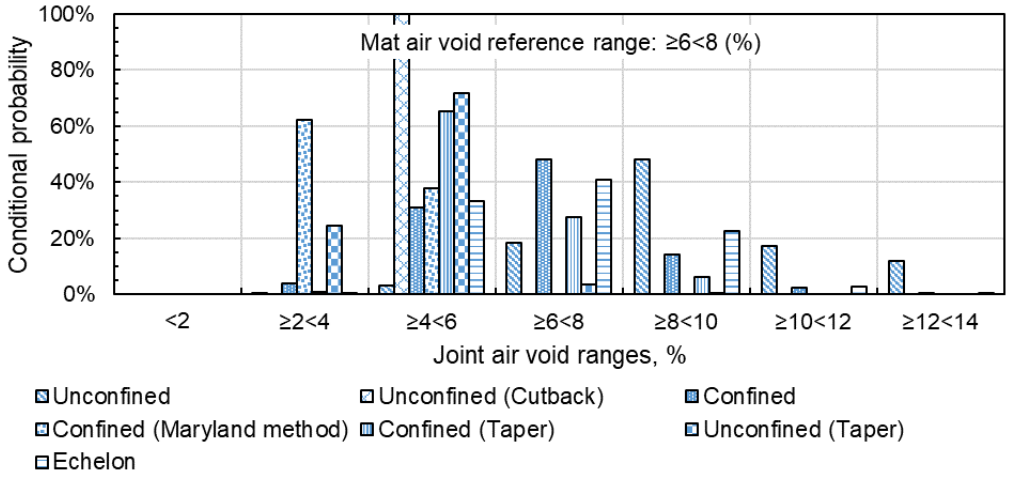

(b) Asphalt mat reference air void range of 6–8%

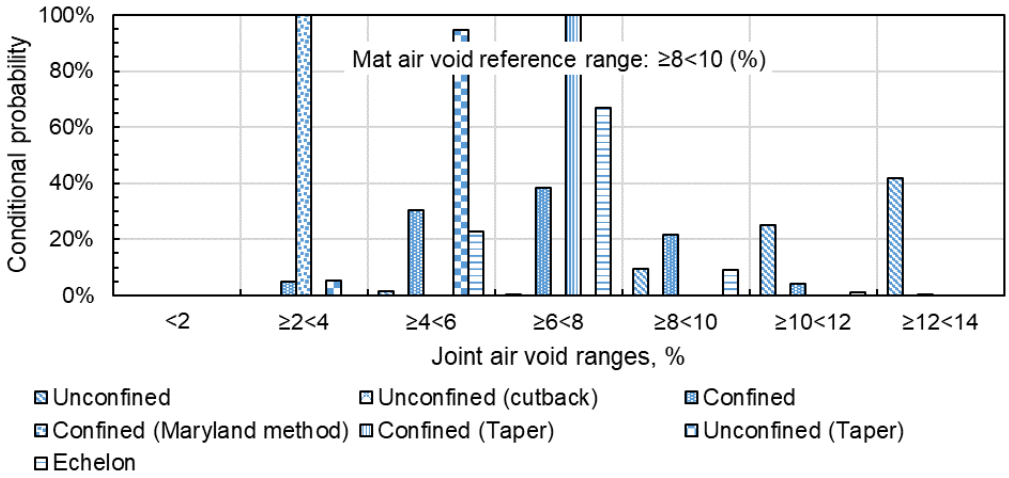

(c) Asphalt mat reference air void range of 8–10%

Figure 4-11 Conditional probabilities of air void categories for varying mat air void reference ranges by joint type

The unconfined (cutback) joint shows the highest probability of having void content within the 4–6% air void range, as seen in Figures 4-11(a) and 4-11(b), irrespective of the mat's reference ranges. Notably, Figure 4-11(c) does not provide any probability data for this joint, as none of the mat values in the projects using the cutback method fell within the 8–10% air void range. The probabilities in Figure 4-11(a) for the confined joint display higher probabilities of matching the reference mat void contents, with a 33% chance of having voids in a higher category. Figures 4-11(b) and 4-11(c) display 31% and 39% probabilities of the joint having voids in a lower category when the reference mat ranges are 6–8% and 8–10%, respectively. In the case of confined joints constructed using the Maryland method, Figure 4-11 shows the highest probability of void content falling within the 2–4% range, regardless of the mat's reference void content.

The confined taper joints primarily exhibit a higher likelihood of matching the reference mat's air void content or falling within a lower air void category, with only a minimal chance of having values in a higher void range relative to the mat reference. Similarly, the unconfined tapered joint shows higher probabilities of matching the mat's reference void content categories, except in the 4–6% air void range shown in Figure 4-11(a), indicating some chances of voids falling in a higher category. A similar trend is observed with the echelon joint, which has the highest probability of matching the mat's reference void group. However, some void contents may fall in the higher 6–8% group when the 4–6% air void range is used as the mat's reference.

The probabilistic analysis results in Figures 4-10 and 4-11 infer that constructing an unconfined joint can lead to a dielectric difference of 0.2 or more compared to the adjacent asphalt mat, with the mat showing higher dielectric values. This difference translates to an air void content of 2% or higher in the joint than in the mat, a trend also reflected in the results of Figure 4-11. These findings align with those from the two statistical approaches detailed in Tables 4-7 to 4-10, further reinforcing the conclusion that unconfined joints should be avoided when possible. Instead, the data suggests that an unconfined cutback joint offers a more effective alternative, where the compacted HMA material at the edge is trimmed before paving the adjacent lane.

4.4 CHAPTER SUMMARY

Various longitudinal joint geometries, rolling patterns, and construction techniques are currently employed in joint construction. However, conventional testing methods offer limited

coverage, which raises the risk of accepting longitudinal joints with insufficient compaction. As a result, relying on any construction technique or traditional quality evaluation method carries the risk of producing a poorly compacted joint, potentially compromising the joint's and the accompanying asphalt pavement's long-term performance. This chapter presented the methods that were used to evaluate the compaction ability of the different longitudinal joints using the continuous dielectric data collected by DPS.

The collected data was visualized using several plots to identify potential compaction differences among the dielectric profiles recorded at varying offsets from the longitudinal joint. The presented example analyses using data from the Xerxes Road project in Minnesota displayed significant dielectric differences between the joint profile, measured at a 6-inch offset from it, compared to the profiles recorded for the mat using 2 ft and 3.5 ft offset from the visible seam location. However, the recorded dielectric profiles were discretized into smaller subsections of 25, 50, 100, and 200 ft for in-depth analyses of the observed differences. These discretized data were analyzed using statistical and probabilistic approaches to evaluate the compaction ability of the different joint construction techniques and methods.

Paired *t*-tests were used to compare the mean joint dielectric values of each subsection of every project with the asphalt mat's mean values using the dielectric profile recorded at 3.5 ft offset from the joint. The paired *t*-tests evaluated the hypothesis of whether or not the relative dielectric difference is insufficient to result in the joint's air voids that are 2% or higher than the mat. The results showed that an unconfined joint produces the highest joint air voids compared to the accompanied asphalt mat. On the contrary, an unconfined joint constructed using a cutback method, where a portion of the compacted HMA material is trimmed off before building the adjacent lane, produces a density comparable to that of the mat. Moreover, confined joints, including those constructed using the Maryland method, tapered (both confined and unconfined) joints, and echelon joints, can produce similar compaction at the joint and the mat.

Before performing a similar analysis using the predicted air voids, the calibrated models were validated using the QA core data. The QA mat and joint cores from the different projects were collected from the sites on the days when DPS testing was conducted. Most of the QA core results agreed with the DPS predictions, validating the calibrated models. Moreover, some projects displayed differences that could be attributed to the fact that the QA cores were not collected within the same 1,000-foot pavement sections that were tested. A more plausible

explanation for the differences is that the collected pavement cores were not representative samples. This is because the measured void contents of the field cores collected from within the tested pavement sections reasonably agreed with the DPS-predicted air voids.

Like the results from the dielectric data, paired *t*-tests, which tested if the joints have 2% or more air voids than the adjacent asphalt mat using the predicted air voids, inferred that constructing an unconfined joint produces the least density at the joint. These joints result in over 2% air void differences relative to the mat. Moreover, using a cutback technique where constructing an unconfined joint cannot be avoided is a better option since it results in comparable joint and mat compaction.

The second statistical approach used to analyze the relative compaction of the different joint types was conducted using PWL analyses. Based on the calibrated models, the PWL calculated the percentage of sections with lower than 60% PWL using a one-sided USL of a dielectric value that would result in 2% or higher joint air voids relative to the mat. A similar analysis was accomplished using the predicted air voids as well. The results from the PWL analyses were consistent in that an unconfined joint construction produces the highest difference between the joint's void content relative to the mat, with the joint having lower density.

Observing the effect of different subsection lengths, the statistical analyses used in this study show that the percentage of sections with compaction issues increases as the subsection length increases from 25 ft to 200 ft. This trend suggests that using a smaller subsection is beneficial and can effectively identify local compaction issues. Moreover, the ability to analyze data using smaller subsection lengths demonstrates the real value of the continuous dielectric data provided by DPS in flexible pavements QA procedures. However, a 25- or 50-foot-long subsection might not be practically feasible. Thus, the results of this study support the use of DPS for the compaction evaluation of flexible pavements in general and the longitudinal joint in particular, as well as the use of a 100-ft subsection length for analysis.

Finally, this chapter also presented the results of the probabilistic analysis. Using different dielectric and air void content groups, the analysis determined the conditional probability of the joint given that the mat compaction (i.e., dielectric or void content) falls within a certain group. The probabilistic analysis results also inferred that constructing an unconfined joint can lead to a dielectric difference of 0.2 or more compared to the adjacent asphalt mat, with the mat showing higher dielectric values irrespective of the reference groups used. This

difference translates to an air void content of 2% or higher in the joint than in the mat. Thus, the results from the probabilistic analyses align with those from the two statistical approaches used in this study.

REFERENCES

1. AASHTO, *Standard specifications for transportation materials and methods of sampling and testing*. 2011.
2. Burati, J., R. Weed, C. Hughes, and H. Hill, "Evaluation of procedures for quality assurance specifications," Turner-Fairbank Highway Research Center, 2004.
3. TRB, "Transportation Research Circular Number E-C235: Glossary of Highway Quality Assurance Terms. ," Transportation Research Board, Washington, D.C., 2018.
4. Willenbrock, J. H., and P. A. Kopac, "Development of a highway construction acceptance plan," *Transportation Research Record*, 1978.
5. Haider, S. W., G. Musunuru, and K. Chatti, Effect of sample size and methods on percent within limits for quality control and assurance. In *Airfield and Highway Pavements 2017*, 2017, pp. 134-144.
6. Gharaibeh, N. G., S. I. Garber, and L. Liu, "Determining optimum sample size for percent-within-limits specifications," *Transportation Research Record,* vol. 2151, pp. 77-83, 2010.
7. Durick, M., "AASHTO Quality Assurance/Quality Control Guide Specification Status Report," In *Selected Committee Meeting Papers Presented at the 78th Annual Meeting of the American Association of State Highway and Transportation Officials* Rapid City, SD, pp. 123-125, 1992.
8. AASHTO, "Asphalt Surface Dielectric Profiling System Using Ground Penetrating Radar, PP98-19," AASHTO, Washington, D.C., 2019.

CHAPTER 5 - LONGITUDINAL JOINT QUALITY INDEX (LJQI)

5.1 SIGNIFICANCE

The dielectric profiling system (DPS) has been developed for adoption in QA and QC testing to address the limitations of traditional compaction evaluation methods (*1*). This system provides a non-destructive way to assess in-place compaction by measuring the dielectric constant of the asphalt concrete (AC) layer, offering real-time, continuous coverage of both the mat and the longitudinal joint. However, converting the measured dielectric values into air voids (or density) requires a calibrated dielectric-air void relationship. Since a hot-mix asphalt (HMA) dielectric value is influenced by its components (i.e., aggregates, binder, and air), models based on the mix's characteristics estimate its dielectric values. These models are used as inputs, either measured or literature-derived dielectric values for aggregates and binders (*2*). However, practical implementation of these mix-characteristic-based models is challenging because the required inputs, such as the dielectric values of aggregates and binders, are typically unavailable.

Alternatively, empirical models have been successfully used for estimating dielectric-air void relationships (*3-6*). These models are calibrated for each mix and need recalibration if significant changes occur in the mix components. While traditional calibration required field cores, Hoegh et al. demonstrated that calibration could be done without cores by using HMA samples compacted in the laboratory with the Superpave Gyratory Compactor (SGC) (*7; 8*). This coreless calibration method has proven reasonably accurate, though few cores are necessary for model verification. As mentioned previously, core extraction is a labor-intensive, costly, and time-consuming process generally avoided by local and state road agencies (*6; 9*).

To optimize the use of the DPS, it is recommended that the recorded dielectric values be directly incorporated into the QA and QC process during construction, eliminating the need for calibration. Such an approach would encourage the adoption of DPS by local and state agencies while minimizing the logistical challenges associated with extracting and testing pavement cores. Using DPS-recorded dielectric values directly for evaluating joint quality during construction could also offer significant advantages by providing real-time feedback, enabling immediate quality assessments and corrective actions during the paving process.

The previous chapters of this study presented a comprehensive comparison of compaction ability between the different longitudinal types relative to their accompanying asphalt mats. These comparisons were based on statistical approaches that primarily used the

recorded dielectric values, utilizing a relative dielectric value difference between the joint and the mat. The results from the dielectric-based comparisons were consistent with those drawn using the predicted air voids.

Although the paired *t*-tests method reasonably detected differences in joint types by comparing the mean mat and joint dielectric values within a subsection, it overlooked cases where the dielectric differences were greater than the ones presented in Table 3-7 (resulting in over 2% air void differences) even when the individual mat and joint had acceptable compaction (i.e., acceptable dielectric, Table 3-7). In other words, the paired *t*-tests treated the relative dielectric difference uniformly, regardless of the specific dielectric values of the mat and joint that constituted the differences.

For instance, a subsection can show a significant dielectric difference (e.g., > 0.145 in the case of the Xerxes Road project) even when both the joint and mat exhibit acceptable compaction (i.e., mat and joint dielectric values are higher than 4.927 and 4.782 corresponding to less than 8% and 10% air voids, respectively). Therefore, considering the compaction at such a subsection as unacceptable due to a large dielectric difference in the paired *t*-test is unreasonable from the contractor's perspective, especially for QA and QC purposes requiring final products' quality-based payment adjustments. Thus, it is essential to account for the individual mean mat and joint dielectric values of the subsections while using the paired *t*-tests method of joint comparison.

Figure 3-1 illustrates such situations occurring at the Xerxes Road project. Figure 3-1(a) shows the mean dielectric differences and their 95% confidence intervals (CI) for every 25 ft subsection of the unconfined joint in the Xerxes Road #1 project. The figure reveals that almost all the mean differences and their corresponding CIs exceed the upper specified limit (USL) of 0.145 for the relative dielectric value difference between the mat and the unconfined joint. Additionally, most of the mean joint dielectric values are above 4.782, the lower specified limit (LSL) that equates to an air void content of 10%, indicating that the joint's void content is below 10% overall. Only subsections 9, 10, and 24 exhibit mean joint dielectric values below this threshold.

In contrast, subsections 8 and 35 have mean joint dielectric values exceeding 4.782, yet their differences are greater than the specified USL value. This is because these subsections display better mat compaction than other project subsections. The mean mat dielectric values for

these subsections are 5.2 or more. As a result, they display the largest mean differences between the mat and the joint.

Similarly, Figure 3-1(b) shows that the mean dielectric differences for all the 25 ft subsections of the unconfined joint of the Xerxes Road #2 project surpass the USL value of 0.145. However, only half of the subsections display a mean dielectric value lower than the LSL for the joint. Since the dielectric values recorded for the accompanying asphalt mat are well above its corresponding LSL values (4.927), the resultant dielectric differences are all greater than 0.145. Such instances suggest a correction strategy that does not penalize the contractor for achieving a higher level of mat compaction relative to an acceptable joint density.

5.2 A DIELECTRIC-BASED INDEX

This study proposes a new dielectric-based index to overcome the limitation of the paired t-test method highlighted in the previous section and enhance the DPS's filed applicability by using the recorded dielectric values directly in the field. This new index is named the Longitudinal Joint Quality Index (LJQI) and is designed to determine the percentage of stations with acceptable compaction by subtracting the proportion of stations with problematic compaction. The LJQI ranges from 0 to 100 and uses the DPS-recorded field dielectric data to assess joint quality while adjusting for the asphalt mat's density. The LJQI requires minimum specified dielectric values for both the mat and the joint and an acceptable dielectric difference between them (mat – joint).

To calculate the index, the dielectric difference between the mat and joint is computed, taking into account the mat's dielectric value at each station. If the mat dielectric value exceeds the specified minimum, the difference is calculated by subtracting the recorded joint dielectric value from the minimum specified mat dielectric value. This correction addresses cases where superior mat compaction might result in a large relative dielectric difference (enough to cause a 2% or more relative air void difference), which could penalize the contractor despite acceptable joint compaction. Additionally, the LJQI evaluates joint dielectric values against a specified threshold and rejects a station's compaction if it fails to meet the individual joint compaction criteria. The LJQI calculation process is as follows:

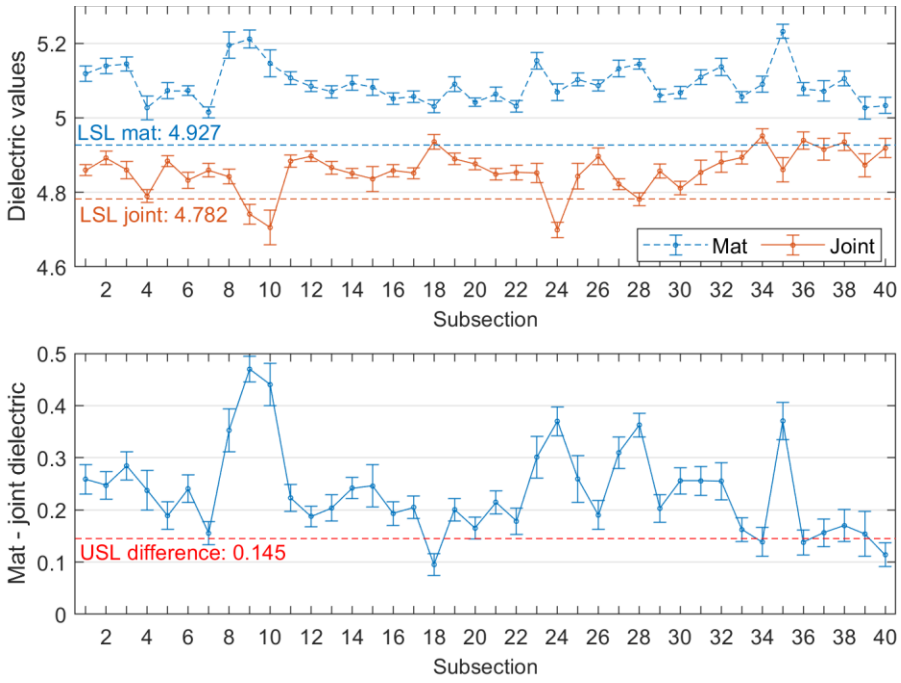

(a) Unconfined joint Xerxes Road #1 project

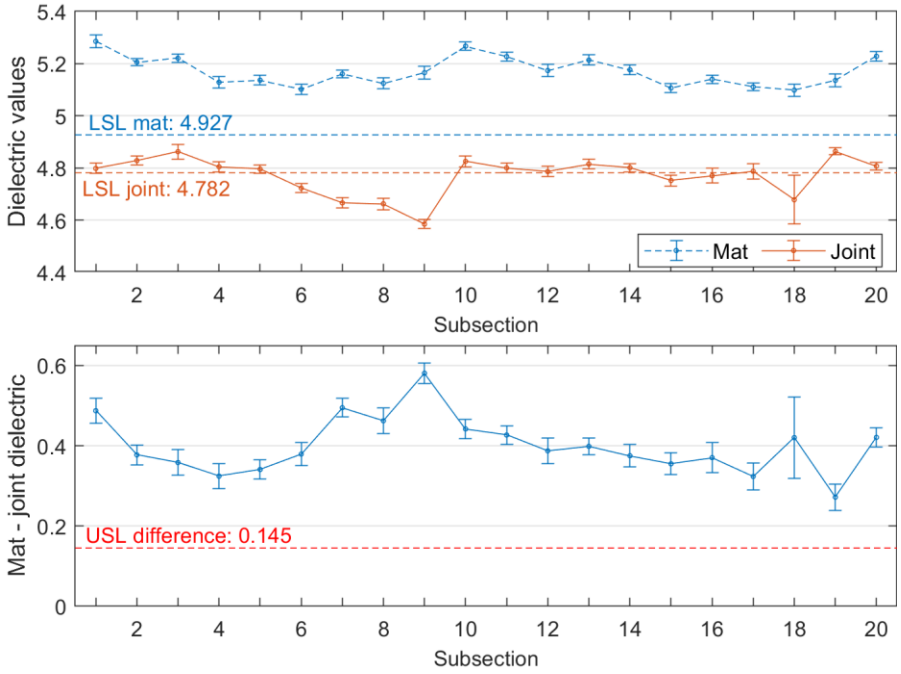

(b) Unconfined joint Xerxes Road #2 project

Figure 5-1 Mean mat and joint dielectric values and their difference with 95% CI for every 25 ft subsection – Xerxes Road project, MN

1. Establish an acceptable dielectric value for the control population (e.g., mat or the confined side of the joint, etc.), $\varepsilon_{mat,min}$.
2. Establish an acceptable dielectric difference value between the joint and the accompanying asphalt mat, $\Delta\varepsilon_{crit}$
3. Establish a minimum acceptable dielectric value for the joint, $\varepsilon_{joint,min}$
4. Compute the number of stations for the two criteria using Equation 5-1. Each criterion determines the number of stations with an unacceptable dielectric value.

$$\varepsilon_{joint} < \varepsilon_{joint,min} \text{ OR } \min(\varepsilon_{mat,}\, \varepsilon_{mat,min}) - \varepsilon_{joint} > \Delta\varepsilon_{crit} \qquad \text{Equation 5-1}$$

   where;

   ε_{joint} = recorded dielectric value at the joint,

   $\varepsilon_{joint,min}$ = minimum specified joint dielectric value,

   ε_{mat} = recorded dielectric value of the control population (e.g., mat),

   $\varepsilon_{mat,min}$ = minimum specified dielectric value of the control population (e.g., mat),

   $\Delta\varepsilon_{crit}$ = minimum specified dielectric difference between the mat (i.e., control population) and the joint (mat – joint).
5. Determine the total percentage of stations with unacceptable dielectric values meeting any of the two criteria defined in *Step 4* above.
6. Calculate the LJQI by subtracting the determined percentage from *Step 5* from 100% to get the percentage of stations with acceptable compaction.

The first criterion in *Step 4* ($\varepsilon_{joint} < \varepsilon_{joint,min}$) assesses the compaction quality of the joint by comparing its dielectric value to the minimum specified threshold ($\varepsilon_{joint,min}$). If the joint dielectric falls below this minimum, the station is deemed unacceptable due to insufficient compaction. The second criterion evaluates the difference between the mat (i.e., the control population) and the joint dielectric value at each station while applying the previously discussed correction for the mat dielectric value. The compaction is considered unacceptable if either of these two criteria is met at a given station.

To demonstrate the outcomes of the two criteria, assume that a dielectric value of 5.0 equates to 8% air voids and 10% air voids result from a dielectric value of 4.8. Thus, the $\Delta\varepsilon_{crit}$ is specified at 0.2, a dielectric difference expected to produce a 2% or more air void content difference between the mat and the joint. Table 5-1 illustrates how both criteria influence the

determination of stations with unacceptable compaction. The first row shows the assumed dielectric values corresponding to 8% and 10% air voids. With the specified mat dielectric of 5 (8% air voids) and joint dielectric of 4.8 (10% air voids), none of the criteria are met, meaning the station is not classified as unacceptable. However, if a station has more than 10% air voids at the joint, even with adequate mat compaction, it will be flagged as unacceptable (as seen in the second and third rows).

Table 5-1 Demonstrating the two LJQI criteria

Row no.	Mat air voids, %	Joint air voids, %	Mat dielectric	Joint dielectric	Criterion 1 (joint)	Criterion 2 (difference)	Unacceptable
1	8	10	5	4.8	No	No	No
2	8	10.5	5	4.75	Yes	Yes	Yes
3	7	11	5.10	4.7	Yes	Yes	Yes
4	10	11	4.8	4.7	Yes	No	Yes
5	8.9	11	4.9	4.7	Yes	No	Yes
6	4	9	5.5	4.89	No	No	No
7	7	10	5.10	4.8	No	No	No

Similarly, stations with poor joint compaction but an acceptable relative difference between the mat and joint dielectrics (as shown in the fourth and fifth rows) will also be classified as unacceptable. On the other hand, if both the mat and joint have adequate compaction, but the dielectric difference exceeds the specified limit due to exceptional mat compaction, the station will not be considered unacceptable (as indicated in the sixth and seventh rows). This demonstrates that the proposed index can account for high mat compaction while evaluating joint density individually to identify stations with compaction issues effectively.

Figure 5-2 illustrates the application of the proposed index for evaluating the compaction of samples of each type of the various longitudinal joints used in this study. The figure uses the project-specific calibration curves to obtain the maximum specified dielectric values of 8% and 10% air voids for the asphalt mat and the longitudinal joint, respectively (Table 3-7). Moreover, the LJQI calculations used the dielectric differences from the table as the maximum value for the relative differences, equating to over 2% air void difference between the mat and the joint. Note that the LJQI values presented in the figure are for all pavement sections (and not subsections).

The results show that only 84%, 51%, 11%, and 89% of stations achieved acceptable joint compaction for unconfined joints in the Xerxes Road #1, Xerxes Road #2, US-23 projects, and the I-496 (2023) projects, respectively. In contrast, the unconfined joint on the I-496 projects

(2022 and 2023), where the contractor trimmed the newly compacted edge before paving the adjacent lane (Cutback method), achieved 100% acceptable compaction throughout the section. Similarly, the confined joints constructed using the Maryland Method on the Manning Trail #1 and #2 projects also resulted in a 100% acceptable compaction. The US-23 (2022) confined joints and Xerxes Road #1 projects also generated 100% LJQI values, indicating perfect joint compaction. Similarly, confined joints constructed using the sequential mill and fill technique as in the M-25 (2022) and M-89 (2022) projects, showed perfect compaction with over 94% LJQI values.

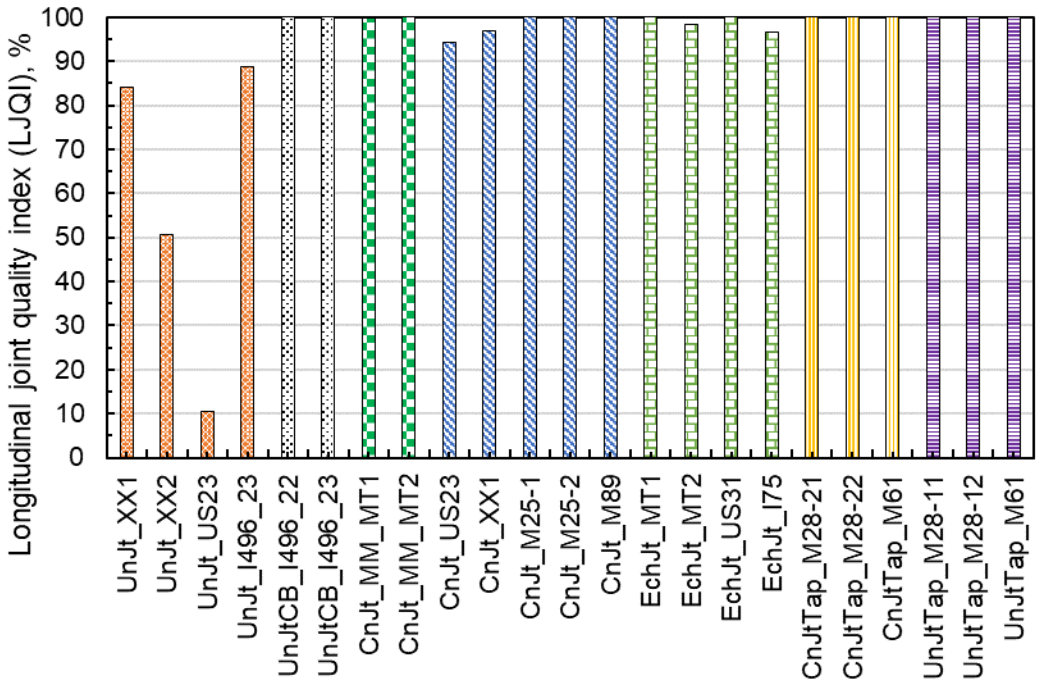

Figure 5-2 Longitudinal joint quality evaluation using the LJQI

The figure also displays that the echelon paved joint of the Manning Trail #1 and #2 projects, US-31 (2022), and the I-75 also resulted in over 97% LJQI values displaying the perfect compaction ability of this construction method. The figure also shows the LJQI values of the joints constructed using tapered geometry (of M-28 and M-61 projects). Whether confined or unconfined, the tapered joint construction technique resulted in perfect density at the joint, indicated by the 100% LJQI values. Comparing the overall results from the LJQI perspective, it is evident that the index can evaluate the individual compaction ability of the different joint types. Moreover, the resulting LJQI values infer similar results to those presented earlier. The LJQI values suggest that unconfined joints are more likely to produce inferiorly compacted

joints. Additionally, its density is enhanced if the unconfined joint is constructed using the cutback method. Also, the LJQI illustrates that both butt and tapered joint geometries are capable of better compaction using any method except for building an unconfined joint.

5.3 DETERMINATION OF AN ACCEPTANCE THRESHOLD FOR LJQI

Muslim et al. recommended using an LJQI value of 60% as the pass/fail criterion for accepting or rejecting joint compaction. This recommendation was based on the LJQI's sensitivity to varying specified minimum mat and joint dielectric values (*10*). However, the suggestion was derived from a relatively small dataset, consisting of just 15 test sections and using a unified (not a project-specific) calibrated model. Moreover, the DPS measurements from the complete 1,000 ft sections generated a single LJQI value for each pavement section (similar to Figure 5-2). The real advantage of DPS's continuous compaction (i.e., in terms of dielectric) data lies in its ability to be segmented into smaller sublots. By dividing DPS data into smaller sublots and calculating LJQI values for each, the minimum acceptable LJQI threshold can be further refined. This approach would help agencies establish a more precise rejection criterion for a longitudinal joint's compaction.

Current QA and QC practices use statistical measures such as percent defective (PD) or percent within limits (PWL) for evaluating achieved quality, as these measures efficiently and simultaneously consider both the mean and the variability of the data (*11; 12*). This study utilizes PWL determined for different joint configurations using DPS dielectric data and compares it with their estimated LJQI values to determine the limiting value for the dielectric-based LJQI. While the PWL for every subsection of each joint type was determined using the predicted air voids, as is the current state of practice for using the DPS's dielectric data, the LJQI for the subsections was determined using the dielectric data alone. The idea was to compute and use the determined PWL values as the control and analyze if the determined LJQI value displays a similar finding as the PWL for every subsection.

Since the subsection PWL was taken as a reference (i.e., considered the truth), the dielectric values from each project were converted into air voids using the individually calibrated models for PWL calculations. The PWL analysis helps assess whether the pavement's density meets the required quality standards, recognizing that local variations are inevitable and achieving 100% compliance is unrealistic. The high sampling rate of the DPS, where each sensor performs 2,000 tests spaced 6 inches apart over a 1,000 ft section, significantly enhances the

accuracy of the PWL analysis. The sample sizes remain substantial even when the data is divided into subsections. Note that establishing acceptable and rejectable quality standards is essential for any PWL analysis. In this case, a rejectable quality level (RQL) of 60% was used to define unacceptable compaction, while an acceptable quality level (AQL) of 90% is shown as a reference but is not used in the analysis.

For the M-100 project in Michigan, mat PWL values were calculated using a USL value of 6% air voids, while joint PWL was determined using three USLs of 6%, 7%, and 8% air voids. Figure 5-3 illustrates the PWL values for the mat and confined joint for every 25 ft subsection (i.e., 1000/25 = 40 subsections). Each value is based on at least 50 dielectric measurements, with two readings per linear foot yielding 50 data points per 25 ft distance. Although stringent, the selected USL values were used to introduce sufficient variation in the PWL results for comparison with LJQI values later in the analysis. The figure indicates that the mat air voids fall below 6% for the majority of subsections, resulting in higher PWL values. In contrast, the air voids in the joint fluctuate across the section, leading to varying PWL values depending on the different USL thresholds.

To optimize the use of DPS and enhance its field applicability, the recorded dielectric values are suggested to be directly incorporated into the QA and QC process during construction, eliminating the need for project-wise calibration. This can be accomplished by developing a comprehensive database of the agency's HMA mixes and determining minimum acceptable dielectric values for both the mat and joints which are required for the LJQI calculation. These values should be based on groupwise calibrations for mixes with similar aggregate types and binder compositions (i.e., sources and proportions) that display comparable dielectric-to-air void relationships. Hoegh et al. demonstrated cases where data could be aggregated to create a single calibration curve for multiple mixes (*13*). Other researchers have also demonstrated the use of combined models for mixes with similar HMA mix component sources and proportions (*6; 10; 14*).

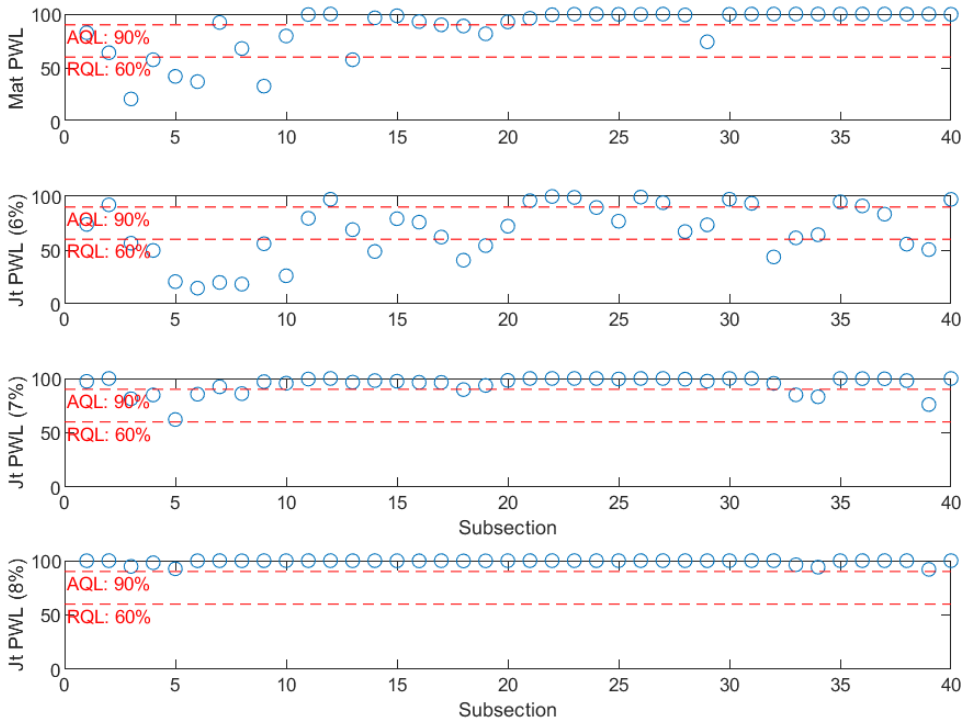

Figure 5-3 Mat and confined joint PWL at varying USL−M-100 project, MI

Table 5-2 presents the grouped dielectric values corresponding to various air void contents using the groupwise calibrated models presented in Chapter 3. The LJQI was calculated for each subsection of a project section based on these values. Unlike PWL, which factors in data variability through standard deviation, the LJQI measures the percentage of stations achieving acceptable compaction by considering the recorded dielectric value at every station. Two tolerances were applied to ensure fair comparison and account for variability: a 1% air void tolerance and a 0.08 dielectric tolerance. The 1% air void tolerance is based on the MDOT HMA production manual, which specifies this tolerance for mix design and QA purposes (*15*). The 0.08 dielectric tolerance follows the acceptable measurement limits for air-launched GPR sensors as per AASHTO PP 98-19 (*16*).

Table 5-2 Groupwise dielectric values for different air void contents

Air void content (%)	Group 1		Group 2		Group 3		Group 4	
	Dielectric values for the air void content (actual) and reduced by 0.08 (-0.08)							
	Actual	(-0.08)	Actual	(-0.08)	Actual	(-0.08)	Actual	(-0.08)
6	4.991	4.911	5.216	5.136	5.280	5.200	5.571	5.491
7	4.886	4.806	5.109	5.029	5.178	5.098	5.460	5.380
8	4.791	4.711	5.007	4.927	5.084	5.004	5.359	5.279
9	4.701	4.621	4.913	4.833	4.996	4.916	5.263	5.183
10	4.615	4.535	4.822	4.742	4.912	4.832	5.171	5.091

5.3.1 Receiver Operating Characteristic (ROC) Curves

A concept from signal detection theory, known as the receiver operating characteristic (ROC) curves, was initially used during World War II for differentiating radar signals between friendly or enemy entities, such as ships, or random noise. In signal theory, this ability to distinguish between different signals is quantified through the receiver operating characteristics (*17*). Today, the ROC curve is a valuable tool for graphically evaluating the performance of binary classification models by adjusting their thresholds. It also aids in statistically estimating false discoveries and classification errors. The ROC curve has widespread use, particularly in the medical field, to establish thresholds for various test parameters that determine the presence or absence of diseases based on test results (*17-19*). While its application in engineering has been limited, it has been explored in some instances (*20*).

Figure 5-4 illustrates the confusion matrix (C) in graphical form, which consists of four possible outcomes: (a) a true negative (TN), where a data point has a PWL value below 60% (the RQL value) and the LJQI is also below the specified threshold (e.g., 60%); (b) a false negative (FN), where the PWL is 60% or higher, but the LJQI is below 60%; (c) a true positive (TP), where both PWL and LJQI values exceed 60%; and (d) a false positive (FP), where the PWL is below 60%, but the LJQI exceeds 60%. After determining these four categories, the confusion matrix is constructed using Equation 5-2.

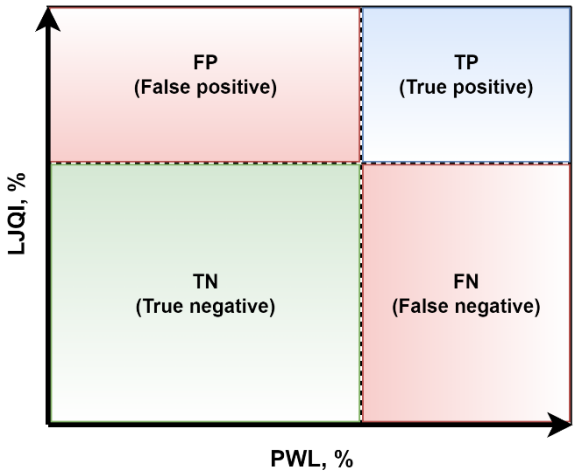

Figure 5-4 A representation of the confusion matrix

$$C = \begin{bmatrix} FP & TP \\ TN & FN \end{bmatrix} \qquad \text{Equation 5-2}$$

The ROC curve is created by plotting two key statistical performance measures: (a) the true positive rate (TPR), also known as sensitivity, against (b) the false positive rate (FPR), across various cutoff points (i.e., thresholds). Sensitivity (S) represents the likelihood of correctly identifying positive cases among the total number of positive instances, and it is calculated using Equation 5-3. In this study, sensitivity refers to the probability that the LJQI accurately identifies stations with acceptable compaction (above the threshold) compared to all stations with a PWL of 60% or higher. On the other hand, the FPR measures the probability of false positives, which occurs when the LJQI incorrectly identifies a station as having acceptable compaction when it does not. The FPR is determined using Equation 5-4 and is equal to 1 minus specificity (SP). Specificity, also called the true negative rate (TNR), reflects the probability of correctly identifying negative cases out of the total number of negative instances. In other words, specificity shows the proportion of stations where the LJQI correctly identifies unacceptable compaction (below the threshold), given that their PWL is less than 60%.

Accuracy is a statistical metric that evaluates how effectively a binary classifier distinguishes between two conditions. It is computed using Equation 5-5, representing the proportion of correct predictions (i.e., true instances) out of the total number of cases analyzed. In simpler terms, Accuracy indicates the percentage of correctly identified instances where both the PWL and LJQI classifiers agree (i.e., TN and TP cases). Another commonly used metric to summarize the performance of an ROC curve is the area under the curve (AUC), calculated using Equation 5-6. The AUC is determined by summing the areas of trapezoids formed by connecting different points on the ROC curve. It measures the test's (i.e., LJQI's) accuracy in distinguishing between specific binary outcomes, such as stations with acceptable or unacceptable compaction (*17*). AUC values range from 0 to 1, where an AUC of 1 signifies perfect agreement between the LJQI and PWL values, with no FP instances (i.e., ideal specificity). Conversely, an AUC of 0.5 suggests that the LJQI cannot differentiate between the scenarios of interest. In general, an AUC above 0.9 is considered excellent, while an AUC between 0.8 and 0.9 indicates good accuracy (*18; 21*).

$$TPR = \frac{TP}{TP + FN} = \frac{No.\,of\ stations\ with\ LJQI\ \geq threshold}{Total\ no.\,of\ stations\ with\ PWL\ \geq 60\%} \qquad \text{Equation 5-3}$$

$$FPR = \frac{FP}{FP + TN} = 1 - SP = \frac{No.of\ stations\ with\ LJQI < threshold}{Total\ no.of\ stations\ with\ PWL < 60\%} \quad \text{Equation 5-4}$$

$$Accuracy = \frac{TN + TP}{TN + TP + FN + FP} \quad \text{Equation 5-5}$$

$$AUC = \int_0^1 ROC(f)\, df = \sum_{i=1}^{n} \frac{(Y_{i+1} - Y_i)(X_{i+1} + X_i)}{2} \quad \text{Equation 5-6}$$

where;

f = indicates the FPR,

$ROC(f)$ = indicates the TPR,

Y= indicates the values of the TPR (i.e., S) on the ROC curve,

X= indicates the values of FPR (i.e., 1-SP) on the ROC curve.

Table 5-2 presents various scenarios where LJQI values were calculated for each subsection (of varying length) within the 1,000 ft sections of different pavement projects. For instance, when the mat and longitudinal joint were specified to have maximum air void contents of 6% and 8%, respectively, LJQI values were computed twice. First, the dielectric values listed in the "Actual" column were used against air void content limits of 7% and 9% (i.e., 4.886 for the mat and 4.701 for the joint in Group 1) while applying a 1% air void tolerance. Second, the dielectric values from the "(-0.08)" column were used for the 6% and 8% air void content limits (i.e., 4.911 for the mat and 4.711 for the joint in Group 1), using a 0.08 dielectric tolerance. Similarly, for the scenario where the mat had a maximum air void content of 6% and the joint was specified at 7%, the dielectric value of 4.886 (for Group 1) was used for the mat, and 4.791 for the longitudinal joint, applying a 1% air void content tolerance. For the same scenario, using the 0.08 dielectric tolerance, the dielectric values from the "(-0.08)" column were applied (i.e., 4.911 for the mat and 4.806 for the joint).

Figure 5-5 illustrates the ROC curves for the scenario where the mat and longitudinal joint were specified to have 6% and 8% as the upper limit for air void content, respectively, using both tolerances for 25 ft subsection lengths. The AUC values for both tolerance methods exceed 0.92, indicating excellent accuracy. The AUC calculated with the 0.08 dielectric tolerance is slightly higher than the 1% air void content tolerance. Both AUC values are

significantly higher than 0.5 (i.e., the null hypothesis), confirming that the LJQI can effectively distinguish compaction quality at the joint compared to the PWL analysis.

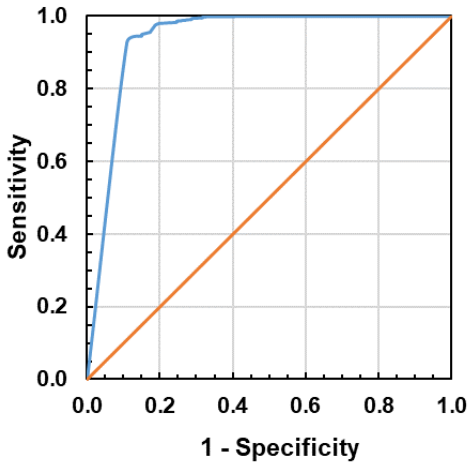

Area	: 0.936
Standard error	: 0.012
95% confidence lower bound	: 0.912
95% confidence Upper bound	: 0.959
Significance (Null hypothesis: AUC = 0.5)	: 0.000

(a) Using 0.08 dielectric tolerance

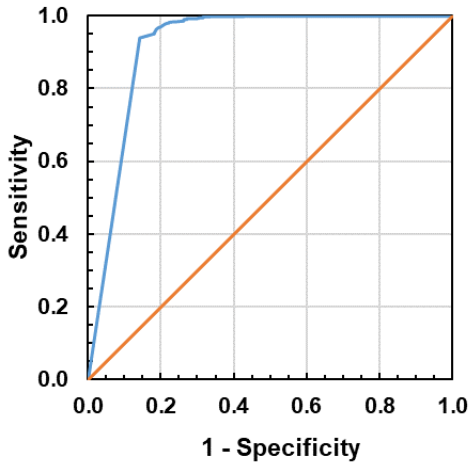

Area	: 0.921
Standard error	: 0.013
95% confidence lower bound	: 0.894
95% confidence Upper bound	: 0.947
Significance (Null hypothesis: AUC = 0.5)	: 0.000

(b) Using 1% air void content tolerance

Figure 5-5 ROC curves using 6% mat and 8% joint specified air voids - 25 ft subsections

Table 5-3 presents the sensitivity (S) and 1-specificity (SP) (i.e., FPR) values for various scenarios and cutoff points using 25 ft subsections. The data suggests that the 60% cutoff for LJQI, recommended based on a previous study using dielectric measurements within 1,000 ft sections from 15 pavement projects, is reasonable but somewhat conservative. The table indicates that applying a 60% LJQI cutoff as an acceptance criterion results in slightly higher FPR, reflected in 1-SP values that range between 35% and 43%. The table also reveals that specifying a USL of 7% air voids for the longitudinal joint with a 1% air void tolerance leads to the lowest 1-SP values. However, using a 7% air void content as the USL for a longitudinal joint may be overly strict.

Alternatively, applying a 0.08 dielectric tolerance with a 6% air void content USL also produces lower SP values, though this remains a stringent quality requirement. Setting the USL at 8% air void content for the joint seems more reasonable. Furthermore, using a 0.08 dielectric tolerance consistently results in lower 1-SP values overall. Moreover, while the LJQI acceptance cutoff could be raised from 60% to 70%, 80%, or even 90%, a 70% cutoff is recommended as it strikes a balance, being neither too conservative nor overly lenient.

Table 5-3 Sensitivity (S) and 1-specificity (SP) for varying scenarios and cutoffs – 25 ft subsections

Cutoffs	S and 1-SP values for various air void content percentages and associated tolerances (tol.)									
	6%, tol. 1%		7%, tol. 1%		8%, tol. 1%		6%, tol. 0.08 DC		8%, tol. 0.08 DC	
	S	1-SP	S	1-SP	S	1-SP	S	1-SP	S	1-SP
50%	1.000	0.469	1.000	0.398	1.000	0.480	1.000	0.429	1.000	0.428
60%	1.000	0.433	1.000	0.339	0.999	0.412	1.000	0.387	0.999	0.354
70%	0.999	0.397	0.999	0.286	0.998	0.321	0.993	0.329	0.995	0.292
80%	0.993	0.340	0.991	0.237	0.991	0.264	0.980	0.290	0.984	0.242
90%	0.963	0.290	0.979	0.185	0.978	0.210	0.931	0.240	0.972	0.183

Figure 5-6 displays the accuracy values derived from confusion matrices (*C* matrices) based on ROC curves generated for different scenarios using 25 ft, 50 ft, and 100 ft subsections. The objective was to assess the effect of varying subsection lengths on accuracy and determine whether the LJQI cutoff would vary. The findings show that the accuracy values change only slightly when using subsections of different lengths. Additionally, the combination of an 8% air void content as a USL, a 0.08 dielectric tolerance, and an LJQI cutoff of 70% yields the highest accuracy, making this scenario the recommended approach, with an LJQI limit of 70%.

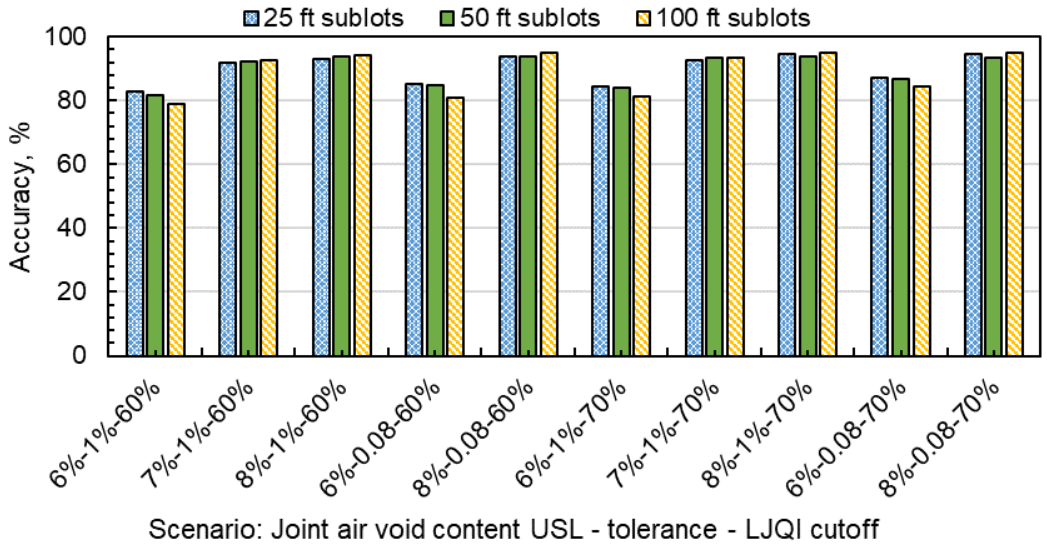

Figure 5-6 Accuracy for each scenario for 25 ft, 50 ft, and 100 ft subsection lengths

Figure 5-7 illustrates the confusion matrix for the selected scenario (i.e., an 8% air void USL and a 0.08 dielectric tolerance), detailing data distribution across the four possible outcomes (i.e., TP, TN, FP, FN) for some projects. The matrix shows that the chosen criterion most accurately identifies the true instances (i.e., TP, TN). Similarly, Figure 5-8 presents the percentages of the four possible outcomes for each pavement section, comparing various sublot

lengths under a 70% LJQI cutoff. Although the accuracy values across different sublot sizes were not significantly different (as seen in Figure 5-6), Figure 5-8 highlights that using 100 ft subsections greatly reduces false instances, particularly FP ones.

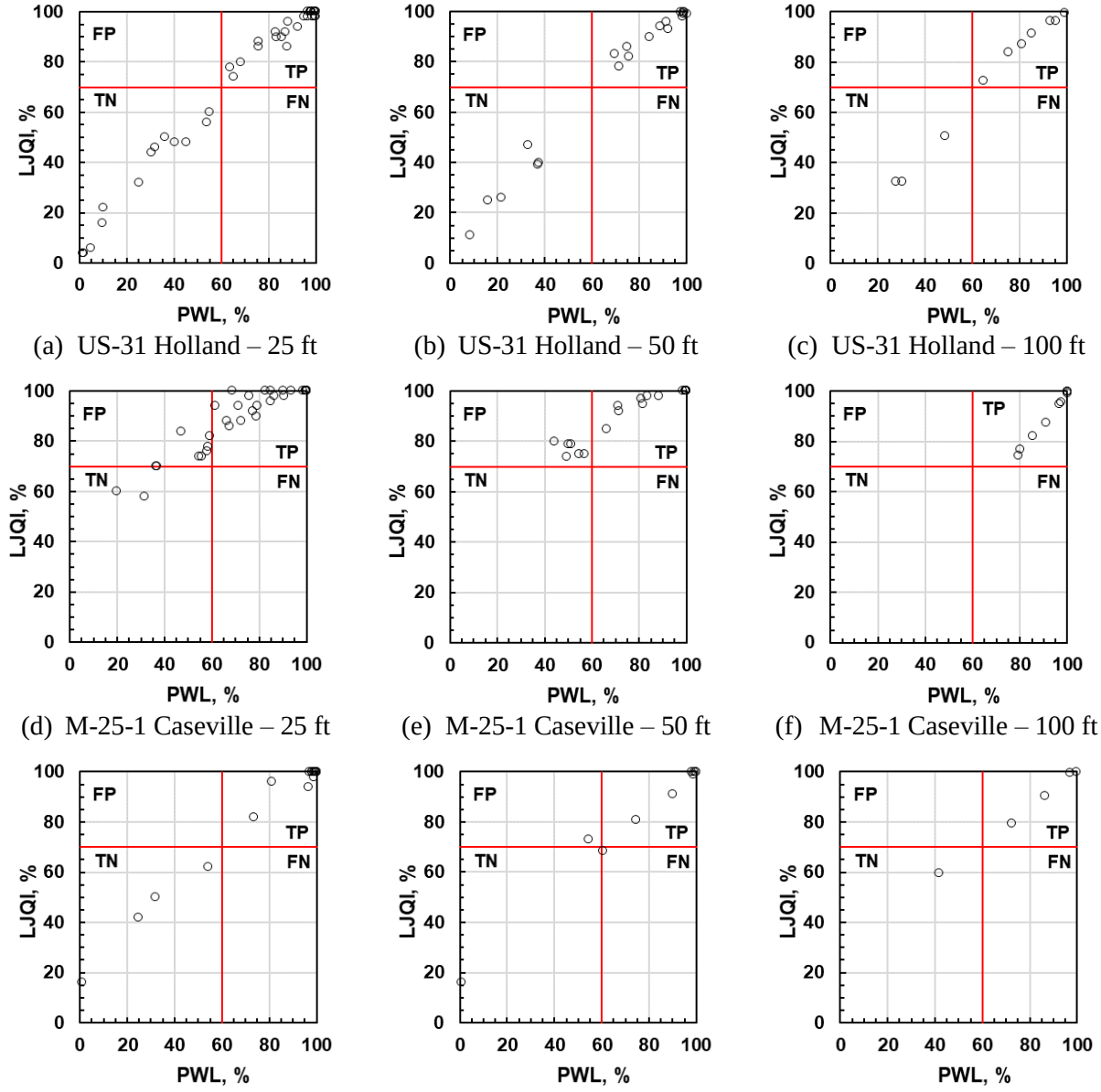

(a) US-31 Holland – 25 ft (b) US-31 Holland – 50 ft (c) US-31 Holland – 100 ft

(d) M-25-1 Caseville – 25 ft (e) M-25-1 Caseville – 50 ft (f) M-25-1 Caseville – 100 ft

(g) US-23SMA Standish – 25 ft (h) US-23SMA Standish – 50 ft (i) US-23SMA Standish – 100 ft

Figure 5-7 Graphical representation of *C* matrix for echelon-paved hot joint (US-31), confined joint (M-25-1), and confined joint (US-23 SMA) using USL of 8% air voids, 0.08 dielectric tolerance, and 70% LJQI cutoff for joint acceptance

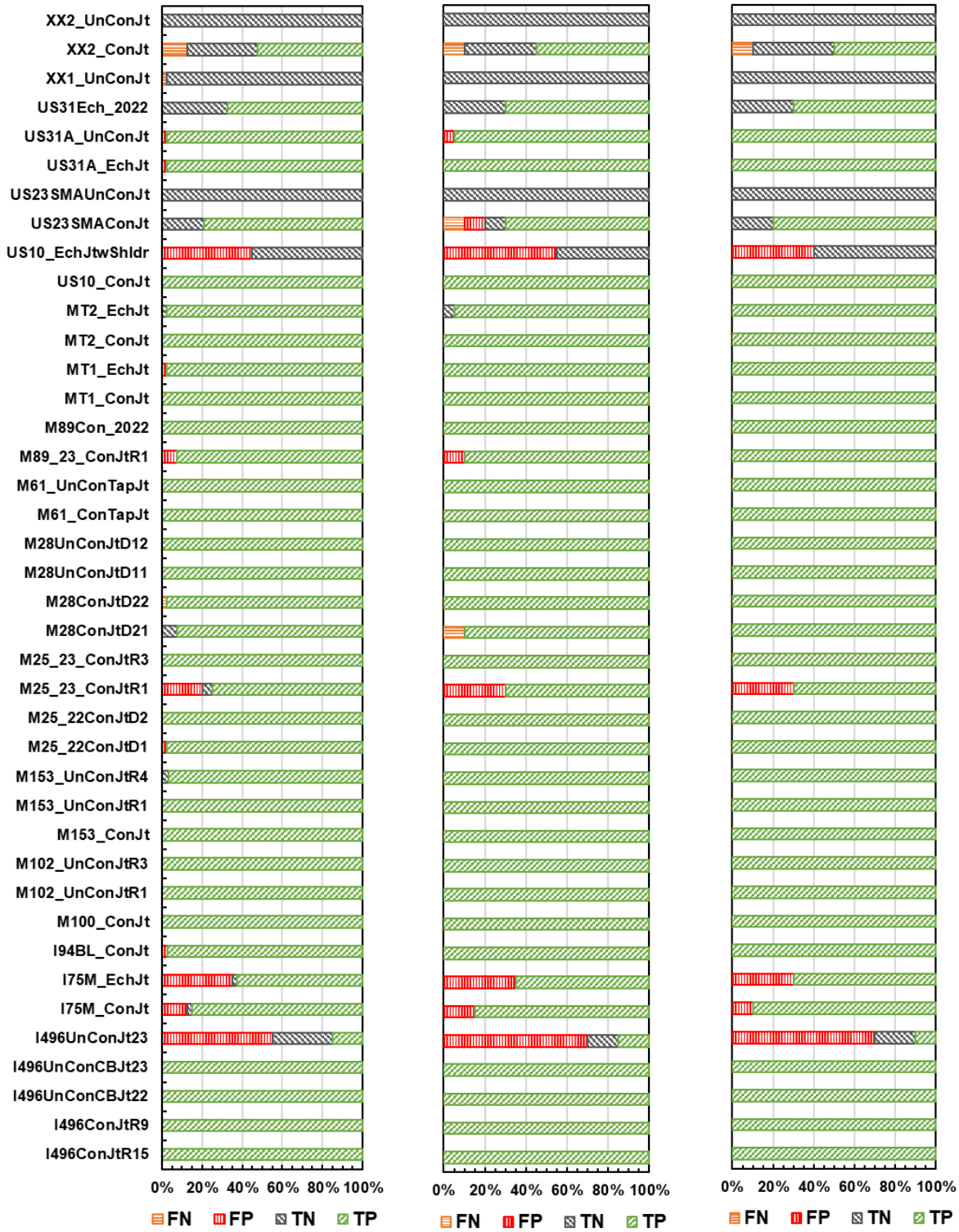

(a) 25 ft sublots (b) 50 ft sublots (c) 100 ft sublots

Figure 5-8 Every possible outcome's percentage for every longitudinal joint of each project using USL of 8% air voids, 0.08 dielectric tolerance, and 70% LJQI cutoff for joint acceptance

5.4 CHAPTER SUMMARY

The quality of asphalt pavement, particularly at the longitudinal joint, is heavily influenced by the level of compaction achieved during construction. Traditional quality assurance (QA) and quality control (QC) methods rely on extracting field cores, which are surface-destructive, time-consuming, and require significant resources in terms of time, cost, and labor. More importantly, core sampling provides limited coverage and may not accurately reflect the overall compaction quality. To overcome these challenges, the Dielectric Profiling System (DPS) offers a more efficient alternative by providing continuous compaction coverage as the recorded dielectric profiles. The DPS is especially advantageous when dielectric values are used directly, without the need to calibrate a dielectric-air void relationship. This direct use of dielectric measurements streamlines QA and QC testing in the field. It encourages the adoption of DPS by local agencies that may not have the resources or capacity to monitor pavement compaction using core samples.

For a calibration-free use of the DPS's dielectric data, groupwise model calibration is possible. In such groupwise calibrations, HMA mixes with similar sources and proportions of the aggregates and binders can be combined to obtain a single dielectric-air void relationship. However, to achieve this capability, highway agencies need to develop a comprehensive database of dielectric-air void relationships for all the HMA mixes they use. Chapter 3 of this dissertation demonstrated the feasibility of groupwise calibrations for the various HMA mixes used by the Michigan Department of Transportation (MDOT).

The paired *t*-test approach presented in the preceding chapter of this dissertation displayed the use of the recorded dielectric values in comparing the compaction ability of the various longitudinal joints. It utilized the mean mat and joint dielectric values within a subsection and effectively evaluated the achieved compaction. However, it overlooked cases where the dielectric differences were greater than the ones presented in Table 3-7, which may result in over 2% relative air void differences even when the individual mat and joint had acceptable compaction. In other words, the relative dielectric difference was treated uniformly in the paired *t*-tests, regardless of the specific dielectric values recorded at the mat and joint locations that constituted the differences.

To address the limitation of the paired *t*-test method's limitation and improve the practical use of DPS by directly utilizing the recorded dielectric values in the field, this study introduces a

new dielectric-based index called the Longitudinal Joint Quality Index (LJQI). The LJQI is designed to evaluate compaction quality by calculating the percentage of stations with adequate compaction. The index ranges from 0 to 100 and leverages field dielectric data recorded by DPS to assess joint quality while factoring in the density of the asphalt mat. The LJQI requires minimum specified dielectric values for both the mat and the joint and an acceptable dielectric difference between them (i.e., mat minus joint).

The results presented in this chapter highlighted the ability of the LJQI to compare the compaction ability of the various longitudinal joints. Using the recorded dielectric values, the LJQI determined for a sample of every type of longitudinal joint and its accompanying asphalt mat reinforced the finding of the previously presented statistical and probabilistic approaches. The LJQI results show, consistent with the results from the methods used earlier, that constructing an unconfined joint has the greatest chance of producing unacceptable joint density. The cutback technique, which requires trimming off a portion of the compacted edge before paving the adjacent lane, improves the compaction quality and produces perfect joint compaction. Moreover, the LJQI could also replicate the results presented earlier by displaying that all the other joint types (i.e., confined joints, echelon-paved joints, and tapered joints) can produce superior compaction at the longitudinal joint. While the LJQI displayed similar findings as the statistical and probabilistic analyses, these were based on section wise dielectric data.

To determine a threshold for joint acceptance using the LJQI, the Receiver Operating Characteristic (ROC) curves were utilized. The percent within limits (PWL) was determined for every subsection (of varying lengths) using the predicted air voids and the project-specific calibrated models and used as a reference. The LJQI was determined for every subsection using different upper specified limits (USL) and tolerances. The ROC curves show that using a 60% LJQI threshold for joint acceptance leads to a false positive rate (FPR) between 35% and 43%. Setting USL of 6% and 7% air void content for longitudinal joint compaction, combined with a 1% air void tolerance or a 0.08 dielectric tolerance, results in the lowest FPR values. However, these stringent quality standards may be impractical for widespread application.

A more reasonable approach involves specifying 8% air void content as the USL for the longitudinal joint. Additionally, using a 0.08 dielectric tolerance instead of the 1% air void tolerance further reduces the FPR values. Based on the results presented, the LJQI cutoff could be raised from 60% to 70%, 80%, or even 90%; a 70% cutoff is recommended as a balanced

choice, neither too conservative nor overly lenient. Furthermore, segmenting the DPS data into smaller sublots of varying lengths did not significantly impact the accuracy of the ROC curves, but using 100 ft subsections considerably reduced the number of false positive (FP) instances.

REFERENCES

1. Khazanovich, L., K. Hoegh, and R. Conway, "Non-destructive Evaluation of Bituminous Compaction Uniformity Using Rolling Density," 2017.
2. Al-Qadi, I. L., Z. Leng, S. Lahouar, and J. Baek, "In-place hot-mix asphalt density estimation using ground-penetrating radar," *Transportation Research Record,* vol. 2152, pp. 19-27, 2010.
3. Böttcher, C. J. F., O. C. van Belle, P. Bordewijk, A. Rip, and D. D. Yue, "Theory of electric polarization," *Journal of The Electrochemical Society,* vol. 121, p. 211Ca, 1974.
4. Haddad, R., and I. L. Al-Qadi, "Characterization of portland cement concrete using electromagnetic waves over the microwave frequencies," *Cement and concrete research,* vol. 28, pp. 1379-1391, 1998.
5. Hoegh, K., L. Khazanovich, S. Dai, and T. Yu, "Evaluating asphalt concrete air void variation via GPR antenna array data," *Case Studies in Nondestructive Testing and Evaluation,* vol. 3, pp. 27-33, 2015.
6. Haider, S. W., H. B. Muslim, L. Khazanovich, M. E. Kutay, and B. Cetin, "BMP For Issues with Asphalt Centerline Joint and Intelligent Compaction for Local Agencies," Minnesota. Department of Transportation. Office of Research & Innovation, 2023.
7. Hoegh, K., R. Roberts, S. Dai, and E. Zegeye Teshale, "Toward core-free pavement compaction evaluation: An innovative method relating asphalt permittivity to density," *Geosciences,* vol. 9, p. 280, 2019.
8. Hoegh, K., T. Steiner, E. Zegeye Teshale, and S. Dai, "Minnesota Department of Transportation case studies for coreless asphalt pavement compaction assessment," *Transportation Research Record,* vol. 2674, pp. 291-301, 2020.
9. Chitnis, V., M. Sukhija, and E. Coleri, "Constructing High-Density Longitudinal Joints To Improve Pavement Longevity," Oregon Department of Transportation. Research Section, 2024.
10. Muslim, H. B., S. W. Haider, and L. Khazanovich, *Dielectric-Based Index for Quality Evaluation of HMA Centerline Longitudinal Joint*. https://ascelibrary.org/doi/abs/10.1061/9780784485538.016.
11. AASHTO, *Standard specifications for transportation materials and methods of sampling and testing*. 2011.
12. Burati, J., R. Weed, C. Hughes, and H. Hill, "Evaluation of procedures for quality assurance specifications," Turner-Fairbank Highway Research Center, 2004.
13. Hoegh, K., S. Dai, T. Steiner, and L. Khazanovich, "Enhanced Model for Continuous Dielectric-Based Asphalt Compaction Evaluation," *Transportation Research Record,* vol. 2672, pp. 144-154, 2018.
14. Muslim, H. B., S. W. Haider, and L. Khazanovich, "Flexible pavement longitudinal joint quality evaluation using non-destructive testing," *Journal of Road Engineering,* vol. 4, pp. 189-202, 2024.

15. MDOT, "HMA Production Manual," Construction Field Services, Michigan Department of Transportation, Lansing, MI, 2020.

16. AASHTO, "Asphalt Surface Dielectric Profiling System Using Ground Penetrating Radar, PP98-19," AASHTO, Washington, D.C., 2019.

17. Kumar, R. V., and G. M. Antony, "A review of methods and applications of the ROC curve in clinical trials," *Drug Information Journal,* vol. 44, pp. 659-671, 2010.

18. Çorbacıoğlu, Ş. K., and G. Aksel, "Receiver operating characteristic curve analysis in diagnostic accuracy studies: A guide to interpreting the area under the curve value," *Turkish Journal of Emergency Medicine,* vol. 23, p. 195, 2023.

19. Zweig, M. H., and G. Campbell, "Receiver-operating characteristic (ROC) plots: a fundamental evaluation tool in clinical medicine," *Clinical chemistry,* vol. 39, pp. 561-577, 1993.

20. Giglioni, V., E. García-Macías, I. Venanzi, L. Ierimonti, and F. Ubertini, "The use of receiver operating characteristic curves and precision-versus-recall curves as performance metrics in unsupervised structural damage classification under changing environment," *Engineering Structures,* vol. 246, p. 113029, 2021.

21. Zhu, W., N. Zeng, and N. Wang, "Sensitivity, specificity, accuracy, associated confidence interval, and ROC analysis with practical SAS implementations," *NESUG proceedings: health care and life sciences, Baltimore, Maryland,* vol. 19, p. 67, 2010.

CHAPTER 6 - PERFORMANCE RELATED SPECIFICATIONS (PRS) FRAMEWORK FOR LONGITUDINAL JOINTS

6.1 SIGNIFICANCE

The air void content in asphalt concrete (AC) plays a crucial role in the performance of hot mix asphalt (HMA) pavements. Linden et al. found that for every 1% increase in air void content beyond 7%, the pavement's service life is reduced by 10% (*1*). The experimental research on the impact of air voids on HMA fatigue performance dates back to the late 1960s (*2*). One study reported that the fatigue performance of HMA mixes decreases by 20.6% to 43.8% for each 1% increase in air voids (*3*). Similarly, other studies found a 15.1% reduction in fatigue performance with a 1% increase in air voids (*4; 5*). Another investigation that combined laboratory and field tests revealed that a 1% decrease in air void content improved fatigue performance by 9% to 13.5% in the lab and 8.2% to 21.3% in the field for different HMA mixes (*6*). In 2010, research on Kentucky mixtures showed a 42% decrease in fatigue performance when air void content increased from 7% to 11.5%, equivalent to a 9.2% reduction in fatigue life for every 1% rise in air voids (*7*).

Several studies have also examined the impact of air void content on the rutting performance of HMA pavements. Field measurements have shown that rutting performance in different HMA mixes deteriorated by 9.6% to 66.3% (*6*). Based on the type of HMA mix, the same study concluded that rutting resistance decreases by 7.3% for every 1% increase in air voids (*6*). Seeds et al. found a 10.9% reduction in rutting performance for a 1% rise in air void content (*3*). Another study, using the flow number test, revealed that as the air void content in an HMA mix increased from 7% to 8.5%, its rutting resistance dropped by approximately 34%, equivalent to a 22.7% reduction per 1% increase in air voids (*7*). These findings underscore that air void content and in-place density are closely linked to the level of compaction achieved during construction, significantly influencing the structural integrity and long-term performance of pavements (*8*). Consequently, AC density is critical in quality control (QC) and quality assurance (QA) procedures for HMA pavement construction.

Many state highway agencies (SHAs) assess pavement construction quality based on the achieved in-place density, tying it to contractor incentives or penalties through specified minimum and maximum thresholds. Hughes recommended a 93% density threshold (7% air voids) with a standard deviation of 1.5% for agencies using end-result specifications for density

measurement (*9*). Later, the Asphalt Institute and Brown et al. suggested a 92% density (8% air voids) to reduce water permeability and binder aging (*10; 11*), a recommendation supported by other studies employing various evaluation methods (*12*). Aschenbrener and Tran reported that 12 agencies aim to minimize density measurements below 92% during in-place pavement compaction assessments (*12*). Three agencies use lot averages, while nine rely on percent within limit (PWL) specifications, with varying testing frequencies. For instance, the Michigan Department of Transportation (MDOT) mandates a minimum lot average of 92.5%, offers incentives for exceeding this threshold, and uses PWL as the quality indicator (*13*). MDOT requires four random QA field cores per sublot (up to 1,000 tons) for projects over 5,000 tons of HMA and one random core at the longitudinal joint for every 2,000 feet of constructed pavement.

The as-constructed density at the longitudinal joint of flexible pavements is just as critical as the density at the center of the lane (i.e., the mat). Many SHAs face challenges in maintaining the joints, as low-density, poorly constructed joints can lead to early failure in otherwise well-built pavements (*14*). Achieving the required density at the centerline joint, where two parallel lanes are constructed at different times, is a common issue in HMA pavement construction. This challenge often arises from limitations in paving equipment or site conditions, such as building one lane while traffic flows in the adjacent lane. Several factors reduce the compaction effort at the joint compared to the asphalt mat, including (a) the unconfined edge at the joint, which allows lateral movement of fresh asphalt instead of reducing its volume during compaction; (b) temperature differences between the materials in the two lanes (*14*); and (c) insufficient HMA material, leaving the joint underfilled (*15*). As a result, joint density is typically lower than mat density, making the joint more susceptible to cracking and moisture infiltration, which can lead to debonding and stripping. Moreover, in colder climates, freeze-thaw cycles of the infiltrated moisture increase the risk of joint failure and pavement raveling near the joint (*16*).

Recognizing the vital role of longitudinal joint quality in pavement performance, some SHAs have implemented specific density requirements for joints separate from those for the overall pavement. These specifications ensure that the joint meets a minimum density standard. Typically, the required density for a longitudinal joint is allowed to be up to 2.0% lower (in terms of $\%G_{mm}$) than the minimum density needed for the asphalt mat (*12*). For example, the MDOT guidelines specify that the average density at the joint for a given lot (usually 2,000 feet)

should be at least 90.5%, which is 2.0% lower than the required 92.5% minimum density for the mat (*17*). Previous studies have shown that a well-constructed joint should have 1 to 2% lower density than the mat, while a poorly constructed joint may show a density drop of 5 to 10% (*14*). Additionally, research into different longitudinal joint construction methods concluded that the joint density should be within 2.0% of the mat density to ensure better performance (*18*).

Many SHAs incentivize contractors to achieve higher joint densities, similar to those offered for better mat compaction (*12; 19*). Conversely, penalties are imposed when joint density falls below the specified minimum. For example, the MDOT offers contractors an incentive of up to $1.00 per linear foot for joints that meet or exceed the minimum density requirement of 90.5%, with a maximum incentive for joint densities of up to 93.5% (*20*). If the joint density falls between 86% and 90.49%, contractors face disincentives, with penalties reaching up to $9.00 per linear foot for joints with 86% density on the top course and up to $4.00 per linear foot for leveling and base courses. Joint densities below 86% (equivalent to 14% air voids) are deemed unacceptable and require different removal strategies based on the layer's position in the pavement structure (*17*). Similarly, the Iowa Department of Transportation (Iowa DOT) offers an incentive of up to $0.40 per foot for joint densities exceeding 97% while imposing a maximum disincentive of $0.80 per foot for densities below 95% (*19*). No payment adjustments for joint densities between 95% and 97% are made.

Most SHAs use specifications focusing on achieved in-place density (or air void content) as a key performance indicator for both the asphalt mat and the longitudinal joint. Moreover, the current QA procedures commonly evaluate the in-place density using pavement cores, which can only provide limited coverage. Thus, the challenges of consistently meeting the required minimum density at joints and the limited coverage provided by core sampling pose a risk to agencies of fully paying for substandard joints. Thus, this study examines the continuous coverage capabilities of the Dielectric Profiling System (DPS) and utilizes its in-field dielectric measurements on road projects in Michigan to assess pavement compaction. Furthermore, the study aims to present a framework for developing performance-related specifications (PRS) based on statistical methods for HMA centerline longitudinal joints, leveraging the DPS's improved sampling capabilities. These PRS can help SHAs in achieving better-performing joints within their budgets.

6.2 HMA COMPACTION EVALUATION

Figure 3-1 compares the recorded dielectric values measured at various offsets from the longitudinal joint. The dielectric data was collected across the entire width of the lane (over a length of 1,000 ft) on the unconfined side of the joint. In contrast, only a limited segment (465 ft) on the confined side was tested using a joint pass with three sensors. The data reveals that dielectric values on the unconfined side of the joint are predominantly 5.6 or lower, with most values falling below 4.8 at a 0.5 ft offset (representing the joint's compaction) from the centerline joint. Conversely, on the confined side, most dielectric values range between 4.8 and 5.6, with very few measurements dropping below 4.8. Such comparison highlights the impact of joint construction methods on compaction quality, emphasizing that unconfined joints tend to result in lower compaction and, consequently, lower dielectric values compared to confined joints. The figure shows that confined joints generally achieve better compaction quality than unconfined joints.

Observing the asphalt mat's dielectric data (i.e., excluding the data from the two outer offsets) throughout the length of the pavement lane, the last 400 ft section (right side in the plot) has significantly lower dielectric values over the lane's width. Suggesting that the later part of the pavement was not compacted consistently as was the first half of the lane. This compaction difference is observed to be translated into significant air void differences as illustrated in the figure (lower heat map). The mat's air voids range between 8% to over 12% while the unconfined joint (i.e., at 0.5 ft offset) has over 12% air voids for the majority of the sections' length. The air voids are below 8% on the confined side of the joint with limited data showing void content between 8% and 12%. The confined joint displays much lower air voids compared to the unconfined joint.

The box plots in Figure 3-1(b) and Figure 3-1(c) show the median values (central line in the box), the 25^{th} and the 75^{th} percentile values (the box's lower and upper box boundary lines), and any outliers (asterisk) in the dielectric and air voids data. Figure 6-1(b) shows that paving conditions affect joint dielectric values, mainly when a confined edge is absent. The dielectric values measured 0.5 ft from the unconfined edge of the joint are noticeably lower than those recorded at greater distances (ranging from 2.5 ft to 17.5 ft). For a joint to be acceptable, air voids should be within 2% of the mat's density. This 2% air void difference equates to approximately a 0.14 dielectric difference (mat versus joint), given that acceptable mat

compaction occurs at 8% air voids (dielectric of 5.057) and 10% air voids (4.921 dielectric) for the joint, according to the project-specific calibration model. However, the unconfined joint's dielectric values show a much higher difference than the 0.14 threshold compared to measurements taken further from the joint.

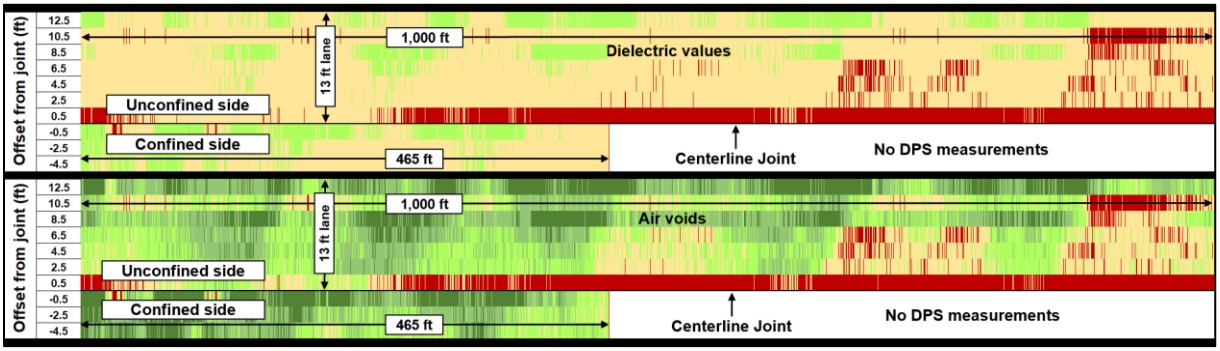

Dielectric scale	< 4.8	≥ 4.8 < 5.2	≥ 5.2 < 5.6	≥ 5.6 < 6.0	≥ 6.0
Air voids scale, %	> 12	> 10 ≤ 12	> 8 ≤ 10	> 6 ≤ 8	≤ 6
Density scale, %	< 88	≥ 88 < 90	≥ 90 < 92	≥ 92 < 94	≥ 94

(a) Heat maps of recorded dielectric and predicted air void values with varying offset from the joint

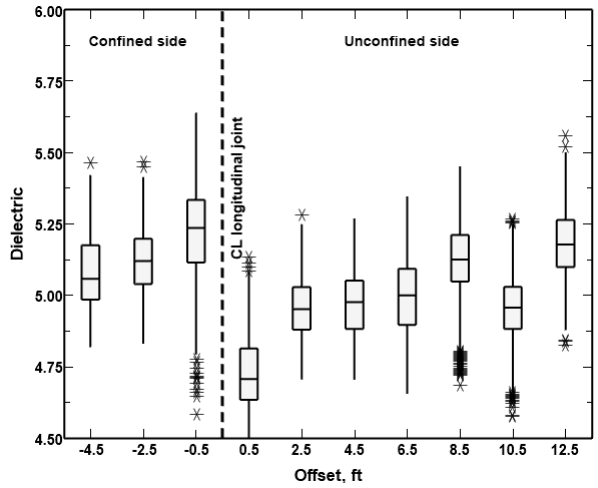

(b) Dielectric value box plots with varying offsets

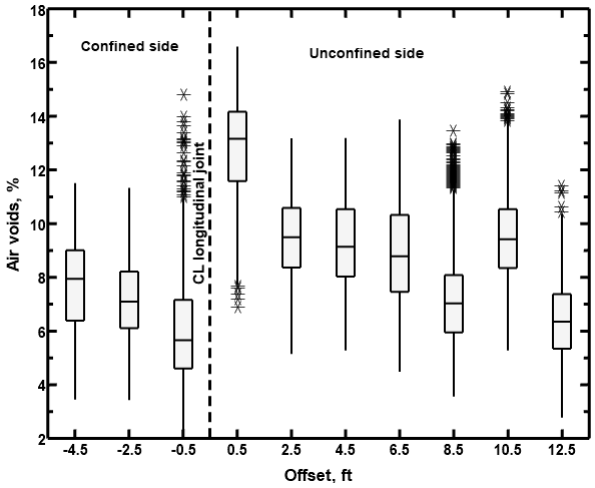

(c) Air void box plots with varying offsets

Figure 6-1 Comparison of dielectric and predicted air void values – US-23 SMA project, MI

Lateral variations in pavement compaction within the lane are apparent from the mat's dielectric values. While these are consistently higher than those recorded at the unconfined joint, the 8.5 ft and 12.5 ft offset measurements surpass the acceptable dielectric threshold for 8% air voids (i.e., 5.057). This level of detailed compaction analysis is essential for pinpointing critical areas of the pavement with lower densities that could influence its long-term performance. Moreover, the confined joint has higher dielectric values than those measured at 2.5 ft and 4.5 ft offsets. Although the values at various offsets are statistically different, all exceed 5.057, indicating air voids below 8%, as seen in Figure 3-1(c). The use of the SMA mix on the US-23,

which typically results in higher field air voids, may have also contributed to these differences. Nonetheless, air voids on the unconfined side of the joint range between 11% and 14%, whereas on the confined side of the second lane, they range between 4.5% and 7%, indicating significantly better compaction for the same HMA mix when constructing against a confined edge.

Figure 6-2 displays the boxplots for the recorded dielectric and predicted air void values for the M-89 and I-69 projects. Like the results from US-23, the confined joint on M-89 demonstrates densities comparable to those of the asphalt mat. For the HMA mix used in this project, a dielectric value of 5.141 corresponds to 8% air voids, while 4.956 equates to 10% air voids. Across all offsets, Figure 6-2(a) shows that dielectric values exceed 5.141, indicating that air voids remain below 8% throughout the lane. The variability in compaction reveals that, aside from the outer shoulder joint (at the 14.5 ft offset), most air void levels seen in Figure 6-2(b) are between 5% and 7%. The figure reinforces that constructing a confined joint produces compaction similar to that of the HMA mat.

Figure 6-2(c) and Figure 6-2(d) show the dielectric and air void value boxplots for the I-69 project, which used echelon paving. The figures show lower dielectric and correspondingly higher air void values at 0.5 ft away from the shoulder (i.e., the shoulder joint). Except for the dielectric values measured 0.5 ft from the shoulder joint, all the other values surpass 5.110, indicating air voids between 4% and 8%. This consistency reflects the effectiveness of the echelon paving method in achieving proper compaction and maintaining acceptable air void levels across the lane.

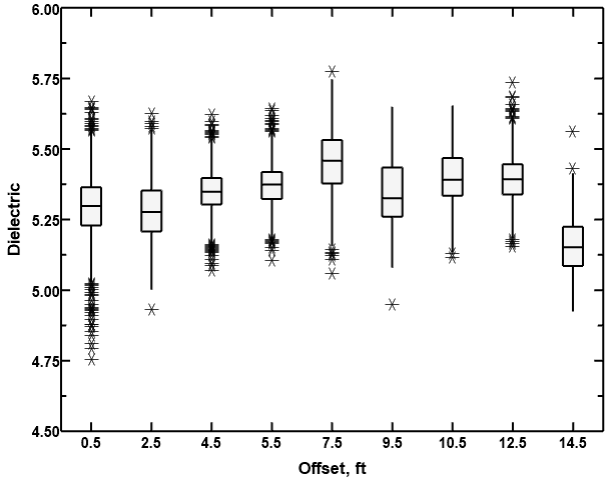

(a) M-89, 2023 (confined joint) dielectric values

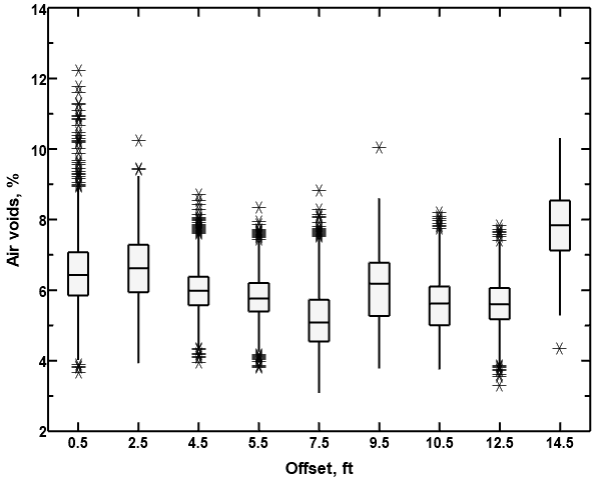

(b) M-89, 2023 (confined joint) air voids

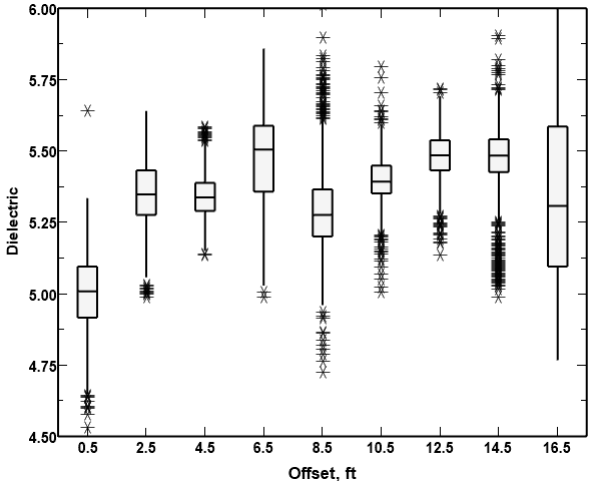

(c) I-69 (echelon paved) dielectric values

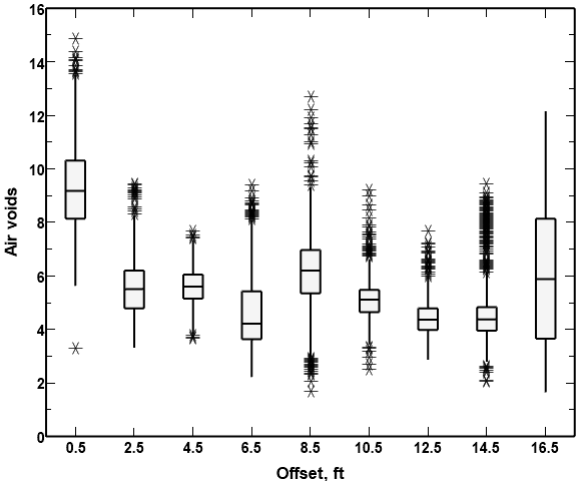

(d) I-69 (echelon paved) air voids

Figure 6-2 Comparison of dielectric and predicted air voids with varying offset from the joint

Figure 6-3 illustrates the recorded dielectric and predicted air void values for the M-61 project, which employed tapered longitudinal joint construction. Figures 6-3(a) and 6-3(b) present the dielectric measurements taken from both sides of the joint. In this project, a 5.027 dielectric value corresponds to 8% air voids, while 10% air voids align with a dielectric value of 4.828 for the specific HMA mix used. Across both sides of the joint, the tapered construction method resulted in higher compaction, reflected by elevated dielectric values and air voids consistently ranging between 4% and 6%. This suggests that constructing an unconfined or confined joint with a tapered geometry can result in similar compaction levels at the joint. Figures 3-1 through 6-3 demonstrate the value of the DPS's continuous compaction coverage capability, allowing for extensive density analysis, which is impossible with conventional spot-

test-based methods. With such a detailed compaction analysis, one can predict future pavement performance variations.

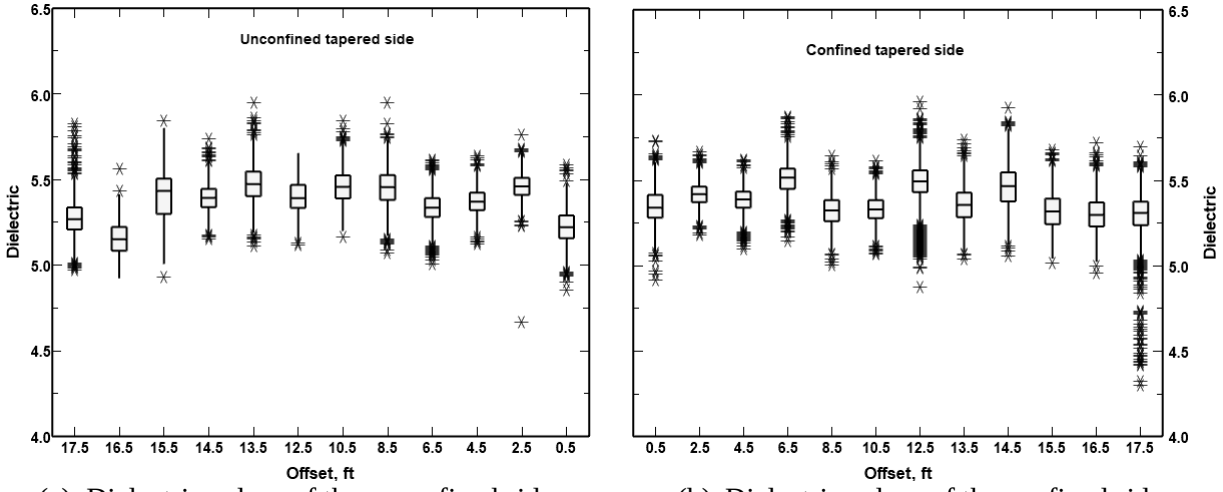

(a) Dielectric values of the unconfined side

(b) Dielectric values of the confined side

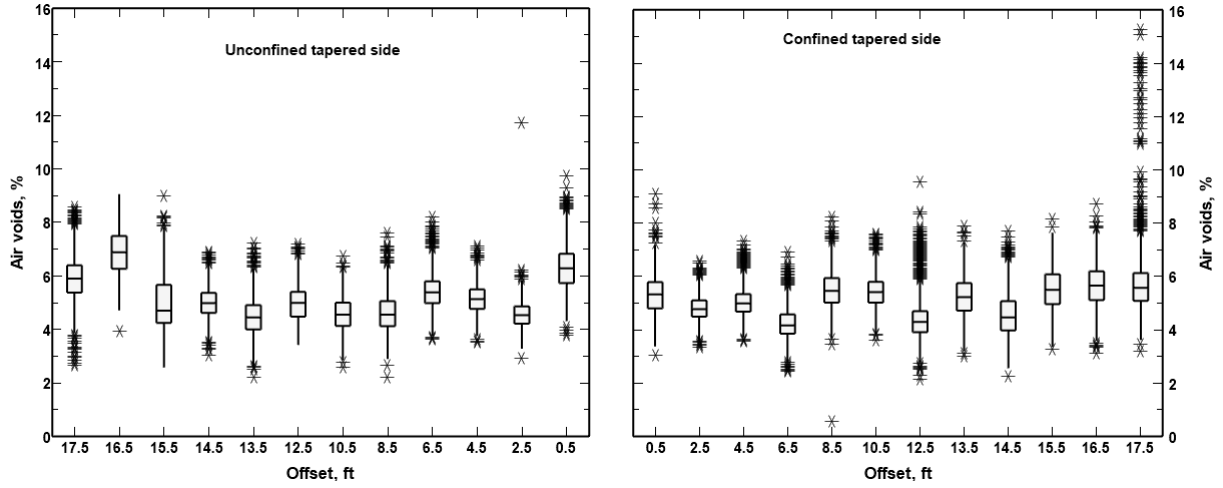

(c) Air voids of the unconfined side

(d) Air voids of the confined side

Figure 6-3 Comparison of dielectric and air voids with varying offset from the joint – M-61, MI

6.3 MECHANISTIC-EMPIRICAL PERFORMANCE RELATIONSHIP

The previous section highlighted the observed differences in the as-constructed density between the mat and the joints using data from four projects in Michigan. While these compaction variations provide valuable insights into the quality achieved at the joints, it is equally important to assess how fluctuations in air void content impact joint performance. Historically, the influence of density on joint performance has been estimated through laboratory tests, pavement cores, or subjective evaluations throughout the pavement's service life. However, joint performance data for the projects in question is currently unavailable, as they were constructed recently (in 2022 or 2023). The AASHTOWare pavement mechanistic-empirical

design (PMED) software is used in this study to establish relationships between air void content and joint performance, with specific assumptions detailed in the following sections. Additionally, since the dynamic modulus (|E*|) is the most critical input for describing the viscoelastic behavior of an HMA mix, this property was measured for the four HMA mixes using the puck samples with varying air void contents.

6.3.1 Sample Preparation and Dynamic Modulus Testing

Test samples were extracted from asphalt pucks that were initially prepared to calibrate the dielectric-air void relationship to evaluate the impact of air voids (or compaction) on the dynamic modulus of the HMA mix. Two specimens, each 1.5 inches in diameter and 4 inches in height, were horizontally cored from each cylindrical gyratory puck. Figure 6-4 illustrates the sample preparation process. The air void content of each specimen was determined according to AASHTO T 166 (*21*). Based on the measured air voids, the specimens were grouped into three categories: *(1)* 2-4% air voids, *(2)* 5-7% air voids, and *(3)* 8-12% air voids. Dynamic modulus tests, as specified in AASHTO TP 132, were then conducted at three temperatures (4°C, 20°C, and either 35°C or 40°C, depending on the high PG temperature of the asphalt binder) and three loading frequencies (10, 1, and 0.1 Hz) (*22*).

Figure 6-4 Small sample preparation from gyratory pucks used in dielectric-air void calibration

6.3.2 Dynamic Modulus Master Curves

|E*| master curves were generated for a reference temperature of 20°C using the time-temperature superposition principle based on the dynamic modulus test results. Figure 6-5 illustrates the |E*| master curves for the M-89 samples, with the legend indicating the air void content of each tested sample (values in parentheses). The |E*| master curve shifts downward as air void content increases, demonstrating that at any reduced frequency (i.e., for a specific temperature and loading frequency), the |E*| of the HMA mixture decreases with increasing air

voids (i.e., reduced density). This observation is consistent with findings reported in the literature (*23; 24*) A noticeable difference in |E*| values is observed within the intermediate temperature range (~20°C) corresponding to the mid-range frequencies. These |E*| differences suggest that variation in compaction levels (i.e., air void content) may influence fatigue damage over time.

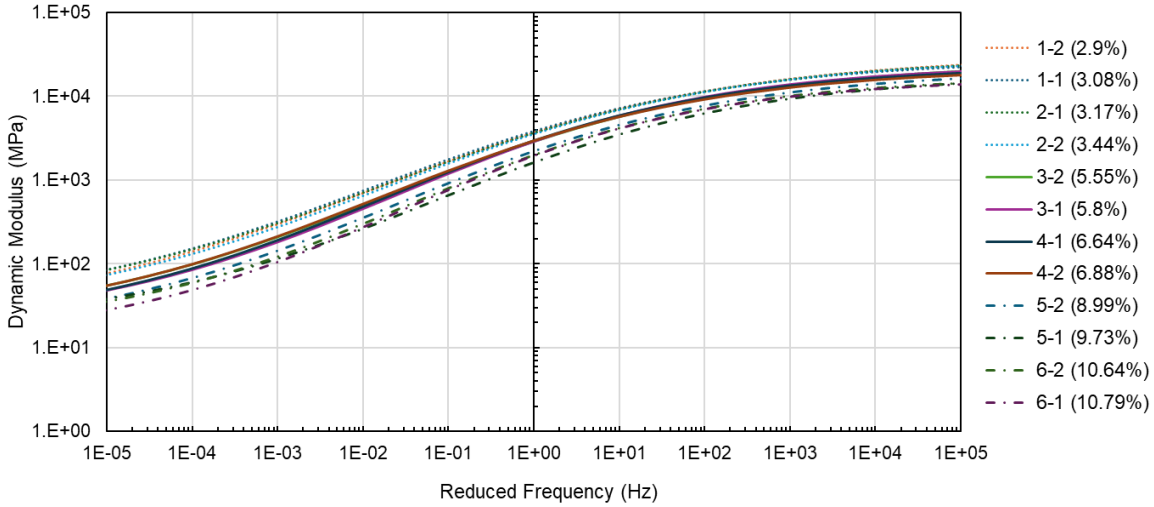

Figure 6-5 Dynamic modulus master curves for M-89 samples with varying air voids

6.3.3 PMED Simulation and Air Void-Performance Relationships

This study used PMED software (v.3.0) with Michigan-calibrated models to estimate the relationship between air void content and joint performance (*25*). Several assumptions were made to focus on air voids' impact on joint performance. The PMED software applies a default wheel wander standard deviation of 10 inches to define the lateral deviation of a wheel from its average path. This value is used probabilistically to estimate cumulative axle load repetitions for distress and performance predictions at a single point. The default distance between the wheel's outer edge and the pavement marking is 18 inches, placing the longitudinal joint approximately 1.75 ft from the outer edge of each tire, based on PMED's default end-to-end axle width of 8.5 ft.

The maximum allowable wheel wander standard deviation of 20 inches was used for this analysis. This adjustment was made because increasing lateral wander reduces the frequency of load applications at the response point (i.e., beneath the tire); increasing the variations (standard deviation) from 10 to 20 inches reduces this frequency by about one-third (*26*). Therefore, this study assumes that the wheel wandering away from the longitudinal joint is comparable to moving the tire away from the response point.

The DPS testing was performed only on the surface layers, with the recorded dielectric values converted to air voids using calibrated relationships. Since the dielectric values were

unavailable for the lower asphalt concrete (AC) layers (i.e., leveling and base), it was assumed that these layers had similar compaction (i.e., air void) levels as the surface layer. This assumption is based on the rationale that if adequate compaction is not achieved at the joint in the surface layer, the underlying layers likely suffer from similar density deficiencies, even if staggered during construction. The |E*| data was also only available for the top layers at varying air void levels. To account for the lower AC layers, |E*| values were extracted from the DynaMOD software and adjusted using the ratio of |E*| values between samples with approximately 7% air voids and those with 4% and 10% air voids. DynaMOD, an MDOT database designed for use with PMED, provided the binder complex shear modulus (|G*|) and the mix's creep compliance values for all pavement layers.

The pavement cross-sections, design speed, and average annual daily truck traffic (AADTT) were obtained from the project plans (see Table 6-1). Traffic distributions for the PMED analysis were based on MDOT's clustered analysis, which factors in Vehicle Class Nine (VC-9) percentage, the number of lanes, road classification (i.e., rural or urban), and functional class. The VC-9 percentages were sourced from MDOT's Traffic Data Management System (TDMS). For the unbound layers and other inputs, the MDOT Mechanistic-Empirical Pavement Design User Guide was referred to (*27*). It should be noted that all pavement simulations were modeled as new flexible pavements within the PMED software.

Figures 6-6(a) and 6-6(b) illustrate the 20-year bottom-up fatigue cracking (BUFC) percentages for the four pavement sections, comparing the results for 20-inch and 10-inch wheel wander scenarios. As expected, BUFC increases as the air void content in the AC layer rises. Specifically, BUFC almost doubles as the air void content increases from 7% to 11% in both wheel wander cases. Additionally, the curve's slope is steeper with the 10-inch wheel wander, a logical expectation. These findings are consistent with trends reported in the literature (*28*). In all simulations, BUFC emerged as the critical distress mechanism, except for the low air voids group (2-4%), where the International Roughness Index (IRI) took precedence, contrary to the expectation of failure due to AC rutting. Figure 6-6(c) presents the predicted design life at failure relative to air void content for the four Michigan projects using a 20-inch wheel wander. The results indicate that for each 1% increase in air voids beyond 7% (taken as the baseline), the predicted design life decreases by approximately 20%. Conversely, Figure 6-6(d) shows a similar percentage reduction in air voids below 7%, leading to a corresponding increase in design life.

These relationships, developed for specific HMA mixes, are reliable for estimating critical design lives across different projects.

Table 6-1 Project details

Project and location	Structure details with layer thicknesses (in) and unbound layer moduli used	Surface mix G_{mm} and nominal maximum aggregate size (NMAS)	Traffic (2-way AADTT), design speed & no. of lanes	Longitudinal joint type (s) tested
US-23 (2022), MI	SMA (PG 70-28P): 1.5 4EML (PG 64-28): 2.0 3EML (PG 58-22): 3.0 Base: 6.0 (33,000 psi) Subbase: 18.0 (20,000 psi) Subgrade (4,400 psi)	2.462, 9.5 mm	375, 75 mph, 2-lanes	Unconfined and confined
M-89 (2023), MI	5EML (PG 64-28): 1.5 4EML (PG 64-28): 1.5 Base: 6.0 (33,000 psi) Subbase: 8.0 (20,000 psi) Subgrade (7,000 psi)	2.455, 9.5 mm	289, 60 mph, 2-lanes	Confined
M-61, MI	4EL (PG 64-28): 2.0 (+1[#]) Base: 10.0 (33,000 psi) Subbase: 21.0 (20,000 psi) Subgrade (7,000 psi)	2.477, 9.5 mm	168, 60 mph, 2-lanes	Unconfined and confined tapered
I-69, MI	5EMH (PG 64-28): 1.5 4EMH (PG 64-28): 2.0 3EMH (PG 64-22): 6.0 Base: 6.0 (33,000 psi) Subbase: 18.0 (20,000 psi) Subgrade (4,400 psi)	2.505, 9.5 mm	3,796, 75 mph, 2-lanes	Echelon

[#]For Pavement-ME simulation.

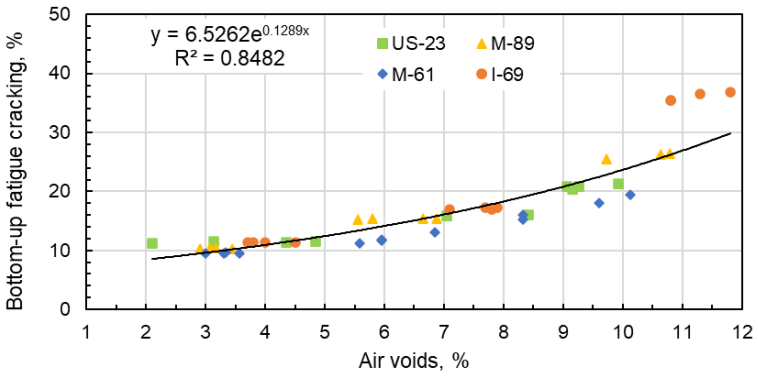

(a) 20 in wheel wander standard deviation

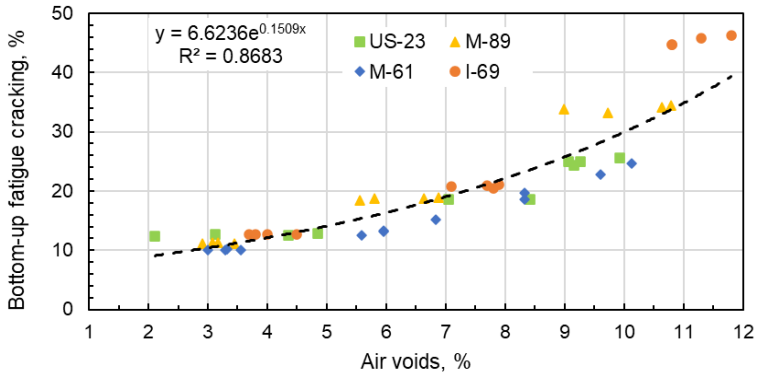

(b) 10 in wheel wander standard deviation

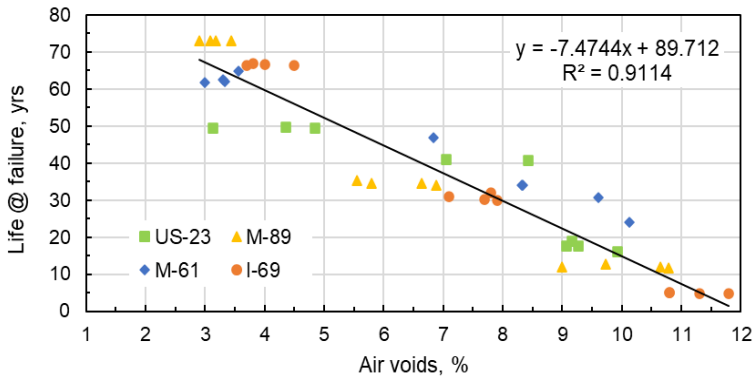

(c) Life vs. air voids (20 in wheel wander)

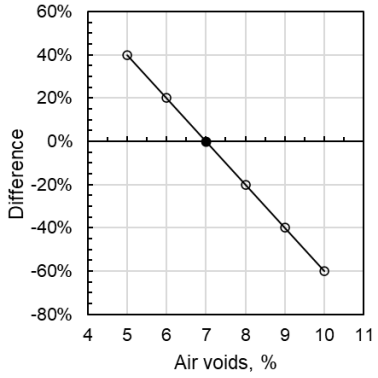

(d) Change in life

Figure 6-6 Relationship of predicted 20-yr BUFC and life with as-constructed HMA air voids

For instance, Figure 6-7 provides box plots showing the predicted design life changes for the US-23 (2022, SMA) and M-89 projects. The graph focuses on the changes in design life under the 20-inch wheel wander scenario, specifically assessing joint performance. While the figure compares estimated lifespans, particularly between confined and unconfined joints, it also highlights significant trends. In the case of US-23, Figure 6-7(a) shows that the unconfined joint substantially reduces predicted design life compared to the confined joint. Additionally, regardless of offset, most stations have values below 1.0, indicating shorter lifespans than

expected at 7% air voids. Conversely, Figure 6-7(b) for the M-89 (2023) project displays that most stations report values exceeding 1.0, suggesting longer lifespans compared to the 7% air void baseline.

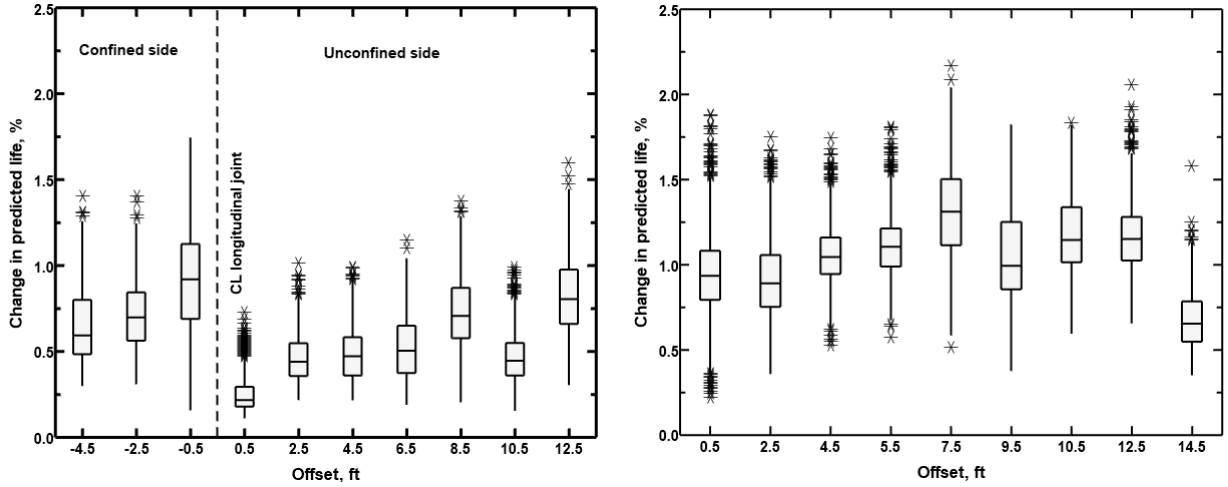

(a) US-23 (2022, SMA) (b) M-89 (confined joint) (2023)

Figure 6-7 Change in predicted lives

6.4 DEVELOPMENT OF PRS FOR LONGITUDINAL JOINTS

Transportation agencies have traditionally relied on QA specifications to determine whether to accept or reject a contractor's work, ensuring the desired pavement construction quality. However, PRS is gaining popularity in pavement construction contracts. PRS employs parameters, known as acceptance quality characteristic (AQC), that influence the long-term performance of the final product (i.e., the pavement), offering a way to account for the value lost or gained when these parameters deviate from their specified target values. Given that as-constructed density (measured as air voids) is widely recognized as the most critical construction-related factor affecting the longevity of both the asphalt mat and the joints, this study adopted air void content at the joint as the AQC. Furthermore, an AQC-performance relationship is essential for developing PRS. The relationship between air void content and the predicted design life at failure—primarily determined by BUFC—was established for the four pavement structures, as shown in Figure 6-6(c) of the previous section.

The percent within limits (PWL) is a highly effective statistical quality measure that accounts for the mean and data variability, making it widely used in highway and pavement construction. As a result, PWL was used to develop the pay factors for this study. An upper specified limit (USL) of 7% air voids was applied to calculate the one-sided PWL across a range of mean air voids, from 2% to 12%, using a standard deviation of 1% in line with MDOT

construction tolerances for air void calculations in design and QA procedures (*29*). The predicted life at failure was estimated using the relationship shown in Figure 6-6(c), based on the same air void values.

Table 6-2 summarizes the relationship between PWL and predicted joint life for a 100 ft subsection/sublot size. Since the DPS collects two dielectric readings per linear foot, a sample size of 200 (n = 200) was used for this analysis. This sample size can be adjusted based on agency requirements. Figure 6-8(a) illustrates this relationship, showing that a USL value of 7% results in a PWL of 50%, corresponding to a predicted joint life of approximately 37 years. Per the MDOT's pavement selection manual, a newly constructed HMA pavement with three maintenance cycles has an expected service life of about 37 years (*30*). Although this is an idealized projection for joint life, it may be somewhat exaggerated as the estimate is based on PMED simulations that primarily focus on the structural performance of the pavement, excluding material and construction-related factors. Additionally, the simulations assume a 20-inch wheel wander, as the joint is not subjected to traffic loading as frequently as the mainline asphalt mat. Therefore, it is reasonable to adjust these predictions downward by 20 years to provide a more realistic expectation.

Table 6-2 Summary of 100 ft sublot mean air voids and the joints performance

Mean AV	Std AV	n	PWL	PL (years)	PL (corrected)
5.0	1.0	200	97.8	52.3	32.3
5.5	1.0	200	93.3	48.6	28.6
6.0	1.0	200	84.1	44.9	24.9
6.5	1.0	200	69.1	41.1	21.1
7.0	**1.0**	**200**	**50.0**	**37.4**	**17.4**
7.5	1.0	200	30.9	33.7	13.7
8.0	1.0	200	15.9	29.9	9.9
8.5	1.0	200	6.7	26.2	6.2

Note: AV = air voids; Std = standard deviation; PL = predicted joint life; n = sample size.

Figure 6-8(b) illustrates the relationship between PWL and the joint's predicted life after the adjustment. Notably, at a USL value of 7%, the PWL remains at 50%, while the predicted joint life is nearly halved (as shown in Table 6-2). Using the PWL and predicted joint life relationship depicted in Figure 6-8(b), the expected performance was converted into pay adjustment factors based on Equation 5-3 and Equation 5-4, adopted from Haider et al. (*31*). A design life of approximately 28 years was assumed, considering that the joints last only 75% of the service life of newly constructed asphalt pavements (i.e., 75% of 37 years). Additionally, subsequent joint repairs are anticipated to occur roughly every 15 years.

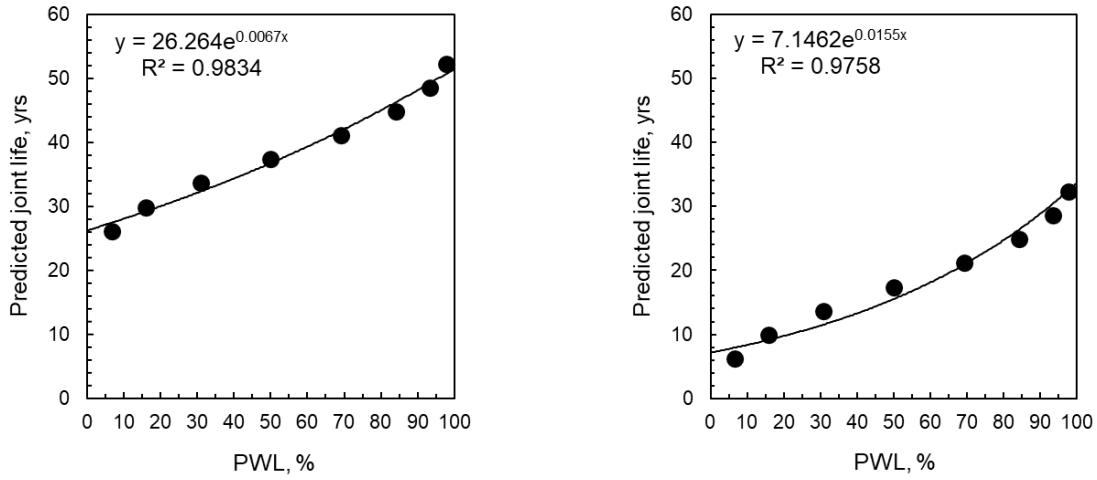

(a) Original (b) After adjustment

Figure 6-8 PWL versus predicted joint life relationship

$$PA = \frac{C(R^D - R^E)}{1 - R^o} \qquad \text{Equation 6-1}$$

$$PF\ (\%) = \left[\frac{(C + PA)}{C}\right] = \left[1 + \frac{PA}{C}\right] \times 100 \qquad \text{Equation 6-2}$$

where;

PF = Pay factor for the joint,

PA = Pay adjustment (same units as *C*),

C = Present total cost of pavement construction, use C = 1 for *PA*,

D = Initial design life of the joint,

E = Expected life of the joint as a function of PWL,

O = the expected life of the successive joint repair (assumed 15 years),

R = (1+ *INF*)/(1 + *INT*),

INF = Long-term annual inflation rate in decimal form,

INT = Long-term annual interest rate in decimal form.

Table 6-3 outlines the relationship between the quality measure (PWL) and the corresponding pay factors (PF). For any acceptance plan that uses PWL to determine pay adjustments, specific quality acceptance thresholds are required, known as the acceptable quality level (AQL) and rejectable quality level (RQL). The AQL represents the minimum level of quality at which the product is accepted based on the AQC, while the RQL defines the point at which the product is rejected. According to the AASHTO *Quality Assurance Guide*

Specification, the AQL is typically set at 90% PWL. Moreover, as per AASHTO R 9-05 recommendations, a PF of 1.00 is assigned for a PWL equal to the AQL (90% PWL in this case). This approach allows for incentives when the PWL exceeds the AQL, while a disincentive applies if the quality falls below the RQL, usually set at around half the design value. The table shows a 100% PF for a joint's life of 28 years with a 100% PWL. The PF reduces by half for a 50% PWL (i.e., the selected RQL) with a joint life of 15 years. The same can be observed in Figure 6-9(a).

Table 6-3 Summary of pay factors with varying PWL levels

PWL	SL (years)	PF (%)
0	7.1	5.1
5	7.7	8.9
10	8.3	12.9
15	9.0	17.1
20	9.7	21.5
25	10.5	26.1
30	11.4	31.0
35	12.3	36.0
40	13.3	41.2
45	14.3	46.6
50 (RQL)	**15.5**	**52.2**
55	16.7	58.0
60	18.1	63.9
65	19.6	69.9
70	21.1	76.0
75	22.8	82.2
80	24.7	88.4
85	26.7	94.7
90 (AQL)	**28.8**	**100.8**
95	31.1	106.9
100	33.6	112.9

Figure 6-9(b) illustrates the operating characteristic (OC) curves, which are essential for evaluating any acceptance plan by assessing the risks associated with the pay received based on the level of quality achieved—in this case, the compaction level at the joint. The plot shows the OC curves for different subsection/lot lengths and their corresponding sample sizes. The contractor’s achieved quality level, represented by the percentage within limits (PWL) on the abscissa, must align with the appropriate OC curve (based on subsection length and sample size) to determine the probability of receiving a pay factor (PF) that reflects the desired quality. For an

unbiased and fair acceptance plan, there should be a 50% probability of achieving a PF ≥ 1, whether the contractor produces above-AQL or below-AQL quality.

For example, if the established AQL for joint density is 90% PWL and the contractor achieves this in the field, aligning the achieved quality level with the OC curve shows the probability of receiving a PF ≥ 1. As seen in Figure 6-9(b), the developed pay adjustment plan awards a 100% PF at AQL with a 50% probability for each lot or subsection (irrespective of the subsection length). This means the contractor will receive more than 100% pay for above-AQL performance half the time and less than 100% pay for below-AQL performance the other half. Since multiple subsections or lots will be sampled throughout the project, the overall pay averages 100%, reflecting a fair adjustment plan. Such a plan encourages contractors to aim for above-AQL performance, increasing their chances of receiving bonus pay.

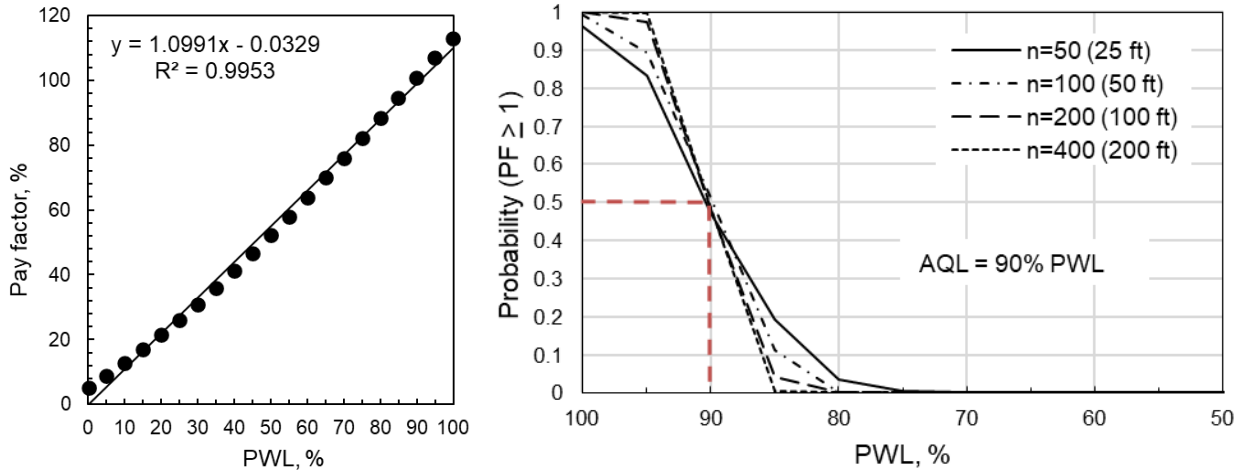

(a) PWL versus PF relationship (b) OC curves for different subsection lengths

Figure 6-9 PF relationship and OC curves for the developed acceptance plan

6.5 CHAPTER SUMMARY

The as-constructed air voids greatly affect the quality of asphalt pavements and longitudinal joints. Current quality assurance (QA) methods predominantly rely on pavement cores to evaluate density, which offers limited spatial coverage and may result in overpayment for subpar field quality. Moreover, many State Highway Agencies (SHAs) use specifications focusing on achieved in-place density (or air void content) as a key performance indicator for both the asphalt mat and the longitudinal joint. The Dielectric Profiling System (DPS) provides extensive compaction coverage and accurately estimates in-place air voids. Incorporating DPS into the QA process and implementing Performance-Related Specifications (PRS) to determine

Pay Factors (PF) for joint quality can aid SHAs in enforcing quality standards better, ensuring the desired outcomes without overpayments.

This study presents a preliminary air void-performance relationship, which can be refined, with several key findings. The DPS offers comprehensive coverage of pavement compaction, effectively identifying low-density areas both longitudinally and laterally. This capability allows SHAs to make more accurate predictions about pavement life and target specific areas for maintenance, optimizing resource allocation. The research highlights significant variability in compaction quality among different longitudinal joints. Unconfined joints demonstrated lower densities and higher air voids, which may shorten pavement service life. In contrast, confined, tapered, and echelon-paved joints exhibited superior compaction and lower air voids, indicating better performance and durability. Given the critical importance of compaction in determining joint performance, the study advocates for a shift in QA methods from traditional spot-test-based approaches to more advanced techniques like DPS that offer continuous coverage.

Furthermore, existing QA procedures often neglect the long-term performance of the longitudinal joint, which this study addresses by proposing a framework that ties service life predictions to air void content, using it as the acceptance quality characteristic (AQC). Finally, PRS was developed by correlating air void content with the predicted service life of the joints and their corresponding pay factors. This was achieved using the widely used percent within limits (PWL) quality measure and a developed service life relationship, offering SHAs a more objective, statistically sound method for evaluating contractor performance and adjusting compensation based on the delivered quality of the joints.

Based on the presented results, the SHAs should strongly consider integrating DPS technology into their QA processes for evaluating asphalt mat destiny in general and joint compaction in particular. Additionally, SHAs are encouraged to investigate and potentially adopt the developed joint PRS framework. By leveraging PWL and air void content as key performance indicators, SHAs can more precisely assess joint quality and adjust contractor payments accordingly, incentivizing the construction of high-quality joints—critical to long-term pavement performance. Continuous monitoring and iterative refinement of the PRS framework based on actual field data and performance outcomes will further ensure its relevance and effectiveness in promoting superior construction practices. Moreover, the study highlights the

need for further research to strengthen the established correlations between dielectric measurements, air voids, and long-term pavement performance. Expanding the dataset to include a broader range of HMA mixes, construction conditions, and geographic locations will improve the accuracy and robustness of the models and specifications, contributing to more reliable and durable pavement systems with durable longitudinal joints in the future.

REFERENCES

1. Linden, R. N., J. P. Mahoney, and N. C. Jackson, "Effect of compaction on asphalt concrete performance," *Transportation Research Record*, 1989.
2. Epps, J., and C. Monismith, "Asphalt mixture behavior in repeated flexure," TE 69-6 (N0. D-6-1). Institute of Transportation and Traffic Engineering., Berkeley, CA, 1969.
3. Seeds, S., G. Hicks, G. Elkins, H. Zhou, and T. Scholz, "NCHRP Project 20-50 (14): LTTP Data Analysis: Significance of "As-Constructed" AC Air Voids to Pavement Performance, Final Report," *Transportation Research Board, Washington, DC*, 2002.
4. Harvey, J. T., and B.-W. Tsai, "Effects of asphalt content and air void content on mix fatigue and stiffness," *Transportation Research Record*, vol. 1543, pp. 38-45, 1996.
5. Harrigan, E. T., "Significance of "as-constructed" HMA Air Voids to Pavement Performance from an Analysis of LTPP Data," *NCHRP Research Results Digest 269*, 2002.
6. Epps, J. A., *NCHRP report 455: Recommended performance-related specification for hot-mix asphalt construction: Results of the WesTrack project*. Transportation Research Board, Washington, DC, 2002.
7. Fisher, J., C. Graves, P. Blankenship, S. Hakimzadeh-Khoee, and R. M. Anderson, "Factors affecting asphalt pavement density and the effect on long term pavement performance," Kentucky Transportation Center, (Research Report KTC-10-05/RSF14-05-1F). Lexington, KY, 2010.
8. Hughes, C. S., *Compaction of asphalt pavement*. Washington, D.C., 1989.
9. Hughes, C. S., *NCHRP Synthesis of Highway Practice 152: Compaction of asphalt pavement*. TRB, National Research Council, Washington, D.C., 1989.
10. Institute, A., "The Asphalt Handbook.," In *Manual Series No. 4 (MS-4), 7th ed.*, Asphalt Institute, Lexington, KY, 2007.
11. Brown, E. R., P. S. Kandhal, F. L. Roberts, Y. R. Kim, D. Y. Lee, and T. W. Kennedy, *Hot Mix Asphalt Materials, Mixture Design, and Construction, 3rd ed.* NAPA Research and Education Foundation, Lanham, MD, 2009.
12. Aschenbrener, T., and N. Tran, "Optimizing in-place density through improved density specifications," *Transportation Research Record*, vol. 2674, pp. 211-218, 2020.
13. MDOT, "Special Provision for Superpave Hot Mix Asphalt Percent Within Limits, 20SP-501R-06," Michigan Department of Transportation, Lansing, MI, 2020.
14. Estakhri, C. K., T. J. Freeman, and C. H. Spiegelman, "Density evaluation of the longitudinal construction joint of hot-mix asphalt pavements," Texas Transportation Institute, Texas A & M University System, 2001.
15. Zinke, S., J. Mahoney, E. Jackson, and G. Shaffer, "Comparison of the use of notched wedge joints vs. traditional butt joints in Connecticut (No. CT-2249-F-08-4)," Connecticut Transportation Institute, 2008.

16. Buchanan, M. S., "Evaluation of notched-wedge longitudinal joint construction," *Transportation Research Record,* vol. 1712, pp. 50-57, 2000.

17. MDOT, "Special Provision for Acceptance of Longitudinal Joint Density in Hot Mix Asphalt Pavements, 20SP-501U-02," Michigan Department of Transportation, Lansing, MI, 2023.

18. Kandhal, P. S., and R. B. Mallick, "Study of longitudinal-joint construction techniques in hot-mix asphalt pavements," *Transportation Research Record,* vol. 1543, pp. 106-112, 1996.

19. Williams, R. C., A. Buss, J. Podolsky, J. Kamau, and N. Tran, "Quantifying Benefits of Improved Compaction," Report No. MN 2021-28, Minnesota Department of Transportation, Office of Research & Innovation, St. Paul, MN, 2021.

20. MDOT, "Special provision for acceptance of longitudinal joint density in hot mix asphalt pavements," 20SP-501U-01, Lansing, MI, 2020.

21. AASHTO, "Bulk Specific Gravity of Compacted Bituminous Mixtures Using Saturated Surface-Dry Specimens," *No. AASHTO T166,* AASHTO, Washington, DC, 2017.

22. AASHTO, "Standard Method of Test for Determining the Dynamic Modulus for Asphalt Mixtures Using Small Specimens in the Asphalt Mixture Performance Tester (AMPT) TP 132," American Association of State Highway and Transportation Officials, Washington, D.C., 2023.

23. Seo, Y., O. El-Haggan, M. King, S. Joon Lee, and Y. Richard Kim, "Air void models for the dynamic modulus, fatigue cracking, and rutting of asphalt concrete," *Journal of Materials in Civil Engineering,* vol. 19, pp. 874-883, 2007.

24. Shu, X., and B. Huang, "Micromechanics-based dynamic modulus prediction of polymeric asphalt concrete mixtures," *Composites Part B: Engineering,* vol. 39, pp. 704-713, 2008.

25. Haider, S. W., M. E. Kutay, B. Cetin, R. R. Singh, H. B. Muslim, C. Santos, Z. You, D. Jin, K. Xin, W. Hansen, and Y. Zhong, "Testing protocol, data storage, and recalibration for pavement-ME design," Michigan Department of Transportation, MDOT, Lansing, MI, 2023.

26. Pais, J., P. Pereira, and L. Thives, "Wander Effect on Pavement Performance for Application in Connected and Autonomous Vehicles," *Infrastructures,* vol. 8, p. 119, 2023.

27. MDOT, "Michigan DOT User Guide for Mechanistic-Empirical Pavement Design: Interim Edition," Michigan Department of Transportation, Lansing, MI, 2021.

28. Heitzman, M., C. Rodezno, F. Leiva, F. Gu, G. Elkins, and P. Serigos, "Investigating the relationship of As-constructed asphalt pavement air voids to pavement performance," 2021.

29. MDOT, "HMA Production Manual," Construction Field Services, Michigan Department of Transportation, Lansing, MI, 2020.

30. MDOT, "Pavement Selection Manual," Michigan Department of Transportation, 2021.

31. Haider, S. W., I. Boz, Y. Kumbargeri, E. Kutay, and G. Musunuru, "Development of performance-related specifications for chip seal treatments," *International Journal of Pavement Engineering*, vol. 22, pp. 382-391, 2021.

CHAPTER 7 - CONCLUSIONS, RECOMMENDATIONS, AND FUTURE WORK

7.1 MAJOR RESEARCH FINDINGS

The quality of longitudinal joint construction is crucial to the longevity of flexible pavements, yet joint deterioration remains a significant challenge for highway agencies. Many highway agencies are dissatisfied with the performance of longitudinal joints, and many local agencies are reporting issues such as raveling along the centerline paving joint of asphalt roads. The persistence of these problems raises questions about whether the root cause lies in materials, construction methods, specifications, or a combination of factors. Despite years of research, training, and industry efforts to improve the construction and compaction of Hot Mix Asphalt (HMA) pavements, joint deterioration continues to cause premature pavement failure. Improving longitudinal joint construction, particularly enhancing compaction to increase density and reduce permeability, is considered one of the most critical remedies for improving overall pavement performance. However, using varying longitudinal joint construction methods coupled with the limited coverage provided by the conventional compaction evaluation methods poses risks in achieving the required compaction levels, potentially affecting the joint's performance.

This study compared various asphalt longitudinal joint construction methods, identified best practices used by highway agencies in general and Minnesota and Michigan in particular, and explored the use of the Dielectric Profiling System (DPS) for joint quality evaluation. Furthermore, the study highlighted the potential use of the recorded dielectric data directly without needing to calibrate project-specific dielectric-air void relationships. In addition, the study demonstrated the DPS's utility for joint quality control (QC) and quality assurance (QA) testing. Moreover, a performance-related specification (PRS) framework was developed to integrate DPS into the joint quality evaluation and subsequent payment schemes. The essential findings of the study can be summarized as follows:

- State Highway Agencies (SHAs), including Michigan and Minnesota, typically do not specify the type of longitudinal joint, though butt joints are commonly constructed. Tapered joints with a vertical notch at the top are used within Michigan. Staggering the longitudinal joints by a 6-inch offset in multiple HMA layers is common. It helps prevent water ingress into the lower layers even if the surface layer's joint opens up. Moreover,

straight or smooth edges are crucial, especially on curves, for ensuring proper compaction during adjacent lane construction.

- Rolling techniques influence joint density; many agencies do not specify rolling methods for unconfined joints, but overhanging the joint by 6 inches is common. Vibratory rolling with a 6-inch overhang can prevent stress cracks, but excessive overhang may damage the joint edge. The hot pinch method is preferred for confined joints, while the hot overlap method is less effective if insufficient material is available for compaction at the joint.
- Overlapping the cold joint edge with 1±0.5 inches of hot asphalt, slightly higher than the adjacent mat, is vital for proper compaction and improved density. Moreover, applying a tack coat to the full lane width and existing joint face is typical and helps with appropriate bonding. Some agencies use joint adhesive or seal (e.g., void-reducing asphalt membrane, VRAM) to improve bonding and reduce permeability.
- Echelon paving is considered the best way to avoid joint construction. Matching lanes daily can eliminate cold joints. The Michigan Department of Transportation (MDOT) allows the removal of up to 4 inches of newly laid HMA from the unconfined edge before paving the adjacent lane, thus eliminating high air void material at the joint.
- Most agencies do not monitor joint density due to the destructive nature of coring and resource constraints. Moreover, the Percent Within Limits (PWL) is used by some agencies, but most rely on a simple average density calculation for compaction evaluation. The simple average method is ineffective for joint quality as it allows half the joint cores to fall below the specified density, unlike PWL, which ensures 90% acceptable void content values for full payment.
- The DPS offers continuous, nondestructive, and comprehensive coverage of the asphalt surface layer. The DPS's ability to provide real-time feedback on pavement density enables immediate quality assessment and corrective actions during the paving process, promoting more uniform compaction.
- The coreless calibration method, which uses laboratory-prepared pucks compacted using a Superpave Gyratory Compactor (SGC), predicts air voids with reasonable accuracy. Moreover, the new regression-based air void prediction model developed and used in this study requires estimating only two parameters compared to the 3-parameter Minnesota

Department of Transportation (MnDOT) model while maintaining similar prediction accuracy.

- Project-wise puck calibration showed reasonable agreement with the extracted core data for most projects. Moreover, the results showed that mix calibration was reproducible and independent of the HMA production day. Additionally, minor fluctuations in the HMA produced on different days for the same design do not impact the calibration curves between surface dielectric and air void content and predict similar density.
- Larger dielectric differences between the calibrated model and core samples were observed for six projects. These differences were hypothesized to be due to moisture on HMA surfaces during DPS testing (from water sprayed by compacting rollers). Additional testing confirmed that ensuring a moisture-free HMA surface is critical for accurate DPS readings. Moreover, the QA core data mostly validated the DPS predictions. However, some discrepancies observed were assumed to be due to unrepresentative core samples or mismatched locations.
- Dielectric measurements conducted over the puck and core samples at varying temperatures (room temperature, freezing at -40°C, and heating to 50°C) revealed the DPS's ability to detect aggregate-absorbed moisture entrapped by binder coating within the HMA. This ability can be beneficial for investigating HMA stripping in pavements with apparently adequate drainage.
- Group-wise calibration was explored using Classification and Regression Trees (CART) analysis to classify HMA mixtures based on the recorded dielectric values and their mix characteristics. The group-wise calibrated models displayed reasonable agreement with individual project curves. Moreover, the group-wise calibration enables the direct use of the recorded dielectric values without the need for model calibration. This would simplify and enhance the DPS's field application, resulting in improved and quicker QA processes.
- Comparing the DPS's dielectric measurements taken on the same asphalt pavement under similar test conditions (i.e., same operator, equipment, sensors, etc.) but several days apart illustrated that these are repeatable. In other words, DPS records similar asphalt dielectric values for a pavement tested multiple times at the same location.
- Comparing the compaction ability of different longitudinal joints constructed using varying joint geometries, rolling patterns, and construction techniques employing

continuous dielectric data demonstrated the DPS's significant advantage over the conventional spot-test-based methods (i.e., coring and nuclear/non-nuclear gauges). The DPS successfully indicated relative compaction differences, where present, between the joint and the accompanied mat.

- The paired *t*-test analysis of discretized dielectric data showed that unconfined joints had the highest air void content, with 50-100% of subsections displaying significant dielectric differences, indicating over 2% more air voids than the mat. In contrast, confined joints (constructed using butt or tapered joint geometry or the Maryland method) achieved similar compaction levels as the mat. Moreover, the cutback method for unconfined joints also resulted in comparable compaction. While echelon-paved joints initially showed higher dielectric differences, this was reduced when analyzing predicted air voids, likely due to using different HMA mixes for the mainline and the shoulder, irregular rolling patterns, or the calibrated model's prediction variability.
- The dielectric-based PWL analysis mirrored the paired *t*-test results, revealing that 60-100% of unconfined joint subsections had PWL values below the rejectable quality level (RQL) of 60%. In contrast, except for echelon-paved joints, all other joint types exhibited comparable compaction, with negligible subsections below 60% PWL. While echelon-paved joints initially showed a higher percentage of subsections with PWL below 60% using dielectric data, the use of predicted air voids significantly reduced the number of subsections falling below the 60% PWL threshold (i.e., RQL).
- Both the statistical and stochastic analyses showed that better joint density can be achieved by either constructing a butt or tapered joint provided the construction of an unconfined joint is avoided.
- Observing the effect of different subsection lengths, the statistical analyses used in this study show that the percentage of sections with compaction issues increases as the subsection length increases from 25 ft to 200 ft. This trend suggests that using a smaller subsection is beneficial and can effectively identify local compaction issues. Moreover, the ability to analyze data using smaller subsection lengths demonstrates the real benefit of the continuous dielectric data provided by DPS in flexible pavements QA/QC procedures.

- The probabilistic joint comparison showed similar results as earlier, indicating that for any compaction level of the asphalt mat, there is a 30-60% chance of the unconfined joints having significantly lower dielectric values, indicating over 2% more air voids than the accompanying mat. All the remaining joint types displayed negligible dielectric differences from the used mat's reference values. Rather, the unconfined joints constructed using the cutback method, confined joints constructed using the Maryland method, and confined tapered and echelon-paved joints display some probability of higher dielectric values than the reference mat value.
- The paired *t*-tests used the relative dielectric differences to compare the joints. However, it did not individually consider the mean mat and joint dielectric values. The Longitudinal Joint Quality Index (LJQI) was introduced to address this limitation and improve the practical use of DPS by directly utilizing the recorded dielectric values in the field. The minimum acceptable dielectric values for mat and joint and an acceptable dielectric difference are determined based on the group-wise calibrated models. Using these values, the calculated LJQI values for the unconfined joints of different projects revealed that 11-89% of the stations within the 1,000 ft sections had unacceptable joint densities, leading to over 2% more void content than the mat.
- An LJQI threshold of 70% was determined, using Receiving Operating Characteristic (ROC) curves, by calculating the LJQI for every subsection of the different projects and comparing it with their void content-based PWL, the latter being used as the reference. The threshold uses a dielectric measurement tolerance of 0.08 and 8% air void content as the upper specified limit (USL) for the longitudinal joint and had an accuracy of about 90% irrespective of the subsection length; using a 100 ft subsection length reduced the occurrence of false positive instances.
- Many State Highway Agencies (SHAs) use specifications emphasizing in-place density or air void content as key quality indicators. However, these specifications overlook the longitudinal joint's performance considerations. Incorporating the DPS's continuous compaction coverage and PRS that link the joint's service life to its void content as the Acceptance Quality Characteristic (AQC) offers a more effective alternative to traditional methods. This approach enables the void content-service life relationship to determine pay factors (PF) based on PWL, providing a more objective, statistically robust method

for assessing contractor performance and adjusting compensation based on the constructed joint's quality.

7.2 RECOMMENDATIONS

The following are recommended based on a comprehensive review of existing longitudinal joint construction practices and literature, findings from surveys conducted in Minnesota and Michigan, and the statistical and stochastic analyses of the collected DPS data.

7.2.1 Best Practices for Longitudinal Joint Construction and Repair of Existing Failed Joints

Although most agencies, including MDOT and MnDOT, do not specify the type and technique of longitudinal joint construction, the following best longitudinal joint construction practices are recommended:

Construction Methods

- The sequential mill and fill technique offers improved compaction for longitudinal joints by avoiding the creation of an unconfined joint. However, the method only applies to mill and fill projects. Proper cleaning of the milled surface and the confined edge of the newly laid mat is crucial before laying the fresh asphalt material in this technique.
- A comparison of different joint types evaluated in this study suggests that constructing an unconfined joint is highly likely to produce significant density differences and should be avoided whenever possible.
- When compacting a single lane during a new HMA pavement construction, utilizing an edge restraint attachment, such as those used for constructing a safety edge or a taper joint, can significantly enhance the unconfined joint's compaction.
- Another method to improve compaction at an unconfined joint is to require the contractor to cut back a minimum of 6 inches from the unconfined edge before paving the adjacent lane. Joints constructed using such practice resulted in similar or slightly better joint compaction than the accompanying mat.
- Echelon paving, which involves multiple lanes simultaneously, showed good compaction results and is recommended for use, where feasible, during the construction of new asphalt pavements. However, proper rolling patterns must be used to ensure a seamless mat with optimum compaction within the vicinity of the interface of hot HMA laid by the adjacent pavers.

- Regardless of the technique employed, ensuring that the joint's edge is paved as straight as possible during construction is essential. A straight edge facilitates improved joint compaction when the adjacent lanes are paved, contributing to the overall quality and longevity of the pavement.
- The survey results and literature indicate that applying a bond, tack coat, or proprietary material to the vertical face and bottom of adjacent joints significantly improves joint quality and aids sealing. Hence, their usage is recommended to enhance bonding at the interface between the two asphalt mats.

Rolling Patterns

- The hot pinch method is recommended for constructing a confined longitudinal joint, which involves keeping the drum of the breakdown roller entirely on the hot asphalt material (i.e., the hot side of the joint), with its edge at least 6 inches away from the joint. The roller operates in vibratory mode, pushing the hot asphalt material toward the joint.
- The Maryland method is recommended for rolling and compacting all confined joints, which involves three sequential steps.
    1. Overlap the edge of the existing adjoining mat (previously constructed) by 1-1.5 inches with hot asphalt material during paving, and bump back any excess material exceeding 1.5 inches.
    2. Compact the hot asphalt material similarly to the hot pinch method, which pushes HMA material into the joint. This helps lock and consolidate the material while pushing additional HMA into the joint.
    3. Finally, the overlapped and pushed material is compacted into the confined joint, utilizing the roller's maximum vibratory force until a thin white line appears on top of the longitudinal joint, indicating the successful execution of the Maryland method.
- For constructing an unconfined longitudinal joint, it is recommended to roll the joint with the drum overhanging the edge by 6 inches with the roller operating in vibratory mode. Exceeding this limit may result in the crushing of the HMA material near the edge, leading to inadequate compaction at the joint.

Joint Geometry

- As far as joint geometry, both butt joints and tapered longitudinal joints can achieve better compaction as long as the traditional unconfined joint construction is avoided.

Joint Repair

- The literature recommends using crack sealing and micro-surfacing to maintain and repair low- to medium-level distressed longitudinal joints. These methods are cost-effective alternatives compared to other repair options.
- For medium and high-severity joint deterioration levels, spray injection treatment and slot paving are recommended. However, slot paving should only be considered a last resort due to its higher cost.

7.2.2 Evaluating Joint Quality During Construction

- The DPS's significant advantage over traditional density evaluation methods (i.e., coring and density gauges) of providing continuous, nondestructive, and comprehensive compaction coverage of the asphalt layers makes it a recommended alternative. The 100% coverage significantly reduces an entity's (agency or contractor) risk associated with random sampling inherent in spot-test-based QA and QC methods, thereby minimizing the likelihood of undetected low-density areas, particularly at critical points such as longitudinal joints, which are prone to premature failure due to lower compaction levels.
- Based on the DPS's ability to offer real-time feedback on pavement density both longitudinally and laterally, enabling immediate quality assessment and corrective actions during the paving process, and distinguishing the compaction ability of varying joint types and construction techniques, SHAs and contractors alike are suggested to adopt DPS for their flexible QA and QC testing.
- The DPS's puck calibration is recommended since it is reliable, free from moisture-related issues, and displayed reasonable agreement with the collected pavement cores as well as QA core data. While project-wise calibration can be adopted, group-wise calibration would make DPS's adoption in the QA and QC process practical and more feasible.
- Moreover, using DPS can enable SHAs to estimate pavement life and optimize maintenance efforts accurately (once an air void-service life relationship exists) by

targeting specific areas of concern, ultimately enhancing overall pavement durability. Therefore, DPS is recommended for comprehensive compaction quality assessment of asphalt pavements in general and longitudinal joints in particular.

7.2.3 Joint Quality Evaluation with DPS

- This study recommends using DPS for the joint quality evaluation, which provides far more data, 2,000 data points within a 1,000 ft section per sensor, compared to limited core/density gauge sampling rates.
- Using the LJQI offers a superior alternative to traditional joint quality evaluation methods. Data analysis from this study shows that the LJQI effectively determines the percentage of stations with acceptable compaction without unfairly penalizing joints due to high compaction in the asphalt mat, which typically skews results based solely on joint-to-mat differences. Thus, the LJQI is recommended for joint quality evaluation utilizing the DPS.
- The recommended use of LJQI also provides an alternative way of using the dielectric data, directly eliminating or significantly minimizing coring needs and calibrating project-wise air void-dielectric relationships. However, this is only possible when using the group-wise calibrated models. An agency could group its HMA mixes based on similarities in mix characteristics and calibrate a group-wise dielectric-air voids relationship like the one presented in this study for the MDOT mixes. Establishing a database for this purpose is beneficial and is recommended to the SHAs.
- This study recommends specifying 8% air void content as the upper specified limit (USL) for longitudinal joints. Moreover, a 0.08 dielectric tolerance is recommended for determining the LJQI. Finally, this study recommends using a 70% LJQI threshold for accepting the delivered longitudinal joint quality.
- The DPS can also pinpoint areas with inadequate compaction within the asphalt mat and joint that may not require immediate intervention according to agency specifications. This capability, which cannot be achieved through traditional coring, allows for targeted maintenance of these areas more frequently during the pavement's service life, helping to extend overall durability.

7.2.4 Construction Specifications for Potential Use of DPS in Quality Assurance Testing

- Given the critical role of compaction quality in pavement performance in general and longitudinal joints in particular, QA and QC methods are recommended to transition from conventional spot-test-based approaches to continuous coverage methods like DPS.
- While the traditional methods fail to provide real-time feedback, the DPS testing can begin as soon as a 500 ft pavement section is ready behind the finish roller. However, in rare circumstances that prevent immediate dielectric recording during paving operations, the DPS testing can occur later, provided that dirt, debris, and moisture have not accumulated on the pavement surface.
- Three DPS passes with the sensors 1.5 – 2 ft apart from each other are recommended for complete coverage of a pavement lane. In addition, a joint pass should have one sensor at 6 in offset from the joint to ensure full coverage of the longitudinal joint.
- The LJQI can be utilized in the QA testing as a pass/fail criterion for directly evaluating longitudinal joints based on the recorded dielectric values in the field. An LJQI passing threshold of 70% is recommended.
- Dielectric-based PWL is recommended for QA, provided acceptable joint and mat dielectric values are obtained. These can be based on project/mix-specific calibrated models; group-wise models are recommended to minimize calibration needs. As mentioned earlier, this is possible if a database is developed that includes data from all HMA mixes used by any SHA.
- Finally, SHAs should consider investigating and potentially adopting the PRS framework proposed in this study. By using PWL as the quality measure and air void content as the key joint performance indicator (i.e., AQC), SHAs can more accurately evaluate the joint quality and make informed pay adjustment decisions to avoid overpayments, ultimately ensuring the construction of high-quality, durable pavements.

7.3 RECOMMENDED FUTURE WORK

While the analyses presented in this study highlight the accuracy of the DPS measurements and the benefits of adopting DPS in the QA and QC procedures, the following are suggestions for future research:

- Further testing and research are needed to validate the accuracy of the DPS in measuring asphalt layer density. Additional DPS testing and data collection across all standard

MDOT HMA mixes are necessary before deciding its future use and implementation in the QA testing plans.

- The possible effect of moisture during the field dielectric data collection by the DPS needs to be explored. Implementing methods to adjust DPS calibration for residual moisture presence could enhance the accuracy of its measurements.
- The group-wise calibration presented using the MDOT mixes and its use for the LJQI determination needs further refined by using all standard MDOT HMA mixes and exploring the index's applicability across different pavement types. Including HMA mixes and projects from all MDOT regions will enhance the applicability of the index and further improve the accuracy of the group-wise models.
- Monitoring the field performance of the longitudinal joints evaluated in this study for the next five years will be beneficial in validating the findings from DPS testing. Moreover, tracking the joints' performance would help refine the air void-service life relationship that was used for developing the PRS. Expanding the dataset to include more HMA mixes and construction conditions will improve the robustness of the relationship.
- SHAs should regularly monitor and adjust the PRS framework based on field data and performance outcomes. This iterative process, including more HMA mixes, will help refine specifications, ensuring they effectively promote high-quality construction practices and achieve the desired pavement performance.